Welding Integrity of HSLA Welds

Houman Alipooramirabad

Thesis submitted for the degree of Doctor of Philosophy

School of Mechanical Engineering

Faculty of Engineering, Computer & Mathematical

Sciences

The University of Adelaide, Australia

March 2017

Table of contents

Abstract

The novel approaches in modelling and experimental investigations on welding integrity for single and multi-pass high strength low alloy steel (HSLA) welds is presented here.

High level of welding stresses (mainly tensile mode) are generated during the construction of pipelines which are due to non-uniform temperature distribution and cooling rates as well as using clamps during welding and mechanical handling loads which occur during lifting the front end of pipeline to place it on supports.

Existing of such high tensile stresses combined with hydrogen rich cellulosic electrodes used by Australian pipeline industry has increased the risk of Hydrogen assisted cold cracking (HACC) in the weld metal, in particular root pass of girth welding, which clearly has detrimental effect on weld integrity and its performance in service. The prediction and measurement of this welding stresses in pipeline construction was limited to a few studies. The current project was therefore started with emphasis on the effect of welding stresses on HACC susceptibility of the root pass of pipeline girth welding using Welding Institute of Canada (WIC) weldability test. 3D finite element models are developed and validated against neutron diffraction measurements to investigate the effects of various welding process parameters and regimes on residual stresses for the root pass of the WIC test. Chapter 4 presents the experimentally validated numerical simulation results of the root pass of the WIC test. However after initial modelling and experimental measurements the project was extended toward measurement of residual stresses (using neutron diffraction) for multi-pass welding in HSLA welds coupled with microstructural characterization and mechanical property studies with the view of full applicability for pipeline/ pressure

vessel applications. It was found that welding parameters have significant effects on the residual stress-microstructural-mechanical property interrelationships of multi-pass HSLA welds. Therefore a set of welded specimens was prepared to investigate such interrelationships for the following welding parameters:

- Heat input effects (variable travel speed)

- The alterations in welding direction (welding sequence)

- The effects of welding process (combination of modified short arc and fluxed core arc welding versus shielded metal arc welding)

It was found that increasing the heat input (reduction in welding speed) is beneficial in reduction of residual stresses. This could be correlated with the formation of microstructural constituent of mainly polygonal ferrite in the weld metal and HAZ of high heat input welds. Furthermore, there was no significant effect on the magnitude of the residual stresses, microstructural characteristics and mechanical properties when the weld deposition direction was changed. The findings also indicated using SMAW lead to significant reduction in residual stresses in comparison with the combination of MSAW+FCAW processes. The results of such investigations are presented in chapters 5-7.

After identifying such interrelationship effects, this research study develops further to investigate the effects of mitigation techniques on relaxation of residual stresses/strains in weldments. In-situ neutron diffraction studies was conducted, coupled with in-depth microstructural/mechanical property studies, in which the rate of relaxation, holding time effects and the underlying mechanism behind stress relaxation for HSLA steel welds was investigated. One of the core finding of this

investigation is the insignificant effects of holding time on stress/strain relaxations of HSLA welds.

It was also found that strain relaxation in the initial stage of heating (temperatures up to about 360-370 ℃) is due to reduced yield strength with increasing temperature, while for the higher temperatures (370-600 ℃) strain relaxation is due to development of creep strain. Microstructural studies also indicate existing of sub-grains in the PWHT specimen, which is due to dislocation climb, pointing out to creep (creep strain development) as the driving mechanism behind stress relaxation during PWHT. The results are presented in chapter 8 of the thesis. Such findings will also be fully elaborated in the up-coming publications. Future work will be investigating the effects of plate thickness and the type of material on strain relaxation behaviour for various weld joints to establish a "time-temperature-rate of relaxation-thickness-holding time-material type" envelope. Such findings could offer the prospect of more economic heat treatment standards that combine cost savings with optimised mechanical properties and residual stress states.

Thesis Declaration

I certify that this thesis contains no material which has been accepted for the award of any other degree or diploma in any university or other tertiary institution, and to best of my knowledge, contains no material previously published or written by other person, except where due reference has been made in the text. In addition, I certify that no part of this work will, in the future, be used in a submission in my name, for any other degree or diploma in any university of tertiary institution without the prior approval of the university of Adelaide and where applicable, any partner institution responsible for the joint-award of this degree.

I give consent to this copy of my thesis, when deposited in the University Library, being made available for loan and photocopying, subject to the provisions of the Copyright Act 1968. The author acknowledges that copyright of published works contained within this thesis resides with copyright holder (s) of those works.

I also give permission for the digital version of my thesis to be made available on the web, via the University's digital research repository, the Library Search and also through web search engines, unless permission has been granted by the University to restrict access for a period of time.

Houman Alipooramirabad

06 February 2017

Acknowledgements

CHAPTER 1

INTRODUCTION

1.1 Background

Welding is one of the major fabrication routes in the manufacturing of a range of structures including aircrafts, ships, pressure vessels and energy pipeline. Welding is usually accomplished by melting the joining parts and adding a filler material or consumable to form a molten weld pool that cools and solidifies to form a strong joint. The quality of the joint and the integrity of the welded structures are dependent on the mechanics of the welding process employed, the chemistry of the consumables, i.e. electrodes and the materials to be joined together, parent metal. A wide range of welding processes and consumables are now available for joining different materials. Amongst the engineering materials, steels are the main class of metals used in fabrication of welded structures using a range of welding processes. The introduction of modern steels with superior mechanical and chemical properties demands more careful selection of welding processes and consumables. One such steels grades are the so-called high strength low alloy (HSLA) steels which resulted from a complex control of rolling procedure and steel chemistry. HSLA steels have now found a wide range of applications for construction of welded structures including energy pipeline for gas and oil distribution. The welded joints of HSLA steels are prone to various failure modes in service such as stress corrosion cracking and hydrogen assisted cold cracking which are related to the generated residual stresses during welding and the microstructure constituents [1, 2].

The use of high strength low alloy (HSLA) steels offers significant weight and cost savings in the construction of pipelines. However, when welded with cellulosic electrodes, in spite of facilitating the high speed construction of pipelines with better weld penetration, the weldment (in particular the root pass) is known to be highly

susceptible to weld metal hydrogen assisted cold cracking (HACC) if not managed properly [3]. This is due to the richer chemistry of the weld metal and lower austenite to ferrite transformation temperature in contrast with the HSLA pipe steels, which result in shifting the risk of HACC from the heat affect zone (HAZ) of line pipe steel to that of the weld metal (WM) [4].

HACC is a very complex phenomenon and several theories and associated criteria have been proposed in the past to describe and characterise HACC, specifically in HAZ. All macroscopic theories agree that HACC is mainly affected by three major factors: (1) hydrogen content; (2) susceptible microstructure; and (3) local stresses [5]. Reflecting the complex nature of HACC, the pipeline industry has developed several empirical evaluation procedures and weldability tests for particular structures, materials and types of welds to assess the risk of HACC. These include the Tekken test [6], Gapped bead on plate weldability test [7], Lehigh U groove restraint test [8] and many others. The review paper by Yurioka and Suzuki [9] provides a comprehensive overview of HACC phenomenon, criteria, theories and the most popular weldability tests.

The Welding Institute of Canada (WIC) has developed an advanced weldability test specifically intended to evaluate the risk of root pass cracking in pipeline girth welds. This test was extensively utilised, over the past three decades, by the industry to qualify pipeline welding procedures [10]. Due to the same local geometry features two main factors affecting HACC in pipes (microstructure and hydrogen diffusion) can be well reproduced in the WIC test, while the appropriate quantitative representation of the third factor, welding stress, currently presents a challenge in the test procedure. This study is therefore carried out to investigate the welding stresses (stresses generated due to self-restraint and external-restraint or anchoring) in WIC test and correlate the

resultant stresses with occurrence of HACC. The other important issue during welding which affects the welded structure integrity and its performance in service is the residual stresses frequently develop during welding.

Residual stresses are self-balancing stresses which are retained within a body when no external forces are acting [11-12]. Local plastic deformation resulted from thermal and mechanical processing of fabricated structures is the main cause of residual stresses generated during a range of manufacturing processes including welding process. Despite the significance of residual stresses on the integrity and life span of structures, the role of residual stress on failure has received relatively little attention. This might be due to complexities associated with the prediction and measurement of residual stresses. There is a common agreement in structural mechanics community that corrosion resistance and fatigue life of welded structures can be improved through a reduction and control of the tensile residual stresses [11-14]. High tensile residual stresses can have a significant effect on the structural integrity and can accelerate significantly the growth of the defects such as micro-cracks and creep voids [15]. As a result, there is a need for more reliable information on the state of residual stresses and magnitude in weldments. It is well-known that the magnitude and distribution of residual stresses are greatly influenced by the welding procedure and weldment geometry. Although the overall effect of welding parameters on the field of residual stresses is relatively well understood; but the effects of individual parameters remain largely unknown for many practical situations [16].

Numerical simulations and experimental techniques have been utilised for evaluation of residual stresses in welded structures. These techniques include ultrasonic [17], hole drilling [16], layer removal techniques [18], X-ray and synchrotron diffraction [19]

and neutron diffractions [20]. It is worth mentioning that residual stress measurements in most of these techniques are only limited to the surface measurements. The latter technique (neutron diffraction) allows the measurement of residual stresses for most alloys and metals with an effective depth of measurements up to several centimetres, which covers many practical applications including multi-pass welding [21-24]. The study was initially conducted to investigate the effect of welding stresses on hydrogen assisted cold cracking (HACC) susceptibility of the root pass of pipeline girth welding using Welding Institute of Canada (WIC) weldability test [25]. 3D finite element models were developed and validated with neutron diffraction results to evaluate the welding stress for matched, under-matched and overmatched welds. The effects of various welding parameters (wall thickness, heat input and variable restraint length) on residual stresses of WIC sample are systematically investigated. As a practical outcome, the presented results can help to select the appropriate anchoring length in WIC tests to simulate the actual stress conditions in the pipeline, and, eventually, reduce the risk of HACC.

It should be noted that the welding of pipeline and pressure vessel were multi-pass procedures and therefore after analysing the root pass of girth weld, it was tried to extend to include multi-pass welding to further highlight the issue of further passes such as the hot, fill and cap passes deposited during pipeline/pressure vessel construction.

Therefore, after initial modelling the project shifted towards measurement and mitigation of residual stresses in multi-pass welds. As a result, neutron diffraction method was applied to investigate the effects of welding parameters (heat input, pass sequence and welding process) and mitigation techniques (post-weld heat treatment)

on the residual stresses in multi-pass welds. Residual strains, and hence stresses, in these samples were analysed quantitatively using neutron diffraction techniques on the KOWARI strain scanning instrument at the OPAL research facility operated by the Australian Nuclear Science and Technology Organisation (ANSTO) [26]. Furthermore, the interrelationship and effects of heat input, pass sequence and welding process on the residual stresses, microstructural, and mechanical properties of multi-pass HSLA weld were also investigated.

After identifying such interrelationship and effects, this research study developed further to investigate the effects of mitigation techniques on reliving residual stresses in weldments. Since the main focus of this study is to optimise and minimize residual stresses in weldments with intentions of being applicable to all welded structures including ship building and pressure vessel fabrication. Post-weld heat treatment (PWHT) is often required for pressure vessel and piping components for relaxing residual stresses, increasing the resistance to brittle fracture and stress corrosion cracking [27]. There are codes and standards to conduct PHWT for steel structures such as ASME Division 2 and API 579RP. All these codes share rather similar regulations for conducting PWHT including applying uniform heating to a sufficiently high temperature below the lower transformation temperature (A1 or AC1), ramping up temperature, hold time and hold temperature depending on the type of steel and for specified wall thickness [28].

According to recent investigations the PWHT related codes can be excessively conservative, particularly for the holding time in thick vessels. For instance Zhang, et al. [29] and Dong and Hong [30] used a series of finite element models to investigate weld residual stress relaxation in a furnace based post weld heat treatment using

Omega creep model. They found the required holding time can be significantly reduced, in comparison with the PWHT standards, with reasonable residual stress reduction as long as a reasonable PWHT temperature is applied.

It is found that the most dominant stress relief mechanism in PWHT is creep strain induced stress relaxation. According to Dong, et al. [28] creep-induced stress relaxation occurs far earlier than recognized by current codes and standards. Therefore, a significant economic benefit can be achieved by reducing the currently implemented PWHT hold time when residual stress relief is the primary objective. With the above discussion the current work was structured to address these fundamental aspects of PWHT.

Although the aforementioned studies improved the understanding of the mechanics of residual stress relief during PWHT, there exist a series of questions that are of practical importance and fundamental in nature particularly for HSLA welds. The questions such as:

1) How to quantitatively inter-relate PWHT temperature, hold time and the rate of stress relaxation to develop a more consistent "time- temperature-rate of relaxation" relationship for residual stress relief?

2) What is the rate of stress relaxation during the hold time? And can it be minimised?

3) What is the relationship between the temperature increase during PWHT and relaxation of residual stress?

4) What is the underlying mechanism behind the stress relaxation during post weld heat treatment?

In order to address these fundamental questions the present study used a novel approach which is based on in-situ neutron diffraction during post-weld heat treatment. This technique enables us to measure the relaxation of residual strains continuously during post weld heat treatment for the welded components. The findings have important economic bearings and can be used to optimize the PWHT process for HSLA steel welds. In addition to the in-situ neutron diffraction studies, microstructural characterization (optical microscopy, scanning electron microscopy, EBSD and TEM) and mechanical testing were also conducted to fully characterize the PWHT effects in multi-pass HSLA welds.

1.2 Objectives

The objectives of this research project were as follows:

I. To develop a numerical procedure capable of predicting and optimising residual stresses of the root pass of pipeline girth weld using Welding Institute of Canada (WIC) weldability test.

II. To investigate the effect of welding sequence and heat input on the residual stress distribution in weld metal (WM) and heat affected zone (HAZ) in high strength low alloy steels (X70).

III. To incorporate the effect of heat input (in the context of travel speed and resulting cooling rate) and pass sequence on microstructure, and residual stresses and how these factors affect the mechanical property (hardness) of the welded joint for multi-pass welds.

IV. To make measurement of the relaxation of residual strains during PWHT. Measuring the relaxation of residual strains/stresses during heat treatment provide a methodology for optimising the post-weld heat treatment of welded components.

V. To study the effects of various post-weld heat treatments (0.5, 1 and 3 hours holding time) on residual stresses, microstructural and mechanical properties of HSLA welds.

VI. To investigate the effects of holding time on strain evaluation during PWHT

It is hoped that the aforementioned aims should provide some information on the driving mechanism responsible for strain/stress relaxation during PWHT.

1.3 Thesis outline

The thesis is presented in ten chapters, the sequence of which highlights the chronology of the knowledge development and research undertaking to meet the defined aims. The first chapter gives an overview of the subject and specifies briefly the gap in knowledge. The principal objective and the aims of the research are also defined in this chapter. Chapter 2 provides a critical review on the measurement techniques of residual stresses, stress relieving techniques and theoretical and numerical models to predict residual stresses. The research gap in each section has been identified.

Chapter 3 presents the experimental procedures employed during the course of this study. It provides information on:

- Welding procedures, processes and parameters;

- The consumables and materials;

- The details of finite element model;

- Neutron diffraction and measurement/calculation of residual stresses;

- Mechanical testing and microstructural characterization used such as hardness test, tensile test and microstructure analysis (optical microscopy, scanning

electron microscopy, electron backscatter diffraction and transmission electron microscopy).

Chapters 4-8 are a collection of five manuscripts that have been published, or currently under review. These publications present the progress made in the course of this study and explain the achievements of this research.

Chapter 4 is the first of the five journal publications. In this chapter the effects of welding parameters (heat input, wall thickness and restraint lengths) on the residual stresses of the WIC weldability test is presented. This chapter also presents the effects of welding parameters on residual stresses for under-matched, matched and over-matched welds using experimentally validated finite element simulations. High level of residual stresses is found in the WIC weldability test which proved that this weldability test is effective in constraining the root run and in consequence enables studying the susceptibility of high-strength pipeline steels to hydrogen assisted cold cracking.

Chapter 5 is the second of the five journal publications. In this chapter the effects of welding speed, pass sequence on residual stresses in multi-pass HSLA steel welds are presented. Residual stress measurements were conducted at ANSTO using KOWARI strain scanning instrument. Substantial reduction in the magnitude of residual stresses is found by reducing the welding speed (higher heat input). The results also indicate that changing the weld deposition direction has no significant effect on the magnitude of the residual stresses.

 Chapter 6 is the third of the five journal publications and aims to identify the effects of welding speed and pass sequence on microstructure, mechanical properties and

residual stresses in multi-pass high strength low alloy steel welds. The welded joints are made by SMAW (Shielded Metal Arc Welding) and combined MSAW (Modified Short Arc Welding) and FCAW (Flux Cored Arc welding) processes. High level of residual stresses is found to be correlated with the existing of microstructural constituents of bainite and Widmanstätten ferrite in the weld metal and HAZ of low heat input specimens. It is also worth mentioning that changing deposition sequence did not have a significant effect on residual stresses and microstructural characteristics of the weldments.

Chapter 7 is the fourth of the five journal publications which presents the effects of welding process on microstructure, mechanical properties and residual stresses in high strength low alloy steel welds. The welded joints are made by SMAW (Shielded Metal Arc Welding) and combined MSAW (Modified Short Arc Welding) and FCAW (Flux Cored Arc welding) processes. Significantly higher level of residual stress was found in the MASW+FCAW combination which is shown to be in line with the microstructural and mechanical properties of these joints.

Chapter 8 is the fifth journal paper and employed in-situ neutron diffraction to measure the relaxation of residual strains during conventional PWHT in multi-pass HSLA weld joints. This chapter also provides the comparative study on the microstructural characterization and mechanical property effects for the as-welded and post-weld heat treated specimens. The findings can be used to characterize comparable material combinations and optimize the PWHT process for HSLA steel welds.

Chapter 9 presents two abstracts of the future publications which the first draft of the papers have been submitted to my principal supervisor A/Prof Reza Ghomashchi.

Finally Chapter 10 lists the conclusions and final remarks from this research along with further development of the present work toward optimising PWHT process for various material combinations.

1.4 Publications and awards arising from this research

The research discussed in this thesis has led to the generation of seven journal, four peer reviewed conference papers and three conferences (non- refereed). The journals in which the papers are published or submitted are amongst the well-respected journals in the field of Materials and Mechanical & Manufacturing Engineering. In addition, this research has won three awards by the Australian Nuclear Science and Technology Organization (ANSTO) to perform experiments at the Kowari strain scanner (total of $75100 AUD).

Journal papers:

- **H. Alipooramirabad**, A. Paradowska, R. Ghomashchi, A. Kotousov, M. Reid. Quantification of residual stresses in multi-pass welds using neutron diffraction. Journal of Materials Processing Technology. 2015; 226:40-9.

- **H. Alipooramirabad**, R. Ghomashchi, A. Paradowska, M. Reid. Residual stress-microstructure-mechanical property interrelationships in multipass HSLA steel welds. Journal of Materials Processing Technology. 2016; 231:456-67.

- **H. Alipooramirabad**, A. Paradowska, R. Ghomashchi, A. Kotousov, N. Hoye. Prediction of welding stresses in WIC test and its application in pipelines. Journal of Materials Science and Technology. 2016; 32: 1462–1470.

- **H. Alipooramirabad**, A. Paradowska, O. Lavigne, R. Ghomashchi, M. Reid. In situ neutron diffraction measurement of strain relaxation in welds during heat treatment. Science and Technology of Joining and Welding. 2016:1-12.

- **H. Alipooramirabad**, R. Ghomashchi, A. Paradowska, M. Reid. Investigating the effects of welding process on residual stresses, microstructure and mechanical properties in HSLA steel welds, Journal of Manufacturing processes (under review).

- **H. Alipooramirabad**, R. Ghomashchi, O Lavigne, A. Paradowska, M. Reid. Post weld heat treatment and its effects on microstructure and mechanical properties of high strength low alloy steel welds (to be submitted).

- **H. Alipooramirabad**, R. Ghomashchi, A. Paradowska, M. Reid. Effect of holding time on strain relaxation in high strength low alloy steel welds: an in-situ neutron diffraction approach (to be submitted).

Conference papers:
- **H. Alipooramirabad**, A. Kotousov, R. Ghomashchi, "Prediction of welding residual stresses in flat plate (X80)", 7th Australian congress on applied mechanics, ACAM, Adelaide, Australia, 2012.

- **H. Alipooramirabad**, A. Kotousov, R. Ghomashchi, "Numerical analysis of welding stresses in WIC weldability test", 8th Australian congress on applied mechanics ACAM, Melbourne, 2014. **Postgraduate best paper award (high commendation)**

- **H. Alipooramirabad,** A. Paradowska, R. Ghomashchi, N. Hoye, M. Reid. Experimental investigation of welding stresses in MWIC weldability test. Materials Research Proceedings, Vol. 2, Vol. 2, pp 557-562, 2017. DOI: http://dx.doi.org /10.21741/9781945291173-94

- **H. Alipooramirabad,** R. Ghomashchi, A. Paradowska, M. Reid. Investigating the effects of mitigation techniques on residual stress and microstructure of HSLA welds. Materials Research Proceedings, Vol. 2, pp 563-568, 2017. DOI: http://dx.doi.org /10.21741/9781945291173-95.

Conference Articles (Non -refereed):

- **H. Alipooramirabad,** R. Ghomashchi, A. Paradowska, M. Reid "development of residual stresses in multi-pass welding of X70 line pipe steel" 6th IIW research and cooperation colloquium, Hyderabad, India, 2016.

- A. Paradowska, M. Reid, **H. Alipooramirabad,** R. Ghomashchi, "Residual stress measurements in welding and manufacturing applications", IIW international conference, Melbourne, Australia, 2016.

- **H. Alipooramirabad,** A. Paradowska, R. Ghomashchi, M. Reid, "Investigation the effects of welding process, heat input and welding sequence on residual stresses in multi-pass welds using neutron diffraction method", AOCNS, Sydney, Australia, 2015.

References

[1] Kurji R, Coniglio N. Towards the establishment of weldability test standards for hydrogen-assisted cold cracking. The International Journal of Advanced Manufacturing Technology. 2015;77:1581-1597.

[2] Ragu Nathan S, Balasubramanian V, Malarvizhi S, Rao AG. Effect of welding processes on mechanical and microstructural characteristics of high strength low alloy naval grade steel joints. Defence Technology. 2015;11:308-317.

[3] Costin WL, Brown IH, Green L, Ghomashchi R. Application of FIB/SEM/EBSD for evaluation of residual strains and their relationship to Weld Metal Hydrogen Assisted Cold Cracking. 9th International Pipeline Conference: American Society of Mechanical Engineers; 2012:343-353.

[4] North T, Rothwell A, Glover A, Pick R. Weldability of High Strength Line Pipe Steels. Welding Journal. 1982;61:243-257.

[5] Yurioka N. Predictive methods for prevention and control of hydrogen assisted cold cracking, IIW Doc. IX-1938-1999;1999.

[6] Suzuki H, Yurioka N, Okumura M. A new cracking parameter for welded steels considering local accumulation of hydrogen. Transactions of the Japan Welding Society. 1982;13:3-12.

[7] Sterjovski Z, Pitrun M, Nolan D, Dunne D, Norrish J. Artificial neural networks for predicting diffusible hydrogen content and cracking susceptibility in rutile flux-cored arc welds. Journal of Materials Processing Technology. 2007;184:420-427.

[8] Glover A, Rothwell B. Specifications and practices for hydrogen crack avoidance in pipeline girth welds. First International Conference on Weld Metal Hydrogen Cracking in Pipeline Girth Welds, Wollongong, Australia1999. p. 8-13.

[9] Yurioka N, Suzuki H. Hydrogen assisted cracking in C-Mn and low alloy steel weldments. International Materials Reviews. 1990;35:217-249.

[10] Graville BA. Interpretive report on weldability tests for hydrogen cracking of higher strength steels and their potential for standardization. Bulletin-Welding Research Council. 1995.

[11] Barsoum Z, Barsoum I. Residual stress effects on fatigue life of welded structures using LEFM. Engineering Failure Analysis. 2009;16:449-467.

[12] Lawrence F, Burk J, Yung J. Influence of residual stress on the predicted fatigue life of weldments. ASTM special technical publication. 1982:33-43.

[13] Teng T-L, Chang P-H, Tseng W-C. Effect of welding sequences on residual stresses. Computers & Structures. 2003;81:273-286.

[14] Wohlfahrt H, Heeschen J. Possibilities for the improvement of the fatigue strength of butt welded joints of high strength structural steels. Mechanical Engineering Publications. 1986:451-458.

[15] Cheng X, Fisher JW, Prask HJ, Gnäupel-Herold T, Yen BT, Roy S. Residual stress modification by post-weld treatment and its beneficial effect on fatigue strength of welded structures. International Journal of Fatigue. 2003;25:1259-1269.

[16] Sattari-Far I, Farahani M. Effect of the weld groove shape and pass number on residual stresses in butt-welded pipes. International Journal of Pressure Vessels and Piping. 2009;86:723-731.

[17] Javadi Y, Akhlaghi M, Najafabadi MA. Using finite element and ultrasonic method to evaluate welding longitudinal residual stress through the thickness in austenitic stainless steel plates. Materials & Design. 2013;45:628-642.

[18] Mahmoodi M, Sedighi M, Tanner DA. Investigation of through thickness residual stress distribution in equal channel angular rolled Al 5083 alloy by layer removal technique and X-ray diffraction. Materials & Design. 2012;40:516-520.

[19] Withers PJ, Bhadeshia HKDH. Residual stress part 1 - Measurement techniques. Materials Science and Technology. 2001;17:355-365.

[20] Pearce SV, Linton VM. Neutron diffraction measurement of residual stress in high strength, highly restrained, thick section steel welds. Physica B: Condensed Matter. 2006;385:590-593.

[21] Paradowska A, Price J, Ibrahim R, Finlayson T, Blevins R, Ripley M. Residual stress measurements by neutron diffraction in multi-bead welding. Physica B: Condensed Matter. 2006;385:890-893.

[22] Paradowska A, Price JW, Ibrahim R, Finlayson T. A neutron diffraction study of residual stress due to welding. Journal of materials processing technology. 2005;164:1099-1105.

[23] Pardowska AM, Price JW, Ibrahim R, Finlayson TR. Neutron diffraction evaluation of residual stress for several welding arrangements and comparison with fitness-for-purpose assessments. Journal of pressure vessel technology. 2008;130:011501.

[24] Pearce SV, Linton VM, Oliver EC. Residual stress in a thick section high strength T-butt weld. Materials Science and Engineering: A. 2008;480:411-418.

[25] Kurji R, Coniglio N, Griggs J, Ghomashchi R. Modified WIC test: an efficient and effective tool for evaluating pipeline girth weldability. Science and Technology of Welding and Joining. 2016:1-13.

[26] Brule A, Kirstein O. Residual stress diffractometer KOWARI at the Australian research reactor OPAL: status of the project. Physica B: Condensed Matter. 2006;385:1040-1042.

[27] McEnerney JW, Dong P. Recommended practices for local heating of welds in Pressure vessels. WRC BULLETIN. 2000.

[28] Dong P, Song S, Zhang J. Analysis of residual stress relief mechanisms in post-weld heat treatment. International Journal of Pressure Vessels and Piping. 2014;122:6-14.

[29] Zhang J, Dong P, Song S. Stress relaxation behavior in PWHT of welded components. ASME 2011 Pressure Vessels and Piping Conference: American Society of Mechanical Engineers; 2011. p. 673-679.

[30] Dong P, Hong JK. Residual stress relief in post-weld heat treatment. ASME 2008 Pressure Vessels and Piping Conference: American Society of Mechanical Engineers; 2008. p. 321-329.

CHAPTER 2

LITERATURE REVIEW

2.1 Background

Welding is a major fabrication route that joins materials through melting the two parts together or by bringing two parts together under pressure, perhaps with the application of heat, to form a metallic bond across the interface. Welding is widely used in the manufacturing of airplanes, heavy machinery, general machinery parts and pipeline construction. Various energy sources can be used for welding such as electric arc, gas flame, electron beam, laser, ultrasound and friction. The most popular welding processes which utilise an electric arc, include Shielded Metal Arc Welding (SMAW), Gas Metal Arc Welding (GMAW), Gas Tungsten Arc Welding (GTAW), Submerged Arc Welding (SAW) and Flux-Cored Arc Welding (FCAW). All these processes use different consumables, methods of deposition and weld shielding techniques. SMAW and FCAW processes are widely used in the fabrication of high strength low alloy steel structures. Welding with SMAW process offers several advantages including lower equipment cost, portability of equipment, welding in various positions and confined spaces. In Australian context, SMAW is used in conjunction with hydrogen rich cellulosic consumables for construction of energy pipeline. The combination of SMAW and cellulosic electrodes renders good weld penetration and faster deposition speeds enabling pipeline constructions at reduced cost. But Cellulosic electrodes generate a substantial amount of dissolved hydrogen in weld metal in comparison with low hydrogen electrodes such as rutile electrodes. The dissolution of hydrogen in weld metal increases the risk of HACC.

Hydrogen assisted cold cracking is a phenomenon that influences the mechanical properties of metals and leads to great expenses with catastrophic failures during

pipeline construction. HACC is unpredictable and it may occur within 24 hours up to one week after the completion of the weld.

As mentioned in the first chapter, three influential factors are contributing to the risk of HACC in pipeline girth welding which are susceptible microstructure, residual stress and hydrogen content. The effects of microstructure and hydrogen content can be found with the great details in the studies conducted by Kurji [1] and Costin [2] at the University of Adelaide (Department of Mechanical Engineering). Furthermore, there are various methods and mechanisms to measure the hydrogen content (i.e. Glycerin Method), specify and control of the microstructure (i.e. steel and consumables chemistry, heat treatment) but the level of the welding stress, which is one of the critical factors affecting the susceptibility of weld metal to HACC, remains largely unspecified. Therefore one of the aims of the present study is to evaluate the welding stresses in the root pass of the girth welding using the WIC test.

Welding processes generate thermal stresses resulted from shrinkage and expansion of weldments during welding and residual stresses when the weld joint cools to room temperature. Such stresses, have significant effects on the structural integrity of the components. The need for the measurement, prediction and control of welding residual stresses is increasing in pressure vessel and structural applications due to recent mandatory requirements for structural integrity assessment of welded structures. The generated stresses affect the performance of welded structures in service as for instance for pipeline welding, the magnitude of stresses affect the critical concentration of residual hydrogen to induce hydrogen embrittlement in the weld joint. Therefore, there is a need for more reliable information on the magnitude and state of residual stresses in the weldment.

The literature review will first discuss the generation of residual stresses in detail, then focuses on several research topics, which are important for the current study. This includes the effects of residual stresses on structural integrity, evaluation of major factors influencing the welding residual stresses, experimental measurement techniques of residual stresses and the development of numerical modelling approaches for evaluation of residual stresses. The gap statement which was briefly described in chapter one, will be further elaborated in this section of the thesis.

2.2 Residual stress

Residual stresses are self-balancing stresses that remain in the material, after manufacturing and processing operations, in the absence of external loading [3]. They can be generated from various sources such as mechanical loading, fabrication and most relevant to the present study by welding. In welded structures, residual stresses are produced by plastic shrinkage that is induced as a result of differential contractions in the welding portion during thermal processes. The typical longitudinal and transverse residual stress profiles for a single pass butt weld are shown in Figure.2.1 [4].
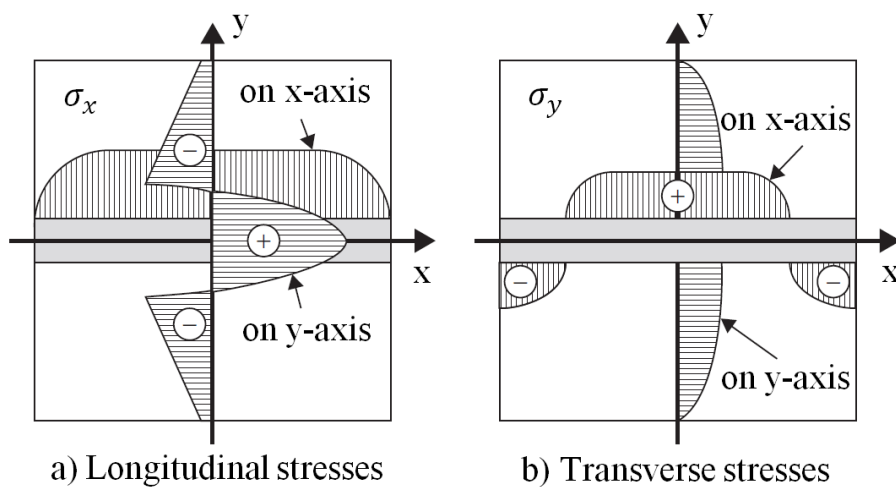
Figure 2.1: Residual stress profiles in a single pass butt weld, (a) longitudinal residual stress and (b) transverse residual stress [4].

It is worth mentioning that residual stresses are three-dimensional and can occur in a component on both macroscopic and microscopic levels [5]. Three kinds of residual stresses are categorized according to their scale, as illustrated in Figure. 2.2 [6]:

- Residual stresses of the first order, or type I residual stresses. These stresses equilibrate over a length scale comparable to the extent of the component in that direction. These stresses are also called macrostresses and the internal forces related to this stress are balanced on all planes.

- Residual stresses of the second kind, or type II residual stresses which act over one particular grain. The internal forces related to these stresses are in balance between the different grains or phases.

- Residual stresses of the third kind or type III residual stresses arising from heterogeneous behaviour at the atomic scale. These stresses act across sub-microscopic areas (over a few interatomic distances). The internal forces coupled with these stresses are in balance in very small domains such as dislocations or point defects.
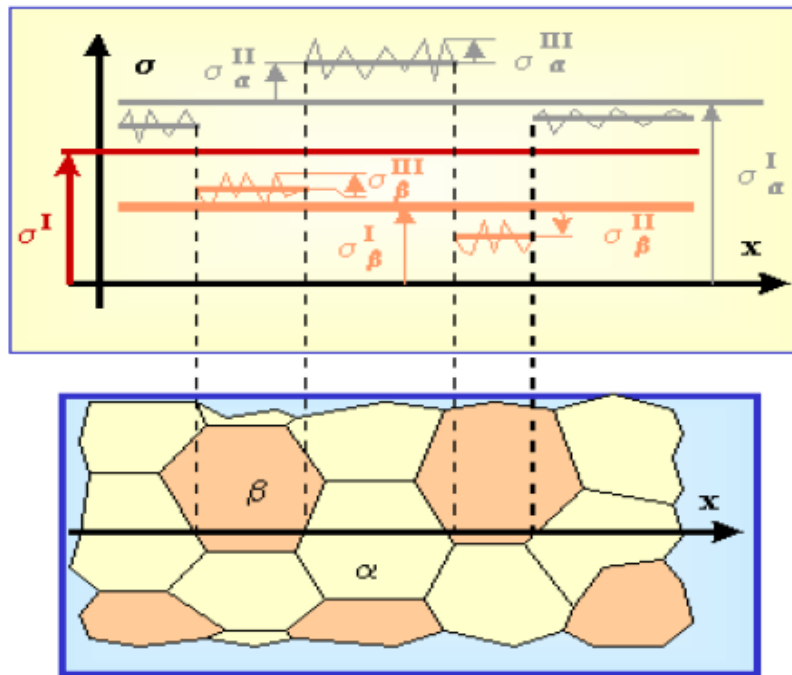
Figure 2.2: Three orders of residual stresses according to their length scale [6].

During welding, localized high temperature region near heat source is resulting in local thermal expansion. The thermal expansion of the high-temperature region is under the restraint of the surrounding area and so the weld material is subject to tensile stress which is balanced by the compressive stress in the parent metal. These stresses may induce distortion and dimensional changes in the welding [7]. The basic deformation patterns in a butt joint weld is shown in Figure.2.3 [4].

a) Transverse shrinkage   b) Longitudinal shrinkage

c) Angular distortion   d) Rotative distortion
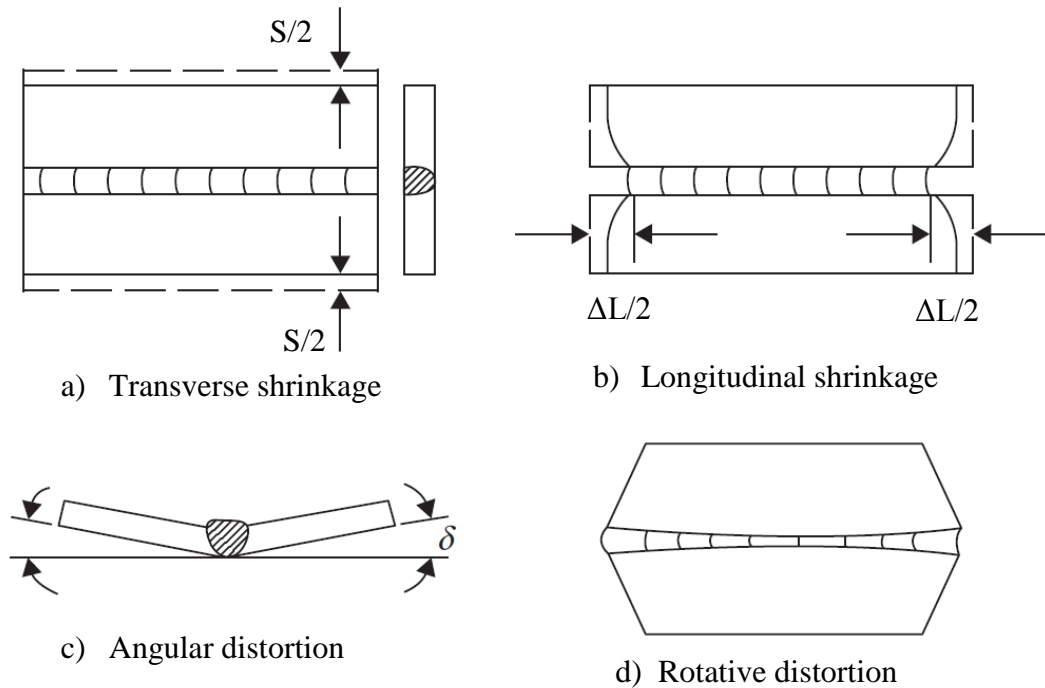
Figure 2.3: Fundamental dimensional changes that occur in welds [4]

A large amount of work has been conducted in the field of residual stresses to identify the causes as well as the remedial work to mitigate the detrimental effects of residual stresses during service for different welding configurations. The review conducted by Lindgren [8] described different numerical modelling aspects to predict the thermal, microstructural and mechanical effects of welding. Based on the review, it was found that the modelling for standard analysis is well developed but further work is required to improve the modelling of material behaviour and its coupling to the microstructural evaluation. In another review conducted by Rossini, et al. [9], different experimental techniques to measure the residual stresses was investigated. They classified residual stress measurement techniques in three distinct categories including destructive, semi destructive and non-destructive and summarized their physical limitations, advantages and disadvantages. According to different investigators the most influential factors

which contribute on the magnitude of residual stresses in the welded structures are [10-12]:

- the temperature of the weld area (heat input);

- yield strength of the material;

- type of welding;

- number of weld runs;

- degree of constraint;

- geometry of parts to be welded;

- pass sequence;

- Phase transformations that occur in the cycle from molten to solid states including solid state transformations.

The magnitude and distribution of residual stresses are influenced by preheat, heat input, shrinkage, and phase transformation as reported by Hot and Seam [13]. The detailed FE studies conducted by Mochizuki [14] and Mochizuki, et al. [15] suggested possible ways to reduce the residual stresses. For example, the transverse stresses in the vicinity of the weld toe of a fillet weld joint can be altered and reduced by changing the welding sequence and locations of weld runs.

However, when the effects of individual parameters are analysed, some contradicting reports are found which generate uncertainty in their applications in real life cases. The work conducted by Peel, et al. [16] reported that an increase in heat input (reduction in travel speed) reduces the magnitude of the residual stresses. While Numerical simulations reported by Qureshi [17] on the effect of weld travel speed on residual stresses in a thick-walled cylinder confirmed higher levels of residual stresses at higher

heat input (lower travel speed). Also there is not much information on the effects of alternating welding sequence on residual stresses. Therefore, one of the aims of the current work is to investigate the effects of welding speed and the pass sequence on the residual stresses in multi-pass welding of high strength low alloy steel.

2.2.1 Effect of residual stresses on structural integrity

Residual stresses can have significant influence on the performance of engineering components. The effect of residual stresses on the performance of welded structures may either be beneficial or detrimental, depending on the magnitude, sign and distribution of the stresses with respect to the load-induced stresses [3, 5]. Tensile residual stresses have detrimental effects on the welded structures and are often in the magnitude of yield strength of the material [18]. As reported by Barsoum and Barsoum [18] tensile residual stresses reduce fatigue life by increasing fatigue crack growth rate while compressive mode of residual stresses decrease fatigue crack growth rate. In another study, the effects of residual stresses on fatigue crack growth in butt welds of a pipeline steel was investigated by Shi, et al. [19]. It was found crack closure is highly dependent on both the transverse and longitudinal residual stresses of welding, and is generally weakened with increasing fatigue crack length due to partial relief of welding residual stresses. There is similar trend for stress corrosion cracking (SCC), as reported by Mochizuki [14], confirming higher susceptibility of welded joints to SCC with increasing tensile residual stresses. In addition, in power plant piping the major area of component cracking is at the welded joints. It is believed that stress corrosion cracking is one of the main causes of failure at these welded joints [20, 21]. The occurrence of this phenomenon is highly dependent on the presence of surface tensile residual stresses of welding which are directly exposed to coolant or affected by

26

condensation [21]. Therefore reliable and accurate prediction and measurement of residual stresses are essential for structural integrity assessment of components in service.

2.2.2 Effects of welding parameters on residual stress in multi-pass welds

As mentioned before, welding parameters play a critical role on the generation of residual stresses and therefore an understanding of the role played by these parameters should enable the welding engineers to appropriately select the parameters to render a more durable welded structure in service. In the following, a brief discussion is presented to highlight the importance of welding parameters on the integrity of welded structures by analysing their effect on the generated residual stresses.

2.2.2.1 Heat input

Heat input is a combination of arc voltage, welding current and travel speed. If not selected properly, the applied heat input leads to generating lower quality welds with poor mechanical properties. This is happening mainly due to segregation in the fusion zone and grain coarsening in the HAZ [12]. However, higher heat input can have a tempering effect on the material through decreasing the cooling rate, thereby producing welds with tougher grain structure [12]. According to Smith, et al. [22] the effects of heat input on mechanical properties of the joint tend to be more significant at the HAZ rather than the weld metal. Welding procedures with higher heat inputs resulted in lower toughness of the HAZ. This can be explained through the presence of microstructure constituent of upper bainite in high heat input welds. Moreover, when the effects of individual heat input parameters are examined, there are some opposing reports which generate uncertainty in their applications in real life cases. Qureshi [17] used experimentally validated FEA to investigate the effect of weld travel

speed ($2\ mms^{-1}$, $3\ mms^{-1}$ and $4\ mms^{-1}$) on residual stresses in a thick-walled cylinder. It was found for the lowest welding speed ($2\ mms^{-1}$) residual stresses were at their highest magnitude for both internal surfaces (tensile stresses) and external surfaces (compressive stresses) of the cylinder. While the study conducted by Peel, et al. [16] which made measurements of residual stresses in 3 mm thick aluminium plates of AA5083 using friction stir welds, showed an increase in heat input due to reduction in travel speed, decreases the magnitude of residual stresses. In addition to travel speed, there are also some contradicting reports on the effect heat input on the residual stresses when considering the applied welding current. The study conducted by Ranjbarnodeh, et al. [23] confirmed that increasing heat input due to increased current (constant travel speed) decreases the magnitude of longitudinal residual stresses. In contradiction with Ranjbarnodeh, et al. [23], Akbari and Sattari-Far [24] used a combination of experimental and numerical methods, demonstrated decreasing heat input due to reduction in current and voltage is beneficial in reducing residual stresses in weldment. Despite the past studies, the effect of welding speeds on the weld properties, particularly for multi-pass welds, remains an area of uncertainty. Therefore, one of the aims of the current work is to investigate the effects of welding speed and the resultant heat input on the residual stresses in multi-pass HSLA welds.

2.2.2.2 Restraint

The structure and the structural boundary conditions (welding fixtures) in which the welding operation is performed have a significant effect on the generation of residual stresses [17]. The restraint in a weld joint can be either external (e.g. jigs, clamps, etc.) or self-induced by structure's own shape. According to Leggatt [11] restraints during welding have significant effect on the distribution and magnitude of welding

distortions in structures. The magnitude of tensile residual stresses was increased with the increase of restraint. It was also reported that high membrane restraint lead to changing of the compressive stresses into tensile stresses at the mid-thickness of the plate [11]. Heinze, et al. [25] resolved that the degrees of restraint experienced by the welded joints due to welding fixtures have a significant influence on the generation of residual stresses. The findings show an increase of 400 MPa for transverse residual stresses due to the transverse shrinkage restraint. In another study, Pardowska, et al. [26] applied neutron diffraction method to investigate the effects of restraints, weld start and end effects and bead deposition sequence on the residual stresses. It was found that more severe restraint conditions increase the magnitude of both longitudinal and transverse residual stresses. The finding showed that bead deposition sequence has significant effect on the final residual stress distribution at the weldments, in particular the appropriate manipulation of the deposition sequence around the weld toes can significantly reduce the residual stresses in that region. Also the highest level of transverse residual stresses was observed for the end of weld in both weld metal and HAZ, which is the last point of solidification.

2.2.2.3 Welding process

Colegrove, et al. [27] investigated the effects of welding process on residual stress and distortion on butt welds in 4 mm thick DH36 shipbuilding steel plate (0.18% C and 0.9-1.6 Mn). They considered six different processes in their investigation including: direct current gas metal arc welding (DCGMAW), submerged arc welding (SAW), autogeneous laser, Fronius cold metal transfer (CMT) and hybrid laser welding. Different residual stress profiles were obtained for different welding processes and the best results come from hybrid laser and pulsed GMAW processes. Also, the effects of

welding process on residual stress distribution and distortion in type 316LN stainless steel weld joints made by A-TIG and TIG welding processes was investigated by Vasantharaja, et al. [28]. Different levels of residual stresses and distortions with varying microstructure were found as a result of using different welding processes and joint geometry configurations. The lowest level of tensile residual stresses was found to be at the weld fabricated with double side A-TIG process. This was due to the intense heat, lower weld metal volume and straight sided joint configuration in the joints fabricated with double side A-TIG process. The effect of welding process (two different welding processes used namely as SMAW and FCAW) on toe-cracking behaviour of fillet-welds on a pressure vessel grade steel was investigated by Balasubramanian and Guha [29]. It was found that the welding process has a significant effect on the toe cracking behaviour and fatigue life of the cruciform joints. It was also found crack initiation is delayed in SMAW joints and as a result crack initiation life is longer as compared to FCAW joints. The delayed initiation of fatigue cracks in SMAW process was explained through better notch impact toughness of this process due to existing of low carbon martensitic microstructure in the toe region of SMAW joints. Lower fatigue crack growth rates were observed in the joints fabricated by SMAW process than the joints fabricated by FCAW process. The superior fatigue performance of SMAW joints was due to the existing microstructure constituent of low carbon martensitic structure in the heat affected zone (HAZ) of these joints, compared to the bainitic HAZ microstructure of FCAW joints. This variation in the microstructure of HAZ was due to the higher heat input involved in fabrication of joints with FCAW process.

2.2.2.4 Welding sequence

Gannon, et al. [30] used finite element modelling to investigate the effects of welding sequence on flat-bar stiffeners in ship hull construction. They reported that welding sequence did not have a significant influence on the distribution of residual stresses. But, peak values of longitudinal residual stresses were changed as a result of changing welding sequence. Ji, et al. [31] developed Finite Element models to investigate the effects of welding sequence on the welding stresses of a thick plate. It was found the peak values of transverse and longitudinal residual stresses decrease by 18.2% and 16.9% respectively in welding in inverse direction in comparison with welding in same direction. Teng, et al. [32] investigated the effects of weld sequence for three different welding sequence including symmetric, progressive and back step welding for single and multi-pass welds (as shown in Figure 2.4). For single pass weld, it was found that the longitudinal residual stresses of symmetric welding are smaller than those of the other welding sequences. This reduction in the longitudinal residual stresses was attributed to the reduction of restrained force of the weldment in the symmetric welding sequence. While in multi-pass welds, the magnitude of transverse residual stresses with symmetric welding sequence was lower than the other sequences. The lower magnitude of transverse residual stresses was found to be related with pre-heating and post heating effects of symmetric welding and reduced residual shrinkage of the plate in these joints.
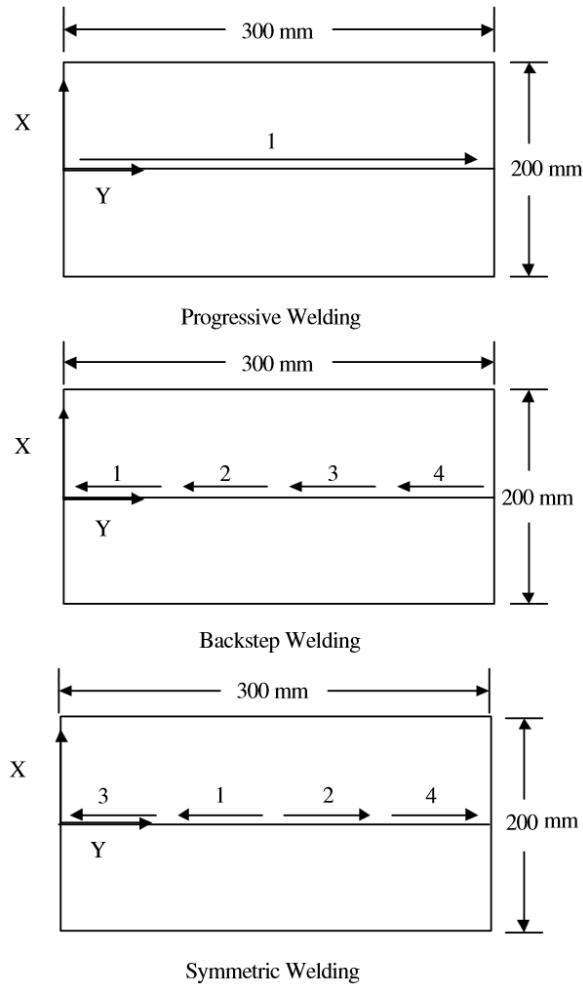
Figure 2.4: Different welding sequences applied for thin wall butt welds [32]

In another study, Kohandehghan and Serajzadeh [33] investigated the effects of weld sequence and weld restraint on residual stresses for Gas Tungsten Arc Welding (GTAW) of aluminium plates. They found that both weld sequence and restraint have a significant effect on both, the transverse and longitudinal residual stresses. An increase of 76% in transverse residual stresses was found as a result of using fixtures. It was also found that using fixtures can affect the geometry of weld pool; where 21% decrease in the weld pool depth was reported due to restraint effects. Additionally, an appropriate selection of the welding sequences can reduce the maximum values of longitudinal residual stresses by 44%. Sattari-Far and Javadi [34] investigated the

effect of welding sequence on welding deformations of pipes (stainless-steel) through a parametric study. The authors utilized a sequentially coupled 3D Finite Element models to study nine different welding sequences and their impact on resultant distortions. It was found that a continuous segment results in higher welding distortions than an alternating joining segments sequence of the weld bead, which ensures the weld metal is deposited evenly across the circumference of a pipe in a progressive fashion.

2.2.2.5 Pre-heat and inter pass temperature

The temperatures of weldments before and during welding have an influence on the residual stress distribution of weldments. The inter-pass temperature is the temperature of the work piece just prior to the depositing additional welds pass for multi-pass welds. The pre-heat temperature is the specific temperature which the work piece is heated before welding commences. According to Keehan [35] preheat and inter-pass temperature have significant impact on the cooling rate, shrinkage stresses and the final microstructure. A preheat temperature is sometimes required to avoid hydrogen cracking, while specific maximum inter-pass temperature in welding procedure is sometimes required to avoid hot cracking. Ramjaun, et al. [36] applied the neutron diffraction method to study the effects of inter-pass temperature on residual stresses in multi-pass welds. The study found if the inter-pass temperature is maintained above the transformation temperature, which means the entire multi-pass weld remains austenitic, there will be a significant reduction of the residual stresses.

2.2.3 Stress relieving

Stress relieving techniques are used to relieve the undesirable residual stresses that remain locked in a structure as a consequence of a manufacturing sequence. Stress

relieving can be either accomplished through heat treatments or mechanical methods. In the following sections these techniques are described.

2.2.3.1 Post weld heat treatment

Post weld heat treatment (PWHT) is a stress reliving process where the uniform heating is applied to the structure at the annealing temperature, holding at this temperature for a specified period of time until the desired stress relief is attained. The temperature and holding time for PWHT depend on the thickness and the type of material [37].

The removal of residual stress is not the only effect of PWHT. It usually conducted with the aim of achieving the following issues:

- To increase the diffusion of hydrogen out of the weld metal;

- To decrease the heat affected zone hardness, noticeably improving the toughness;

- To improve the dimensional stability during machining;

- To improve in ductility due to recovery that takes place;

- To increase the resistance to stress corrosion cracking;

Once PWHT is applied it is crucial to examine the microstructure, tensile and impact strength of the material to confirm the effectiveness of stress relieving treatment. This is because inappropriate stress relief heat treatment will lead to increasing residual stresses, distortion and degradation of the microstructure precipitation of carbides and embrittlement [38].

So far several experimental and numerical investigations have been done on the comparison of residual stress levels before and after PWHT. Paddea, et al. [39] used neutron diffraction method to measure the residual stress distributions in a P91 steel-

pipe girth welded before and after PWHT. The boundary between the HAZ and the adjacent parent material, close to inner surface of the pipe, was found to have the highest level of tensile residual stresses with the magnitude of 600MPa. Similarly, the peak of tensile residual stresses after PWHT was remained in the vicinity of the HAZ which was 120 MPa. Smith and Garwood [40] investigated the effects of PWHT on the magnitude and distribution of residual stresses in a submerged-arc weld in a 50 mm thick ferritic steel using drill holing technique. A significant reduction in the surface residual stress levels was observed as a result of PWHT (the peak of residual stresses was 740 MPa for as welded condition which reduced to 140 MPa).

Cho, et al. [41] developed a 2D thermal elastic-plastic finite element model to evaluate the residual stresses for welded and after PWHT. It was found that maximum residual stress for K- and V-type weld joints of thick plates were 316 and 256 MPa, respectively, which were reduced to 39.3 and 3.7 MPa. Aba-Perea, et al. [42] performed in-situ residual stress analysis using neutron diffraction during annealing treatments in Ni-base superalloy Inconel 718. Residual stress measurements were also conducted before and after annealing treatments and were found to be 700 MPa and 420 MPa, respectively. It was found the stress relaxation is mainly due to the reduction of the yield strength with increasing temperature, while creep play a minor role in the stress relaxation during the isothermal treatment.

Chen, et al. [43] used in-situ neutron diffraction during PWHT to measure the residual stress relaxation on two circumferentially butt-welded steel pipes. It was found stress was relaxed instantaneously, when the temperature reached to 650ºC. This might be due to the reduction in the yield stress of the material with temperature. However, as stated by the authors, during the experiments two practical problems occurred. The

major problem was cutting the electrical supply during heating stage which leads to temperature drops for a period of 90 minutes. Also neutron beam flux was varied and sometimes could drop to a level where measurements were not able to be made.

In spite of the studies carried out in the past, there exist a series of questions for the mechanics of residual stress relief during PWHT which have practical implications. The rate of stress relaxation during holding time, the starting temperature for relaxation of residual strain/stresses and the relationship between the temperature increase during PWHT with relaxation of residual strains/stresses have not been fully answered yet. Moreover, to the best of our knowledge, there is not any report on the strain/stress relaxations during PWHT for high strength low alloy steel welds.

Therefore one of the main aims of this research study is the evaluation of residual strains during the PWHT process. This will help to optimise the current PWHT codes and standards, which can result in significant economic benefits.

2.2.3.2 Mechanical methods

The relaxation of residual stresses can be done through mechanical methods. In mechanical treatments an external load is applied on the welded structure where a residual stress exists. As a consequence of the effects of external load, localized yielding with the combination of applied and residual stresses will be resulted. Once the external enforcing load is removed the residual stresses can be reduced [44]. There are three commonly used techniques: overloading, vibration and peening techniques. We will briefly discuss laser peening and vibration techniques in the following sections.

Laser peening

Laser peening is a surface engineering process that is used to minimize the potential for stress corrosion cracking, fatigue and other failure modes [44]. There are several surface processes to impart the beneficial residual stress (compressive residual stress) namely as shot pinning, micro-shot pinning, ultrasonic peening and laser peening. Among these peening techniques, laser peening is a competitive treatment technique with deeper, higher compressive residual stresses as well as lower surface roughness [45, 46]. Compressive stresses induced by laser peening can have significant impact on the life span of the components due to the fact that failures are mostly initiated at the surface of the components [47].

Vibration techniques

Vibration stress relief refer to the reduction of residual stress through cyclic loading treatments. The vibration is created by an eccentric mass electric motor which is attached to the component [48]. The basic theory is that the cyclic vibratory stresses added to the residual stresses exceed the yield strength of the material which leads to local plastic deformation and substantial reduction of residual stresses. The high degree of residual stress relaxation can be achieved in different mechanical structures through running these motors close to a resonant frequency of the combined assembly. This technique has some advantages over conventional heat treatment including lower energy and equipment costs, higher efficiency for the large and complex structures. But there are some disadvantages such as the softening of HAZ and other desirable metallurgical changes (i.e. tempering of the weld metal and HAZ) which do not take place with this technique [49].

2.2.4 Numerical Residual stress models

2.2.4.1 Heat source models

Selection of the most appropriate model for the heat source of the welding process becomes the crucial step in the simulation. Different types of heat source models have been developed by researchers, depending upon the scope of their works. Goldak and Akhlaghi [50] give a comprehensive account of various generations of heat source models used by many researchers over the years.

The temperature field caused by the weld heat source is the main driving force of the weld. Temperature histories particularly soaking time at high temperatures determine the microstructure and chemical composition of the weld. Also cooling time (t_{100}) is a major factor in hydrogen diffusion and cold cracking of the welds. Due to the fact that residual stresses, plastic strains, distortions and microstructural changes in the WM and HAZ are directly related to the temperature history, therefore it is necessary to model the transient thermal analysis accurately [50].

The calculation of the temperature history during welding operation can be done through considering the process to be transient thermal analysis with a moving heat source. Due to complexity of heat transfer in welding operations, numerical thermal models have been developed to reduce the complexity to the manageable levels. The mass transfer and fluid flow (convective heat transfer in the weld pool) were not considered and in order to consider these effects an artificial higher rate of heat conductivity at melting point was considered [51-53]. Also the conduction was considered to be the only way of heat transfer through the material. Although these models ignoring most of the physics of the welding process but except for the interior part of the weld they can give remarkably accurate results [50].

Heat distribution models

Knowledge about welding heat sources mainly come from experimental observations or detailed models of the welding process and the mathematical models. Different types of equipment including video cameras, infra-red cameras and thermocouples can be used to measure the weld pool temperature and its surroundings, i.e. HAZ [50]. In order to mathematically model the welding arc, different geometries from point sources to complicated shape functions based on the type of application have been developed.

Rosenthal [54] and Rykalin [55] developed the first models for the point, line and plane heat source models. However these models have some shortcomings which were explained earlier throughout the literature [56]. Later on, Pavelic, et al. [57] developed a circular disc heat source model based on the Gaussian distribution heat flux model. This model gives quite accurate results in the cases where the depth of penetration is small. This model was widely used by many researchers because of simplicity and accuracy of such assumptions [23, 58, 59].

Eagar and Tsai [60] modified the Rosenthal's model by using Gaussian distributed heat source. They used similar simplifying assumptions on their model such as using constant temperature material properties, disregarding convective heat flow and a quasi-steady state semi-infinite medium. Goldak, et al. [61] developed a mathematical model, based on Gaussian distribution of power density to calculate the thermal history of the welds. A double-ellipsoid heat flux, which could be able to measure the thermal history of deep penetration and shallow welds, is used. The governing Equation of power density distribution for this model can be expressed as:

$$q(x,y,z,t) = \frac{6\sqrt{3}\,\eta VI}{abc\pi\sqrt{\pi}}\, e^{\frac{-3x^2}{a^2}}\, e^{\frac{-3y^2}{b^2}}\, e^{\frac{-3z^2}{c^2}} \tag{2.1}$$

Where v is the welding speed; ηVI is the total heat input (η the heat source efficiency V the welding voltage and I the welding current); and a, b, c are Goldak' s double ellipsoidal heat source geometric parameters. Sabapathy, et al. [62] modified Goldak's double ellipsoidal model [61] and introduced an analytical model with a differential distribution at the front and back portion of the arc. This model can be used for modelling of different welding applications.

Numerical modelling of heat transfer during welding

Due to complexity in the governing equations of heat transfer, nonlinearity associated with the material properties and latent heat effects in welding applications, numerical modellings have been developed to overcome these challenges. Finite element and finite difference methods are widely used to solve the thermal analysis of welds [50]. The temperature field can be obtained by imposing the temperature in the weld as the thermal load in the finite element simulation. The weld metal is held for the certain lapse of time and the prescribed temperature is solved by heat conduction equation. Carmet, et al. [63]; Goldak, et al. [64] and Camilleri, et al. [65] used specified temperatures in their simulations. Lindgren, et al. [66] used the prescribed temperature for multi-pass butt welding of a thick steel plate. The temperature for each weld pass is specified during the heat input phase. Andersson [67] used constant heat flux as the thermal loading with the ramping function to calculate the transient stress fields in a submerged arc welding.

The accuracy of thermal analysis, to a large extent, depends on the type of heat source used. Many researchers have used distributed heat sources in their welding numerical simulations. As for example double ellipsoid heat source model was used by [68-73] while Kermanpur, et al. [58]; Lee and Chang [74] and Ranjbarnodeh, et al. [23] applied Gaussian distribution in their numerical simulations.

One of the objectives of this research study will be developing a numerical model to calculate the transient temperature history of welding. A moving heat source will be considered for the modelling of the welding arc, based on the Gaussian distribution of surface heat flux model. The results of numerical analysis will be validated with the published literature results.

2.2.4.2 Mechanical analysis

2D thermo-mechanical models

Solving the nonlinear thermal-structural problems for a welding application requires extensive computational power. In order to reduce the computational costs of the simulations, two dimensional models were extensively used to predict the residual stresses of welding [52, 70, 75, 76]. These models assumed that the entire girth is welded simultaneously. These 2D models considered the residual stress fields on the plane perpendicular to the welding direction. The out of plane behaviour of these models were assumed to be plane stress (zero out of plane stress), plane strain (zero out of plane strain), generalized plane strain (constant strain normal to the model plane) or axi-symmetric condition.

According to Lindgren [77], the first 2D finite element models to calculate the welding residual stresses were developed by Iwaki and Masubuchi [78], Ueda and Yamakawa

[79] and Fujita, et al. [80]. Prasad and Sankaranarayanan [81] used plain stress models to simulate the welding residual stresses in a thin plate. Sarkani, et al. [52] investigated the possibility of replacing 3D finite element analysis by 2D analysis in single and multi-pass welded T-joint. Quite similar results for temperature histories (within the central zone of weld joint) for 2D and 3D finite element analysis were found. Also for residual stresses, the generalized plane strain model gave quite similar results for both 2D and 3D finite element model. But the maximum discrepancy was found in plane stress states, which were mainly due to the mechanical boundary conditions of the 2D and 3D models.

Camilleri, et al. [65] and Camilleri and Gray [82] developed simplified 2D finite element models to predict the out-of-plane distortion caused by fusion butt welding. Their simplified approach dealt with using temperature for the thermal analysis and replacing thermo-elastic-plastic model with a simple analytical algorithm. Their results showed a reasonable accuracy with the experimental data. Deng and Murakawa [70] and Deng, et al. [53] developed finite element models (2D axi-symmetric) to predict the welding residual stresses in multi-pass stainless steel pipe. The FE results were compared with the experimental measurements and a reasonable accuracy was achieved. According to their investigation the yield strength of weld metal has a significant effect on the final residual stresses in the weld zone.

There are some limitations associated with 2D models to calculate welding residual stresses which are including inability to compute longitudinal residual stresses and their effect on the corresponding normal and transverse components in real life applications (assuming plane stress and strain conditions), and not being able to simulate weld start-end effects. In spite of these limitations, the 2D models provides

faster computational times (compare with the 3D models) with the reasonable accuracy for both circumferential and butt-joint welds [83, 84].

3D thermo-mechanical models

In recent years through developments in computational power, efforts toward comprehensive 2D and 3D thermo-elastic-plastic analysis have been further facilitated. In one of the earliest attempts, Karlsson [85] developed a 3D FE model in single pass girth butt welding of a carbon manganese steel pipe. The FE model was used to investigate the effects of welding parameters, geometries and material properties on radial and hoop residual stresses. Based on the results, material properties and in particular thermal strain behaviour have a significant effect on the residual stress characteristics. It was also found that pipe geometry (pipe diameter) did not have any significant effect on hoop and axial residual stresses. Later on, Zhu and Chao [86] developed a 3D thermo-elasto-plastic finite element model to predict the transient temperature and residual stresses of 304L stainless steel during friction stir welding. The effects of fixture release after welding on the residual stresses is considered. They found that fixture release has a significant effect on the residual stress developments and it should be considered in the numerical simulations of friction stir welding. Deng and Murakawa [76] employed a combination of 3D finite element model (using large and small deformation theory) and experimental validation to predict welding distortion and residual stresses in low carbon steel in thin plate butt-welded joint. Comparing the results of large and small deformation theory with the experiments indicated that the results of large deformation finite element model is in a good agreement with the measurements, especially for mid-thickness deformations. Lee, et al. [87] developed a three dimensional thermo-elasto-plastic finite element model to

investigate the residual stress distributions of high strength steel plates. Highest level of transverse residual stress was found near the weld toe on the joint middle section, which could be significantly reduced by using proper PWHT (40% reduction in the magnitude of transverse residual stress). They also found changing the welding direction between successive weld passes could significantly reduce the maximum residual stress near the weld toe.

The effects of solid state phase transformation on the residual stress distributions were considered in the welding simulations. It was found the volumetric strains during solid-state phase transformations (austenite to martensite) have a significant effect on the welding residual stresses [69, 83, 88].

Deng [89] used finite element method (ABAQUS) to investigate the effects of solid-state phase transformation on welding residual stress in low and medium carbon steels. Based on the results of simulations, it was concluded that phase transformation does not have a significant influence on the final residual stress and the welding distortion in low carbon steel; while in medium carbon steel phase transformation has a significant effect on the welding residual stress and the distortion because of relatively large dilation and a low transformation temperature. Heinze, et al. [90] investigated residual stress development in a six bead multi pass gas metal arc welding of a structural steel, both numerically and experimentally. They developed 2D and 3D finite element models to conduct the numerical investigations. They considered the effects of phase transformations, volume change due to phase transformation, thermal-tempering, transformation plasticity and strain hardening effects in their numerical simulations. It was found that preheat temperature has a small effect on residual stress while inter-pass temperature is quite significant parameter in the residual stress

development of multi-pass weld. The findings also indicated the significant effects of tempering in reduction of longitudinal and transverse residual stresses with a reduction of 131 and 53 MPa, respectively.

2.2.5 Measurement of residual stress

Numerical simulations provide a useful insight of the generation of residual stresses in weldments; however, all theoretical approaches are very prone to various errors and uncertainties in mechanical behaviour at elevated temperatures. Therefore, various experimental techniques were developed for the measurement of residual stresses including ultrasonic [91], hole drilling [92], layer removal techniques [93], exhaustively discussed in the literature including their many limitations, and X-ray and neutron diffractions [3, 9].

There are a wide range of techniques available to measure residual stresses in welded structures. However, they may be divided into two main groups depending on the preservation or destruction of the test piece. In the following, brief accounts of two methods of destructive and non-destructive of measuring residual stresses are given.

2.2.5.1 Destructive methods

The destructive techniques are called stress relaxing methods, which measure the deformation and analyse the stress-relaxation generated in the metal upon the removal of the material. Several destructive techniques have been developed including sectioning [94], slitting and layer removal [95] while others such as the contour method [96] and the deep hole method [97] are novel techniques receiving attention in fewer laboratories. It is also worth mentioning that while sectioning provides single stress measurements, the contour method provides area maps and deep hole drilling and slitting provide depth profiles of residual stress.

Sectioning

Sectioning technique is a destructive method which is based on the measurement of deformation due to relaxation of residual stress by removal of material from the specimen. This method has been widely used to measure the residual stresses in various applications including aluminium, structural steel and stainless steel sections [9, 98, 99].

Counter method

Counter method is a fully destructive technique providing residual stress measurement capability, developed by Prime [100]. It requires only one straight cut through a sample on the plane of interest, followed by measurement of the resulting deformation due to redistribution of the residual stress field [3]. The theory is based on the variation of Bueckner's superposition principle [101]. A specimen is parted in two using wire electric discharge machining (WEDM) causing the residual stresses to relax. Finite element modelling is then used to compute the residual stress form the measured displacement data. It is worth noting that this method provide area maps of residual

stress [102]. This technique can be applied in various applications and to complex geometries. A reasonably good correlation was found for the results of counter method with the results of other measurement techniques such as neutron diffraction and numerical modelling [102].

Hole drilling techniques

Hole-drilling method is an established technique for measuring residual stresses [103]. This method is suitable for applications of strain gauges. The machining operation usually involves drilling a blind hole (usually 1.6 mm or 3.2 mm in diameter) and measuring the strain using strain gauges. The stresses are calculated based on the measured released strain by strain gauges [104]. The ideal application of the hole-drilling method is one in which the uniform stress exist with depth and it has been determined that this method leads to significant errors, particularly where large stress gradients exist through the hole depth [105]. In order to alleviate the shortcomings of this method, deep hole drilling (DHD) technique have been developed which can measure the linear and non-linear stress distributions [106]. In this case, an incremental method is used in which the relieved strains are measured during a series of small, hole-depth increments.

Deep hole method

The deep hole is a semi destructive mechanical method employed to measure through-thickness residual stress distributions in components up to 100 mm thick. In the deep-hole method, a reference hole is first gun drilled through the thickness of the component. The reference hole is then polished to remove any abrupt changes of the diameter. The diameter of the hole is measured accurately and then a core of material around the hole is trepanned out using a plunge electric discharge machine, relaxing

the residual stresses in the core. The diameter of the hole is re-measured and the changes in the diameter of the reference hole is used to calculate the through-thickness distribution of residual stresses [9, 97].

It is worth mentioning that mechanical methods are limited by assumptions concerning the nature of the residual stress field and geometry and they cannot be checked by repeated measurements.

2.2.5.2 Non-destructive diffraction technique

The non-destructive methods are based on the application of high energy photons or particles beam and their interaction with materials' crystal lattice, i.e. elastic scattering, generally known as diffraction techniques. Diffraction methods are based on determining the elastic deformation which will cause changes in the crystallographic inter-planar spacing, d, from their stress free value, d_0. Then, the strain could be calculated by using Bragg's law and of course it is necessary to have an accurate measure of stress-free inter-planar spacing. The most common diffraction methods are as follows.

X-rays diffraction

X-ray diffraction strain measurement, which does not require stress relaxation, offers a non-destructive alternative to the foregoing methods, but has its own limitations. Due to the low energy of the X-rays, the method is primary applied to surface measurements (the practical depth limit is about 1 mm) [107]. Due to this limitation it is assumed that the stress normal to the free surface is zero, which reduces the system to two dimensional plane stress components. The principles of this method is based on peak broadening and lateral peak shift when compared with stress free condition [108].

Synchrotron X-ray diffraction

Third generation synchrotron sources such as the Advanced Photon Source (APS) and the European Synchrotron Radiation Facility (ESRF) provide intense beams with high energy x-rays and high penetration capability (significantly higher intensity than the laboratory X-ray techniques). With such capabilities, synchrotron x-ray beamlines are expanding for measurement of subsurface residual stresses with high spatial resolution [109]. The intense white beam is generated, with energies in the range of 15-100 keV, through powerful magnets which bend the beam of electrons orbiting in a synchrotron. The intense flux of the white beam is then modified to provide a spectrum of wavelengths that is useful for diffraction experiments [109]. Due to the novelty of this technique, limited studies have been conducted and engineering potential for this technique is largely untapped [109]. The work was carried out by Paradowska, et al. [110] used both neutron and synchrotron X-ray diffraction techniques to investigate variations in measured d spacing in two reference samples. The findings showed the negligible effects of texture and microstructure in the weld area on d_0 results. This technique was also applied to measure the residual stresses on laser welded NiTi shape memory alloys [111].

Neutron diffraction

Neutron diffraction technique is able to penetrate a few centimetres through the thickness for most of the metals and alloys which enables the measurement of residual stresses in bulk components to be made [112-121]. Neutrons are sub-atomic particles with approximately the mass of a proton but no electric charge. The thermal neutrons may be generated with the same wavelength as the lattice spacing of typical engineering materials to make them very suitable for strain measurements. The thermal

neutrons for materials research are generated by two main sources: nuclear reactors or spallation sources. Reactor sources are optimized for research purposes, instead of energy production, which means that instead of high temperature they produce high neutron flux. In these reactors the produced neutrons are moderated by heavy water to bring their energies at around room temperature, which provides a useful wavelength spectrum ($\lambda \geq 0.05$ nm) for diffraction in engineering materials [122].

Past studies of residual stresses in weldments with neutron diffraction method include Lorentzen and Ibsø [123] who utilized neutron diffraction technique to investigate the residual strains in two test welded samples of steel plates. The results showed high tensile strains with the magnitude of $+10^{-3}$ near the outer surface and compressive strains of -4×10^{-4} near the surface of the plates. Paradowska, et al. [115] applied this method to investigate and compare the residual stresses distributions in fully restrained and unrestrained samples with different numbers of weld runs. This study has achieved a new level of resolution of the measurements revealing many important features of the residual stress distributions. The finding showed that the peak of residual stresses exceeded the minimum yield stress and it occurred in the middle of the weld bead. The measured stresses in their experimental study were much lower than those structural integrity assessment standards such as BS 7910. Kim, et al. [124] utilised the neutron diffraction method to evaluate residual stresses for a modified 9Cr-1Mo steel weldments. This steel is a strong candidate to be used in future power plants and reactors. The measurements were performed for two types of welds: V-butt and T joints. The maximum longitudinal residual stresses for both T-plate and V-butt welded specimen was found to be near the weld toe. Also the distribution of transverse and longitudinal residual stresses in V-butt welded specimen was generally higher than the

T-plate welded specimen. Martinson, et al. [125] conducted neutron diffraction measurements for laser and resistance spot welding procedures. The experiments were performed to gain an understanding of residual stresses of different joint geometries and techniques widely used in automotive industry. Comparing the results of both welding procedures (resistance and laser spot welding) showed that laser spot welding has higher level of tensile residual stresses than those found in resistance spot welding. Higher level of compressive residual stresses with the larger size was also found at the vicinity of weld region in laser spot welding in comparison with resistance spot welding.

2.2.5.3 Non-destructive nonlinear elastic model

Ultrasonic techniques

Ultrasonic stress measurement techniques are based on variations in the velocity of ultrasonic waves, which can be employed for residual stresses measurements on welded joints [126]. Measuring of stresses can be done through propagating a sound wave with a frequency of several megahertz into the metal specimen and measuring the sound velocity. The velocity of Ultrasonic wave can be affected by microstructural in-homogeneities and in such cases there are difficulties in distinction between the effects of tri-axial stresses and materials non-uniformity [9]. But despite this shortcoming, ultrasonic method is cheap and portable and can be used in routine inspections and can be applied to measurements of residual stresses of large components.

Barkhausen noise method

This method is applicable to ferromagnetic materials, which are composed of small order magnetic fields called magnetic domains. In this technique magnetization

changes lead to inducing electrical pulse on the coil. When all electrical pulses produced by all domain movements added together a noise like signal called as Barkhausen Noise is generated [9]. There is an interaction between elastic properties, domain structure and magnetic properties of the material which is called "magneto-elastic interaction". Because of this interaction (magneto-elastic), in materials with positive magnitic anisotrophy (iron, cobalt and most steels), tensile stresses increase the intensity of Barkhausen noise while compressive stresses decrease it [9]. Similar with ultrasonic technique, this approach is sensitive to both stress and the microstructure and they cannot distinct between microstructural changes and the residual stress variations [127]. This indicates that the stress dependent Barkhausen signal varies from one material to the subsequent and in order to have accurate and effective measurement of residual and applied stresses MBM needs to be calibrated individually [9].

2.3 Conclusions

Experimental measurement techniques are used to evaluate the residuals stress (magnitude, sign and distribution of residual stresses) in welded components within acceptable limits. There are various methods for characterization of residual stresses in engineering components including semi-destructive, destructive and non-destructive methods. It is clear that neutron diffraction method has the outstanding capability of providing residual stress measurements in sub-surface of the engineering components. Neutron diffraction technique was selected in this study because it has been widely reported as accepted technique for providing reliable sub-surface residual stress measurements in various engineering applications [3].

References:

[1] Kurji R. Thermo-Mechanical Factors Influencing Weld Metal Hydrogen Assisted Cold Cracking: The University of Adelaide; 2017.

[2] Costin WL. On the relationship between microstructure mechanical properties and weld metal hydrogen assisted cold cracking: The University of Adelaide; 2016.

[3] Withers PJ, Bhadeshia HKDH. Residual stress part 1 - Measurement techniques. Materials Science and Technology. 2001;17:355-365.

[4] Ueda Y, Murakawa H, Ma N. Welding deformation and residual stress prevention: Elsevier; 2012.

[5] Withers P, Bhadeshia H. Residual stress. Part 2–Nature and origins. Materials Science and Technology. 2001;17:366-375.

[6] Fitzpatrick ME, Lodini A. Analysis of residual stress by diffraction using neutron and synchrotron radiation: CRC Press; 2003.

[7] Blackburn J, Kirk M, Brand P. An Overview of Some Current Research on Welding Residual Stresses and Distortion in US Navy. IIW Document Nos X-1359-96. 1998.

[8] Lindgren LE. Numerical modelling of welding. Computer Methods in Applied Mechanics and Engineering. 2006;195:6710-6736.

[9] Rossini NS, Dassisti M, Benyounis KY, Olabi AG. Methods of measuring residual stresses in components. Materials & Design. 2012;35:572-588.

[10] Anca A, Cardona A, Risso J, Fachinotti VD. Finite element modeling of welding processes. Applied Mathematical Modelling. 2011;35:688-707.

[11] Leggatt RH. Residual stresses in welded structures. International Journal of Pressure Vessels and Piping. 2008;85:144-151.

[12] Zondi MC. Factors that Affect Welding-Induced Residual Stress and Distortions in Pressure Vessel Steels and their Mitigation Techniques: A Review. Journal of Pressure Vessel Technology. 2014;136:040801.

[13] Hot CC, Seam H. Residual stress formation processes during welding and joining. Handbook of Residual Stress and Deformation of Steel. 2002:391.

[14] Mochizuki M. Control of welding residual stress for ensuring integrity against fatigue and stress–corrosion cracking. Nuclear Engineering and Design. 2007;237:107-123.

[15] Mochizuki M, Hayashi M, Hattori T. Residual stress distribution depending on welding sequence in multi-pass welded joints with X-shaped groove. Journal of pressure vessel technology. 2000;122:27-32.

[16] Peel M, Steuwer A, Preuss M, Withers PJ. Microstructure, mechanical properties and residual stresses as a function of welding speed in aluminium AA5083 friction stir welds. Acta Materialia. 2003;51:4791-4801.

[17] Qureshi ME. Analysis of residual stresses and distortions in circumferentially welded thin-walled cylinders: National University of Sciences and Technology; 2008.

[18] Barsoum Z, Barsoum I. Residual stress effects on fatigue life of welded structures using LEFM. Engineering Failure Analysis. 2009;16:449-467.

[19] Shi YW, Chen BY, Zhang JX. Effects of welding residual stresses on fatigue crack growth behaviour in butt welds of a pipeline steel. Engineering Fracture Mechanics. 1990;36:893-902.

[20] Janin YJ. Characterisation of residual stress and investigation of environmental effects on atmospheric-induced stress corrosion cracking of austenitic stainless steel nuclear waste containers: University of Manchester; 2013.

[21] Haigh R, Hutchings M, James J, Ganguly S, Mizuno R, Ogawa K, Okido S, Paradowska A, Fitzpatrick M. Neutron diffraction residual stress measurements on girth-welded 304 stainless steel pipes with weld metal deposited up to half and full pipe wall thickness. International Journal of Pressure Vessels and Piping. 2013;101:1-11.

[22] Smith C, Pistorius PGH, Wannenburg J. The effect of a long post weld heat treatment on the integrity of a welded joint in a pressure vessel steel. International Journal of Pressure Vessels and Piping. 1997;70:183-195.

[23] Ranjbarnodeh E, Serajzadeh S, Kokabi AH, Fischer A. Effect of welding parameters on residual stresses in dissimilar joint of stainless steel to carbon steel. Journal of Materials Science. 2011;46:3225-3232.

[24] Akbari D, Sattari-Far I. Effect of the welding heat input on residual stresses in butt-welds of dissimilar pipe joints. International Journal of Pressure Vessels and Piping. 2009;86:769-776.

[25] Heinze C, Schwenk C, Rethmeier M. Numerical calculation of residual stress development of multi-pass gas metal arc welding under high restraint conditions. Materials & Design. 2012;35:201-209.

[26] Pardowska AM, Price JW, Ibrahim R, Finlayson TR. Neutron Diffraction Evaluation of Residual Stress for Several Welding Arrangements and Comparison With Fitness-for-Purpose Assessments. Journal of pressure vessel technology. 2008;130:011501.

[27] Colegrove P, Ikeagu C, Thistlethwaite A, Williams S, Nagy T, Suder W, Steuwer A, Pirling T. Welding process impact on residual stress and distortion. Science and Technology of Welding & Joining. 2009;14:717-725.

[28] Vasantharaja P, Vasudevan M, Palanichamy P. Effect of welding processes on the residual stress and distortion in type 316LN stainless steel weld joints. Journal of Manufacturing Processes. 2015;19:187-93.

[29] Balasubramanian V, Guha B. Effect of welding processes on toe cracking behaviour of pressure vessel grade steel. Engineering Failure Analysis. 2004;11:575-587.

[30] Gannon L, Liu Y, Pegg N, Smith M. Effect of welding sequence on residual stress and distortion in flat-bar stiffened plates. Marine Structures. 2010;23:385-404.

[31] Ji SD, Fang HY, Liu XS, Meng QG. Influence of a welding sequence on the welding residual stress of a thick plate. Modelling and Simulation in Materials Science and Engineering. 2005;13:553.

[32] Teng T-L, Chang P-H, Tseng W-C. Effect of welding sequences on residual stresses. Computers & structures. 2003;81:273-286.

[33] Kohandehghan AR, Serajzadeh S. Experimental Investigation into the Effects of Weld Sequence and Fixture on Residual Stresses in Arc Welding Process. Journal of Materials Engineering and Performance. 2012;21:892-899.

[34] Sattari-Far I, Javadi Y. Influence of welding sequence on welding distortions in pipes. International Journal of Pressure Vessels and Piping. 2008;85:265-274.

[35] Keehan E. Effect of microstructure on mechanical properties of high strength steel weld metals: Chalmers University of Technology and Göteborg University; 2004.

[36] Ramjaun T, Stone H, Karlsson L, Kelleher J, Moat R, Kornmeier JR, Dalaei K, Bhadeshia, H. Effect of interpass temperature on residual stresses in multipass welds produced using low transformation temperature filler alloy. Science and Technology of Welding and Joining. 2014;19:44-51.

[37] Olabi A-G. Residual stresses and heat treatments for metallic welded components: Dublin City University; 1994.

[38] Aloraier AS, Ibrahim RN, Ghojel J. Eliminating post-weld heat treatment in repair welding by temper bead technique: role bead sequence in metallurgical changes. Journal of Materials Processing Technology. 2004;153–154:392-400.

[39] Paddea S, Francis JA, Paradowska AM, Bouchard PJ, Shibli IA. Residual stress distributions in a P91 steel-pipe girth weld before and after post weld heat treatment. Materials Science and Engineering: A. 2012;534:663-672.

[40] Smith DJ, Garwood SJ. Influence of postweld heat treatment on the variation of residual stresses in 50 mm thick welded ferritic steel plates. International Journal of Pressure Vessels and Piping. 1992;51:241-256.

[41] Cho JR, Lee BY, Moon YH, Van Tyne CJ. Investigation of residual stress and post weld heat treatment of multi-pass welds by finite element method and experiments. Journal of Materials Processing Technology. 2004;155–156:1690-1695.

[42] Aba-Perea PE, Pirling T, Preuss M. In-situ residual stress analysis during annealing treatments using neutron diffraction in combination with a novel furnace design. Materials & Design. 2016;110:925-931.

[43] Chen B, Skouras A, Wang YQ, Kelleher JF, Zhang SY, Smith DJ, Flewitt P, Pavier, MJ. In situ neutron diffraction measurement of residual stress relaxation in a welded steel pipe during heat treatment. Materials Science and Engineering: A. 2014;590:374-383.

[44] Yang YS, Lee SH. A study on the mechanical stress relieving in a butt-welded-pipe. International Journal of Pressure Vessels and Piping. 1997;73:175-182.

[45] Wang T, Wang D, Huo L, Zhang Y. Discussion on fatigue design of welded joints enhanced by ultrasonic peening treatment (UPT). International Journal of Fatigue. 2009;31:644-650.

[46] Zhou JZ, Huang S, Zuo LD, Meng XK, Sheng J, Tian Q, Han Y, Zhu W. Effects of laser peening on residual stresses and fatigue crack growth properties of Ti–6Al–4V titanium alloy. Optics and Lasers in Engineering. 2014;52:189-194.

[47] Habibi N, H-Gangaraj SM, Farrahi GH, Majzoobi GH, Mahmoudi AH, Daghigh M, Yari A, Moridi A. The effect of shot peening on fatigue life of welded tubular joint in offshore structure. Materials & Design. 2012;36:250-257.

[48] Rao D, Ge J, Chen L. Vibratory stress relief in manufacturing the rails of a Maglev system. Journal of manufacturing science and engineering. 2004;126:388-391.

[49] Walker C, Waddell A, Johnston D. Vibratory stress relief—an investigation of the underlying processes. Proceedings of the Institution of Mechanical Engineers, Part E: Journal of Process Mechanical Engineering. 1995;209:51-58.

[50] Goldak JA, Akhlaghi M. Computational welding mechanics: Springer Science and Business Media; 2005.

[51] Michaleris P, Feng Z, Campbell G. Evaluation of 2D and 3D FEA models for predicting residual stress and distortion. ASME PVP- Approximate Methods in the Design and Analysis of Pressure Vessels and Piping Components. 1997;347:91-102.

[52] Sarkani S, Tritchkov V, Michaelov G. An efficient approach for computing residual stresses in welded joints. Finite Elements in Analysis and Design. 2000;35:247-268.

[53] Deng D, Murakawa H, Liang W. Numerical and experimental investigations on welding residual stress in multi-pass butt-welded austenitic stainless steel pipe. Computational Materials Science. 2008;42:234-244.

[54] Rosenthal D. Mathematical theory of heat distribution during welding and cutting. Welding Journal. 1941;20:220-234.

[55] Rykalin.R.R. Calculations of Heat Processes in Welding, Educational Lecture. American Welding Society. New York1961.

[56] Nguyen N, Ohta A, Matsuoka K, Suzuki N, Maeda Y. Analytical solutions for transient temperature of semi-infinite body subjected to 3-d moving heat sources. Welding Journal-New York. 1999;78:265-s.

[57] Pavelic V, Tanbakuchi R, Uyehara O, Myers P. Experimental and computed temperature histories in gas tungsten-arc welding of thin plates. Welding Journal. 1969;48:295-305.

[58] Kermanpur A, Shamanian M, Yeganeh VE. Three-dimensional thermal simulation and experimental investigation of GTAW circumferentially butt-welded Incoloy 800 pipes. Journal of Materials Processing Technology. 2008;199:295-303.

[59] Lee C-H, Chang K-H. Temperature fields and residual stress distributions in dissimilar steel butt welds between carbon and stainless steels. Applied Thermal Engineering. 2012;45:33-41.

[60] Eagar T, Tsai N. Temperature fields produced by traveling distributed heat sources. Welding Journal. 1983;62:346-355.

[61] Goldak J, Chakravarti A, Bibby M. A new finite element model for welding heat sources. Metallurgical Transactions B. 1984;15:299-305.

[62] Sabapathy PN, Wahab MA, Painter MJ. Numerical models of in-service welding of gas pipelines. Journal of Materials Processing Technology. 2001;118:14-21.

[63] Carmet A, Debiez S, Devaux J, Pont D, Leblond J. Experimental and numerical study of residual stresses and strains in an electron-beam-welded joint. International Conference on Residual Stresses: Springer; 1989. p. 491-496.

[64] Goldak J, Zhou J, Breiguine V, Montoya F. Thermal Stress Analysis of Welds : From Melting Point to Room Temperature. Transactions of JWRI. 1996;25:185-189.

[65] Camilleri D, Comlekci T, Gray TF. Computational prediction of out-of-plane welding distortion and experimental investigation. The Journal of Strain Analysis for Engineering Design. 2005;40:161-176.

[66] Lindgren L-E, Runnemalm H, Näsström MO. Simulation of multipass welding of a thick plate. International Journal for Numerical Methods in Engineering. 1999;44:1301-1316.

[67] Andersson BAB. Thermal stresses in a submerged-arc welded joint considering phase transformations. Journal of Engineering Materials and Technology. 1978; 100(3):356-362.

[68] Michaleris P, DeBiccari A. Prediction of welding distortion. Welding Journal-Including Welding Research Supplement. 1997;76(4):172s.

[69] Bonifaz E. Finite element analysis of heat flow in single-pass arc welds. Welding Journal-New York. 2000;79(5):121-s.

[70] Deng D, Murakawa H. Numerical simulation of temperature field and residual stress in multi-pass welds in stainless steel pipe and comparison with experimental measurements. Computational Materials Science. 2006;37:269-277.

[71] Dong Z, Wei Y. Three dimensional modeling weld solidification cracks in multipass welding. Theoretical and applied fracture mechanics. 2006;46:156-165.

[72] Attarha MJ, Sattari-Far I. Study on welding temperature distribution in thin welded plates through experimental measurements and finite element simulation. Journal of Materials Processing Technology. 2011;211:688-694.

[73] Kohandehghan AR, Serajzadeh S. Arc welding induced residual stress in butt-joints of thin plates under constraints. Journal of Manufacturing Processes. 2011;13:96-103.

[74] Lee C-H, Chang K-H. Prediction of residual stresses in high strength carbon steel pipe weld considering solid-state phase transformation effects. Computers & Structures. 2011;89:256-265.

[75] Chang P-H, Teng T-L. Numerical and experimental investigations on the residual stresses of the butt-welded joints. Computational Materials Science. 2004;29:511-522.

[76] Deng D, Murakawa H. Prediction of welding distortion and residual stress in a thin plate butt-welded joint. Computational Materials Science. 2008;43:353-365.

[77] Lindgren L-E. Finite element modeling and simulation of welding part 1: increased complexity. Journal of thermal stresses. 2001;24:141-192.

[78] Iwaki T, Masubuchi K. Thermo-elastic analysis of orthotropic plastic by the finite element method. J Soc Naval Arch Japan. 1971;130:195-204.

[79] Ueda Y, Yamakawa T. Analysis of thermal elastic-plastic stress and strain during welding by finite element method. Transactions of the Japan Welding Society. 1971;2:186-96.

[80] Fujita Y, Takeshi Y, Kitamura M, Nomoto T. Welding stresses with special reference to cracking. IIW Doc X-655-72. 1972.

[81] Prasad NS, Sankaranarayanan TK. Estimation of residual stresses in weldments using adaptive grids. Computers & Structures. 1996;60:1037-1045.

[82] Camilleri D, Gray TGF. Computationally efficient welding distortion simulation techniques. Modelling and Simulation in Materials Science and Engineering. 2005;13:1365.

[83] De A, DebRoy T. A perspective on residual stresses in welding. Science and Technology of Welding & Joining. 2011;16:204-208.

[84] Dunstone A. Numericall modelling of pipeline construction: The University of Adelaide; 2004.

[85] Karlsson C. Finite element analysis of temperatures and stresses in a single-pass butt-welded pipe—influence of mesh density and material modelling. Engineering Computations. 1989;6:133-141.

[86] Zhu XK, Chao YJ. Numerical simulation of transient temperature and residual stresses in friction stir welding of 304L stainless steel. Journal of Materials Processing Technology. 2004;146:263-272.

[87] Lee C, Chiew S, Jiang J. 3D residual stress modelling of welded high strength steel plate-to-plate joints. Journal of Constructional Steel Research. 2013;84:94-104.

[88] Karlsson CT, Josefson BL. Three-dimensional finite element analysis of tempratures and stresses in a single-pass butt welded pipe. Journal of Pressure Vessel Technology. 1990;112:76-84.

[89] Deng D. FEM prediction of welding residual stress and distortion in carbon steel considering phase transformation effects. Materials & Design. 2009;30:359-366.

[90] Heinze C, Schwenk C, Rethmeier M. Numerical calculation of residual stress development of multi-pass gas metal arc welding. Journal of Constructional Steel Research. 2012;72:12-19.

[91] Javadi Y, Najafabadi MA. Comparison between contact and immersion ultrasonic method to evaluate welding residual stresses of dissimilar joints. Materials & Design. 2013;47:473-482.

[92] Sattari-Far I, Farahani MR. Effect of the weld groove shape and pass number on residual stresses in butt-welded pipes. International Journal of Pressure Vessels and Piping. 2009;86:723-731.

[93] Mahmoodi M, Sedighi M, Tanner DA. Investigation of through thickness residual stress distribution in equal channel angular rolled Al 5083 alloy by layer removal technique and X-ray diffraction. Materials & Design. 2012;40:516-520.

[94] Tebedge N, Alpsten G, Tall L. Residual-stress measurement by the sectioning method. Experimental Mechanics. 1973;13:88-96.

[95] Treuting R, Read Jr. A mechanical determination of biaxial residual stress in sheet materials. Journal of Applied Physics. 1951;22:130-134.

[96] Prime MB, Martineau RL. Mapping residual stresses after foreign object damage using the contour method. Materials science forum: Trans Tech Publ; 2002. p. 521-526.

[97] Leggatt R, Smith D, Smith S, Faure F. Development and experimental validation of the deep hole method for residual stress measurement. The Journal of Strain Analysis for Engineering Design. 1996;31:177-186.

[98] Young B, Lui W-M. Behavior of cold-formed high strength stainless steel sections. Journal of structural engineering. 2005;131:1738-1745.

[99] Lagerqvist O, Olsson A. Residual stresses in welded I-girders made of stainless steel and structural steel. Helsinki: Proceedings of the ninth nordic steel construction conference 2001. p. 737-744.

[100] Prime MB. Cross-sectional mapping of residual stresses by measuring the surface contour after a cut. Transactions-American society of mechanical engineers journal of engineering materials and technology. 2001;123:162-168.

[101] Pagliaro P, Prime MB, Swenson H, Zuccarello B. Measuring multiple residual-stress components using the contour method and multiple cuts. Experimental Mechanics. 2010;50:187-194.

[102] Zhang Y, Ganguly S, Edwards L, Fitzpatrick ME. Cross-sectional mapping of residual stresses in a VPPA weld using the contour method. Acta Materialia. 2004;52:5225-5232.

[103] Schajer G. Measurement of non-uniform residual stresses using the hole-drilling method. Part I—Stress calculation procedures. Journal of Engineering Materials and Technology. 1988;110:338-343.

[104] Vishay M. Measurement of residual stresses by the hole drilling strain gage method. Tech Note TN. 2005:503-506.

[105] Flaman M, Manning B. Determination of residual-stress variation with depth by the hole-drilling method. Experimental Mechanics. 1985;25:205-207.

[106] Woo W, An GB, Kingston EJ, DeWald AT, Smith DJ, Hill MR. Through-thickness distributions of residual stresses in two extreme heat-input thick welds: A neutron diffraction, contour method and deep hole drilling study. Acta Materialia. 2013;61:3564-3574.

[107] Prevey PS. X-ray diffraction residual stress techniques. ASM International, ASM Handbook. 1986;10:380-392.

[108] Culity B, Stock S. Elements of X-ray Diffraction. Reading: Addition-Wesley. 1978.

[109] Withers P. Residual stress and its role in failure. Reports on Progress in Physics. 2007;70:2211.

[110] Paradowska A, Finlayson TR, Price JWH, Ibrahim R, Steuwer A, Ripley M. Investigation of reference samples for residual strain measurements in a welded specimen by neutron and synchrotron X-ray diffraction. Physica B: Condensed Matter. 2006;385–386, Part 2:904-907.

[111] Oliveira JP, Fernandes FMB, Miranda RM, Schell N, Ocaña JL. Residual stress analysis in laser welded NiTi sheets using synchrotron X-ray diffraction. Materials & Design. 2016;100:180-187.

[112] Mochizuki M, Hayashi M, Hattori T. Numerical analysis of welding residual stress and its verification using neutron diffraction measurement. Journal of engineering materials and technology. 2000;122:98-103.

[113] Stacey A, MacGillivary H, Webster G, Webster P, Ziebeck K. Measurement of residual stresses by neutron diffraction. The Journal of Strain Analysis for Engineering Design. 1985;20:93-100.

[114] Owen RA, Preston RV, Withers PJ, Shercliff HR, Webster PJ. Neutron and synchrotron measurements of residual strain in TIG welded aluminium alloy 2024. Materials Science and Engineering: A. 2003;346:159-167.

[115] Paradowska A, Price JWH, Ibrahim R, Finlayson T. A neutron diffraction study of residual stress due to welding. Journal of Materials Processing Technology. 2005;164:1099-1105.

[116] Paradowska A, Price JWH, Ibrahim R, Finlayson TR, Blevins R, Ripley M. Residual stress measurements by neutron diffraction in multi-bead welding. Physica B: Condensed Matter. 2006;385:890-893.

[117] Park MJ, Yang HN, Jang DY, Kim JS, Jin TE. Residual stress measurement on welded specimen by neutron diffraction. Journal of Materials Processing Technology. 2004;155:1171-1177.

[118] Skouras A, Paradowska A, Peel MJ, Flewitt PEJ, Pavier MJ. Residual stress measurements in a ferritic steel/In625 superalloy dissimilar metal weldment using neutron diffraction and deep-hole drilling. International Journal of Pressure Vessels and Piping. 2013;101:143-153.

[119] Price JWH, Paradowska A, Joshi S, Finlayson T. Residual stresses measurement by neutron diffraction and theoretical estimation in a single weld bead. International Journal of Pressure Vessels and Piping. 2006;83:381-387.

[120] Florea RS, Hubbard CR, Solanki KN, Bammann DJ, Whittington WR, Marin EB. Quantifying residual stresses in resistance spot welding of 6061-T6 aluminum alloy sheets via neutron diffraction measurements. Journal of Materials Processing Technology. 2012;212:2358-2370.

[121] Jung M, Kang M, Woo W, Lee Y-K. Evaluations of stress-free lattice spacings and residual stresses in a quenched carbon steel cylinder using neutron diffraction. Materials Science and Engineering: A. 2013;565:392-395.

[122] Paranjpe S. Measurement of Residual Stress in Materials using Neutrons: Proceedings of a Technical Meeting Held in Vienna, 13–17 October 2003. International Atomic Energy Agency. 2005.

[123] Lorentzen T, Ibsø J. Neutron diffraction measurements of residual strains in offshore welds. Materials Science and Engineering: A. 1995;197:209-214.

[124] Kim S-H, Kim J-B, Lee W-J. Numerical prediction and neutron diffraction measurement of the residual stresses for a modified 9Cr–1Mo steel weld. Journal of Materials Processing Technology. 2009;209:3905-3913.

[125] Martinson P, Daneshpour S, Kocak M, Riekehr S, Staron P. Residual stress analysis of laser spot welding of steel sheets. Materials & Design. 2009;30:3351-3359.

[126] Javadi Y, Akhlaghi M, Najafabadi MA. Using finite element and ultrasonic method to evaluate welding longitudinal residual stress through the thickness in austenitic stainless steel plates. Materials & Design. 2013;45:628-642.

[127] Withers PJ, Turski M, Edwards L, Bouchard PJ, Buttle DJ. Recent advances in residual stress measurement. International Journal of Pressure Vessels and Piping. 2008;85:118-127.

CHAPTER 3

EXPERIMENTAL WELDING AND TESTING

METHODS

3.1 Welding set up description

The welding of the Welding Institute of Canada (WIC) test was conducted using Lincoln Electric Invertec V 350 Pro. The Lincoln Electric Invertec V 350 Pro with the Advanced Process Module (K1728-7), an inverter-type model that allows for an accurate selection of output current, as the system is digitally controlled. It has an output range of 5–425A and has an open current voltage of 80V DC.

The welding of the plates (multi-pass) was conducted with a multi-purpose Lincoln Electric power wave S350, as shown in Fig.3.1. Lincoln Electric power wave S350 automatically adjusts to input power from 200-600V, 50 or 60 Hz, single phase or three phase.
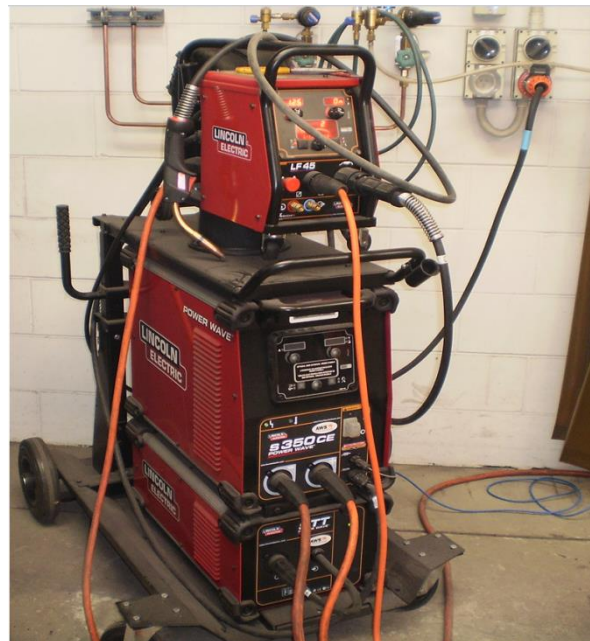
Figure 3.1: Lincoln Electric power wave S350 welding machine

The root pass of WIC test was completed with shielded metal arc welding process (SMAW). As explained in the first chapter, the experiments were also conducted for multi-pass welds including SMAW as well as combination of modified short arc welding (MSAW) with flux cored arc welding process (FCAW). The root pass of

multi-pass weldments with combination of MSAW+FCAW was completed with modified short arc welding (MSAW) and flux cored arc welding process (FCAW) was utilised for the remaining passes, which is quite common in modern welding procedures. The MSAW offers many advantages such as low distortion, freedom from spatter, high quality of welded joints and lower cost for post-weld machining. FCAW ensures high deposition and productivity rates. It does not require a highly trained personnel; the process is simple and more adaptable for various welding configurations than other types of welding, such as submerged arc welding (SAW) for example.

Similarly, welding with SMAW process offers several advantages including lower equipment cost, portability of equipment, and welding in various positions and confined spaces [1]. The root pass of combination of MSAW+FCAW was completed with ER70-6 electrode; and the remaining passes with E81TNi class Flux cored wire. The weld consumable for the SMAW specimens was specified to be E6010 electrode with a diameter of 3.2 mm for the root pass and E8010 electrode of 4 mm diameter for deposition of remaining passes. The experimental set-up is shown in Figure.3.2.

Figure 3.2: Experimental set-up for multi-pass welds

3.2 Material selection and consumables

The selected material for the parent metal was API 5L grade X70. This material was selected due to its widespread use in pipeline construction and pressure vessel applications. The plates were cut from a single slab hot rolled to 20 mm thick and were provided by Bao Steel, China. The yield strength of the parent metal is about 490-520 MPa.

The chemical compositions of the materials and weld metal are shown in Table 3.1. All the MSAW+FCAW welds were produced using an Argon shield 52 (CO_2 25%) shielding gas (with gas flow rate 18 l/min).

Table 3.1: Chemical compositions of the parent and weld metal consumables

Chemical composition	ER 70S-6	E81T1-Ni 1M	E6010	E8010	Parent metal
%C	0.09	0.04-0.05	0.16	0.20	0.052
%Mn	<1.60	1.26-1.36	0.62	1.20	1.55
%S	0.007	0.006-0.009	0.009	0.03	0.0011
%Si	0.90	0.25-0.29	0.19	0.60	0.21
%P	0.007	0.005-0.008	0.009	0.03	0.0097
%Cu	0.20	-			0.15
%Cr	0.05	0.04-0.05	0.02	0.30	0.026
%Ni	0.05	0.86-0.96	0.2	1.00	0.19
%Mo	0.05	0.01	0.01	0.50	0.18
%V	0.05	0.02-0.03	$\leq$0.01	$\leq$0.10	0.029
%Ti	-	-			0.012
%NB	-	-			0.041

3.3 Metallographic inspection

The metallographic weld specimen examination was carried out at the materials lab (university of Adelaide) and Adelaide microscopy. The selected sections were prepared according to the Australian standard AS.2205.5.1 (method 5.1) for either macro or microscopic inspection. Cross- sections of welded specimens were prepared and the surfaces were polished down to 1 μm diamond paste and etched using Nital 5% (95% Ethanol and 5 % Nitric acid) or prepared by a double etching procedure using 2% Picral (2% picric acid in ethanol) and 2% Nital solutions (2 % nitric acid in ethanol). The microstructure of the as etched samples was examined within the weld metal, HAZ and parent metal using optical and scanning electron microscopy.

3.4 Hardness testing

Hardness testing was conducted according to the Australian standard AS.2205.6.1 (method 6.1). Cross- sections of test specimens were prepared and the surfaces were polished (down to 1 μm diamond paste) and the hardness of the weld metal, HAZ and parent metal were measured. Measurements were taken in cross sections of weld in nine lines (2, 4, 6, 8, 10, 12, 14, 16 and 18 mm away from weld top surface) at intervals of 0.5 mm apart and one line in the weld centreline (through the thickness) at intervals of 0.5 mm. In all cases the hardness testing was conducted using a Vickers (HV) indenter with the load of 0.5 Kg and with a loading time of 15 seconds.

3.5 EBSD analysis

Sample surfaces were polished using a semi-automatic TegraPol polishing machine (Struers). Final polishing was achieved using a porous neoprene disc with a colloidal silica suspension (0.04 μm). A FEI Helios Nanolab 600-SEM equipped with EBSD detector (EDAX Hikari™) was utilised to collect the EBSD scans from the identified microstructural regions. The acceleration voltage and current of electron beam for the EBSD measurements were 30 kV and 2.7 nA, respectively. The step size was 30 nm with a hex-agonal scan grid (scans were100x100 μm^2). Data collection and analyses were made using TSL-OIM software.

3.6 TEM analysis

TEM analysis was carried out to fully characterize the morphology of microstructure for the as-welded and post-weld heat treated specimens. TEM thin foils were prepared using focused ion beam (FIB) with the foil's dimension of 15 μm x 10 μm x 75 nm. TEM Tecnai G2 Spirit type transmission electron microscope was employed to carry out the investigations

3.7 Finite Element modelling

3D thermo-elasto-plastic Finite Element models were developed and the numerical results for root pass of the WIC test were obtained with ANSYS 14.5 software package utilising the eight-node 3D thermal element SOLID70 with a single degree of freedom at each node (temperature) for both parent and weld metal and a Newton-Raphson iterative procedure. SOLID185 element was used for structural analysis. This 3D element is characterised by eight nodes, which have three degrees of freedom each: translations in the nodal x, y, and z directions. The analysis of stresses was conducted by using an uncoupled formulation, because the dimensional changes were found negligible [2] and the corresponding mechanical energy was insignificant when compared with the thermal energy from the welding arc. The element length size in the simulations was varied from 1 mm to 1.3 mm which was based on the mesh sensitivity analysis. The temperature-dependant thermo-physical and mechanical properties were used in the numerical simulations of the WIC test. Further details of Finite Element modelling can be found in the published paper (chapter 4).

3.8 Tensile and Charpy impact tests

Standard and sub-sized specimens tensile testing were performed at room temperature with strain rate of $4 \times 10^{-4} s^{-1}$ using two different tensile testing machines (INSTRON 1282 Servo-hydraulic and MTS FXSA305A). Tensile testing procedure and specimen specifications were according to the ASTM-A370. The tensile tests were carried out to investigate the PWHT effects on both the parent and weld metal. Charpy impact tests were performed at room temperature for the as-welded and post-weld heat treated specimens on standard Charpy V-notch specimens (size; 10×10×55mm^3). The dimensions of the specimens are presented, in Figure 3.3.
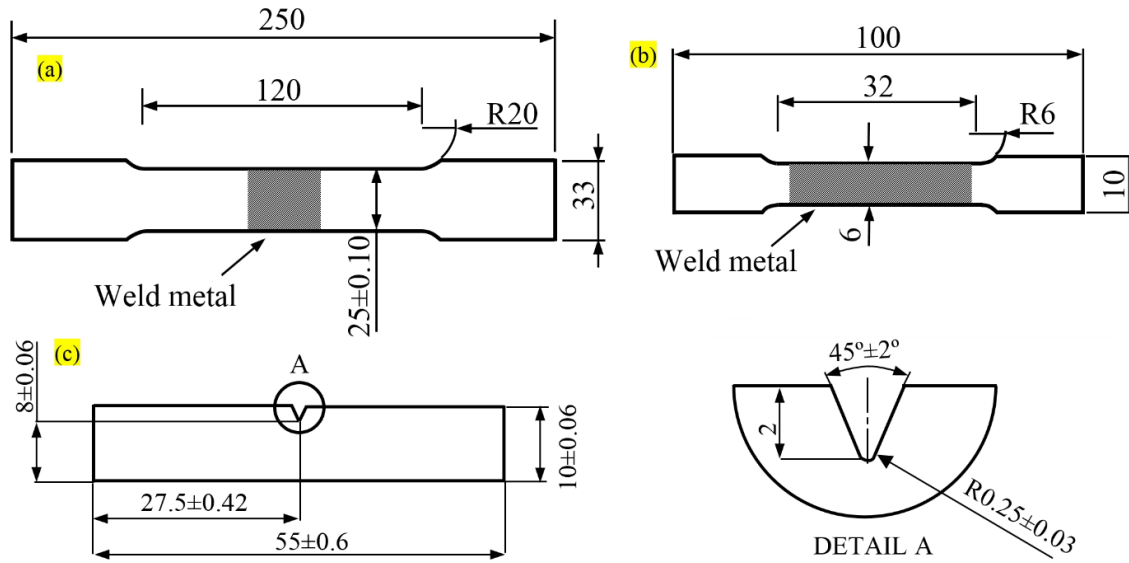
Figure 3.3: Shape and dimensions of (a) standard tensile; (b) sub-sized tensile and (c) Charpy specimens (all dimensions are in mm).

3.9 Neutron diffraction method

Neutron diffraction method represents a non-destructive deep scanning technique for generation of three-dimensional strain maps in engineering components. This method utilises a beam of neutrons with a momentum p, and associated wavelength λ:

$$\lambda = \frac{h}{p} \qquad (3.1)$$

where h is the Planck's constant. When the neutron beam penetrates crystalline materials, a diffraction pattern with sharp maxima is produced. The diffraction pattern can be described in terms of Bragg's law, see Figure 3.4 for illustration:

$$2d_{hkl} \cdot \sin\theta_{hkl} = n\lambda , \qquad (3.2)$$

where d_{hkl} is the crystal lattice interplanar spacing, n is an integer number representing the order of the reflection plane and θ is the angle between the incident ray and the scattering planes as shown in Figure 3.4. A small change in the lattice spacing (Δd_{hkl})

will result in a change in the angular position of the diffraction peak ($\Delta\theta_{hkl}$) given by the following equation:

$$\Delta\theta_{hkl} = -\tan\theta_{hkl} \cdot \frac{\Delta d_{hkl}}{d_{hkl}} \qquad (3.3)$$

The lattice normal strain ε is given by:

$$\varepsilon = \frac{d_{hkl} - d_{0,hkl}}{d_{0,hkl}} = -\Delta\theta_{hkl} \cdot \cot\theta_{0,hkl} \, , \qquad (3.4)$$

Where $d_{0,hkl}$ is the strain-free lattice spacing for the hkl planes, and $\theta_{0,hkl}$ is the diffraction angle of the unrestrained lattice [3].
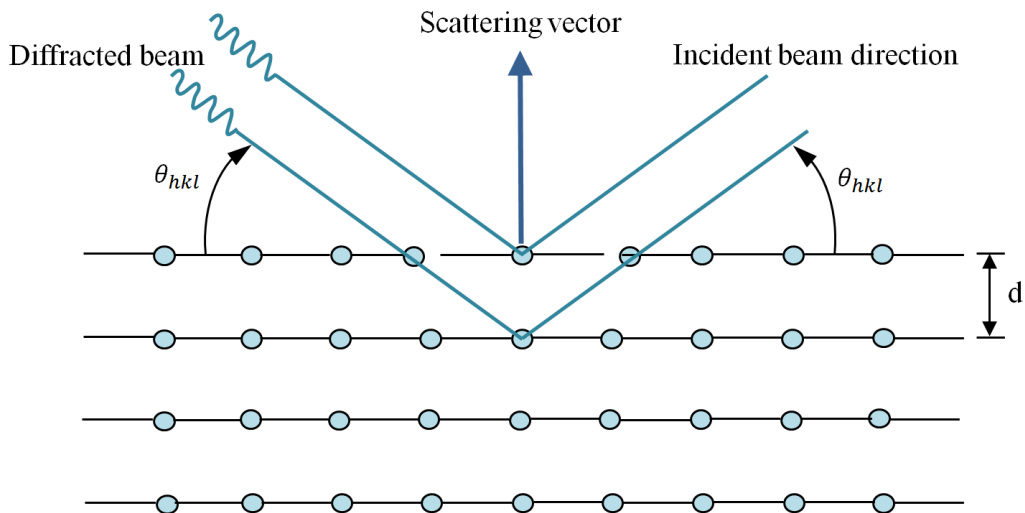
Figure 3.4: Schematic illustration of Bragg's law.

The principles of the ND technique showing a Bragg reflection from crystal planes is shown in Figure 3.5. It is important to note that the grain size is exaggerated for clarity.
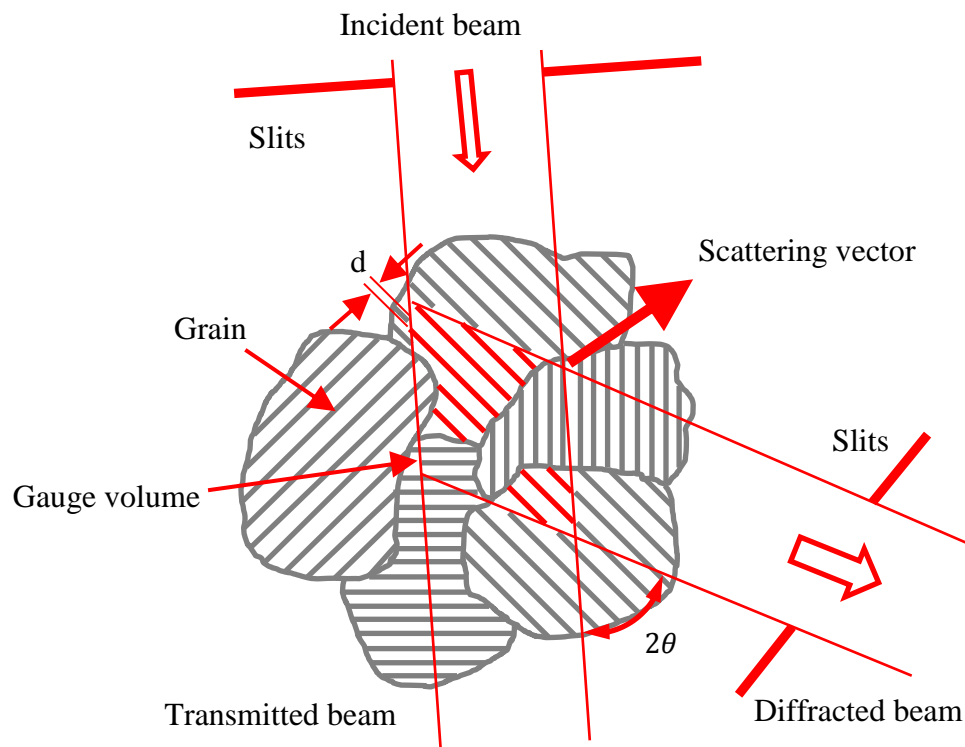
Figure 3.5: Principles of the diffraction technique showing Bragg's reflection from the crystal plane *d* [4].

In the present study, the measurements of strains were conducted in three directions; longitudinal (parallel to the welding direction), transverse (perpendicular to the weld) and normal to the plate (through thickness), as illustrated in Figure 3.6:
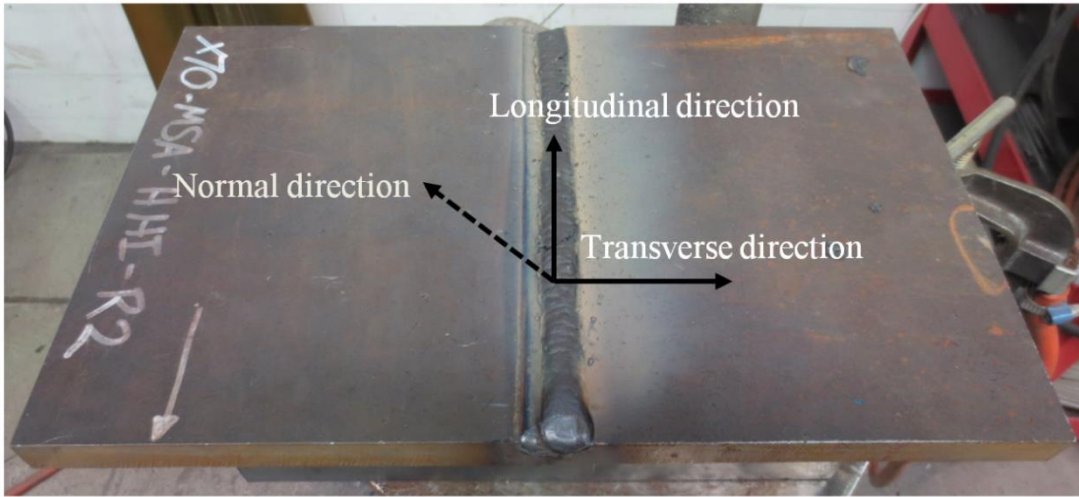
Figure 3.6: Welding specimen showing three directions of strain measurements.

The three-dimensional stresses can be calculated from the measured strains using the

generalized Hook's law as [5]:

$$\sigma_{xx} = \frac{E}{(1+v)(1-2v)}\left[(1-v)\varepsilon_{xx} + v(\varepsilon_{yy} + \varepsilon_{zz})\right]$$

$$\sigma_{yy} = \frac{E}{(1+v)(1-2v)}\left[(1-v)\varepsilon_{yy} + v(\varepsilon_{xx} + \varepsilon_{zz})\right]$$

(3.5)

$$\sigma_{zz} = \frac{E}{(1+v)(1-2v)}\left[(1-v)\varepsilon_{zz} + v(\varepsilon_{xx} + \varepsilon_{yy})\right]$$

where E is Young's modulus and v is the Poisson's ratio. The uncertainties of the stress

components in there directions (x, y and z) were derived as the following Equations

[5]:

$$\Delta\sigma_{xx} = \frac{E}{(1+v)}\sqrt{\left(\frac{v}{1-2v}\right)(\Delta\varepsilon_{xx})^2 + \left(\frac{v}{1-2v}\right)^2\left(\Delta\varepsilon_{xx}^2 + \Delta\varepsilon_{yy}^2 + \Delta\varepsilon_{zz}^2\right)}$$

$$\Delta\sigma_{yy} = \frac{E}{(1+v)}\sqrt{\left(\frac{v}{1-2v}\right)(\Delta\varepsilon_{yy})^2 + \left(\frac{v}{1-2v}\right)^2\left(\Delta\varepsilon_{xx}^2 + \Delta\varepsilon_{yy}^2 + \Delta\varepsilon_{zz}^2\right)}$$

(3.6)

$$\Delta\sigma_{ZZ} = \frac{E}{(1+\nu)} \sqrt{\left(\frac{\nu}{1-2\nu}\right)(\Delta\varepsilon_{ZZ})^2 + \left(\frac{\nu}{1-2\nu}\right)^2 \left(\Delta\varepsilon_{xx}{}^2 + \Delta\varepsilon_{yy}{}^2 + \Delta\varepsilon_{zz}{}^2\right)}$$

The residual stresses were derived from the elastic strain (Equation 3.5) measurements of the (211) reflection of αFe. Young's modulus of 224 GPa and Poisson's ratio of 0.27 were used for these constants in the present work. Residual stress measurements were performed at Australian Nuclear Science and Technology Organization (ANSTO) using KOWARI strain scanner and a $3 \times 3 \times 3$ mm^3 gauge volume. The Si (400) type double focusing monochromator generated a neutron beam with the wavelength of 1.67Å. A detector angle, 2θ, was set at 90° corresponding to the αFe (211) diffraction peak. Strain measurements was made with the scattering vector parallel to each of the three axes including transverse, longitudinal and normal as illustrated in Figure 3.6. This was implemented through changing the sample orientations as shown in Figure 3.7.

To determine the diffraction angle for the unrestrained lattice, $\theta_{0,211}$, the reference samples were stress relieved by sectioning through thickness using electro-discharge machining (EDM) with a wire diameter of 0.2 mm. The reference samples were examined in three principal directions to account for variation in chemical composition heterogeneity around the weld and HAZ.
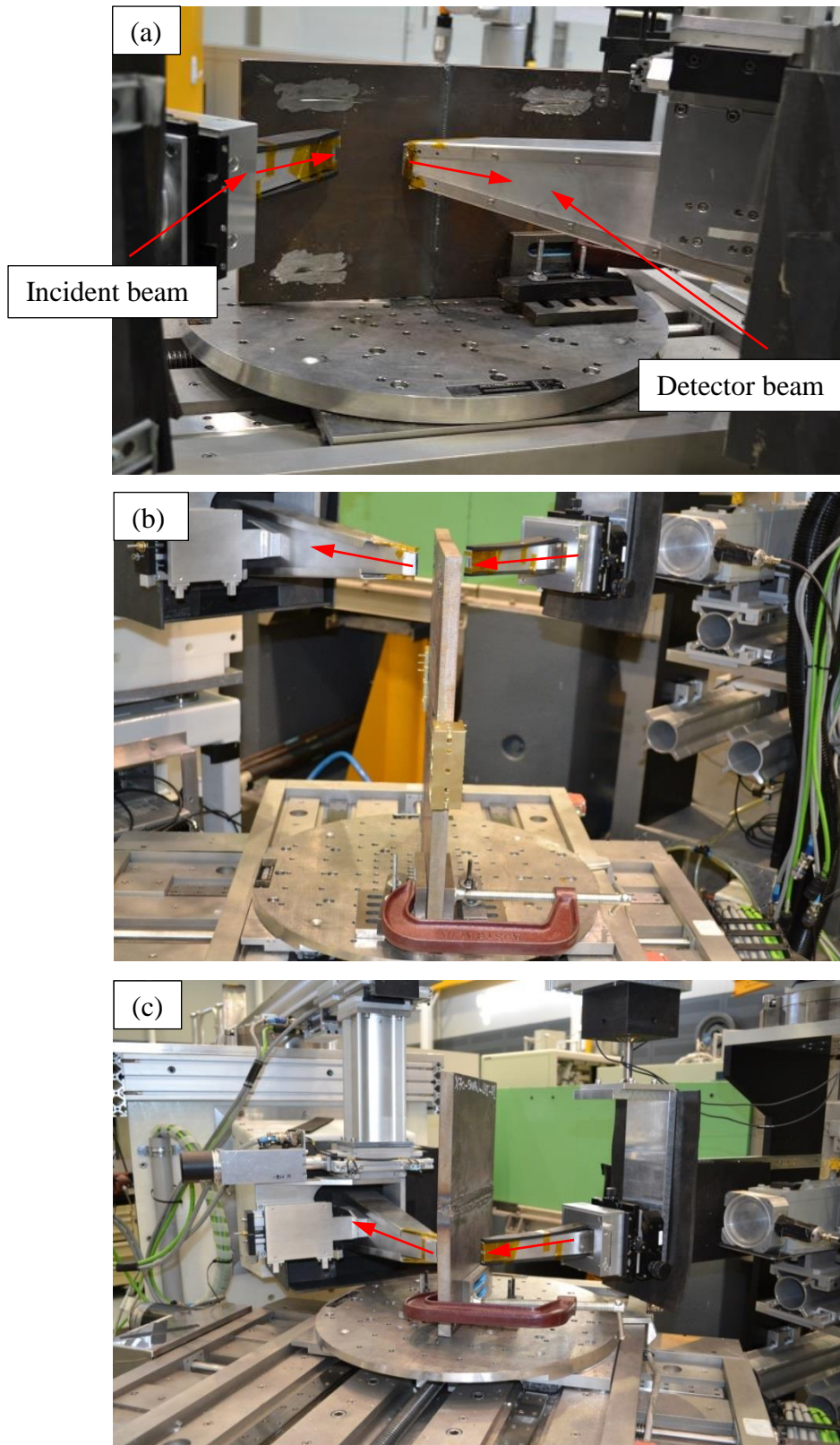
Figure 3.7: Different orientations of specimen for residual stress measurements using KOWARI strain scanner; (a) normal, (b) transverse and (c) longitudinal direction.

3.10 PWHT

In situ neutron diffraction was employed to measure the relaxation of residual strains during conventional PWHT in multi-pass high strength low alloy steel welds. The full details of in situ neutron diffraction is explained in chapter 8, therefore it is not repeated here. However, some parts of PWHT need further explanation and the details is given in this section. PWHT was carried out using the heating blankets which were made up from block shaped elements of sintered alumina containing resistance heating Ni-Cr wire, as shown in Figure 3.8. The heating blankets was controlled using an Advantage3 controller to regulate the input current according to a centrally mounted control thermo-couple. The Advantage3 controller has three modes of operation which are off (indicator only), programmer and controller. When the mode of operation is off, the heat input remains off (no control action) and the display alternates between the thermocouple load temperature reading and OFF. In the controller mode the unit receive the incoming set point from the Programmer unit with the display continuously showing load temperature.

As shown in Figure 3.9, the Advantage3 controller was used in order to perform the following functions:

- Temperature measurement, display and control (°C or °F)

- Start and end temperature

- Temperature ramp up and down in degrees per hour

- Hold/soak temperature set point and hold/soak time period sett

In order to monitor the temperature uniformity during the experiment six thermocouples (K type) were spot welded to the specimen at different locations in the

weld and parent metal. The temperature distribution across the entire sample did not vary more than 10ºC from the set PWHT temperature during the entire experiment.

The as-welded samples were reheated at 5ºC/min to soaking temperature of 600ºC (below the subcritical temperature) and was held isothermally at this temperature for three different holding times (0.5, 1 and 3 hours), followed by slow controlled-cooling at a rate of 5 °C /min, back to room temperature. A graph of temperature measurements during PWHT for the holding time of 0.5 hour is shown in Figure. 3.10.
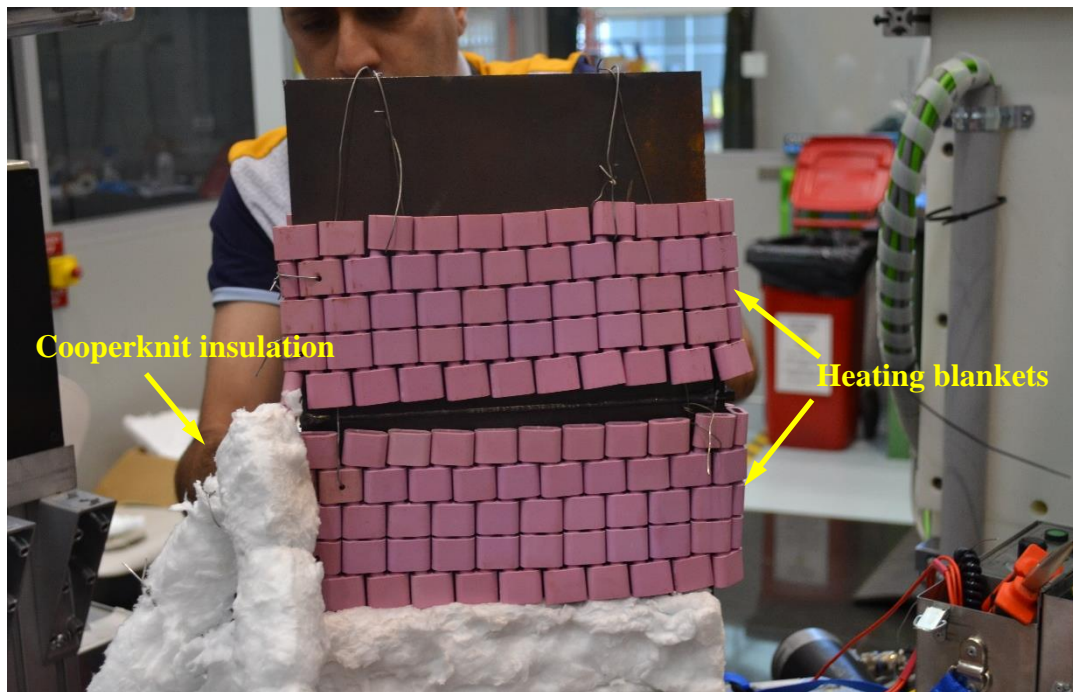
Figure 3.8: Experimental set-up for the measurement of strain relaxation by ND during PWHT.

Figure 3.9: Advantage 3 programmer/controller heat treatment unit used during PWHT.
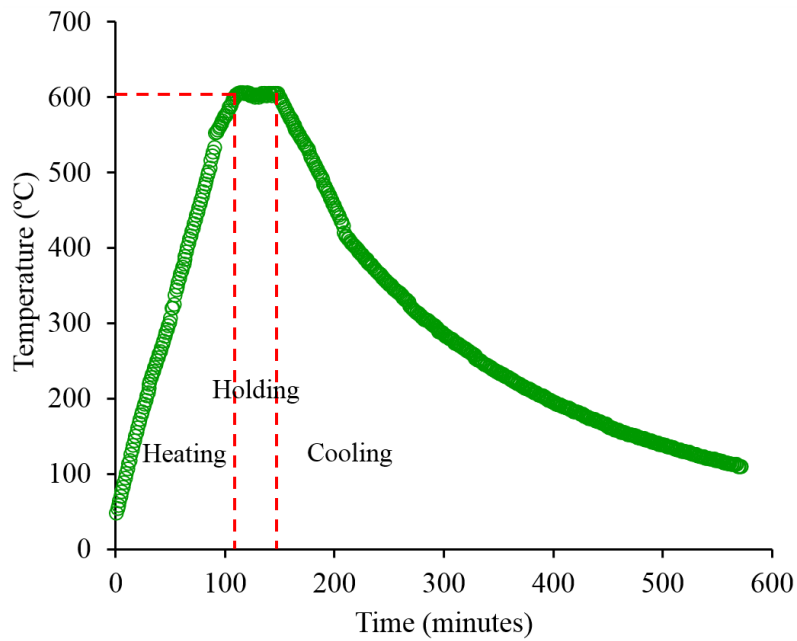
Figure 3.10: Thermal cycle during post-weld heat treatment (0.5 hour holding time).

References:

[1] Kotousov A, Borkowski K, Fletcher L, Ghomashchi R. A model of hydrogen assisted cold cracking in weld metal. 2012 9th International Pipeline Conference: American Society of Mechanical Engineers; 2012. p. 329-334.

[2] Javadi Y, Akhlaghi M, Najafabadi MA. Using finite element and ultrasonic method to evaluate welding longitudinal residual stress through the thickness in austenitic stainless steel plates. Materials & Design. 2013;45:628-642.

[3] Grunitz L. Buckling strength of welded HY-80 spherical shells: A direct approach: Hamburg; 2004.

[4] Pardowska AM, Price JW, Ibrahim R, Finlayson TR. Neutron Diffraction Evaluation of Residual Stress for Several Welding Arrangements and Comparison With Fitness-for-Purpose Assessments. Journal of pressure vessel technology. 2008;130:011501.

[5] Paradowska A. Investigation of residual stress in steel welds using neutron and synchrotron diffraction, Ph.D thesis. Melbourne: University of Monash; 2007.

CHAPTER 4

PREDICTION OF WELDING STRESSES IN WIC

TEST AND ITS APPLICATION IN PIPELINES

Houman Alipooramirabad[1], Anna Paradowska[2]*, Reza Ghomashchi[1] and Andrei Kotousov[1], Nicholas Hoye[2, 3]

[1]Mechanical Engineering Department, University of Adelaide, Adelaide, Australia

[2] Bragg Institute, Australian Nuclear Science and Technology Organisation (ANSTO), Lucas Heights, NSW 2234, Australia

[3]University of Wollongong, Wollongong,, Australia

Statement of Authorship

Title of Paper	Prediction of welding stresses in WIC test and its application in pipelines
Publication Status	☑ Published ☐ Accepted for Publication ☐ Submitted for Publication ☐ Unpublished and Unsubmitted w ork w ritten in manuscript style
Publication Details	Alipooramirabad H, Paradowska AM, Ghomashchi R, Kotousov A, Hoye N. Prediction of welding stresses in WIC test and its application in pipelines. Materials Science and Technology. 2016;32(14):1462-70.

Principal Author

Name of Principal Author (Candidate)	Houman Alipooramirabad
Contribution to the Paper	I was responsible for the literature review required for this work, and idea development. I performed simulations and calculations, wrote the first draft of the manuscript and incorporated and addresses all comments and suggestions by other authors in subsequent revesions of the manuscript. Interpertation of the data was primary my responsibility.
Overall percentage (%)	95%
Certification:	This paper reports on original research I conducted during the period of my Higher Degree by Research candidature and is not subject to any obligations or contractual agreements with a third party that would constrain its inclusion in this thesis. I am the primary author of this paper.
Signature		Date	30/01/2017

Co-Author Contributions

By signing the Statement of Authorship, each author certifies that:
  i.   the candidate's stated contribution to the publication is accurate (as detailed above);
  ii.   permission is granted for the candidate in include the publication in the thesis; and
 iii. the sum of all co-author contributions is equal to 100% less the candidate's stated contribution.

Name of Co-Author	Anna Paradowska
Contribution to the Paper	I was supervisor of this work for the validating experiments at the ANSTO, and jointly contributed to refining the manuscript.
Signature		Date	02/02/2017

Name of Co-Author	Reza Ghomashchi
Contribution to the Paper	I was joint supervisor for the work, helped in developing ideas and contributed to refining the manuscript.

Signature		Date	31/01/2017

Name of Co-Author	Andrei Kotousov
Contribution to the Paper	I was joint supervisor of the work, and helped in developing ideas and contributed to refining the manuscript.

Signature		Date	02/02/2017

Name of Co-Author	Nicholas Hoye
Contribution to the Paper	I jointly contributed to conducting some part of the validating experiments.

Signature		Date	02/02/2017
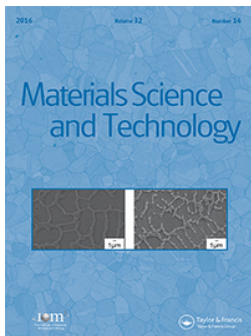
Prediction of welding stresses in WIC test and its application in pipelines

H. Alipooramirabad, A. M. Paradowska, R. Ghomashchi, A. Kotousov & N. Hoye

Published online: 20 Jul 2016.

Submit your article to this journal ⬀

Article views: 84

View related articles ⬀

View Crossmark data ⬀

Prediction of welding stresses in WIC test and its application in pipelines

H. Alipooramirabad[1], A. M. Paradowska[*2], R. Ghomashchi[1], A. Kotousov[1] and N. Hoye[2,3]

In the present study, the Welding Institute of Canada (WIC) restraint test was used to simulate the restraint conditions of full-scale girth welds on energy pipelines to ascertain the influence of welding process parameters on welding stresses. Finite element models are developed, and validated with neutron diffraction measurements, to evaluate the welding stresses for under-matched, matched and over-matched welds. The effects of heat input, wall thickness and variable restraint lengths of WIC sample are systematically investigated. As a practical outcome, this work can help in selection of the appropriate restraint length for WIC tests to simulate the specified stress conditions in the pipeline, and, ultimately, reduce the risk of Hydrogen Assisted Cold Cracking (HACC) in high strength low alloy.

This paper is part of a Themed Issue on Measurement, modelling and mitigation of residual stress.

Nomenclature

ρ	density
C	specific heat
T	temperature
t	time
$\{q\}$	heat flux
Q	the rate of internal heat generation
η	unit outward normal vector
h_f	film coefficient
T_B	bulk temperature of adjacent fluid
T_A	temperature at the surface of model
$[N]$	element shape functions
$\{T_e\}$	nodal temperature vector
$[C]$	$\rho \int C[N]^T[N]\mathrm{d}V$
$[K]$	$\int [B]^T[D][B]\mathrm{d}V + \int h_f[N][N]^T\mathrm{d}A$
σ	stress tensor
b_i	body force
$\{\Delta\sigma_e\}$	nodal stress incremental matrix
$\{D^{ep}\}$	$\{D^e\} + \{D^p\}$
$\{D^e\}$	elastic stiffness matrix
$\{D^p\}$	plastic stiffness matrix
$\{U_e\}$	nodal displacement vector
$\{\Delta T\}$	temperature increment matrix
$\{C^{\mathrm{th}}\}$	thermal stiffness matrix
$\{\Delta T_e\}$	nodal temperature matrix
$\{M\}$	temperature shape function
$\{F_e\}$	$\int Q[N]\,\mathrm{d}V + \int h_f T_B[N]\mathrm{d}A$
$\{\varepsilon\}$	strain vector
$\{u\}$	displacement vector

[1]Mechanical Engineering Department, University of Adelaide, Adelaide, Australia
[2]Australian Nuclear Science and Technology Organisation (ANSTO), Lucas Heights, Australia
[3]University of Wollongong, Wollongong, Australia

*Corresponding author, email anna.paradowska@ansto.gov.au

Introduction

The construction of Australian oil and gas pipeline networks is carried out using high strength low alloy (HSLA) steels line pipe and employing shielded metal arc welding (SMAW) in conjunction with hydrogen rich cellulosic consumables.[1] The application of cellulosic electrode at ambient temperature ensures good weld penetration and shorter construction lead time with huge cost saving.[2] The drawback however is the risk of hydrogen cracking emanated from high hydrogen content of cellulosic electrodes and the high levels of restraint as a result of clamping and lifting stresses the pipeline is subjected to during construction. The use of HSLA steels with low carbon contents ($\sim$0.05–0.09 wt-%) along with improvement in steel mechanical properties due to control rolling during line pipe manufacture has resulted the risk of Hydrogen Assisted Cold Cracking (HACC) formation to shift from the heat affected zone (HAZ) to weld metal (WM).[2,3] It is now firmly confirmed that the root pass is the most vulnerable and susceptible pass to HACC.[4]

The susceptibility of weldments to HACC is largely affected by three major factors of hydrogen content; microstructure; and stresses, all controlled by the steel and consumables chemistry and welding procedure. Several weldability tests and empirical evaluation procedures have also been proposed to assess the risk of HACC in particular structures, materials and different types of welds. These include the Tekken test,[5] Gapped bead on plate,[6] Lehigh U groove restraint[7] weldability tests, to mention just a few. A comprehensive overview of HACC phenomenon, theories, criteria and the most popular weldability tests can be found in the review paper by Yurioka and Suzuki.[8]

The Welding Institute of Canada (WIC) has developed a weldability test specifically intended to examine HACC in the WM. This test is widely considered to be the most representative of actual pipeline girth welding. It has been widely endorsed and utilised by the pipeline industry over the past 30 years[9] and was demonstrated to be capable of characterising the risk of HACC in both the HAZ and WM.[8,10,11] During the WIC test a single weld pass is deposited into a V groove, same size and geometry as the pipeline joint, machined out on between two restrained test plates attached to a T shaped strong backing as shown in Fig. 1. This similarity ensures that the thermal conditions are the same in the weldability test and the actual pipe welding. Therefore, one can expect a very similar microstructure as well as the same rate of hydrogen diffusion (two main factors affecting HACC in pipes) if the same welding regimes (parameters) and consumables are used. The third factor influencing HACC susceptibility, the welding stresses, is estimated by the level of restraint, i.e. restraint length – Fig. 1, selected for the WIC test coupon. This is a crude approach in estimating stresses generated during pipeline construction and considering the important role stresses play in HACC formation,[12] it is desirable to develop means that are able to simulate stresses better and evaluate the risk of HACC more accurately when qualify welding procedures.[8,10,11]

In the WIC test, the restraint conditions are controlled by the length of the anchor weld free region, i.e. the restraint length, see Fig. 1. The restraint length can simulate the girth weld root pass subjected to lifting, and a good correlation of cracking results between the WIC test and full-scale tests has been observed.[9,10] The restraint length also leads to similar thermal conditions and cooling rates in the weldability test and the actual pipe welding. The shims are used to create a gap between the testpiece and the backing bar, and hence facilitate welding. The backing T is used to provide high stiffness and prevent joint rotation. The welded joint is removed from the WIC sample, usually 24 h after welding completion by sawing the test assembly just inside the restraint length, avoiding the ends of the anchoring welds, and the weld zone is assessed for cracking.

The restraint (anchoring) length, see Fig. 1, can be varied from the standard length (25 mm) up to 150 mm. However, no direct link has been established so far between the welding parameters of the WIC test and the welding stresses. Only a limited number of experiments have been conducted to investigate the stress conditions in a WIC test. For example, North *et al.*,[12] and Alam *et al.*,[10] investigated the HACC risk in HSLA steel welding, using WIC test methodology. They found that the increasing restraint length not only leads to a decrease in restraint intensity, but it also reduces the cooling rate to allow more hydrogen effusion. In addition to stress reduction as a result of increasing the restraint length, both studies[10,12] reported that HACC is more likely to occur in WM rather than the HAZ of the HSLA parent metal of X70 and X80.

Simplified approaches were applied to evaluate the applied stresses, corresponding to different restraint lengths in the WIC test. For example, according to Alam *et al.*,[10] the magnitude of the restraint stress in the WIC test can be evaluated from the following semi-empirical relationship:

$$\sigma_R = 0.04 R_F \tag{1}$$

where R_F and σ_R are the restraint intensity and restraint stress, respectively. The restraint intensity (R_F) can be calculated as

$$R_F = \frac{Eh}{3.1L(1 + (hB/A))} \tag{2}$$

where E is Young's modulus, h is the plate thickness, L is the restraint length, B the weld length and A is the cross-
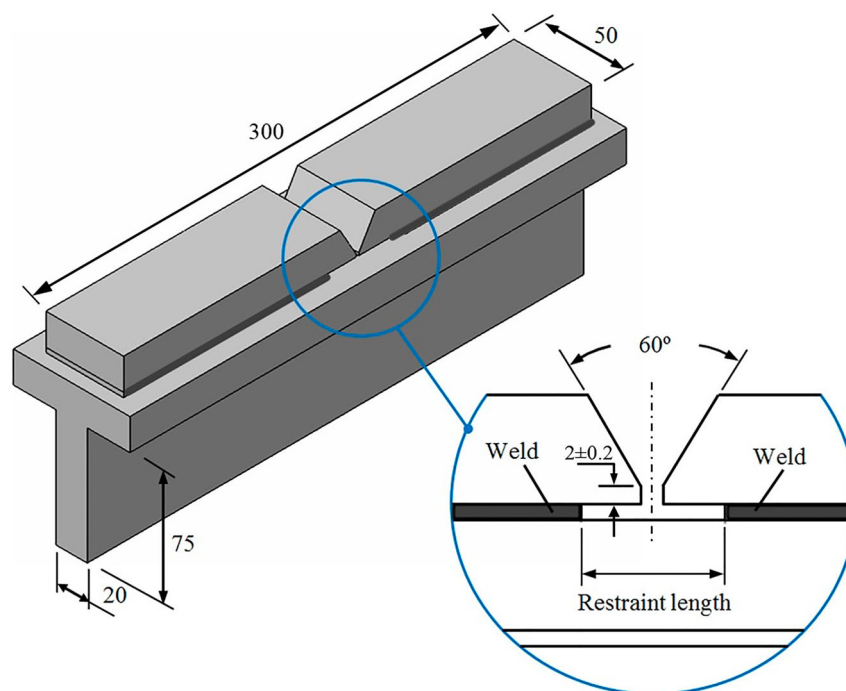
1   Geometry of Welding Institute of Canada (WIC) Test[8,10,11] (all dimensions are in mm)

sectional area of the restraining plates. However in the presence of undercuts and other defects restraint stress (σ_R) can be magnified such that the local stress (σ_L) is given by

$$\sigma_L = k \, (0.04 R_F) \qquad (3)$$

where k is the stress concentration factor (constant), which mainly related with defects in the root pass of the WIC test including undercuts, lack of fusion or an unusually convex root shape, for a particular welded geometry.

In particular, the above equation (3) predicts an increase in the local stress with an increase in the plate thickness and decrease of the restraint length, L. It is obvious that this simplified equation does not take into account many factors, for example, the relative strength of the WM and parent pipe, as well as the effect of the heat input, which are expected to influence significantly the magnitude of the local stresses.[13] Moreover, equation (3) ignores the existence of high residual stresses in the weld region.[14] Meanwhile, the combined effect of the restraint stress and welding residual stresses, which are in practice very difficult to separate, is expected to contribute to the risk of HACC as reported by Yurioka.[13]

The current study is therefore developed to address the issue of welding stresses generated due to self-restraint and external-restraint during welding. However, our focus is the root pass WM only, since, as mentioned before, it is the segment of the joint which is more susceptible to HACC cracking than the HAZ of parent metal. A number of transient 3D Finite Element models were developed to evaluate this stress and investigate the effect of various welding parameters (heat input, plate thickness and restraint length) on its magnitude for matched, under-matched and over-matched welds. The developed Finite Element models were validated against neutron diffraction measurements for the WIC sample; this provided a high level of confidence in the numerical approach. The outcomes of the numerical simulations can help to relate the stress conditions in the WIC test and the actual pipeline, and so, ultimately, reduce the risk of HACC. The adaptation of the WIC test methodology (instead a full-scale testing) for the development of safe welding procedures facilitating a fast construction of pipelines can result into significant financial benefits. In the following sections the numerical procedure is described, which is followed by presenting selected results of the validation study using neutron diffraction method. Further, the main outcomes of the simulation of the welding stresses in the WIC test are demonstrated.

Overview of the finite element model

The temperature, $T(x, y, z, t)$, as a function of spatial coordinates, (x, y, z), and time, (t), satisfies the following governing differential equation:

$$\frac{\partial}{\partial x}\left(k_x \frac{\partial T}{\partial x}\right) + \frac{\partial}{\partial y}\left(k_y \frac{\partial T}{\partial y}\right) + \frac{\partial}{\partial z}\left(k_z \frac{\partial T}{\partial z}\right) + \dot{Q}$$
$$= \rho C_p \frac{\partial T}{\partial t} \qquad (4)$$

where k_x, k_y and k_z are thermal conductivity in x, y and z directions, Q is the power generation per unit volume in the domain, ρ is the density, C_p is the specific heat. The

particular solution can be obtained by applying the appropriate initial and boundary conditions.

The initial conditions in the case of the uniform temperature distribution are:

$$T(x, y, z, 0) = T_0 \qquad (5)$$

The boundary condition on free surfaces can be written as:

$$k_n \frac{\partial T}{\partial n} + q_s + h_c(T - T_\infty) + \sigma \varepsilon F(T^4 - T_r^4) = 0 \qquad (6)$$

where k_n is the thermal conductivity normal to the surface, q_s the surface heat flux, h_c is the convection heat transfer coefficient, σ is the Stephan–Boltzman constant, F the configuration factor, ε the emissivity, T_∞ the surrounding temperature and T_r is the temperature of radiation heat source. Equation (4) incorporates both the thermal radiation and convection mechanisms of heat dissipation. From previous simulations of welding,[15,16] it was found that the radiation mechanism dominates for higher temperatures near and in the weld zone; and the convection mechanism governs the temperature field away from the weld zone or at low temperatures. In this work, the temperature-dependant heat transfer coefficient was employed similar to other numerical studies.[14,17] The temperature-dependant thermo-physical and mechanical properties corresponding to X80 was considered to be similar to the work conducted by Yan et al.,[18] and are all listed in Table 1 of the Appendix.

Standard Gaussian heat flux model was adopted to simulate the surface heat loading due to arc welding. In this model the surface flux, q, is fully symmetric and the flux density can be represented as:

$$q(r) = \left(\frac{3Q}{\pi r_b^2}\right) \exp\left[-3\left(\frac{r}{r_b}\right)^2\right], \qquad (7)$$

where $Q = \eta VI$ is the heat input, (η the heat source efficiency ($\eta = 0.9$ for SAW), V the welding voltage and I the welding current), r is the distance from the centre of the heat flux region and r_b is the radius of the region, which releases 95% of the total heat input, Q. In Finite Element simulations it was assumed that the weld torch is attached to the origin of the moving coordinate system. The coordinate system was therefore translated through the discrete domain of the Finite Element model based on the welding speed and the mesh size. The fluid flow and mass transfer (convective heat transfer in the weld pool) was not considered in the present work. To consider the heat effects related with the molten metal of the welded pool, an artificial rate of heat conductivity of around 2.5 times higher than the conductivity in room temperature was assumed at melting temperature to allow for the convective heat transfer, following the works of.[19–21]

The numerical results were obtained with ANSYS 14.5 software package utilising the eight-node 3D thermal element SOLID70 with a single degree of freedom at each node (temperature) for both parent and WM and a Newton–Raphson iterative procedure.

SOLID185 element is used for structural analysis. This 3D element is characterised by eight nodes, which have three degrees of freedom each: translations in the nodal x, y, and z directions. The analysis of stresses is conducted by using an uncoupled formulation, because the

dimensional changes were found negligible and the corresponding mechanical energy is insignificant when compared with the thermal energy from the welding arc. In the mechanical analysis, the time-dependent temperature field obtained from the transient thermal analysis was incorporated into the mechanical model. The thermally induced strains and stresses are then calculated at discrete times.

The elastic stress and strain state is modelled using the isotropic Hook's law with temperature-dependent isotropic elastic constants (Young's modulus and Poisson's ratio).

The plastic behaviour of the material is modelled by utilising a bilinear kinematics hardening model because material points typically undergo both loading and unloading in course of the welding process. The tangent modulus is considered to be 0.5% of the Young's modulus at corresponding temperature. This small value of strain hardening (small positive values of tangent modulus) was set to allow numerical convergence. Moreover in the studies conducted by Bhatti *et al.*,[22] Deng *et al.*[23] and Liang and Murakawa[24] it was assumed that the influence of strain hardening is insignificant and the material behaviour was considered to be elastic perfectly plastic model. The temperature-dependant mechanical properties considered in this work are listed in Table 1 of Appendix A.

Experimental validation

To verify the approach, the numerical results were compared against the experimental data obtained from neutron diffraction for the same materials and conditions as utilised in the FEM. The neutron diffraction measurements for the WIC sample were carried out at ANSTO, using KOWARI neutron strain scanner, Australia. The neutron diffraction is non-destructive deep scanning technique capable of measuring residual stresses non-destructively within the interior of components. This method utilises a beam of neutrons with a momentum p, and associated wavelength λ:

$$\lambda = \frac{h}{p} \qquad (8)$$

where h is the Planck's constant. When the neutron beam penetrates crystalline materials, a diffraction pattern with sharp maxima is produced. The diffraction pattern can be described in terms of Bragg's law:

$$2d_{hkl} \cdot \sin \theta_{hkl} = n\lambda , \qquad (9)$$

where d_{hkl} are the lattice spacing, n is an integer number representing the order of the reflection plane and θ is the angle between the incident ray and the scattering planes. A small change in the lattice spacing (Δd_{hkl}) will result in a change in the angular position of the diffraction peak ($\Delta \theta_{hkl}$) given by the following equation:

$$\Delta \theta_{hkl} = -\tan \theta_{hkl} \cdot \frac{\Delta d_{hkl}}{d_{hkl}} \qquad (10)$$

The lattice normal strain ε is given by:

$$\varepsilon = \frac{d_{hkl} - d_{0,hkl}}{d_{0,hkl}} = -\Delta d_{hkl} \cdot \cot \theta_{0,hkl}, \qquad (11)$$

Where $d_{0,hkl}$ is the strain-free lattice spacing for the *hkl*
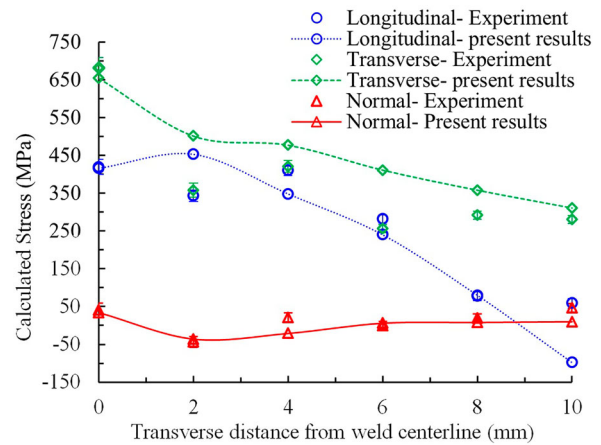
2 Comparison of the current approach with neutron diffraction measurements

planes, and $\theta_{0,hkl}$ is the diffraction angle of the unrestrained lattice.[25] The strains (ε_{xx}, ε_{yy}, ε_{zz}) convert to the three-dimensional stress (σ_{xx}, σ_{yy}, σ_{zz}) state by using the generalised Hooke's law, as follows:

$$\sigma_{xx} = \frac{E}{(1+\nu)(1-2\nu)}[(1-\nu)\varepsilon_{xx} + \nu(\varepsilon_{yy} + \varepsilon_{zz})] \quad (12)$$

Stresses in three directions can be calculated, using equation (12). It should be noted that the Young's modulus of 224 GPa and Poisson's ratio (ν) of 0.27 was used for stress calculations.[26] Figure 2 shows the distribution of residual stresses in tri-axial directions for both experimental and numerical results. As it can be seen reasonable agreement can be seen between the experimental and numerical results. Measurements of residual stresses were performed using the KOWARI instrument with neutron diffraction for the α-Fe (2 1 1) reflection using a nominal gauge volume of $2 \times 2 \times 2\text{mm}^3$. The experimental results were processed with SScanSS virtual laboratory software to determine the optimum sample orientations to minimise path length and hence count times during measurements. The measurements of the unstrained ($d0$) were performed on the free reference cube ($6 \times 6 \times 6\text{ mm}^3$).

As it can be seen from Fig. 2 the results of numerical simulations are generally in a good agreement with the experimental results. However, some discrepancies exist for the transverse stresses at distances 2 and 6 mm away from weld centreline. This can be explained through the lack of symmetry in the weld bead profile about the weld centreline which may result in the non-symmetric stress and strain profiles (neutron diffraction measurements) observed. The full details of experimental work and basic principles of neutron diffraction will be presented in the upcoming publications.

The welds were produced using a SMAW process using E8010 electrode. The welding parameters which was used during the experimental study is shown in Table 1.

Results and discussion

A set of 96 thermo-elasto-plastic 3D FE models was developed and numerical analysis was performed with ANSYS 14.5 APDL in accordance with the general methodology developed in.[27] The element length size in the

Table 1 Parameters used in the experimental work

Electrode diameter	4 mm
Current	133 [A]
Voltage	23.5 [V]
Travel speed	335 [mm min^{-1}]
Heat input range	0.56 [kJ mm^{-1}]
Polarity	DC$^+$

simulations was varied from 0.8 to 1.3 mm (Fig. 3). This mesh density represents the trade-off between the accuracy of the results and the computational time. The latter factor was very important considering the amount of computational work conducted. A mesh sensitivity analysis was also performed to determine the appropriate mesh size for the models. It was found that the results were varied slightly between the aforementioned element size and the models with higher mesh density, with the element sizes of 0.5(mm), 0.6 (mm) and 0.7 (mm).

Fixed supports are applied to the left and right ends of the FE model to simulate the effect of restraints as indicated in Fig. 3. All other faces of the FE model are free from stresses. The focus of the modelling was the investigation of the effects of heat input (0.3 and 0.5 kJ mm^{-1}), section thickness (between 8.6 and 20 mm) and restraint (anchoring) length (from 25 to 150 mm) on the maximum transverse residual stresses in WM (or at the centreline). The selected range of welding parameters corresponds to the actual welding conditions of the root pass of girth pipe welding in Australia, which are normally characterised by a low heat input and very high welding speed. For comparative purposes, the numerical simulations were performed for matched, under-matched and over-matched welds. The first two represent a major focus of the current study as these conditions are relevant to HSLA. For the under-matched weld the yield strength of WM is lower than the parent metal while for over-matched weld the yield strength of WM is higher than the parent metal, as specified in Table A.2 (Appendix A). Figure 4a–c shows the variations of the longitudinal, transvers and normal stresses, for matched weld, under-matched weld and over-matched welds (20 mm thickness, restraint length of 25 mm and heat input of 0.3 kJ mm^{-1}), respectively. The figures show that the magnitude of transverse residual stresses is higher than the other stress components (longitudinal and normal) for matched, under-matched and over-matched welds.
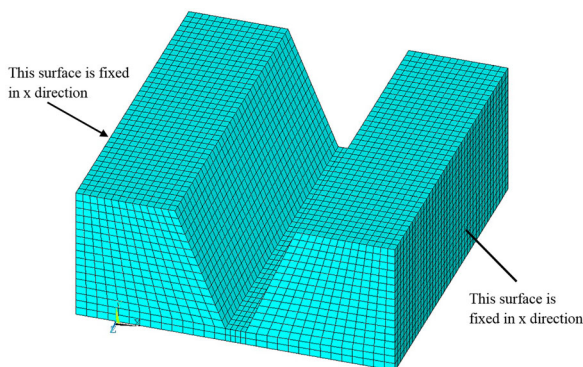
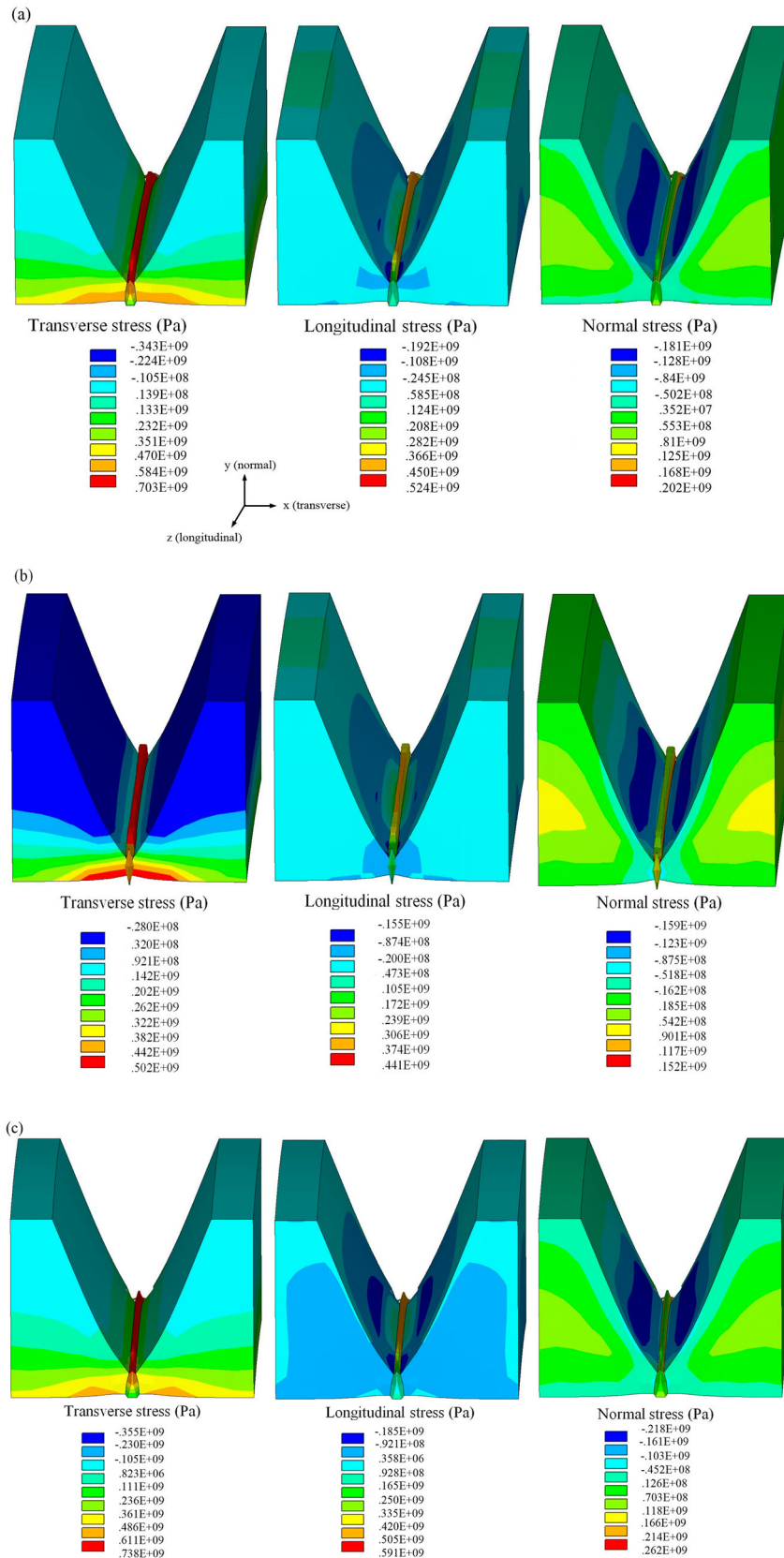**3 The snap shot of the FE mesh used for the analysis of WIC test**

In order to evaluate the effects of restraint (anchoring) length on the maximum transverse residual stresses in WIC samples, different restraint lengths (see Fig. 1) were considered in the numerical simulations, namely, 25 (standard), 50, 100 and 150 mm.

The results of the simulations were first compared with the empirical equation (3). According to Alam *et al.*,[10] for the standard restraint length of 25 mm, and with the 8.6 mm plate thickness, in the WIC test, the restraint intensity was $R_F = 16400$ N mm^{-2}, which produced an equivalent restraint stress (σ_R) of about 656 MPa. However due to conservative nature of WIC test, i.e. over-estimation of stresses, stress concentration factor (k) was considered to be 1 and therefore welding stresses is calculated to be 656 MPa which is a realistic value. Therefore the magnitude of local stresses is calculated to be 656 MPa.[10,28] Subsequently, the equation predicts an equivalent stress of about 656 MPa. In FE simulations for the same conditions, the maximum transverse residual stress was found to be 685 MPa (as shown in Fig. 5b), which indicates a very good agreement between two approaches for the specified welding conditions and weld geometry.[10]

Several WIC tests with an increased restrain length (reduced restraint intensities) were completed in Alam *et al.*[10] For the restraint length of 100 mm and plate thickness of 8.6 mm the welding stress was measured and found to be around 525 MPa. This restraint length corresponds to the restraint intensity of 4100 N mm^{-2}, restraint stress (σ_R) of 164 MPa and considering a stress concentration factor (k) of 3.2 for the root weld of WIC.[10,28] In the present FE simulation, the welding residual stress (for a restraint length of 100 mm and with a plate thickness of 8.6 mm) is predicted to be 562 MPa (as shown in Fig. 5b), which indicates a good correlation between the current approach and the experimental measurements for the considered plate thickness and matched weld. These values are plotted in the diagrams for comparison with the results obtained from the FE simulations. Figure 6 also shows the effects of restraint length on transverse stresses across the weld in 1 mm below the weld surface for the 12 mm plate thickness and heat input of 0.3 kJ mm^{-1}. The results of the FE simulations are also summarised in Tables A2 and A3 in the Appendixes. Below, we will briefly discuss the effect of various parameters on the magnitude of the welding stress in WIC samples.

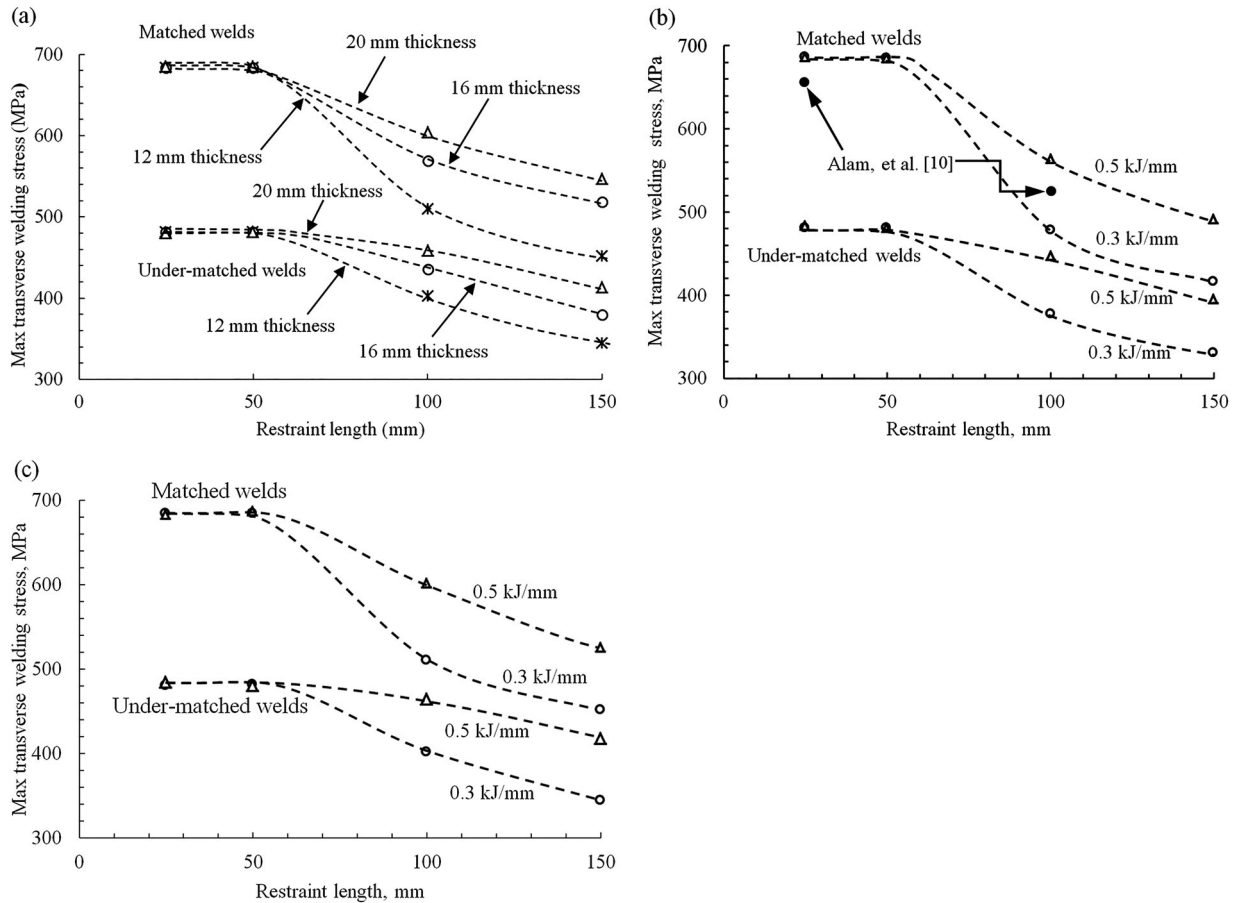## Effects of thickness on transverse welding stresses

Figure 5a shows the effect of the plate thickness on the magnitude of the welding stress in the centreline of the weld for matched and under-matched welds. The results for over-matched welds are undistinguished from those obtained for matched welds (when the yield stress of the parent material is the same as the WM). As expected, an increase of the plate thickness leads to an increase of welding stresses for the restraint lengths above a critical length, $L = 50$ mm, which was found to be the same for all combinations of welding parameters (heat input and plate thickness). This critical length generates a very high restraint intensity, which causes an extensive yielding in the WM for matched, under-matched and over-matched welds.

(a)

Transverse stress (Pa)

- -.343E+09
- -.224E+09
- -.105E+08
- .139E+08
- .133E+09
- .232E+09
- .351E+09
- .470E+09
- .584E+09
- .703E+09

Longitudinal stress (Pa)

- -.192E+09
- -.108E+09
- -.245E+08
- .585E+08
- .124E+09
- .208E+09
- .282E+09
- .366E+09
- .450E+09
- .524E+09

Normal stress (Pa)

- -.181E+09
- -.128E+09
- -.84E+09
- -.502E+08
- .352E+07
- .553E+08
- .81E+09
- .125E+09
- .168E+09
- .202E+09

y (normal)

x (transverse)

z (longitudinal)

(b)

Transverse stress (Pa)

- -.280E+08
- .320E+08
- .921E+08
- .142E+09
- .202E+09
- .262E+09
- .322E+09
- .382E+09
- .442E+09
- .502E+09

Longitudinal stress (Pa)

- -.155E+09
- -.874E+08
- -.200E+08
- .473E+08
- .105E+09
- .172E+09
- .239E+09
- .306E+09
- .374E+09
- .441E+09

Normal stress (Pa)

- -.159E+09
- -.123E+09
- -.875E+08
- -.518E+08
- -.162E+08
- .185E+08
- .542E+08
- .901E+08
- .117E+09
- .152E+09

(c)

Transverse stress (Pa)

- -.355E+09
- -.230E+09
- -.105E+09
- .823E+06
- .111E+09
- .236E+09
- .361E+09
- .486E+09
- .611E+09
- .738E+09

Longitudinal stress (Pa)

- -.185E+09
- -.921E+08
- .358E+06
- .928E+08
- .165E+09
- .250E+09
- .335E+09
- .420E+09
- .505E+09
- .591E+09

Normal stress (Pa)

- -.218E+09
- -.161E+09
- -.103E+09
- -.452E+08
- .126E+08
- .703E+08
- .118E+09
- .166E+09
- .214E+09
- .262E+09

4 **Typical results of numerical simulations for stress components; *a* matched weld; *b* under-matched weld; and *c* over-matched weld with 20 mm thickness, restraint length of 25 mm and heat input of 0.3 kJ mm^{-1}**

The effect of the plate thickness is also acknowledged in the simplified approach, equation (3), which indicates a proportional increase of the local stresses with an increase of the plate thickness. However, in comparison with this equation, the plate thickness effect is highly non-linear and disappears either with the decrease of the restraint length or with an increase of the restraint intensity.

5 **Maximum transverse welding stresses for matched and under-matched welds; *a* effects of restraint length and plate thickness when heat input is 0.3 kJ mm⁻¹, *b* and *c* effects of restraint length and heat input when plate thickness is 8.6 and 12 mm, respectively**

The simplified approach also assumes that the local stresses decrease with an increase of the restraint length. This is also confirmed by FE simulations but the dependence is different to L^{-1} as predicted by Alam *et al.*[10] It is also expected that the welding stress will reach saturation (plateau) at low restraint intensities, which will represent the welding residual stress in the free from restraint specimen. However, this level is not reached with the maximum restraint length of 150 mm in the WIC test.

Effects of heat input on transverse welding stresses

Figure 5*b* and *c* shows the effect of the heat input on the generation of welding stresses for different restraint lengths and plate thicknesses. As can be seen, the generated welding stresses are higher for higher heat inputs above the critical restraint length. This is attributed to the higher portion of thermal energy which is transformed into strain energy associated with welding stresses. Therefore, the use of lower heat inputs, i.e. higher travel speeds, in girth welding provides not just shorter construction times as highlighted in the introduction but also generates lower welding stresses. However, low heat input also results in shorter cooling times, which in turn increases the susceptibility of the welded joint to HACC directly related to the microstructure. Therefore, there are two competitive mechanisms affecting HACC formation with the changes in heat input which seems to be

dominated by the latter, shorter cooling times and more susceptible microstructure. Again, the effect of heat input on welding stress takes place only for relatively low restrain intensity (larger restraint lengths), which can be related to small plate thicknesses and small pipeline diameters. For large diameter pipes, the effect of the heat input is expected to be negligible as the welding stress
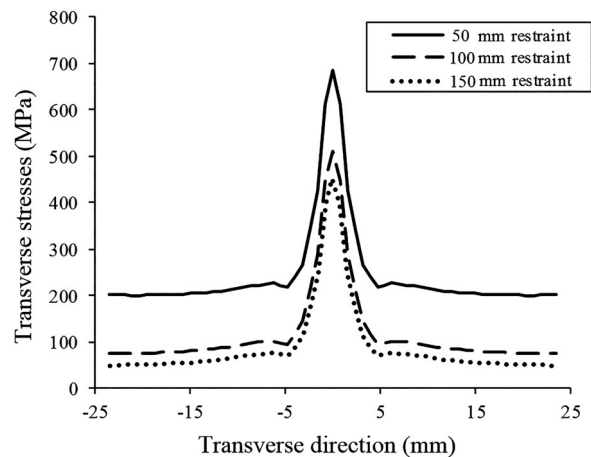
6 **Effects of restraint length on transverse stresses across the weld (heat input is 0.3 kJ mm⁻¹ and plate thickness of 12 mm)**

reaches a plateau and the stresses are limited by the lowest value of yield stress either WM or parent material. It should be noted that transverse stress is the stress in the transverse direction to the welding. The maximum transverse stress is located in 1 mm below the weld surface in the middle of the specimen. In general, the obtained numerical results follow the tendencies of equation (3) and numerical values correlate rather well for a particular plate thickness of 8.6 mm for matched welds only, see Fig. 5b. However, this simplified equation fails to describe many other features as highlighted above.

Conclusions

In this paper welding stresses in WIC tests are evaluated with different restraint lengths. Also the effect of basic welding parameters, corresponding to pipeline girth welding (low heat input and relatively high welding speed), on the magnitude of this stresses in WM are investigated. The key findings of this study were:

- The present results of the calculations generally support general tendencies incorporated into the empirical equation of Alam *et al.*,[10] such as an increase of the welding stresses with an increase of the plate thickness and restraint intensity. Despite the correct tendencies, the difference between numerical and the empirical equation are not within a reasonable range, especially for the samples with higher thickness values.
- The numerical results indicate the existence of the critical restraint length (between 25 and 50 mm), below which the further decrease of the restraint length has no effect on the welding stress field.
- The welding stresses depend significantly on the heat input, specifically at low restraint intensity or for relatively small diameter pipelines and small wall thicknesses. This is an interesting justification for the use of low heat inputs at least for the first weld pass, which is the most critical with respect to the risk of HACC. On the other hand, low heat inputs also lead to higher cooling rates of the WM which in turn can result in trapping more hydrogen within the weld. However, it is not clear how these trade-off (lower cooling time and lower welding stresses) affects the overall risk of HACC.[1] This should be subject to further investigation.
- Finally, the numerical results were obtained and tabulated for a wide range of welding parameters corresponding to pipeline girth welding. These results can be used to relate the actual conditions to the welding conditions of the small-scale weldability test (WIC test). Of course, these results have to be used with caution as even the most sophisticated FE studies are currently unable to capture all features and effects associated with the extremely complex processes accompanying welding procedures. However, these studies can be extremely useful to guide the design of welding procedures.

Acknowledgements

References

1. A. Kotousov, K. Borkowski, L. Fletcher and R. Ghomashchi: 'A model of hydrogen assisted cold cracking in weld metal', 9th International Pipeline Conference: American Society of Mechanical Engineers, 2012, 329–334.
2. R. Ghomashchi, W. Costin and R. Kurji: 'Evolution of weld metal microstructure in shielded metal arc welding of X70 HSLA steel with cellulosic electrodes: A case study', *Mater. Charact.*, 2015, **107**, 317–326.
3. M. Law, D. Nolan and R. Holdstock: 'Method for the quantitative assessment of transverse weld metal hydrogen cracking', *Mater. Charact.*, 2008, **59**, 991–997.
4. R. Kurji, J. Griggs, V. Linton, A. Kotooussov, E. Gamboa, R. Ghomashchi and N. Coniglio: 'An improved Welding Institute of Canada test for evaluation of high-strength pipeline steel weldability', International Pipeline Technology Conference (06 Oct 2013–09 Oct 2013: Ostend) 2013.
5. H. Suzuki, N. Yurioka and M. Okumura: 'A new cracking parameter for welded steels considering local accumulation of hydrogen', *Transactions of the Japan Welding Society*, 1982, **13**, 3–12.
6. Z. Sterjovski, M. Pitrun, D. Nolan, D. Dunne and J. Norrish: 'Artificial neural networks for predicting diffusible hydrogen content and cracking susceptibility in rutile flux-cored arc welds', *J. Mater. Process. Technol.*, 2007, **184**, 420–427.
7. A. Glover and B. Rothwell: Specifications and practices for hydrogen crack avoidance in pipeline girth welds. First International Conference on Weld Metal Hydrogen Cracking in Pipeline Girth Welds, Wollongong, Australia1999. p. 13.1–0.8.
8. N. Yurioka and H. Suzuki: 'Hydrogen assisted cracking in C-Mn and low alloy steel weldments', *Int. Mater. Rev.*, 1990, **35**, 217–249.
9. B. A. Graville: 'Interpretive report on weldability tests for hydrogen cracking of higher strength steels and their potential for standardization', 1995, WRC Bulletin, available at https://forengineers.org/bulletin/wrc-400.
10. N. Alam, D. Dunne and F. Barbaro: Weld metal crack testing for high strength cellulosic electrodes. First International Conference on Weld Metal Hydrogen Cracking in Pipeline Girth Welds, Wollongong, Australia1999. p. 9.1–9.23.
11. E. Signes and P. Howe: 'Hydrogen-assisted cracking in high-strength pipeline steels', *Weld J.*, 1988, **67**, 1635–1705.
12. T. North, A. Rothwell, A. Glover and R. Pick: 'Weldability of high strength line pipe steels', *Weld J.*, 1982, **61**, 243–257.
13. N. Yurioka: Predictive methods for prevention and control of hydrogen assisted cold cracking, IIW Doc. IX-1938–99; 1999.
14. D. Deng and H. Murakawa: 'Numerical simulation of temperature field and residual stress in multi-pass welds in stainless steel pipe and comparison with experimental measurements', *Comput. Mater. Sci.*, 2006, **37**, 269–277.
15. Y. Ueda, H. Murakawa and N. Ma: 'Welding deformation and residual stress prevention', 2012, Osaka, Elsevier.
16. L.-E. Lindgren: 'Finite element modeling and simulation of welding part 1: Increased complexity', *J. Therm. Stresses*, 2001, **24**, 141–192.
17. F. Vakili-Tahami and A. Ziaei-Asl: 'Numerical and experimental investigation of T-shape fillet welding of AISI 304 stainless steel plates', *Mater. Des.*, 2013, **47**, 615–623.
18. C. Yan, C. Liu and B. Yan: '3D modeling of the hydrogen distribution in X80 pipeline steel welded joints', *Comput. Mater. Sci.*, 2014, **83**, 158–163.
19. C.-H. Lee and K.-H. Chang: 'Temperature fields and residual stress distributions in dissimilar steel butt welds between carbon and stainless steels', *Appl. Therm. Eng.*, 2012, **45–46**, 33–41.

20. B. Taljat, B. Radhakrishnan and T. Zacharia: 'Numerical analysis of GTA welding process with emphasis on post-solidification phase transformation effects on residual stresses', *Mater. Sci. Eng. A*, 1998, **246**, 45–54.
21. D. Deng, H. Murakawa and W. Liang: 'Numerical and experimental investigations on welding residual stress in multi-pass butt-welded austenitic stainless steel pipe', *Comput. Mater. Sci.*, 2008, **42**, 234–244.
22. A. A. Bhatti, Z. Barsoum, H. Murakawa and I. Barsoum: 'Influence of thermo-mechanical material properties of different steel grades on welding residual stresses and angular distortion', *Mater. Des.*, 2015, **65**, 878–889.
23. D. Deng, W. Liang and H. Murakawa: 'Determination of welding deformation in fillet-welded joint by means of numerical simulation and comparison with experimental measurements', *J. Mater. Process. Technol.*, 2007, **183**, 219–225.
24. W. Liang and H. Murakawa: 'An inverse analysis method to estimate inherent deformations in thin plate welded joints', *Mater. Des.*, 2012, **40**, 190–198.
25. H. Alipooramirabad, A. Paradowska, R. Ghomashchi, A. Kotousov and M. Reid: 'Quantification of residual stresses in multi-pass welds using neutron diffraction', *J. Mater. Process. Technol.*, 2015, **226**, 40–49.
26. H. Alipooramirabad, R. Ghomashchi, A. Paradowska and M. Reid: 'Residual stress-microstructure-mechanical property interrelationships in multipass HSLA steel welds', *J. Mater. Process. Technol.*, 2016, **231**, 456–467.
27. Swanson Analysis Systems. ANSYS Version14.5. 2012.
28. R. Singh: Weld cracking in ferrous alloys: London, Elsevier; 2008.

Appendix A

Table A.1   Thermo-physical properties and mechanical properties of X-80 (high strength low carbon steel)[19]

Temperature (°C)	Specific heat/J Kg°C	Conductivity/ J m°C s	Yield stress/MPa	Thermal expansion/°C^{-1}	Young's modulus/Gpa	Density g cm^{-3}
20	423	54.42	560	11.0×10^{-6}	210.0	7.81
100	473	54.01	540	11.5×10^{-6}	207.0	7.79
200	536	52.75	525	12.2×10^{-6}	204.0	7.77
400	662	47.71	485	1.35×10^{-5}	187.50	7.72
800	914	27.55	70	1.48×10^{-5}	118.600	7.61
1200	1160	40.00	12	1.34×10^{-5}	39.50	7.50
1500	652	120	8	…	–	7.48

Table A.2   The yield strength of WM for the under-matched and over-matched weld

Temperature (°C)	Under-matched weld	Over-matched weld
20	420	645
100	408	612
200	390	581
400	358	525
800	53	101
1200	9	21
1500	8.5	14

Table A.3   Maximum transverse residual stresses (MPa) with the heat input of 0.3 kJ mm^{-1}

	Thickness (mm)															
	8.6				12				16				20			
Restraint length (mm)	25	50	100	150	25	50	100	150	25	50	100	150	25	50	100	150
Matched welds	686	685	478	415	684	682	510	452	684	682	570	517	684	683	604	546
Under-matched welds	482	481	377	330	482	480	401	345	482	481	436	380	483	482	458	413
Over-matched welds	716	713	493	424	718	716	516	461	721	718	588	534	719	717	608	566

Table A.4   Maximum transverse residual stresses (MPa) with the heat input of 0.5 kJ mm

	Thickness (mm)															
	8.6				12				16				20			
Restraint length (mm) Length mmmmmmm(mm)	25	50	100	150	25	50	100	150	25	50	100	150	25	50	100	150
Matched welds	686	685	565	491	685	683	601	525	688	684	642	580	691	686	667	620
Under-matched welds	484	480	446	395	484	481	464	418	487	484	479	452	489	485	481	473
Over-matched welds	719	717	563	494	722	718	613	532	725	722	655	588	726	718	677	638

CHAPTER 5

QUANTIFICATION OF RESIDUAL STRESSES IN MULTI-PASS WELDS USING NEUTRON DIFFRACTION

Houman Alipooramirabad[1]*, Anna Paradowska[2], Reza Ghomashchi[1], Andrei Kotousov[1] and Mark Reid[2]

[1]School of Mechanical Engineering, the University of Adelaide, SA 5005

[2] Bragg Institute, Australian Nuclear Science and Technology Organisation (ANSTO), Lucas Heights, NSW 2234, Australia

Statement of Authorship

Title of Paper	Quantification of residual stresses in multi-pass welds using neutron diffraction
Publication Status	☑ Published ☐ Accepted for Publication ☐ Submitted for Publication ☐ Unpublished and Unsubmitted work written in manuscript style
Publication Details	Alipooramirabad H, Paradowska A, Ghomashchi R, Kotousov A, Reid M. Quantification of residual stresses in multi-pass welds using neutron diffraction. Journal of Materials Processing Technology. 2015;226:40-9.

Principal Author

Name of Principal Author (Candidate)	Houman Alipooramirabad		
Contribution to the Paper	I was responsible for the literature review required for this work, and designed the framework for the experimental conditions. I carried out mechanical property analysis, wrote the first draft of the manuscript and incorporated and addresses all comments and suggestions by other authors in subsequent revesions of the manuscript. Interpertation of the data was primary my responsibility.		
Overall percentage (%)	90%		
Certification:	This paper reports on original research I conducted during the period of my Higher Degree by Research candidature and is not subject to any obligations or contractual agreements with a third party that would constrain its inclusion in this thesis. I am the primary author of this paper.		
Signature		Date	30/01/2017

Co-Author Contributions

By signing the Statement of Authorship, each author certifies that:

    i.   the candidate's stated contribution to the publication is accurate (as detailed above);

    ii.   permission is granted for the candidate in include the publication in the thesis; and

    iii.   the sum of all co-author contributions is equal to 100% less the candidate's stated contribution.

Name of Co-Author	Anna Paradowska		
Contribution to the Paper	I was supervisor of this work while it was carried out in the Australian Nuclear Science and Technology Organization (ANSTO), and jointly contributed to refining the manuscript.		
Signature		Date	02/02/2017

Name of Co-Author	Reza Ghomashchi		
Contribution to the Paper	I was joint supervisor for the work, and contributed to refining the manuscript.		
Signature		Date	31/01/2017

Name of Co-Author	Andrei Kotousov		
Contribution to the Paper	I was joint supervisor of the work, and contributed to refining the manuscript.		
Signature		Date	02/02/2017

Name of Co-Author	Mark Reid		
Contribution to the Paper	I jointly contributed to conducting some part of the experiments at the Australian Nuclear Science and Technology Organization (ANSTO) .		
Signature		Date	31/01/2017

Quantification of residual stresses in multi-pass welds using neutron diffraction

Houman Alipooramirabad [a,*], Anna Paradowska [b], Reza Ghomashchi [a], Andrei Kotousov [a], Mark Reid [b]

[a] *School of Mechanical Engineering, The University of Adelaide, SA 5005, Australia*
[b] *Bragg Institute, Australian Nuclear Science and Technology Organisation (ANSTO), Lucas Heights, NSW 2234, Australia*

ARTICLE INFO

ABSTRACT

Neutron diffraction results highlighted the effect of heat input through changes of travel speed and welding sequence (direction) on the residual stresses in multi-pass weldments of high strength low alloy steel. Residual stresses in excess of yield strength were developed in the weld metal and HAZ particularly for the upper-layers of welds which were not affected by the tempering of the subsequent weld layers. The magnitude of the residual stresses was significantly reduced by increasing the heat input. There was no substantial difference in the magnitude of the residual stresses when the direction of weld deposition was varied but the distribution was more uniform.

1. Introduction

Local plastic deformation resulted from thermal and mechanical processing of fabricated structures is the prime cause of residual stresses generated during a range of manufacturing processes. For welding, the non-uniform temperature distribution and cooling rates are responsible for residual stresses form in welded structures. The nature and magnitude of residual stresses have significant effect on the integrity and life span of welded structures and could be beneficial or detrimental. Barsoum and Barsoum (2009) showed tensile residual stresses reduce fatigue life by increasing fatigue crack growth rate while compressive residual stresses have the reverse effect. There is similar trend for stress corrosion cracking (SCC), as the numerical analysis coupled with experimental work by Mochizuki (2007) confirm higher susceptibility of welded joints to SCC with increasing residual stresses. Cheng et al. (2003) also confirmed the deterimental effect of tensile residual stresses on the structural integrity of welded structures through significant acceleration of the growth rate of the defects, such as micro-cracks and creep voids.

The magnitude and distribution of residual stresses are greatly influenced by the welding procedure and parameters and joint geometry. However, when the effects of individual parameters are scrutinized, there are some contradicting reports generating uncertainty in their applications in real life cases. It is expected the value of heat input to be inversely related to the magnitude of residual stresses where a higher heat input is to result in less stressed weld joint (Jiang et al., 2011). However, since heat input is a combination of welding travel speed, and applied current and voltage, its effects become less straight forward. In other words, the general trend mentioned above may vary depending on the heat input changes originated from changes in welding travel speed or applied current. Ranjbarnodeh et al. (2011) reported that an increase in heat input due to increased current (constant travel speed) reduces the magnitude of longitudinal residual stresses. For travel speed, Peel et al. (2003) showed an increase in heat input due to reduction in travel speed is beneficial in reducing residual stresses in weldment. In contradiction to the above-mentioned studies, Akbari and Sattari-Far (2009), using experimentally validated FEA, demonstrated decreasing heat input due to reduction in current and voltage decreases the magnitude of residual stresses. Numerical simulations by Qureshi (2008) on the effect of weld travel speed ($2\,\mathrm{mm\,s^{-1}}$, $3\,\mathrm{mm\,s^{-1}}$ and $4\,\mathrm{mm\,s^{-1}}$) on residual stresses in a thick-walled cylinder confirmed higher magnitudes of residual stresses at lower travel speed ($2\,\mathrm{mm\,s^{-1}}$), i.e. higher heat input.

In addition to heat input effects on residual stresses, for multi pass welding which is the theme of this report, the weld sequence including the direction of weld passes could alter the magnitude of residual stresses. Mochizuki (2007) and Deng (2013) studied the effect of the deposition sequence on residual stresses and reported a significant effect on the distribution and magnitude of residual stress. However, there is not much report on the issue of reversing the welding direction effect on the residual stresses although the FEA modelling by Ji et al. (2005) have shown that the peak values of longitudinal and transverse residual stresses decrease by 16.9% and 18.2% in welding in inverse direction in comparison with the welding in the same direction. They did not report any significant changes in the distribution of residual stresses.

Therefore, the main aim of the current work was to investigate the effects of welding heat input (travel speed) and reversing the welding sequence (direction) on the residual stresses in a most common situation of multi-pass welding of high strength low alloy steel.

2. Neutron diffraction

A range of experimental techniques were developed for the measurement of residual stresses and used by different investigators (Javadi and Najafabadi, 2013), ultrasonic, (Sattari-Far and Farahani, 2009), hole drilling, (Mahmoodi et al., 2012), layer removal techniques, (Withers and Bhadeshia, 2001), X-ray and (Pardowska et al., 2008), neutron diffractions. However, as pointed out by Paradowska et al. (2006) the latter technique (neutron diffraction) allows the measurement of residual stresses for most metals and alloys with an effective depth of measurements up to several centimetres, which covers many practical applications including multi-pass welding as the theme of the current report.

Neutron diffraction method represents a non-destructive deep scanning technique for generation of three-dimensional strain maps in engineering components. This method utilises a beam of neutrons with a momentum p, and associated wavelength λ:

$$\lambda = \frac{h}{p} \tag{1}$$

where h is the Planck's constant. When the neutron beam penetrates crystalline materials, a diffraction pattern with sharp maxima is produced. The diffraction pattern can be described in terms of Bragg's law, see Fig. 1 for illustration:

$$2d_{hkl} \times \sin\theta_{hkl} = n\lambda, \tag{2}$$

where d_{hkl} is the lattice spacing, n is an integer number representing the order of the reflection plane and θ is the angle between
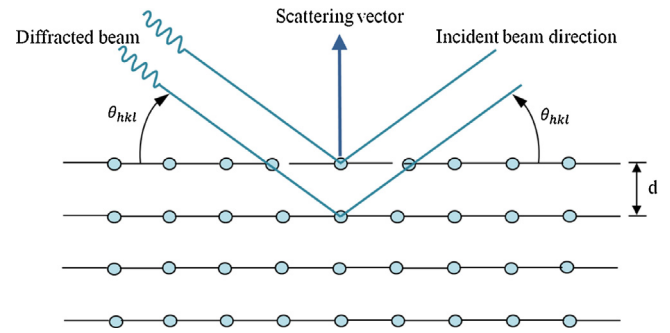

Fig. 1. Schematic illustration of Bragg's law.

the incident ray and the scattering planes as shown in Fig. 1. A small change in the lattice spacing (Δd_{hkl}) will result in a change in the angular position of the diffraction peak ($\Delta\theta_{hkl}$) given by the following equation:

$$\Delta\theta_{hkl} = -\tan\theta_{hkl} \times \frac{\Delta d_{hkl}}{d_{hkl}} \tag{3}$$

The lattice normal strain ϵ is given by:

$$\epsilon = \frac{d_{hkl} - d_{0,hkl}}{d_{0,hkl}} = -\Delta\theta_{hkl} \times \cot\theta_{0,hkl}, \tag{4}$$

where $d_{0,hkl}$ is the strain-free lattice spacing for the hkl planes, and $\theta_{0,hkl}$ is the diffraction angle of the unrestrained lattice (Grünitz, 2004).

The strains can be measured in an arbitrary directions and the magnitude of residual stresses can be found using the generalised Hooke's law. In this study, the measurements of strains were conducted in three directions; longitudinal (parallel to the welding direction), transverse (perpendicular to the weld) and normal to the plate (through thickness), as illustrated in Fig. 2.

Details of instruments set up and other general principles of neutron diffraction method can be found in the works done by Park et al. (2004) for T-type and a double V butt joint welded stainless steel specimens and Webster and Wimpory (2001) for different practical welding applications.

3. Experiemental procedures

3.1. Weld deposition

The root pass of all V-prep weld joints was completed with modified short arc welding (MSAW); and flux cored arc welding
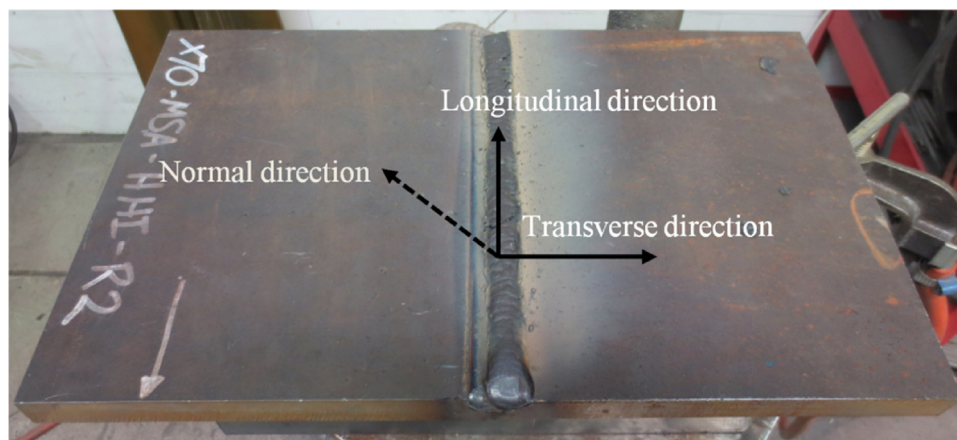

Fig. 2. Welding specimen showing three directions of strain measurements.
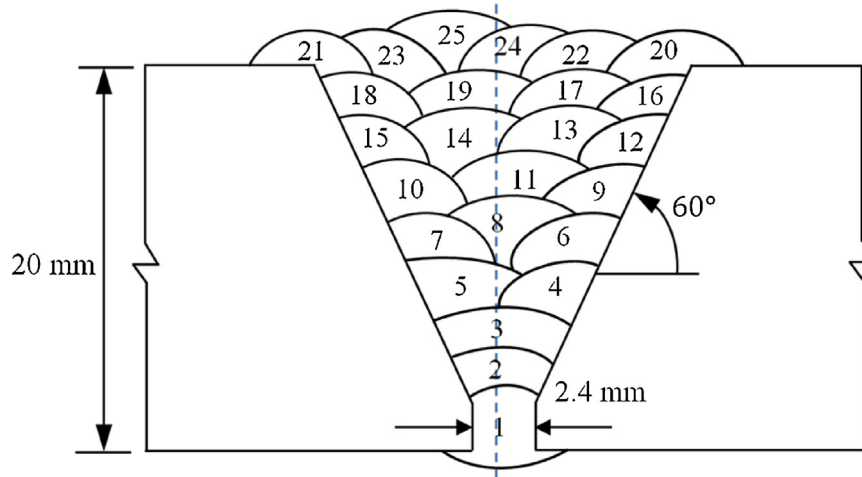
Fig. 3. Weld deposition sequence in Specimen I.

process (FCAW) was utilised for the remaining passes, which is quite common in modern welding procedures. The MSAW offers many advantages including low distortion, freedom from spatter, high quality of welded joints and lower cost including post-weld machining. FCAW ensures high deposition and productivity rates. It does not require a highly trained personnel; the process is less complex and more adaptable than other types of welding, such as submerged arc welding. The root pass was completed with ER70s-6 welding wire; and the remaining passes with E81TNi class Flux cored wire. The yield strength of ER70s-6 welding wire is 482 MPa while the yield strength of E81TNi class Flux cored wire is about 470 MPa. The chemical composition for ER 70s-6 and E81TNi wires can be seen in Table 1 of the Appendix A.

The test specimens comprised two 20 mm thick steel plates (API 5L grade X70) with the dimensions of 250×200 mm. The selected sample size was based on minimizing the end-effects during welding to provide sufficient weld length with uniform thermal distribution for residual stresses measurements. This was confirmed by simple analytical modelling and FE calculations as reported by Lu et al. (1999) and Kotousov (2000). These specimen dimensions also exceed those used in the previous studies (Paradowska et al., 2006; Pardowska et al., 2008). Therefore, the outcomes of the present experiments can be applicable to a wide range of geometries and situations.

The yield strength of the parent metal is about 485 MPa. The preparatory joint geometry is shown in Figs. 3 and 4. A total of six (6)
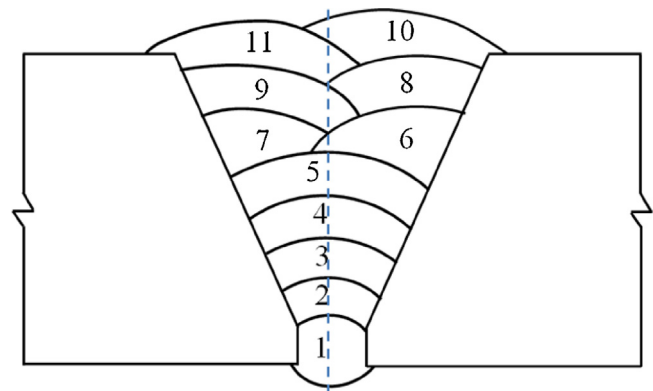
Fig. 4. Weld deposition sequence in Specimens II and III.

samples were fabricated. Three samples were used to measure the lattice spacing ($d_{0,hkl}$) in stress free mode and the other 3 samples were used to evaluate the residual stresses.

Specimen series I: The welding direction was the same for all passes. The weld run placement sketch for this welding process is shown in Fig. 3. The welding specification is provided in Table 2 of the Appendix A. Fig. 3 also specifies the preparatory geometry of all samples.
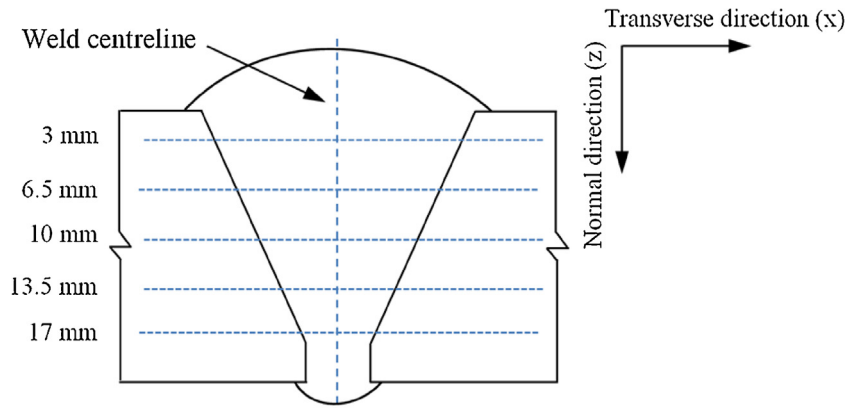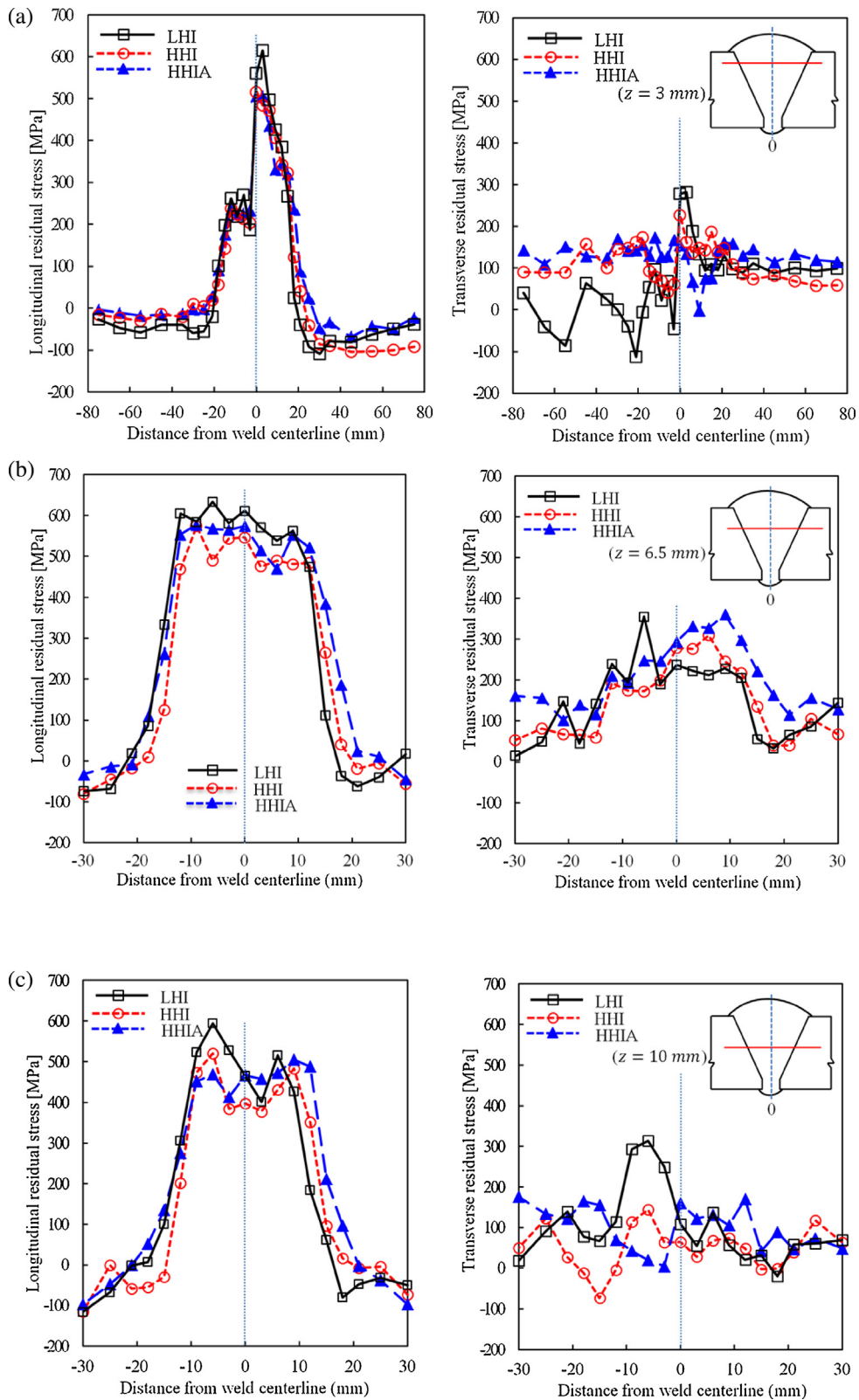

Fig. 5. Schematic of measurement points.

Fig. 6. Effects of heat input and pass sequence on longitudinal and transverse residual stresses: (a) 3 mm from the top surface (b) 6.5 mm (c) 10 mm (d) 13.5 mm and (e) 17 mm from the top surface; LHI—low heat input specimen (Specimen I), HHI—high heat input (Specimen II), HHIA: high heat input alternate weld sequence (Specimen III).
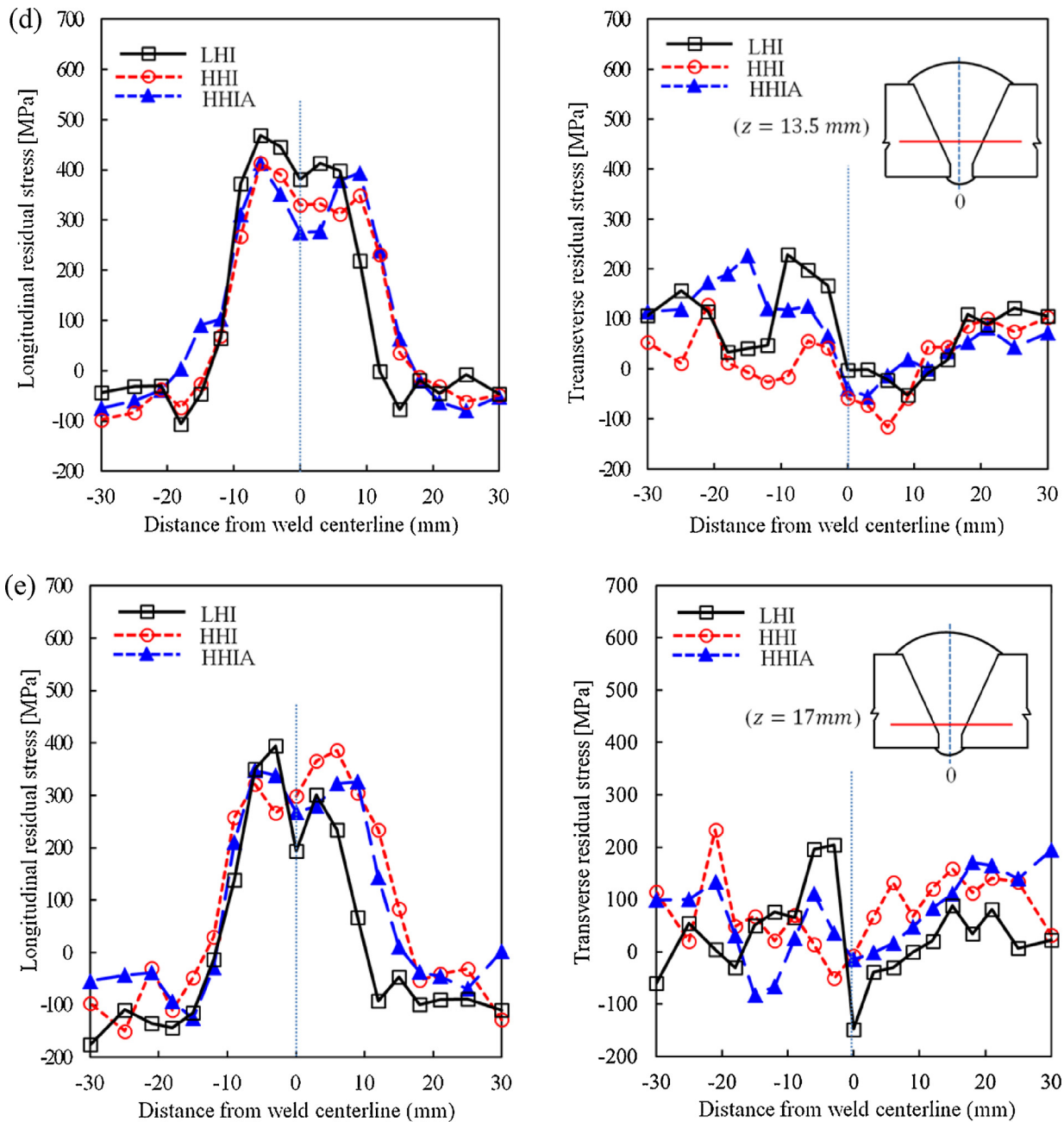
Fig. 6. (Continued).

Specimen series II: The number of weld runs is reduced to 11, and the speed of weld runs was lower than specimen series I (heat input of each run is higher than those of the Specimen series I). The weld runs in Specimen series II were also deposited in the same direction. The welding specification is provided in Table 3 of the Appendix A. The weld deposition sketch of Specimen series II is shown in Fig. 4.

Specimen series III: The welding parameters and the number of passes are the same as for Specimen series II. The converse welding sequence (alternating directions) was used to complete the weld.

3.2. Measurement procedure

Residual stress measurements were performed at ANSTO using KOWARI strain scanner and a $3 \times 3 \times 3\,mm^3$ gauge volume. The Si

(400) type double focusing monochromator generated a neutron beam with the wavelength of 1.67 Å. A detector angle, 2θ, was set at 90° corresponding to the αFe (211) diffraction peak. The locations of measurement points are shown in Fig. 5. Positioning of the gauge volume within the sample surface is very important for the near surface measurements with neutron diffraction method. In the present study, this was achieved by utilizing 'entering curves' by which the gauge volume position can be placed with a high precision with respect to the specimen surface (Cheng et al., 2003).

Residual strains were evaluated at 258 points (86 points for each sample) in three principal directions. To determine the diffraction angle for the unrestrained lattice, $\theta_{0,211}$, the reference samples were stress relieved by sectioning through thickness using electro-discharge machining (EDM) with a wire diameter of 0.2 mm. Counting times were determined by the accuracy required for the strain measurements. Counts were collected until the peak was

clearly identified. The reference samples were examined in three principal directions to account for variation in chemical composition heterogeneity around the weld and HAZ.

4. Results and discussion

The results are presented for residual stresses evaluated across the weld (transverse direction) and through thickness (normal direction) and the effect of welding heat input and sequence (direction) is discussed, respectively.

4.1. Across the weld

4.1.1. Heat input (welding speed)

The effect of heat input (welding speed) on residual stresses should be extracted from comparison of the residual stress distribution for Specimens I and II. The heat input was controlled by weld travel speed since the welding voltage and current were kept constant. A total of twenty five (25) weld runs were deposited for Specimen I (Low Heat Input specimen-LHI) and 11 for Specimen II (High Heat Input specimen-HHI). Fig. 6(a–e) shows the longitudinal and transverse residual stresses for both heat inputs.

The highest residual stresses have been experienced in longitudinal direction for both high and low heat input samples at a depth of 6.5 mm below the surface. The highest value of the generated residual stress is about 120–150 MPa above the nominated weld yield strength of both the parent and weld metals. It is also evident that increasing the heat input decreases the longitudinal residual stresses notably. The maximum difference in longitudinal residual stress for low and high input welds was 145 MPa at a depth of 10 mm below the plate free surface. A similar trend was also found for transverse residual stresses where the peak stress was lower for higher heat input. This difference in some cases could even reach up to 220 MPa. However, there is a distinct difference on the magnitude of residual stresses in transverse direction which is almost half of that for longitudinal direction. It is worth noting that in most cases the highest magnitude of both longitudinal and transverse residual stresses was experienced within the HAZ. In addition, with the increase of heat input, the fusion zone and HAZ area also increased. As a result, the maximum tensile residual stresses (longitudinal stresses) were located further away from weld centreline for the samples with higher heat input. The distribution of longitudinal and transverse residual stresses, Fig. 6(c and d), agrees with the results reported by Kim et al. (2009) who employed finite element simulation and neutron diffraction measurements for a V-butt steel. Also consistent trend can be found for the distribution of longitudinal residual stresses with the study (using experimentally validated FEA) carried out by Venkata et al. (2014). The consis-
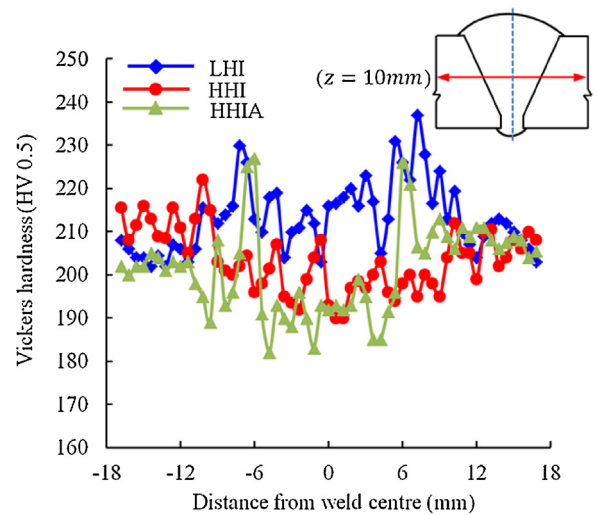

Fig. 7. Microhardness profile showing hardness across the weld at 10 mm below the surface.

tent trend in the distribution of longitudinal residual stress profile (mainly comparable with mid-thickness of the plate) can also be found in the work of Liang et al. (2015).

It is also interesting to note that the distribution of the residual stresses have the same trend as microhardness measurement where an example of hardness distribution, depth of 10 mm below the surface, Fig. 7, is comparable with that of stress distribution at the similar depth. The hardness values for low heat input weld are greater than that of high heat input in support of the residual stresses measurement. The fact that lower heat input renders higher stresses may be related to the total number of passes with lower amount of weld metal deposited in each pass. Since the heat sink is the same for both specimens, the rate of cooling of deposited weld in each run is expected to be higher for low heat input meaning higher thermal stresses. In addition, the heat generated by the following weld pass may not be as effective as for the high heat input weld run in implementing some degree of stress relieving. The other possibility could be due to phase transformation and the associated residual stress where a faster cooling rate may generate structures with higher transformation stresses. This is an on-going study and the microstructural analysis of the both welds along with the measurement of hardness will be reported in details later.

It is a well-established fact that hardness and residual stresses have significant effects on the fatigue life of the welded structures. There are two competing factors affecting the fatigue life in these
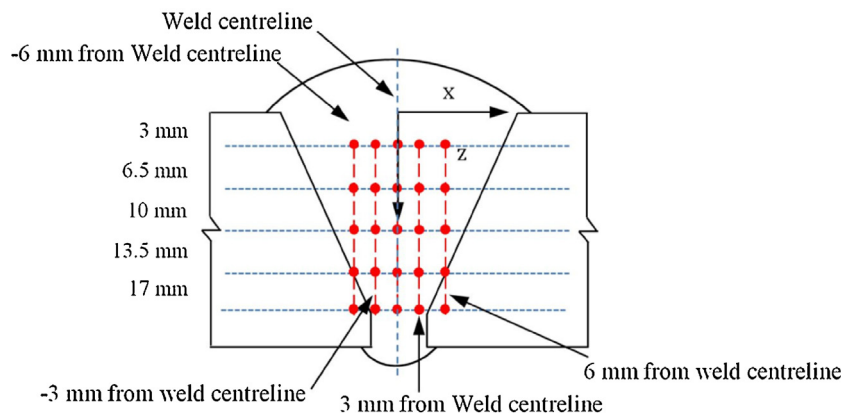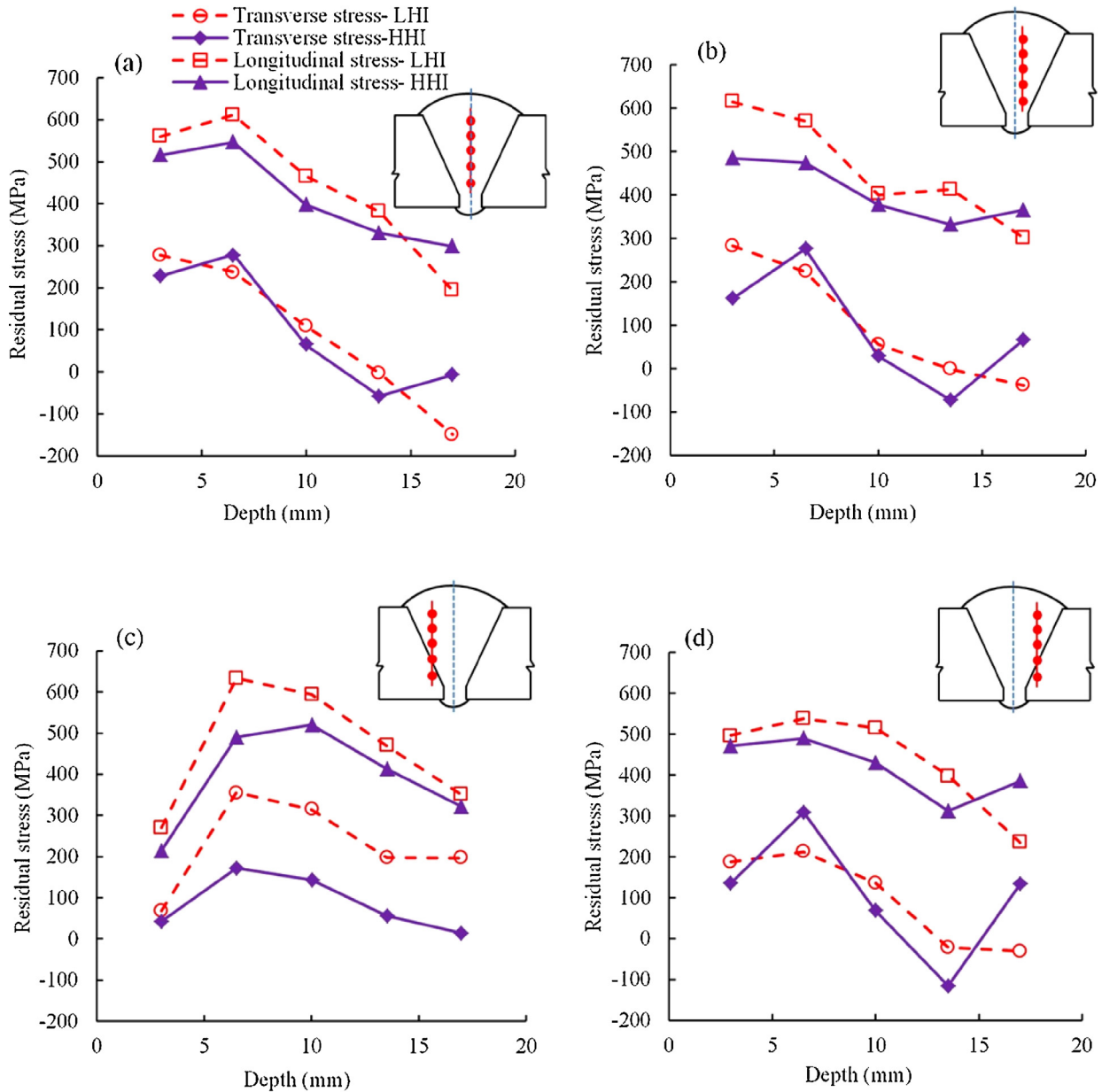

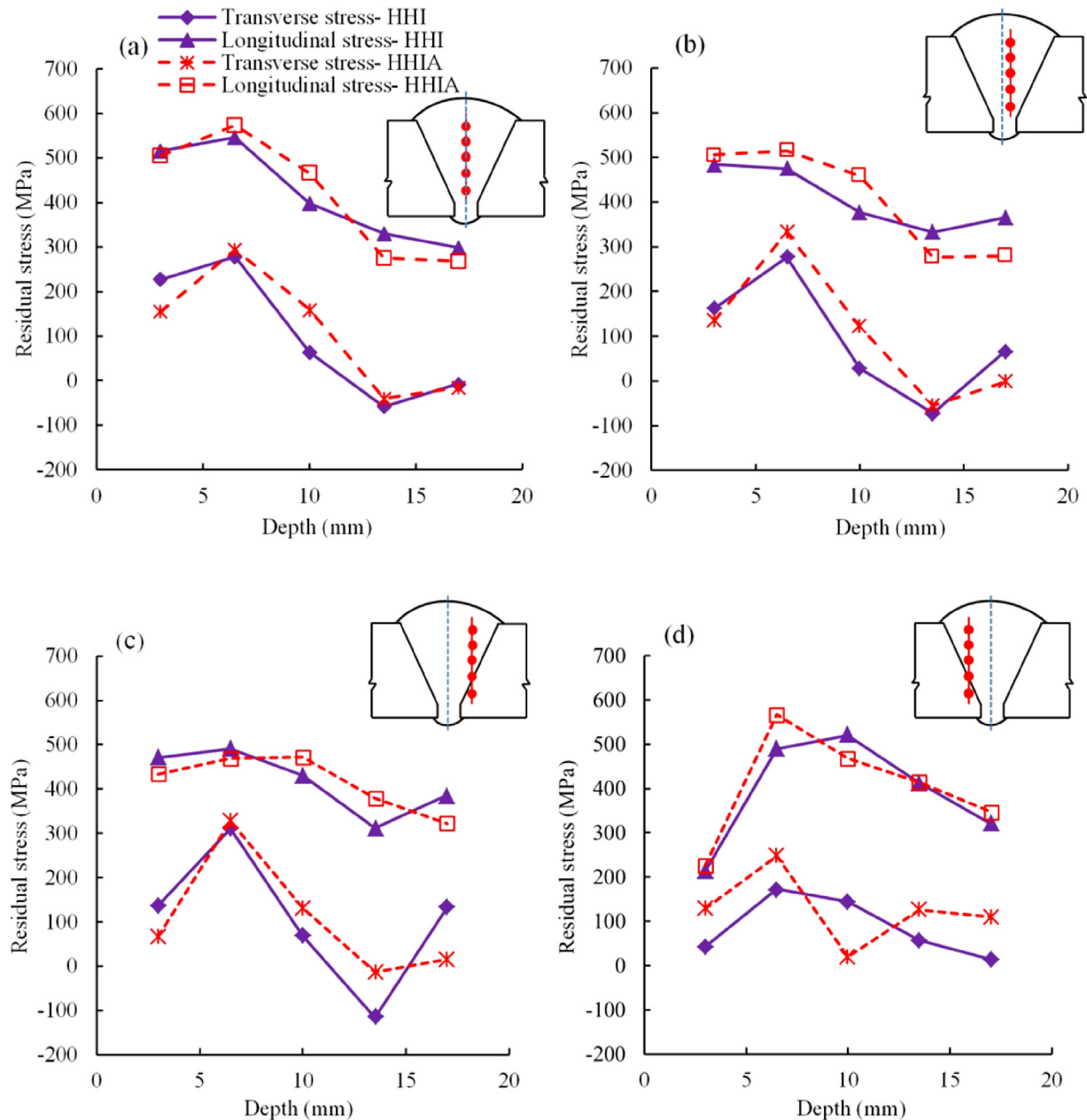**Fig. 8.** Schematic of through thickness measurement points.

Fig. 9. Comparison between the through thickness residual stress profiles measured for low heat input (specimen I) and high heat input (specimen II) welds: (a) weld centreline, (b) 3 mm away from the weld centreline, (c) −6 mm away from the weld and (d) 6 mm away from the weld centreline; (solid line) high heat input (dashed line) low heat input.

welded joints. With the increase of heat input the magnitude of residual stresses were decreased while it has reduced the hardness values to some extent. Decreasing the residual stresses in the welded specimens with higher heat input may correspond with grain coarsening and lowering the hardness of these specimens. As evident in the literature, reduction in the magnitude of residual stresses, particularly tensile residual stresses, can improve the fatigue behaviour of welded joints (Harati et al., 2015). But at the same time it was reported that fatigue life can be reduced by a decrease in hardness value (Fratini et al., 2009). Therefore the combined influence of these factors on fracture resistance can be very complex, and at this stage it is quite difficult to evaluate its effect without additional tests and studies. In other words, further tests are required to clarify the effect of the changes in residual stresses and hardness on fatigue life, which is beyond the scope of the current paper.

4.1.2. Pass sequence

As for pass sequence effect on residual stresses (Specimens II: unidirectional weld deposition; and Specimen III: converse weld deposition), a comparison of the field of residual stresses is presented in Fig. 6(a–e). Our results clearly demonstrate that the change in weld deposition direction does not have a significant effect on the magnitude of the longitudinal residual stresses. However, the distribution of residual stresses in the specimen with alternating welding sequence (HHIA) is more uniform in comparison with the other two specimens (LHI and HHI). In general, the uncertainties in the measured stresses were no greater than ±16 MPa, to the point that the error bars do not extend beyond the data point markers.

It is also noteworthy to point out the effect of subsequent passes on the relieving of the residual stresses within the earlier passes, as for instance the peak longitudinal stress of 630 MPa measured

Fig. 10. Comparison between the through thickness residual stress profiles measured for direct (specimen II) and alternating (specimen III) welds: (a) weld centreline; (b) 3 mm away from the weld centreline; (c) 6 mm away from the weld centreline and (d) −6 mm away from the weld centreline; (solid line) direct welding method (dashed line) alternating welding method.

within the final passes has reduced to less than 400 MPa at a depth of 17 mm below the surface (initial passes).

4.2. Through thickness

4.2.1. Heat input

Fig. 9(a–d) shows the effect of the heat input on the residual stress profiles in the normal direction (z-direction) for different locations from the weld centreline: 3 mm, −6 and 6 mm away from the weld centreline. The locations of the measurement points are shown in Fig. 8.

The heat input has a significant effect on residual stress distribution along the normal (through thickness) direction. Fig. 9 demonstrates that in most of the cases the longitudinal and transverse residual stresses for low heat input specimen (LHI) are higher than of the high heat input. The maximum difference for two differ-

ent heat inputs can be seen in Fig. 9c where the difference between the longitudinal residual stresses reaches to 145 MPa while in the transverse direction this difference is about 185 MPa. For the low heat input specimen (Specimen I) both the longitudinal and transverse residual stresses gradually decreases with the depth and reach the minimum at 17 mm from the top surface. This is attributed to the tempering effects of the subsequent weld runs, which reduce the magnitude of residual stresses for both the longitudinal and transverse stress components.

4.2.2. Weld sequence

Fig. 10(a–d) shows the effect of the change of the weld pass direction on the residual stress profiles for different locations from the weld centreline. A very similar trend for longitudinal and transverse residual stresses can be seen for both samples. The differences in the magnitudes of the residual stresses are quite

small, generally less than 18%. This could be attributed to the length of the specimen, which was rather long and negated the thermal effects associated with the change of the weld deposition direction. Another reason may be related to the location of the measurements that taken from the central part of the Specimens, which is lesser affected by this change. It is expected the effect to be more pronounced at the weld start and end locations.

5. Conclusions

Neutron diffraction method was used to measure residual stresses in multi-pass weldments of high strength low alloy steel. The key findings of this experimental study were:

- Residual stresses in excess of yield strength were developed in the weld metal and HAZ particularly for the upper-layers of welds which were not affected by tempering due to the subsequent weld layers. The magnitude of residual stresses for the specimen with lower heat input (higher welding travel speed) was significantly higher than the specimens with higher heat input (lower welding travel speed).
- The magnitude of residual stresses decreased substantially with weld depth as a consequence of tempering effects of the later weld passes onto the earlier weld runs.
- With the increase of heat input, the fusion zone and HAZ area also increased. As a result, the maximum tensile residual stresses (longitudinal stresses) were located further away from weld centreline for the samples with higher heat input.
- The results indicated no significant effect on the magnitude of the longitudinal residual stresses as a result of changing the weld deposition direction. However, the distribution of resid-

ual stresses in the specimen with alternating welding sequence (HHIA) was more uniform.
- The peak of longitudinal residual stresses was mainly found to be at the HAZ for all of specimens (particularly from 6.5 mm to 17 mm from the weld surface).

Appendix A.

Table 1
Chemical composition of ER70S-6 and E81T1-Ni 1 M.

Chemical composition	ER 70S-6	E81T1–Ni 1M
%C	0.09	0.04–0.05
%Mn	<1.60	1.26–1.36
%S	0.007	0.006–0.009
%Si	0.9	0.25–0.29
%P	0.007	0.005–0.008
%Cu	0.2	–
%Cr	0.05	0.04–0.05
%Ni	0.05	0.86–0.96
%Mo	0.05	0.01
%V	0.05	0.02–0.03

Table 2
Welding parameters used for Specimen I—low heat input (LHI).

Pass number	Filler/electrode		AMP	Gas		Volts	Speed	HI
	Size	Class	DCEP	Type	Class	DCEP	mm/min	kJ/mm
1	0.9	ER70S-6	98	Argoshield	52	21	244	0.5
2	1.2	E81TNi	153	Argoshield	52	25	354	0.65
3	1.2	E81TNi	153	Argoshield	52	25	298	0.77
4	1.2	E81TNi	153	Argoshield	52	25	354	0.65
5	1.2	E81TNi	153	Argoshield	52	25	323	0.71
								.0.71
6	1.2	E81TNi	153	Argoshield	52	25	372	0.62
7	1.2	E81TNi	153	Argoshield	52	25	354	0.65
8	1.2	E81TNi	153	Argoshield	52	25	338	0.68
9	1.2	E81TNi	153	Argoshield	52	25	331	0.69
10	1.2	E81TNi	153	Argoshield	52	25	346	0.66
11	1.2	E81TNi	153	Argoshield	52	25	304	0.75
12	1.2	E81TNi	153	Argoshield	52	25	323	0.71
13	1.2	E81TNi	153	Argoshield	52	25	338	0.68
14	1.2	E81TNi	153	Argoshield	52	25	438	0.53
15	1.2	E81TNi	153	Argoshield	52	25	331	0.69
16	1.2	E81TNi	153	Argoshield	52	25	338	0.68
17	1.2	E81TNi	153	Argoshield	52	25	372	0.62
18	1.2	E81TNi	153	Argoshield	52	25	402	0.57
19	1.2	E81TNi	153	Argoshield	52	25	372	0.62
20	1.2	E81TNi	153	Argoshield	52	25	298	0.77
21	1.2	E81TNi	153	Argoshield	52	25	346	0.66
22	1.2	E81TNi	153	Argoshield	52	25	354	0.65
23	1.2	E81TNi	153	Argoshield	52	25	310	0.74
24	1.2	E81TNi	153	Argoshield	52	25	323	0.71
25	1.2	E81TNi	153	Argoshield	52	25	317	0.73

Table 3
Welding parameters used for specimen II and III- High heat input (HHI).

Pass number	Filler/electrode		AMP	Gas		Volts	Speed	HI
	Size	Class	DCEP	Type	Class	DCEP	mm/min	kJ/mm
1	0.9	ER70S-6	98	Argoshield	52	21	240	0.51
2	1.2	E81TNi	153	Argoshield	52	25	271	0.85
3	1.2	E81TNi	153	Argoshield	52	25	210	1.1
4	1.2	E81TNi	153	Argoshield	52	25	149	1.54
5	1.2	E81TNi	153	Argoshield	52	25	120	1.91
								.0.71
6	1.2	E81TNi	153	Argoshield	52	25	162	1.42
7	1.2	E81TNi	153	Argoshield	52	25	160	1.44
8	1.2	E81TNi	153	Argoshield	52	25	173	1.33
9	1.2	E81TNi	153	Argoshield	52	25	150	1.53
10	1.2	E81TNi	153	Argoshield	52	25	153	1.5
11	1.2	E81TNi	153	Argoshield	52	25	155	1.46

It is important to note that similar heat input was used for Specimens II and III, but in Specimen III the direction for each subsequent weld pass was changed.

References

Akbari, D., Sattari-Far, I., 2009. Effect of the welding heat input on residual stresses in butt-welds of dissimilar pipe joints. Int. J. Press. Vessels Pip. 86, 769–776.

Barsoum, Z., Barsoum, I., 2009. Residual stress effects on fatigue life of welded structures using LEFM. Eng. Fail. Anal. 16, 449–467.

Cheng, X., Fisher, J.W., Prask, H.J., Gnäupel-Herold, T., Yen, B.T., Roy, S., 2003. Residual stress modification by post-weld treatment and its beneficial effect on fatigue strength of welded structures. Int. J. Fatigue 25, 1259–1269.

Deng, D., 2013. Influence of deposition sequence on welding residual stress and deformation in an austenitic stainless steel J-groove welded joint. Mater. Des. 49, 1022–1033.

Fratini, L., Pasta, S., Reynolds, A.P., 2009. Fatigue crack growth in 2024-T351 friction stir welded joints: longitudinal residual stress and microstructural effects. Int. J. Fatigue 31, 495–500.

Grünitz, L., 2004. Buckling Strength of Welded HY-80 Spherical Shells: A Direct Approach. Arbeitsbereiche Schiffbau, Technische Universität, Hamburg–Harburg.

Harati, E., Karlsson, L., Svensson, L.-E., Dalaei, K., 2015. The relative effects of residual stresses and weld toe geometry on fatigue life of weldments. Int. J. Fatigue 77, 160–165.

Javadi, Y., Najafabadi, M.A., 2013. Comparison between contact and immersion ultrasonic method to evaluate welding residual stresses of dissimilar joints. Mater. Des. 47, 473–482.

Ji, S.D., Fang, H.Y., Liu, X.S., Meng, Q.G., 2005. Influence of a welding sequence on the welding residual stress of a thick plate. Modell. Simul. Mater. Sci. Eng. 13, 553.

Jiang, W.C., Wang, B.Y., Gong, J.M., Tu, S.T., 2011. Finite element analysis of the effect of welding heat input and layer number on residual stress in repair welds for a stainless steel clad plate. Mater. Des. 32, 2851–2857.

Kim, S.-H., Kim, J.-B., Lee, W.-J., 2009. Numerical prediction and neutron diffraction measurement of the residual stresses for a modified 9Cr-1Mo steel weld. J. Mater. Process. Technol. 209, 3905–3913.

Kotousov, A., 2000. Thermal stresses and fracture of thin plates during cutting and welding operations. Int. J. Fract. 103, 361–372.

Liang, W., Murakawa, H., Deng, D., 2015. Investigation of welding residual stress distribution in a thick-plate joint with an emphasis on the features near weld end–start. Mater. Des. 67, 303–312.

Lu, G., Kotousov, A., Siores, E., 1999. Elementary mathematical theory of thermal stresses and fracture during welding and cutting. J. Mater. Process. Technol. 89–90, 298–302.

Mahmoodi, M., Sedighi, M., Tanner, D.A., 2012. Investigation of through thickness residual stress distribution in equal channel angular rolled Al 5083 alloy by layer removal technique and X-ray diffraction. Mater. Des. 40, 516–520.

Mochizuki, M., 2007. Control of welding residual stress for ensuring integrity against fatigue and stress–corrosion cracking. Nucl. Eng. Des. 237, 107–123.

Paradowska, A., Price, J., Ibrahim, R., Finlayson, T., Blevins, R., Ripley, M., 2006. Residual stress measurements by neutron diffraction in multi-bead welding. Physica B: Condens. Matter 358, 890–893.

Pardowska, A.M., Price, J.W., Ibrahim, R., Finlayson, T.R., 2008. Neutron diffraction evaluation of residual stress for several welding arrangements and comparison with fitness-for-purpose assessments. J. Press. Vessel Technol. 130, 011501.

Park, M.J., Yang, H.N., Jang, D.Y., Kim, J.S., Jin, T.E., 2004. Residual stress measurement on welded specimen by neutron diffraction. J. Mater. Process. Technol. 155, 1171–1177.

Peel, M., Steuwer, A., Preuss, M., Withers, P.J., 2003. Microstructure, mechanical properties and residual stresses as a function of welding speed in aluminium AA5083 friction stir welds. Acta Mater. 51, 4791–4801.

Qureshi, M.E., 2008. Analysis of Residual Stresses and Distortions in Circumferentially Welded Thin-Walled Cylinders. National University of Sciences and Technology.

Ranjbarnodeh, E., Serajzadeh, S., Kokabi, A.H., Fischer, A., 2011. Effect of welding parameters on residual stresses in dissimilar joint of stainless steel to carbon steel. J. Mater. Sci. 46, 3225–3232.

Sattari-Far, I., Farahani, M., 2009. Effect of the weld groove shape and pass number on residual stresses in butt-welded pipes. Int. J. Press. Vessels Pip. 86, 723–731.

Venkata, K.A., Kumar, S., Dey, H.C., Smith, D.J., Bouchard, P.J., Truman, C.E., 2014. Study on the effect of post weld heat treatment parameters on the relaxation of welding residual stresses in electron beam welded P91 steel plates. Procedia Eng. 86, 223–233.

Webster, G.A., Wimpory, R.C., 2001. Non-destructive measurement of residual stress by neutron diffraction. J. Mater. Process. Technol. 117, 395–399.

Withers, P.J., Bhadeshia, H.K.D.H., 2001. Residual stress part 1—measurement techniques. Mater. Sci. Technol. 17, 355–365.

CHAPTER 6

RESIDUAL STRESS-MICROSTRUCTURE-MECHANICAL PROPERTY INTERRELATIONSHIPS IN MULTIPASS HSLA STEEL WELDS

Houman Alipooramirabad[1]*, Reza Ghomashchi[1], Anna Paradowska[2], Mark Reid[2]

[1]School of Mechanical Engineering, the University of Adelaide, SA 5005

[2] Bragg Institute, Australian Nuclear Science and Technology Organisation (ANSTO), Lucas Heights, NSW 2234, Australia

Statement of Authorship

Title of Paper	Residual stress- microstructure- mechanical property interrelationships in multipass HSLA steel welds
Publication Status	☑ Published ☐ Accepted for Publication ☐ Submitted for Publication ☐ Unpublished and Unsubmitted work written in manuscript style
Publication Details	Alipooramirabad H, Ghomashchi R, Paradowska A, Reid M. Residual stress- microstructure- mechanical property interrelationships in multipass HSLA steel welds. Journal of Materials Processing Technology. 2016;231:456-67.

Principal Author

Name of Principal Author (Candidate)	Houman Alipooramirabad		
Contribution to the Paper	I was responsible for the literature review required for this work, and designed the framework for the experimental conditions. I carried out mechanical property and microstructural behaviour analysis, wrote the first draft of the manuscript and incorporated and addresses all comments and suggestions by other authors in subsequent revesions of the manuscript. Interpertation of the data was primary my responsibility.		
Overall percentage (%)	90%		
Certification:	This paper reports on original research I conducted during the period of my Higher Degree by Research candidature and is not subject to any obligations or contractual agreements with a third party that would constrain its inclusion in this thesis. I am the primary author of this paper.		
Signature		Date	30/01/2017

Co-Author Contributions

By signing the Statement of Authorship, each author certifies that:

  i.   the candidate's stated contribution to the publication is accurate (as detailed above);
  ii.   permission is granted for the candidate in include the publication in the thesis; and
  iii. the sum of all co-author contributions is equal to 100% less the candidate's stated contribution.

Name of Co-Author	Reza Ghomashchi		
Contribution to the Paper	I was joint supervisor for the work, helped in developing ideas and contributed to refining the manuscript.		
Signature		Date	31/01/2017

Name of Co-Author	Anna Paradowska
Contribution to the Paper	I was joint supervisor of this work, assisted for conducting some part of the experiments, and jointly contributed to refining the manuscript.

Signature		Date	2/02/2017

Name of Co-Author	Mark Reid
Contribution to the Paper	I jointly contributed to conducting some part of the experiments and refining the manuscript.
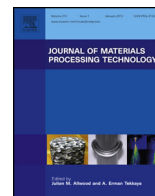
Signature		Date	31/01/2017

Residual stress- microstructure- mechanical property interrelationships in multipass HSLA steel welds

Houman Alipooramirabad [a,*], Reza Ghomashchi [a], Anna Paradowska [b], Mark Reid [b]

[a] School of Mechanical Engineering, The University of Adelaide, Adelaide, SA 5005, Australia
[b] Bragg Institute, Australian Nuclear Science and Technology Organization (ANSTO), Lucas Heights, NSW 2234, Australia

ARTICLE INFO

ABSTRACT

Higher levels of residual stresses in excess of yield strength of the both weld and parent metals were developed within the upper-layers of the modified short arc and flux cored arc welding combination of HSLA steel. The magnitude of the residual stresses was significantly reduced by increasing the heat input. High level of residual stresses was found to be correlated with the existing of microstructural constituents of bainite and Widmanstätten ferrite in the weld metal and HAZ of low heat input specimens. There was no substantial difference in the magnitude of the residual stresses, microstructural characteristics and mechanical properties when the direction of weld deposition was changed.

© 2016 Elsevier B.V. All rights reserved.

1. Introduction

High strength low alloy steels (HSLA) not only provide economic advantages in relation to the consumption of expensive alloy elements, but also provide unique thermo-mechanical capabilities such as high strength, excellent ductility, good weldability, and outstanding low temperature impact toughness superior to that of high yield strength steels. HSLA steels are widely used in a range of applications where welding is the primary mode of fabrication. This includes construction of large ships, oil and gas transmission lines, and offshore oil drilling platforms, pressure vessels, building construction, bridges and storage tanks. The welded structures of HSLA steels are susceptible to a range of failure modes in service such as stress corrosion cracking (Zhang et al., 2013), fatigue damage (Ragu Nathan et al., 2015) and hydrogen assisted cold cracking (Alipooramirabad et al., 2014), all are indirectly related to the microstructure and the residual stresses generated during welding. Therefore, minimizing the tensile residual stresses along with some control over the formation and distributions of a range of microstructures can assist against the various failures in these joints. The development of microstructure and distribution of residual stresses within the welded area and heat affected zone are greatly influenced by the welding procedure and weldment geometry as reported by Leggatt (2008). One of the parameters that affect the temperature history and thus controls the cooling rate, constituent microstructure and residual stresses is the heat input (Kumar and Shahi, 2011).

Heat input is interpreted in terms of a combination of welding travel speed, and applied current and voltage. If not properly selected, incorrect heat input tends to generate lower quality welds with poor mechanical properties. A high heat input may result in excess segregation within the fusion zone and encourage grain coarsening in the HAZ (Zondi, 2014). However, higher heat input may be beneficial by having a tempering effect on the welded joint by slowing down the cooling rate, thereby producing tougher weld structure (Zondi, 2014). According to Smith, et al. (1997) the effects of heat input, (through changes in welding speed and current), on the mechanical properties of normalised ASTM A302 Gr B steel (manganese–molybdenum alloy steel) welded joint tend to be more significant at the HAZ rather than the weld metal. Welding procedures with higher heat inputs resulted in lower toughness of the HAZ. This is due to the presence of upper bainite in the coarse grained heat-affected zone. Welding travel speed is arguably one of the most influential welding heat input parameters with significant effect on the mechanical properties and quality of weld. Yang (2008) reported that high welding speeds could lead to surface defects such as porosity and under cuts while lower weld speeds may lead to uncontrollable weld pool resulting in slag inclusions. Welding travel speed also controls the geometry and size of weld
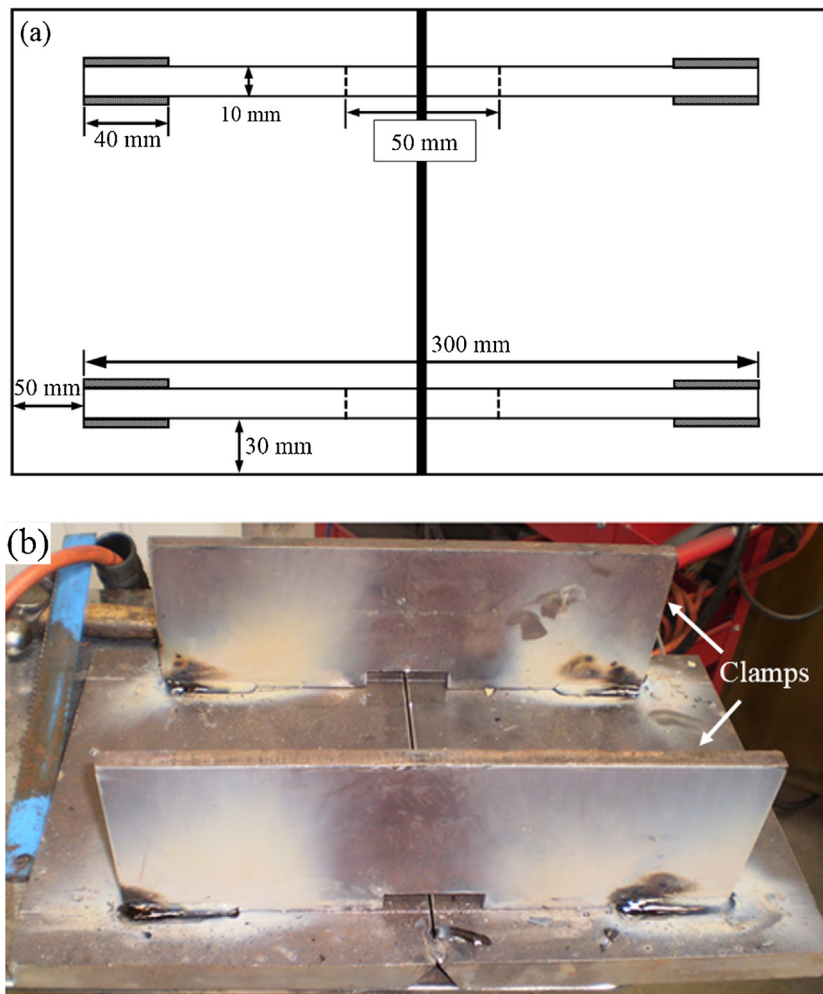

Fig. 1. Experimental set up with (a) a schematic of the clamp position and (b) welding specimen.

metal pool with bearings on cooling rate and thus the resultant microstructure and residual stresses. Qureshi (2008) carried out numerical simulations to investigate the effect of weld travel speed on residual stresses in a thick-walled cylinder. The outcomes of these simulations demonstrated that for low weld travel speeds (2 mms^{-1}) the magnitudes of residual stresses are normally higher at both the inner (tensile stresses) and outer (compressive stresses) surfaces of the cylinder.

Shi and Han (2008) investigated the effects of weld thermal cycle on microstructure and fracture toughness of simulated HAZ for high strength low alloy steel confirming a longer cooling time ($t_{8/5}$) reduces toughness. The increasing cooling time was also resulted in increasing the size of prior austenite grain, as well as the volume fraction of bainitic ferrite and martensite/austenite (M/A) constituent. It was particularly noted that the formation of M/A constituent and increasing prior austenite grain size were responsible for fracture toughness reduction. Keehan (2004) showed that increasing heat input (from 1.1 to 1.8 kJmm^{-1}) increases the area of weld bead, and results in fewer passes being required to completely fill up the weld. However, in contrast to Shi and Han (2008), Keehan (2004) argued that high heat input improves toughness due to removing most of the columnar structure in a multi-pass weld.

As briefly mentioned here, there is no report to incorporate the effect of heat input (in the context of travel speed and resulting cooling rate) and pass sequence on microstructure, and residual stresses and how these factors affect the mechanical property (hardness) of the welded joint for multi-pass welds. This is the focus of this article to elucidate on heat input-microstructure-residual stress- weld sequence and hardness interrelationship for API 5L grade X70 line pipe steel.

2. Experiemental procedure

2.1. Weld deposition

The root pass of all V-prep weld joints was completed with modified short arc welding (MSAW) and flux cored arc welding (FCAW) was utilised for the remaining passes, which is quite common in modern welding procedures. The MSAW offers many advantages including low distortion, freedom from spatter, high quality of welded joints and lower cost including post-weld machining. FCAW ensures high deposition and productivity rates. It does not require a highly trained personnel; the process is less complex and more adaptable than other types of welding, such as submerged arc welding. The root pass was completed with ER70s-6 welding wire; and the remaining passes with E81T1-Ni1 m class Flux cored wire. The yield strength of ER70s-6 welding wire is 482 MPa while the yield strength of E81TNi class Flux cored wire is about 470 MPa. The chemical composition for ER 70s-6 and E81TNi wires can be seen in Table A1 of the Appendix. The mechanical properties of the parent metal and welding consumables, provided by the manufactures, are given in Table A2 of the Appendix.

The test specimens comprised two 20 mm thick steel plates (API 5L grade X70) with the dimensions of 250×200 mm. The
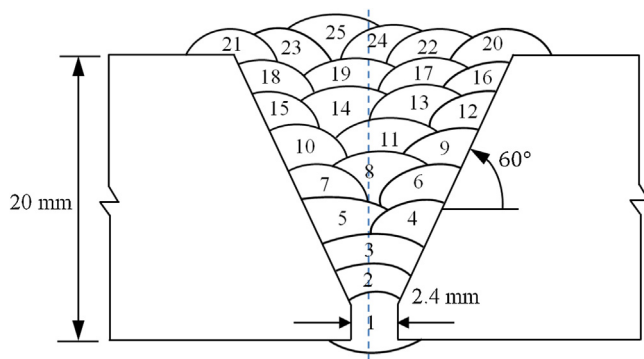
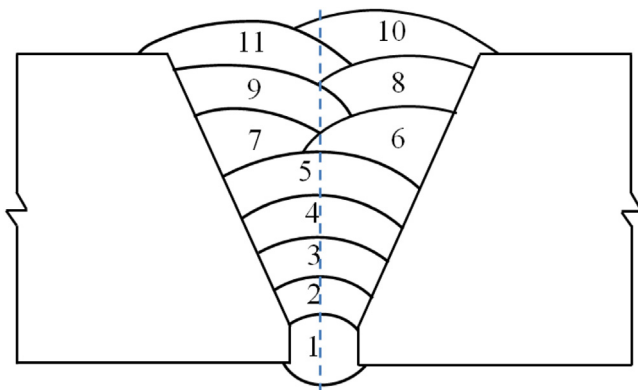**Fig. 2.** Weld deposition sequence in specimen I.

Fig. 3. Weld deposition sequence in specimen II and III.

experimental set up with the clamp position is shown in Fig.1. The yield strength of the parent metal is about 485 MPa (the chemical composition of parent metal can also be seen in Table A1 of the Appendix). The preparatory joint geometry is shown in Figs. 2 and 3. Three sets of samples were prepared (two samples each) for the measurement of residual stresses and microstructural analysis. One sample of each set was to measure the lattice spacing ($d_{0,hkl}$) in stress free mode and the other for the measurement of residual stresses. Both samples were analysed for microstructural characterization.

Specimen series I (low heat input—LHI)

The welding direction was the same for all passes. The weld run placement sketch for this welding process is shown in Fig. 2. The welding specification is provided in Table A3 of the Appendix. Fig. 2 also specifies the preparatory geometry of all samples.

Specimen series II (high heat input—HHI)

The number of weld runs is reduced to 11, and the speed of weld runs was lower than specimen series I (heat input of each run is higher than those of the specimen series I). The welding specification is provided in Table A4 of the Appendix. The weld runs in specimen series II was also deposited in the same direction. The weld deposition sketch of specimen series II is shown in Fig. 3.

Specimen series III (alternating high heat input—AHHI)

The welding parametes and the number of passes are the same as for specimen series II. The converse welding sequence (alternating directions) was used to complete the weld.

2.2. Characterization techniques

Neutron diffraction residual stress measurements were performed at ANSTO using KOWARI strain scanner and a $3 \times 3 \times 3\,mm^3$ gauge volume. The Si (400) type double focusing monochromator generated a neutron beam with the wavelength of 1.67 Å. A detector angle, 2θ, was set at $90°$ corresponding to the αFe (211) diffraction peak. A schematic drawing of the welded samples with the locations of the weld cross section (middle of the plate) and the measurement points for residual stress analysis are shown in Fig. 4. The details of the neutron diffraction analysis to evaluate the residual stresses during welding are given in the works done by Park et al. (2004) for *T*-type and a double V butt joint welded stainless steel specimens and Alipooramirabad et al. (2015) for high strength low alloy steel welds.

Hardness testing was conducted according to the Australian standard AS.2205.6.1 (method 6.1). Cross-sections of test specimens (I, II and III) were prepared by conventional metallography down to 1 μm diamond paste and micro-hardness measurement were taken for the weld metal, HAZ and parent metal. Measurements were taken over the cross sections of the weld in nine locations at distances of 2, 4, 6, 8, 10, 12, 14, 16 and 18 mm away from weld surface at intervals of 0.5 mm. Hardness measurements were carried out on the middle cross-section of the welded specimens (similar location for residual stress measurement and microstructural characterization), as shown in Fig. 4a. A second traverse of hardness was taken along the weld centreline (through the thickness) at intervals of 0.5 mm. In all cases the microhardness testing was conducted using a Vickers (HV) indenter with the load of 0.5 Kg and with a loading time of 15 s. Optical and scanning electron microscopy were used to characterize the microstructure in different areas of the parent metal (PM), the heat affected zone (HAZ), and weld metal (WM). All samples were etched in 5% Nital (5% nitric acid in ethanol) or prepared by a double etching procedure using 2% Picral (2% picric acid in ethanol) and 2% Nital solutions (2% nitric acid in ethanol).

3. Results and discussion

The welding process and resulted thermal distribution along with the thickness of parent metal control the cooling rate of the weld joint fusion zone and the width of the heat affected zone. The cooling rate itself is the controlling parameter for the microstructure of weld metal and HAZ and resulted residual stresses. Both microstructure and residual stress are indicators for expected hardness of weldmetal. Therefore, the following sections are chronologically concentrated on the microstructure, residual stresses and hardness with a final conclusion on weld integrity.

3.1. Microstructural analysis

The macrographs of the welded specimens with alternating, high, and low heat inputs, (AHHI, HHI and LHI,), are given in Fig. 5. The size of each weld pass along with the HAZ and root pass are clearly visible on the macrographs. The size of weld pass decreases with decreasing heat input but not much variation detectable with the sequence changes. It is also noticble that final passes have some degree of directionality which confirms effective cooling was through weld top surface especially for the last passes. The directionality of the inner weld passes was removed as a result of reheating effect of subsequent weld runs.The width of HAZ was measured to be around 1.78 and 2.65 mm for LHI and HHI respectively. However when the direction of welding changed to alternating welding sequence the width of HAZ appears to have not changed but becoming less straight and more wavey and patchy.
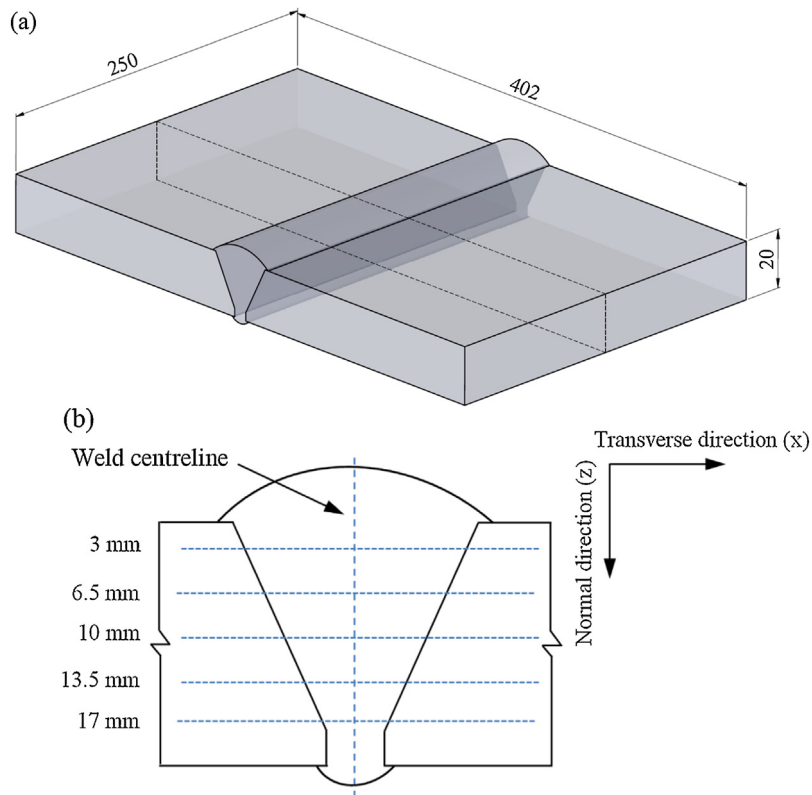
Fig. 4. schematic of (a) weld cross section for residual stress measurements and (b) measurement points.
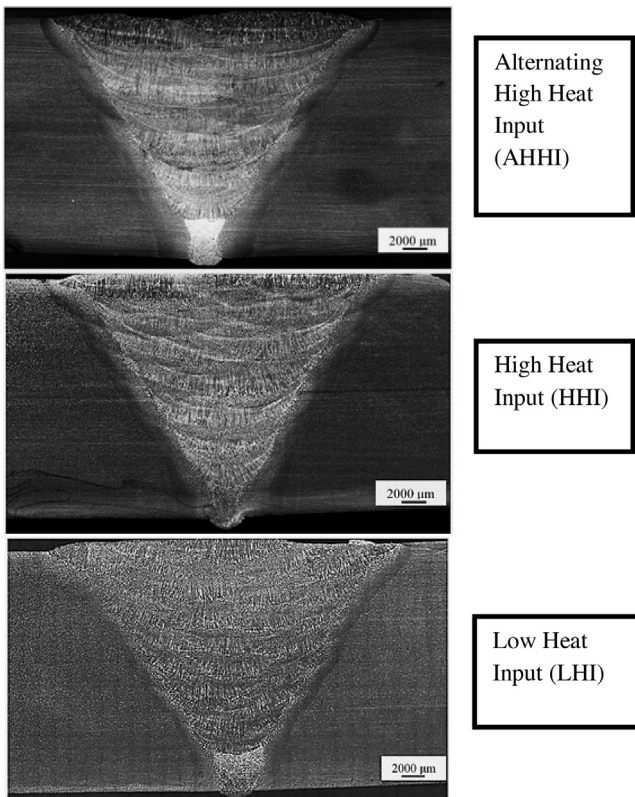

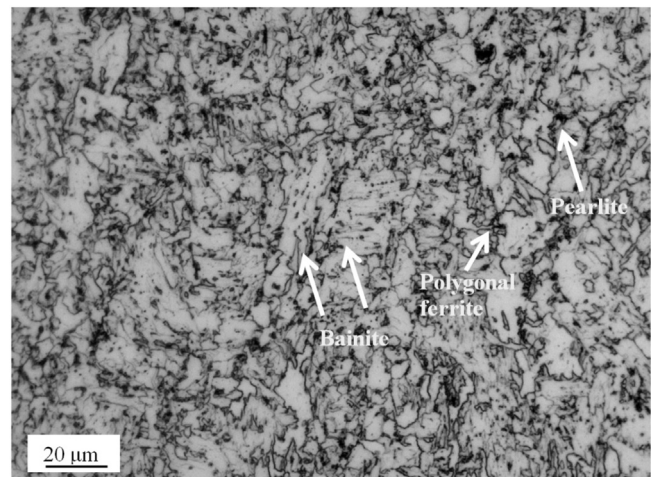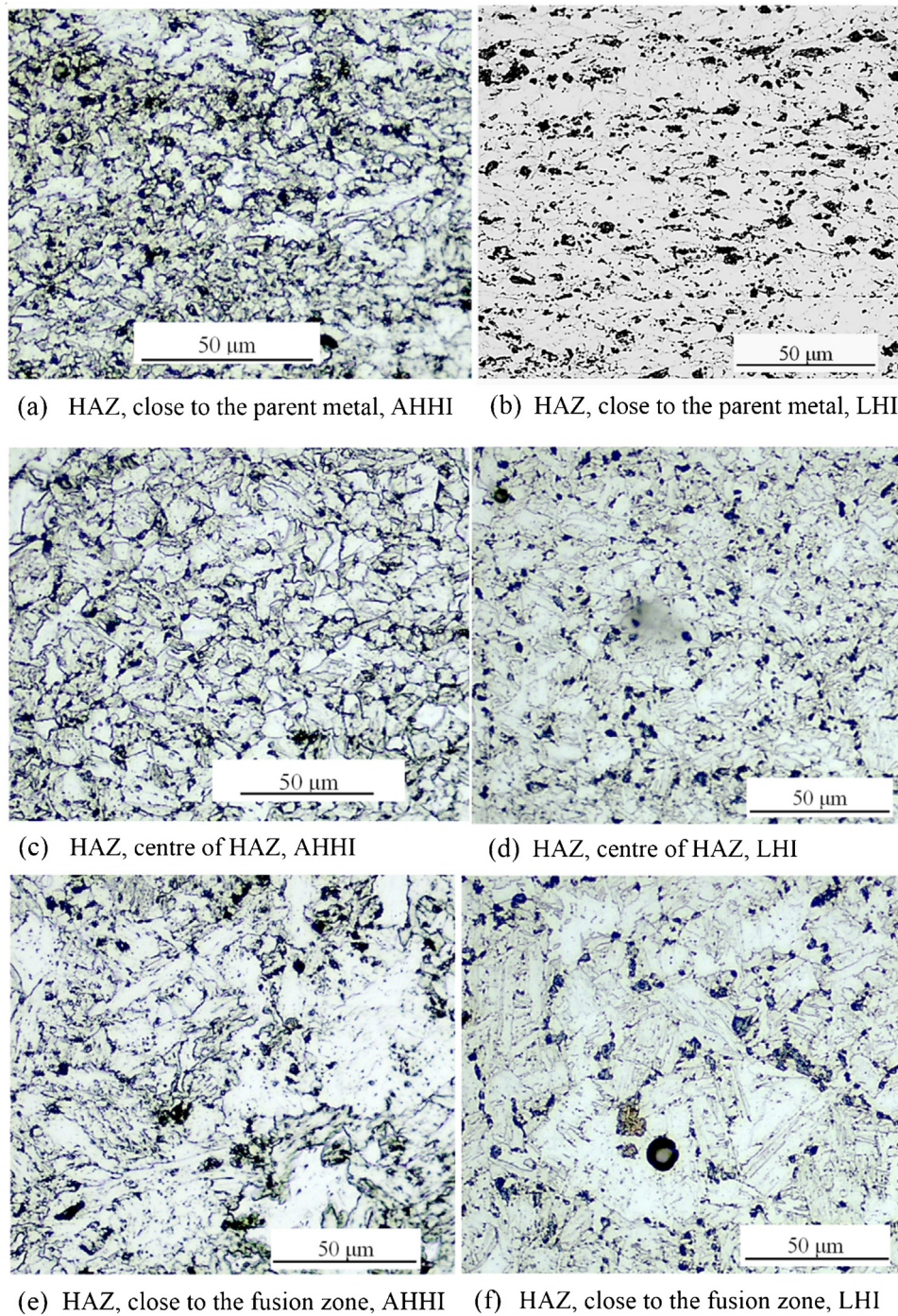Fig. 5. Optical macrographs to show the geometry of three welded geometry.

Fig. 6. Optical micrograph of the as-received X70 steels showing a mainly acicular ferrite with some bainite and polygonal ferrite.

The X70 parent plate steel has a mainly acicular ferrite sturucture with some bainite and polygonal ferrite as illustrated by the optical micrograph in Fig. 6. There is small percentage of pearlite as expected with only 0.05% C. The HAZ, as expected, comprises two distinct regions of coarse grained (CGHAZ) and fine grained (FGHAZ) heat affected zone, as shown in Fig. 7. However, there is continous grain growth toward the fusion zone with microstructure predominately acicular ferrite near the parent metal but changing to polygonal ferrite and bainitic ferrite as it approaches fusion zone. The degree of grain growth and formation of bainite are the dominant feature of HAZ all the way up to the fusion zone. Such changes

(a) HAZ, close to the parent metal, AHHI

(b) HAZ, close to the parent metal, LHI

(c) HAZ, centre of HAZ, AHHI

(d) HAZ, centre of HAZ, LHI

(e) HAZ, close to the fusion zone, AHHI

(f) HAZ, close to the fusion zone, LHI

Fig. 7. Optical micrographs to show the HAZ in both high (a, c, e) and low heat inputs (b, d, f). The weld structure mainly comprises acicular ferrite replaced by bainite and polygonal ferrite with closing towards the fusion zone.

is expected to influence residual stresses and the hardness as will be discussed later where in spite of massive grain growth, there is some increase in hardness which could be attributed to formation of bainite.

It is further evident that the concentration of polygonal ferrite is greater in the HAZ of the high heat input weld when compared to that of low heat input weld. This in itself is expected to be revealed when measuring the residual stresses and hardness, i.e., reduction in residual stress and hardness should be expected. The process of alternating weld pass appears to have negligible effect on the microstructure of HAZ for both fine and coarse grained regions.

The weld fusion zone was also examined in great details to highlight the morphology of the weldmetal microstructure, and the interface between weld passes to identify if passes are well fused together. The porosity formation was also inspected to reveal if heat input and in our case the weld travel speed affects porosity content and its morphology, size and distribution. Finally the formation of inclusions was also studied, but the main emphasis in this article is on the microstructure.

As shown in Fig. 8, the root pass which is carried out by MSAW is mainly acicular ferrite but Widmanstätten, polygonal and bainitic ferrite morphologies are also detectable. It is interesting to see that
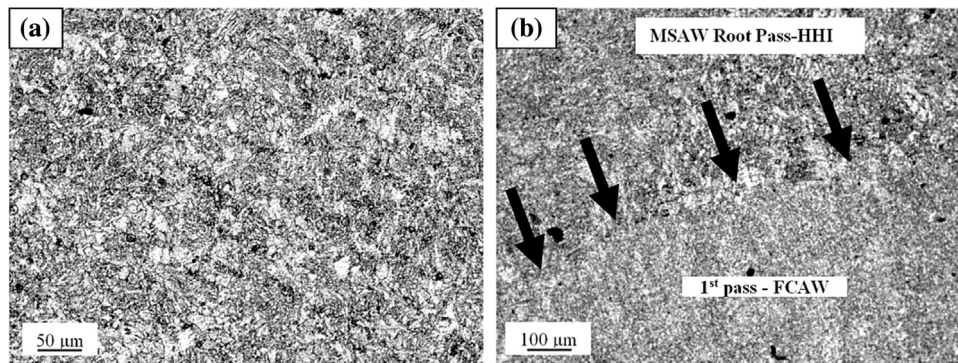
Fig. 8. Optical micrographs to show (a) the morphology of weld for the root pass—HHI and (b) the boundary (arrows) between the MSAW root pass and FCAW 1st pass.
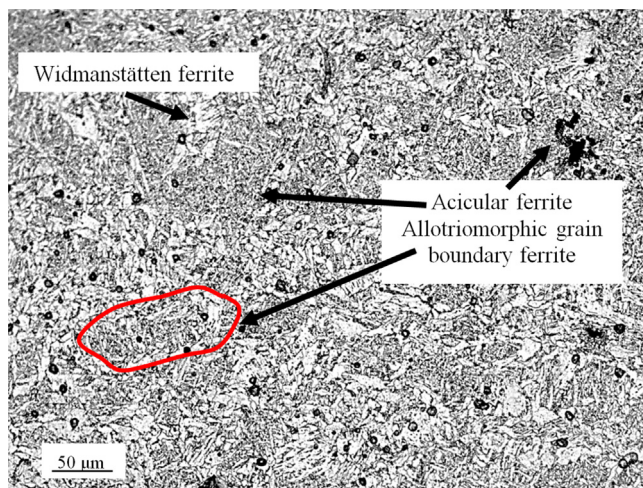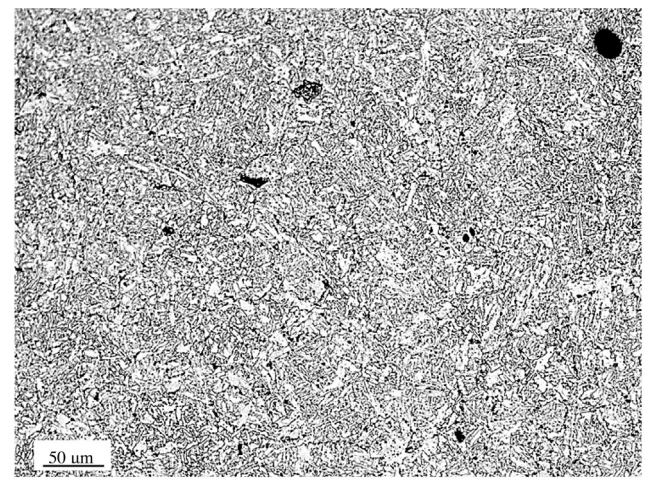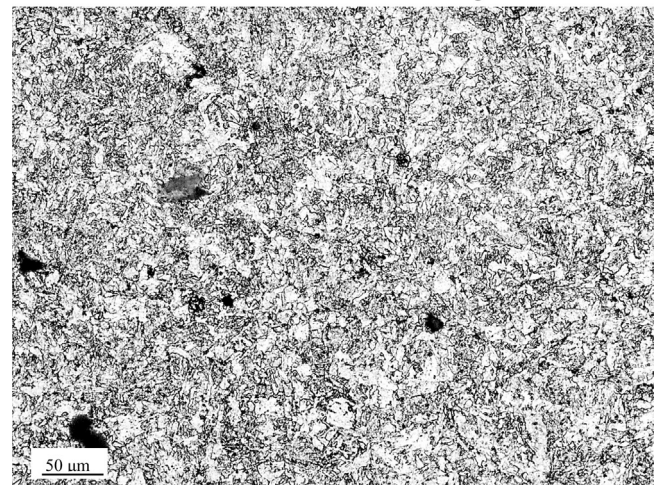

Fig. 9. Optical micrograph – middle of throat length to show the MSAW root pass of low heat input weld. (For interpretation of the references to colour in the text, the reader is referred to the web version of this article.)

LHI-Middle of weld throat length

HHI – middle of throat length

Fig. 10. Optical micrographs to show typical microstructure for mid-throat length pass of low heat input (LHI) and high input (HHI) FCAW welds.

there is a clear interface between the root pass and that of first pass of FCAW as shown by the arrows in Fig. 8b.

The microstructure of root pass of the LHI, Fig. 9, is distinctly different from that of the HHI (Fig. 8a) where there is more Widmanstätten ferrite with smaller grain size and more refined ferrite morphologies. The size of prior austenite grains is discernible if the allotriomorphic grain boundary ferrites are traced on the micrograph (one such prior austenite grain is shown on the micrograph in Fig. 9—red broken line). The changes in grain size and morphology of the weld will certainly affect the residual stresses and the resulted hardness as discussed later.

The optical micrographs in Fig. 10, taken from corresponding regions of the low and high heat input welds, highlight that it is basically the heat input that affects the scale and morphology of the weld metal. The high heat input contains more polygonal ferrite but less bainitic ferrite with a weld which is mainly acicular. The low heat input however, contains more Widmanstätten ferrite and bainite but still is a mainly acicular ferritic weld. Apart from the quantity of various ferritic morphologies, the main distinct difference between the low and high heat input welds (the heat input range used in this study) is the scale of microstructure with smaller prior austenite grains and more refined ferritic structure for low heat input welds. The formation of more Widmanstätten ferrite and bainite for the low heat input specimens fits well with the theoretical principles where a smaller prior austenite grain provides more nucleation sites for phases with nucleation preference at the
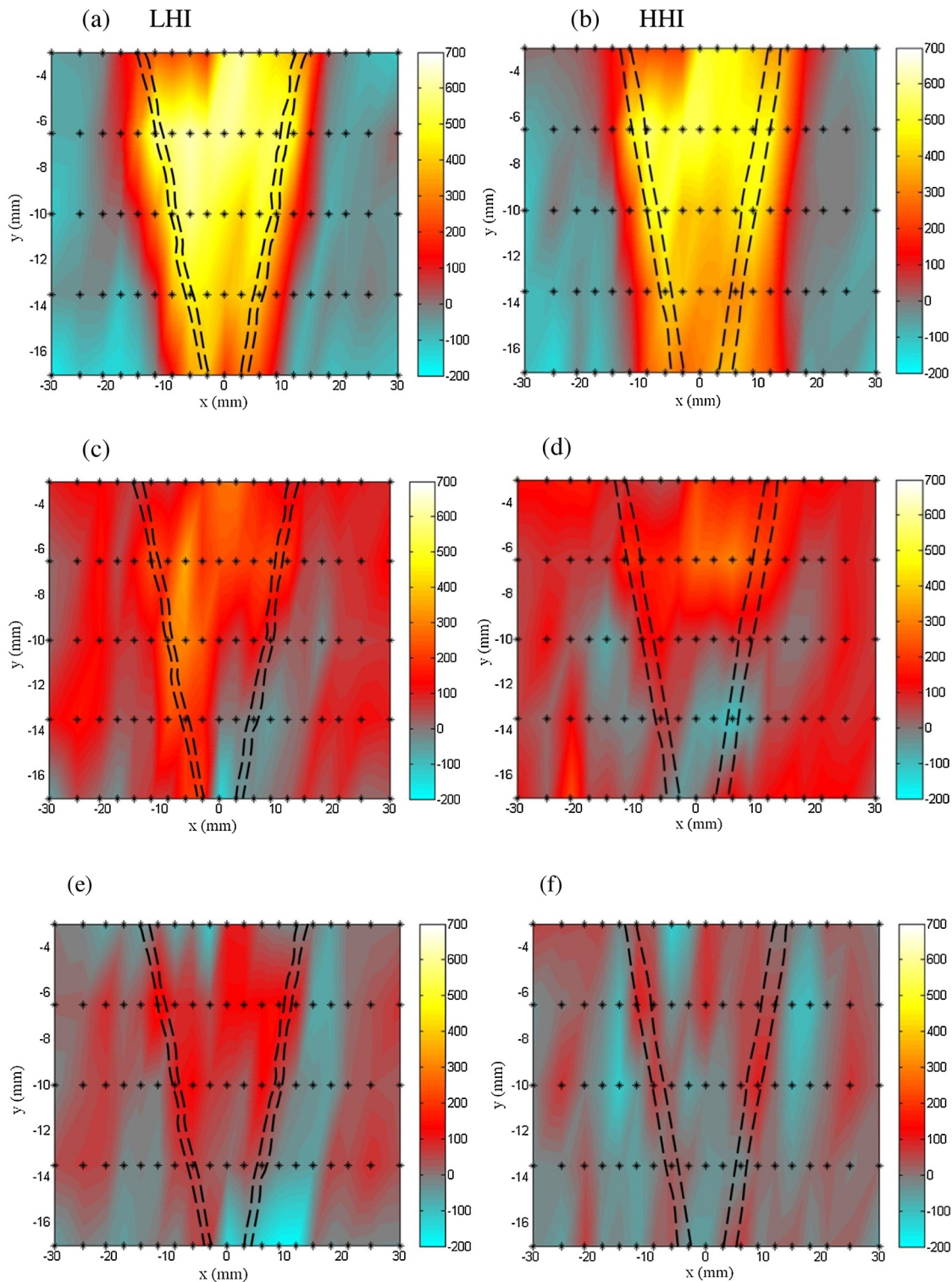
prior austenite grain boundaries, i.e., bainite and Widmanstätten ferrite (Ghomashchi et al., 2015).

3.2. Residual stresses

3.2.1. Heat input (welding speed)

A total of twenty five (25) weld runs were deposited for specimen I (Low Heat Input specimen-LHI) and 11 for specimen II (High
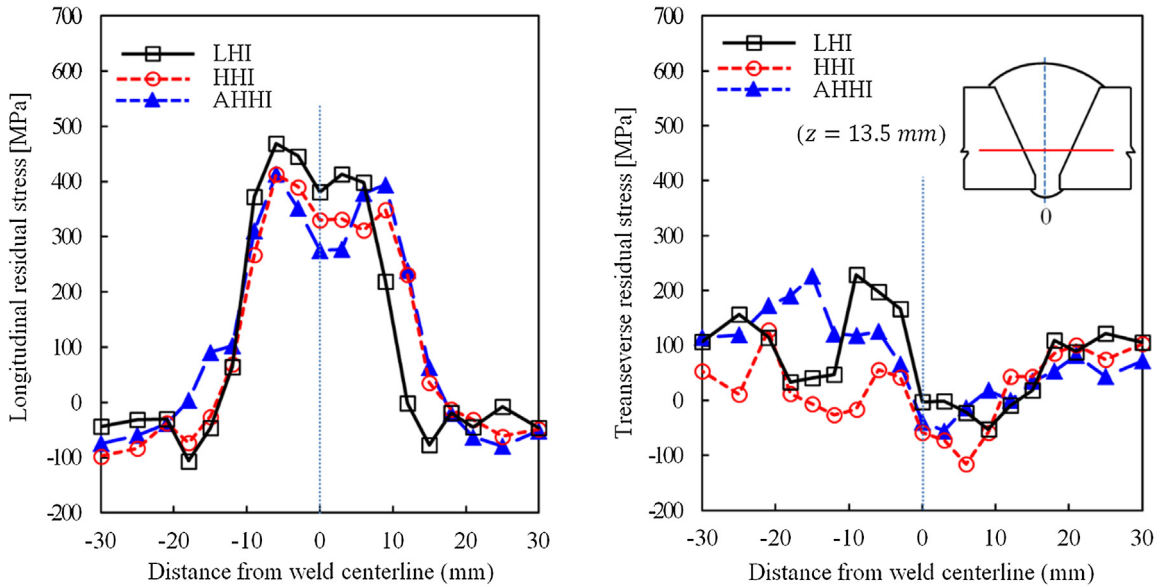
Fig. 11. Contour maps for longitudinal (a, b), transverse (c, d) and normal (e, f) components, as measured by neutron diffraction method for low heat input (LHI), left, and high heat input (HHI), right.

Heat Input specimen-HHI). The measured stresses were used to create contour maps in order to get an overall impression of the residual stress distributions, as shown in Fig. 11(a–e). The black cross markers on the contour plots show the measurement positions, while the broken lines indicate the HAZ regions. The area which represents the region of 3 mm–17 mm from weld surface, as identified from the micrographs for each specimen.

The highest residual stresses have been experienced in longitudinal direction for both high and low heat input samples at a depth of 6.5 mm below the surface. The peak tensile stress exceeds the yield stress of both the parent and weld metals reaching a magnitude of 633 ± 15 MPa. It is also evident that increasing the heat input decreases the longitudinal residual stresses notably. This is in line with microstructural analysis where a higher heat input resulted
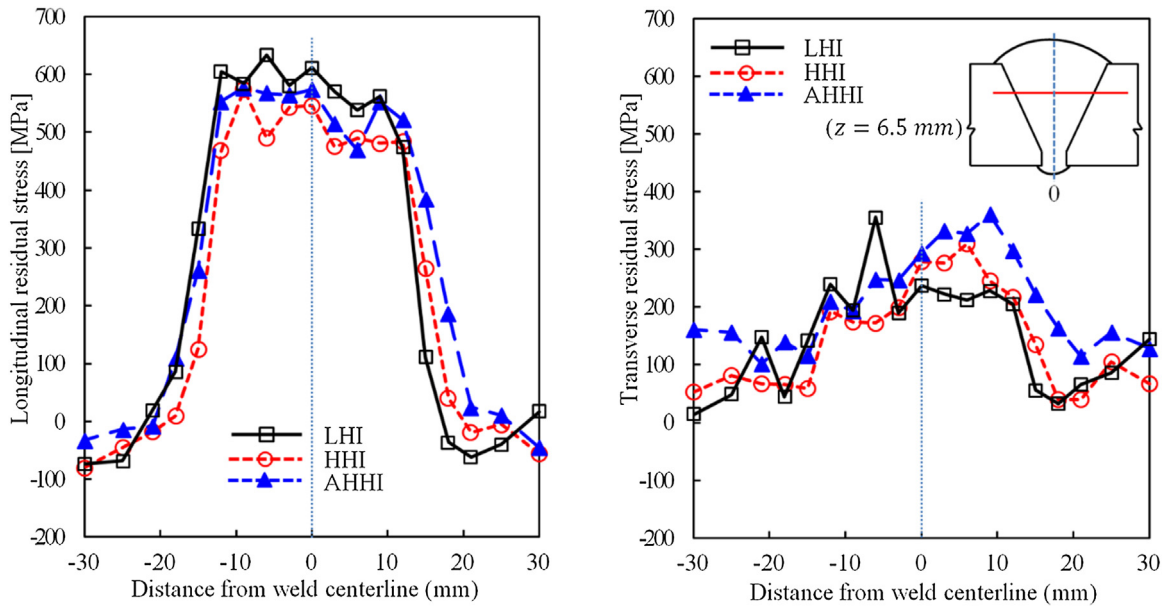
12(a): 6.5 mm from top surface (z = 6.5 mm);

12(c): 13.5 mm from top surface (z = 13.5 mm);

Fig. 12. Effects of heat input and pass sequence on longitudinal and transverse residual stresses: (a) 6.5 mm from the top surface (b) 10 mm and (c) 13.5 mm from the top surface; LHI—low heat input specimen (specimen I), HHI—high heat input (specimen II), AHHI: alternating high heat input weld sequence (specimen III).

HHI- 2nd weld pass (FCAW) after the root pass

HHI- last weld pass (FCAW)
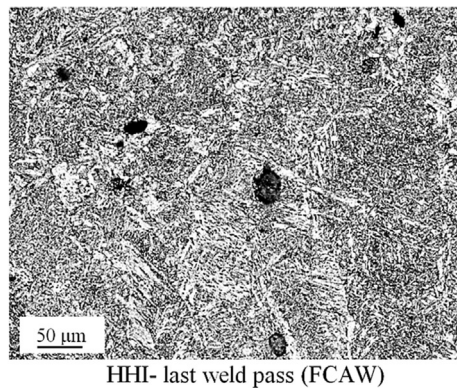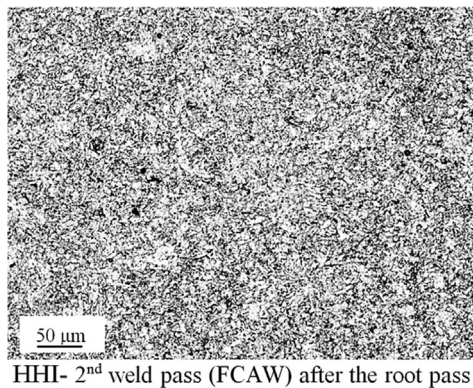
Fig. 13. Optical micrographs of weld metal microstructure for high heat input (HHI) specimens to highlight the effect of tempering of the later passes on the earlier ones.
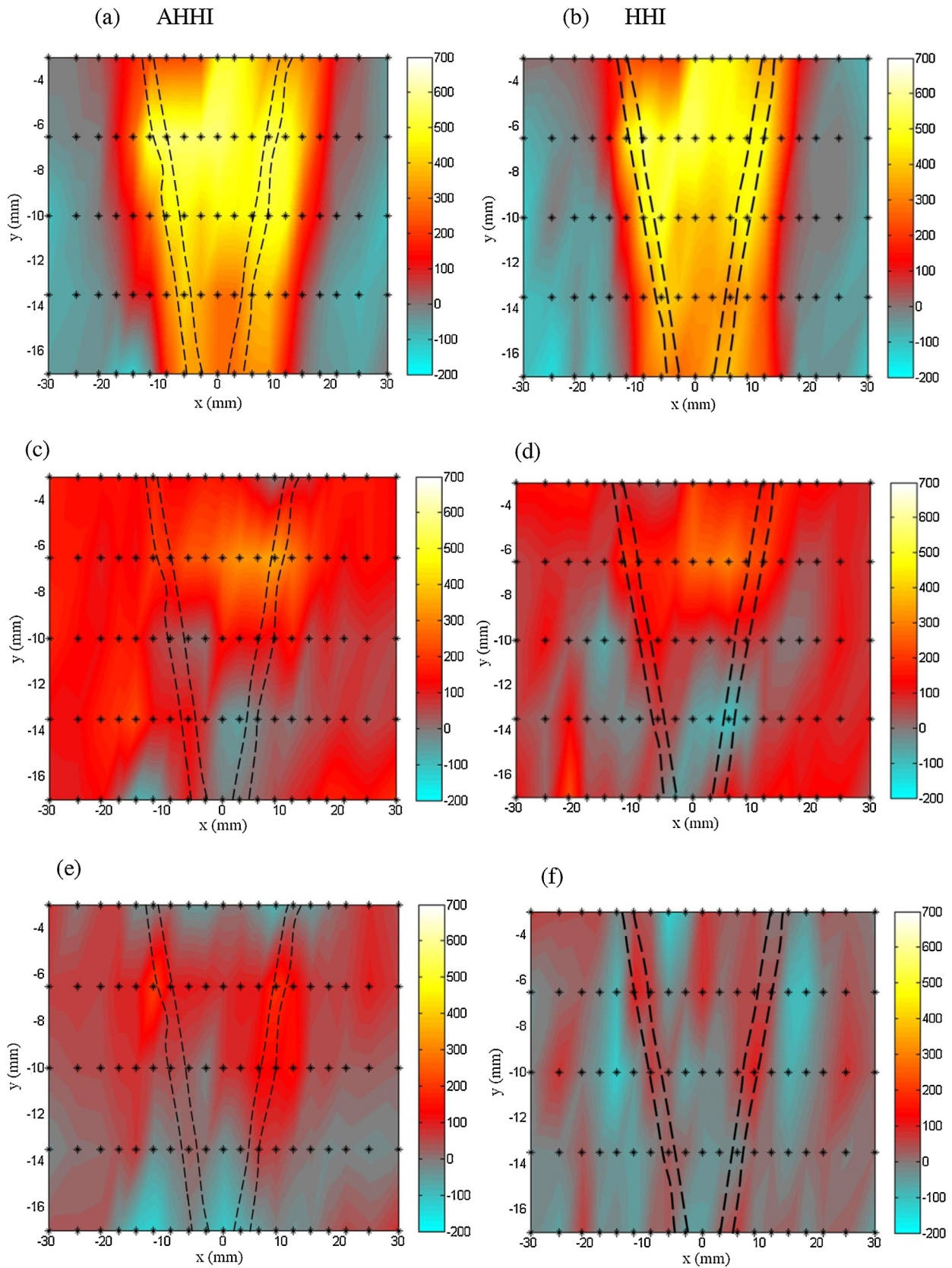
Fig. 14. Contour maps for longitudinal (a, d), transverse (b, e) and normal (c, f) components, as measured by neutron diffraction method for alternating welding sequence (AHHI), left, and high heat input (HHI), right.

in coarser prior austenite grains with coarser acicular ferrite. It is worth noting that in most cases a high level of residual stresses have developed within the HAZ. This may be attributed to the formation of more bainitic ferrite as the microstructure of the HAZ at the vicinity of fusion zone is examined closely, as shown in Fig. 7e and f. An important feature of these plots is the overall stress distribution within the weld joint and parent metal and whether the resulted tensile stresses are compensated by compressive stresses within the parent metal. The distribution of longitudinal and transverse residual stresses, Fig. 11(a–d), agrees with the results reported by Kim et al. (2009) who employed finite element simulation and neutron diffraction measurements for a V-butt steel. There is a distinct difference on the magnitude and distribution of transverse residual stresses for both low and high heat input specimens. The distribution of transverse stresses for the low heat input specimen in most regions in the weld metal and HAZ is mainly in tensile mode, but turns to compressive mode when the heat input is increased. This is practically evident around the mid thickness of about 10 mm below the weld surface. This shift in the distribution of transverse stresses is complex to be interpreted but may be due to tempering effect of final passes on the more inner passes. This can be explained through higher deposition rate in the lower layers of welds which lead to lower cooling rate and increased time for stress relaxation in HHI specimen. Fig. 12 also shows the comparative line plots of longitudinal and transverse residual stresses to better comprehend the residual stress distribution contour maps given in Fig. 11 for low and high heat input welds.

The magnitude of transverse stresses are notably higher for the low heat input welded specimen. This difference in some cases could even reach up to 220 MPa. In addition to faster cooling rate due to mass of weld metal for low heat input, it may also be explained through microstructural constituents, i.e., formation of bainite and Widmanstätten ferrite as discussed before. Similar finding was also reported in the literature where bainitic microstructure could lead to generation of higher level of residual stresses in welded structures (Smith et al., 1997).

It is also noteworthy to point out the effect of subsequent passes on the relieving of the residual stresses within the earlier passes, as for instance the peak longitudinal stress of 630 MPa measured within the final passes has reduced to less than 400 MPa at a depth of 17 mm below the surface (initial passes). This reduction could be related with the reduction of yield strength as a result of increasing cooling time and tempering effects. The contrast in the microstructure between the first and last passes of the high heat input specimen is clearly visible in Fig. 13.

The normal stress component for high heat input in most of the regions exhibits compressive stresses while for low heat input specimen the reversed effect can be observed.

3.2.2. Pass sequence

As for pass sequence effect on residual stresses a comparison of the field of residual stresses is presented in Fig. 14(a–e). Our results clearly demonstrate that the change in weld deposition direction doesn't have a significant effect on the magnitude and distribution of the longitudinal residual stresses which is well in line with microstructural analysis i.e., negligible differences were detected when alternating weld sequence was employed. The line plots of Fig. 12 provide quantitative values to better illustrate the residual stress distributions, counter maps, due to pass sequence.

3.3. Hardness analysis

Fig. 15(a–c) shows the hardness map across the weld for different welded specimens. Generally hardness values for the sample with lower heat input was higher than those with higher heat input. This is due to the fact that cooling rate for the sample with lower
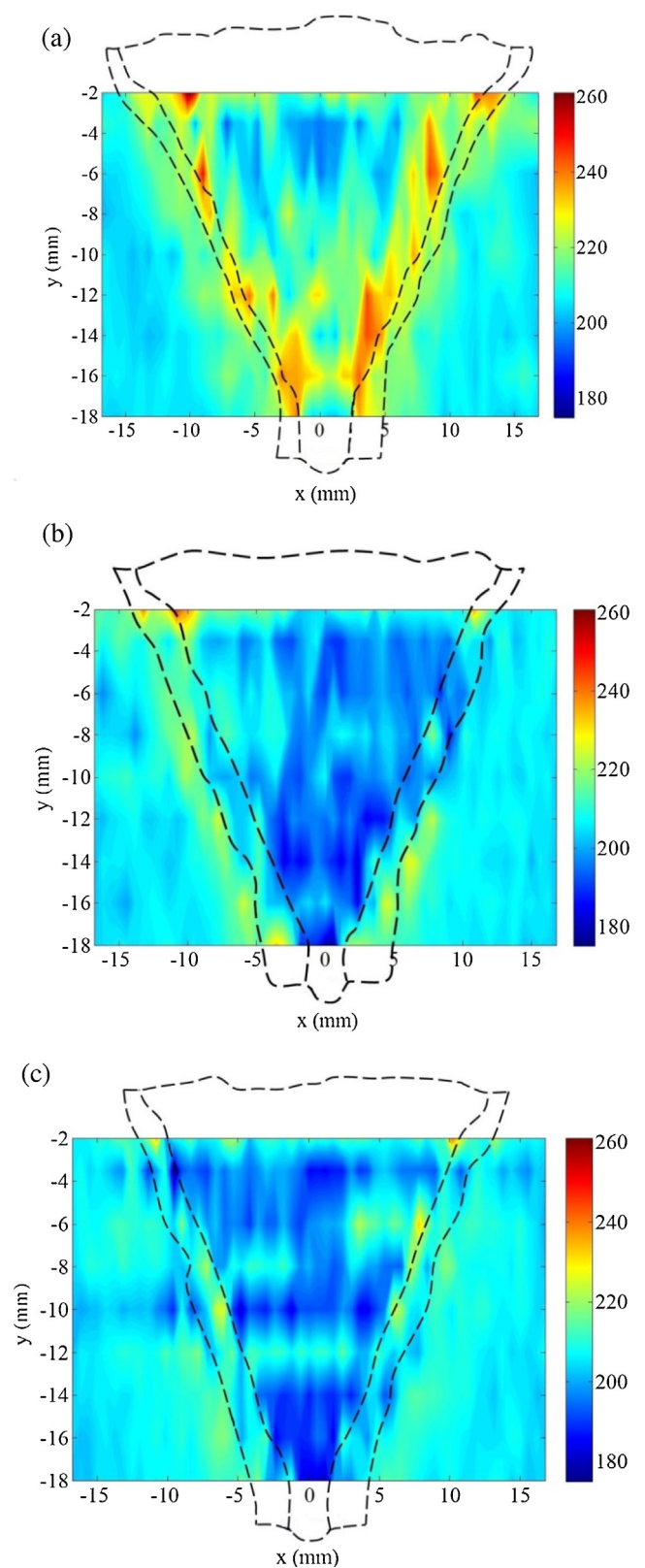

Fig. 15. Microhardness map for (a) low heat input specimen; (b) high heat input specimen and (c) alternating high heat input welding sequence.
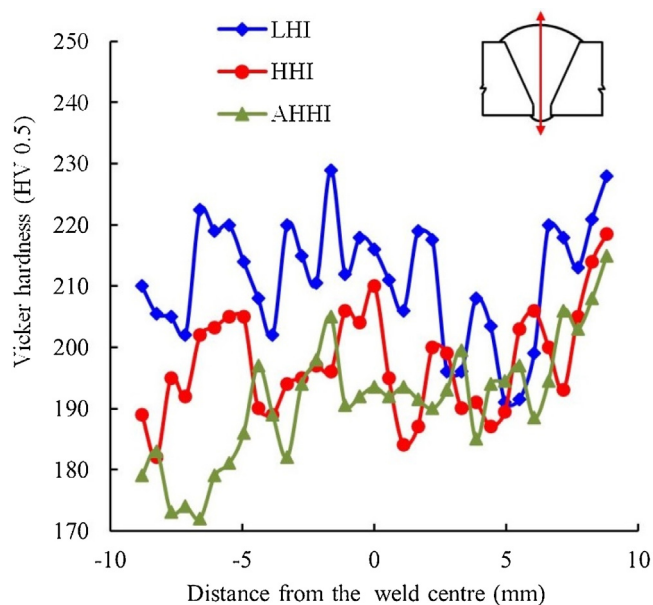
Fig. 16. Microhardness profile showing hardness through the thickness for different welded specimens.

heat input is higher with its direct effect on the microstructure. The smaller prior austenite grains, and the formation of more bainitic and Widmanstätten ferrite, as clearly demonstrated in Fig. 10, are responsible for changes in hardness. However, due to un-even temperature distribution across the weld the magnitude of hardness has fluctuations. Furthermore, the higher residual stresses for the low heat input specimens are another indication of expecting higher hardness values.

Fig. 16 shows the microhardness measurements in the weld centreline (through the thickness). The high hardness value near the surface of the plate is due to higher cooling rate. The fluctuations in the micro hardness values, specifically for the low heat input specimen, is attributed to the number of passes where the weld metal is exposed to higher number of heating and cooling cycles. It is also interesting to note that the distribution and magnitude of the residual stresses have similar trend as microhardness measurements, as shown in Fig. 11(a–e). The hardness values for low heat input weld is greater than that of high heat input in support of the residual stresses measurement. It is important to note that changing the welding sequence did not have significant impact on hardness distributions.

4. Conclusions

The key findings of this experimental study were:

- The microstructure of weld changes with heat input where a lower heat input renders more bainitic and Widmanstätten ferrite resulted from smaller prior austenite grain size.
- Residual stresses in excess of yield strength were developed in the weld metal and HAZ particularly for the upper-layers of welds. The magnitude of residual stresses for the specimen with lower heat input (higher welding travel speed) was significantly higher than the specimens with higher heat input (lower welding travel speed). This could be explained through the existing microstructure constituents of bainite and Widmanstätten ferrite in weld

metal and HAZ of LHI specimen. Similar trend was also found for the hardness measurements where higher hardness was found for the LHI specimen.

- The magnitude of residual stresses decreased substantially with weld depth due to tempering effects of the later weld passes onto the earlier weld runs. The tempering effect was also more pronounced for the HHI specimens due to increased cooling time for stress relaxations.
- Compressive transverse residual stresses were found for the HHI specimens, particularly from the mid thickness down of the plate in most regions of weld metal and HAZ. This has a favorable effect on structural integrity of welded structures.
- The results indicated no significant effect on the magnitude of the longitudinal residual stresses as a result of changing the weld deposition direction. The results were in line with microstructural and hardness analyses where negligible differences were detected when alternating weld deposition sequence was used.

Appendix A.

Table A1
Chemical composition of ER70S-6, E81T1-Ni 1 M and parent metal.

Chemical composition	ER 70S-6	E81T1-Ni 1 M	Parent metal
%C	0.09	0.04–0.05	0.052
%Mn	<1.60	1.26–1.36	1.55
%S	0.007	0.006–0.009	0.0011
%Si	0.90	0.25–0.29	0.21
%P	0.007	0.005-0.008	0.0097
%Cu	0.20	–	0.15
%Cr	0.05	0.04–0.05	0.026
%Ni	0.05	0.86–0.96	0.19
%Mo	0.05	0.01	0.18
%V	0.05	0.02–0.03	0.029
%Ti	–	–	0.012
%NB	–	–	0.041

Table A2
Mechanical properties of parent metal and welding consumables provided by the manufacturer.

	Yield strength (MPa)	Tensile strength (MPa)	% elongation	Charpy V–notch test (−40 °C)
X70	485	565–758	17	–
E81T1-Ni1m	470	590	21	95 J
ER 70S-6	482	592	25	–

Table A3
Welding parameters used for specimen I—Low heat input (LHI).

Pass number	Filler/electrode		AMP DCEP	Gas		Volts DCEP	Speed mm/min	HI kJ/mm
	Size	Class		Type	Class			
1	0.9	ER70S-6	98	Argoshield	52	21	244	0.5
2	1.2	E81TNi	153	Argoshield	52	25	354	0.65
3	1.2	E81TNi	153	Argoshield	52	25	298	0.77
4	1.2	E81TNi	153	Argoshield	52	25	354	0.65
5	1.2	E81TNi	153	Argoshield	52	25	323	0.71
6	1.2	E81TNi	153	Argoshield	52	25	372	0.62
7	1.2	E81TNi	153	Argoshield	52	25	354	0.65
8	1.2	E81TNi	153	Argoshield	52	25	338	0.68
9	1.2	E81TNi	153	Argoshield	52	25	331	0.69
10	1.2	E81TNi	153	Argoshield	52	25	346	0.66
11	1.2	E81TNi	153	Argoshield	52	25	304	0.75
12	1.2	E81TNi	153	Argoshield	52	25	323	0.71
13	1.2	E81TNi	153	Argoshield	52	25	338	0.68
14	1.2	E81TNi	153	Argoshield	52	25	438	0.53
15	1.2	E81TNi	153	Argoshield	52	25	331	0.69
16	1.2	E81TNi	153	Argoshield	52	25	338	0.68
17	1.2	E81TNi	153	Argoshield	52	25	372	0.62
18	1.2	E81TNi	153	Argoshield	52	25	402	0.57
19	1.2	E81TNi	153	Argoshield	52	25	372	0.62
20	1.2	E81TNi	153	Argoshield	52	25	298	0.77
21	1.2	E81TNi	153	Argoshield	52	25	346	0.66
22	1.2	E81TNi	153	Argoshield	52	25	354	0.65
23	1.2	E81TNi	153	Argoshield	52	25	310	0.74
24	1.2	E81TNi	153	Argoshield	52	25	323	0.71
25	1.2	E81TNi	153	Argoshield	52	25	317	0.73

Table A4
Welding parameters used for specimen II and III—High heat input (HHI).

Pass number	Filler/electrode		AMP DCEP	Gas		Volts DCEP	Speed mm/min	HI kJ/mm
	Size	Class		Type	Class			
1	0.9	ER70S-6	98	Argoshield	52	21	240	0.51
2	1.2	E81TNi	153	Argoshield	52	25	271	0.85
3	1.2	E81TNi	153	Argoshield	52	25	210	1.1
4	1.2	E81TNi	153	Argoshield	52	25	149	1.54
5	1.2	E81TNi	153	Argoshield	52	25	120	1.91
6	1.2	E81TNi	153	Argoshield	52	25	162	1.42
7	1.2	E81TNi	153	Argoshield	52	25	160	1.44
8	1.2	E81TNi	153	Argoshield	52	25	173	1.33
9	1.2	E81TNi	153	Argoshield	52	25	150	1.53
10	1.2	E81TNi	153	Argoshield	52	25	153	1.5
11	1.2	E81TNi	153	Argoshield	52	25	155	1.46

**It is important to note that similar heat input was used for specimens II and III, but in specimen III the direction for each subsequent weld pass was changed.

References

Alipooramirabad, H., Kotousov, A., Ghomashchi, R., 2014. Numerical analysis of welding stresses in WIC weldability test.

Alipooramirabad, H., Paradowska, A., Ghomashchi, R., Kotousov, A., Reid, M., 2015. Quantification of residual stresses in multi-pass welds using neutron diffraction. J. Mater. Process. Technol. 226, 40–49.

Ghomashchi, R., Costin, W., Kurji, R., 2015. Evolution of weld metal microstructure in shielded metal arc welding of X70HSLA steel with cellulosic electrodes: a case study. Mater. Charact. 107, 317–326.

Keehan, E., 2004. Effect of Microstructure on Mechanical Properties of High Strength Steel Weld Metals. Chalmers University of Technology and Göteborg University.

Kim, S.-H., Kim, J.-B., Lee, W.-J., 2009. Numerical prediction and neutron diffraction measurement of the residual stresses for a modified 9Cr–1Mo steel weld. J. Mater. Proc. Technol. 209, 3905–3913.

Kumar, S., Shahi, A.S., 2011. Effect of heat input on the microstructure and mechanical properties of gas tungsten arc welded AISI 304 stainless steel joints. Mater. Des. 32, 3617–3623.

Leggatt, R.H., 2008. Residual stresses in welded structures. Int. J. Press. Vessels Pip. 85, 144–151.

Park, M.J., Yang, H.N., Jang, D.Y., Kim, J.S., Jin, T.E., 2004. Residual stress measurement on welded specimen by neutron diffraction. J. Mater. Proc. Technol. 155, 1171–1177.

Qureshi, M.E., 2008. Analysis of Residual Stresses and Distortions in Circumferentially Welded Thin-Walled Cylinders. National University of Sciences and Technology.

Ragu Nathan, S., Balasubramanian, V., Malarvizhi, S., Rao, A.G., 2015. Effect of welding processes on mechanical and microstructural characteristics of high strength low alloy naval grade steel joints. Def. Technol. 11, 308–317.

Shi, Y., Han, Z., 2008. Effect of weld thermal cycle on microstructure and fracture toughness of simulated heat-affected zone for a 800 MPa grade high strength low alloy steel. J. Mater. Proc. Technol. 207, 30–39.

Smith, C., Pistorius, P.G.H., Wannenburg, J., 1997. The effect of a long post weld heat treatment on the integrity of a welded joint in a pressure vessel steel. I. J. Press. Vessels Pip. 70, 183–195.

Yang, Y., 2008. The Effect of Submerged Arc Welding Parameters on the Properties of Pressure Vessel and Wind Turbine Steels Department of Mechanical Engineering University of Saskatchewan, Canada.

Zhang, C., Lu, P., Hu, X., Song, X., 2013. Residual stress-induced deformation and fatigue crack growth in weld-repaired high-strength low-alloy steel with soft buffer layer. Mater. Sci. Eng.: A 564, 147–157.

Zondi, M.C., 2014. Factors that affect welding-induced residual stress and distortions in pressure vessel steels and their mitigation techniques: a review. J. Press. Vessel Technol. 136, 040801.

CHAPTER 7

INVESTIGATING THE EFFECTS OF WELDING PROCESS ON RESIDUAL STRESSES, MICROSTRUCTURE AND MECHANICAL PROPERTIES IN HSLA STEEL WELDS

Houman Alipooramirabad[1]*, Anna Paradowska[2, 3], Reza Ghomashchi[1], Mark Reid[2]

[1]School of Mechanical Engineering, the University of Adelaide, SA 5005

[2] Bragg Institute, Australian Nuclear Science and Technology Organisation (ANSTO), Lucas Heights, NSW 2234, Australia

[3]School of Mechanical and Manufacturing Engineering, UNSW, Sydney, NSW 2052, Australia

Statement of Authorship

Title of Paper	Investigating the effects of welding process on residual stresses, microstructure and mechanical properties in HSLA steel welds
Publication Status	☐ Published ☐ Accepted for Publication ☑ Submitted for Publication ☐ Unpublished and Unsubmitted work written in manuscript style
Publication Details	Alipooramirabad H, Paradowska A, Ghomashchi R, Reid M. Investigating the effects of welding process on residual stresses, microstructure and mechanical properties in HSLA steel welds. Journal of Manufacturing Processes (under review)

Principal Author

Name of Principal Author (Candidate)	Houman Alipooramirabad		
Contribution to the Paper	I was responsible for the literature review required for this work, and designed the framework for the experimental conditions. I carried out mechanical property and microstructural behaviour analysis, wrote the first draft of the manuscript and incorporated and addresses all comments and suggestions by other authors in subsequent revesions of the manuscript. Interpertation of the data was primary my responsibility.		
Overall percentage (%)	90%		
Certification:	This paper reports on original research I conducted during the period of my Higher Degree by Research candidature and is not subject to any obligations or contractual agreements with a third party that would constrain its inclusion in this thesis. I am the primary author of this paper.		
Signature		Date	30/01/2017

Co-Author Contributions

By signing the Statement of Authorship, each author certifies that:

     i.   the candidate's stated contribution to the publication is accurate (as detailed above);

    ii.   permission is granted for the candidate in include the publication in the thesis; and

   iii.   the sum of all co-author contributions is equal to 100% less the candidate's stated contribution.

Name of Co-Author	Anna Paradowska		
Contribution to the Paper	I was joint supervisor of this work, assisted for conducting some part of the experiments, and jointly contributed to refining the manuscript.		
Signature		Date	02/02/2017

Name of Co-Author	Reza Ghomaschchi
Contribution to the Paper	I was joint supervisor for the work, helped in developing ideas and contributed to refining the manuscript.
Signature		Date	31/01/2017

Name of Co-Author	Mark Reid
Contribution to the Paper	I jointly contributed to conducting some part of the experiments and jointly contributed to refining the manuscript..
Signature		Date	31/01/2017

Corresponding Author: Mr. Houman Alipooramirabad, PhD student

Corresponding Author's Institution: University of Adelaide

First Author: Houman Alipooramirabad, PhD student

Order of Authors: Houman Alipooramirabad, PhD student; Anna Paradowska, PhD; Reza Ghomashchi, PhD; Mark Reid, PhD

Abstract: One of the important steps in the design and fabrication of welded structures is the selection of the welding process and the filler consumables. This is because these two factors control the mechanics of thermal distribution and the chemistry of the welded join, which in turn affect weld integrity through the resulting microstructure and residual stresses. The present study employed neutron diffraction to investigate the effects of welding process on the residual stresses in high-strength low-alloy steel weld joints made by SMAW (Shielded Metal Arc Welding) and combined MSAW (Modified Short Arc Welding) and FCAW (Flux Cored Arc welding) processes. A significantly higher level of residual stress was found in the MASW+FCAW combination which was shown to be in line with the microstructural and mechanical properties. Higher levels of residual stresses may be related to the formation of bainite and Widmanstätten ferrite in the weld metal and HAZ of the combined MSAW and FCAW processes.

Suggested Reviewers:

Opposed Reviewers:

Cover Letter

SCHOOL OF MECHANICAL ENGINEERING
FACULTY OF ENGINEERING, COMPUTER &
MATHEMATICAL SCIENCES

Houman Alipooramirabad
PhD student

THE UNIVERSITY OF ADELAIDE
SA 5005
AUSTRALIA

TELEPHONE +61 8 83135439
FACSIMILE +61 8 83134367

houman.alipooramirabad@adelaide.edu.au

12 December 2016

Professor Shiv Kapoor, Editor-in-Chief Journal of Manufacturing Processes

Dear Professor Shiv Kapoor,

On behalf of my co-authors let me begin by thanking you for the review of our article "*No: SMEJMP-D-16-00374, "*Investigating the effects of welding process on residual stresses, microstructure and mechanical properties in HSLA steel welds". The remarks made by the referees have been insightful and addressing them has the addition of other relevant material and contributed significantly to the quality of the paper. Attached to this letter is a detailed overview of changes that have been made to the paper, which includes a point-by-point response to each query made by the reviewers. The amendments have been highlighted with a blue colour through Marked-Manuscript.

We trust that you will find the revised paper to be suitable for publication in the Journal of Manufacturing Processes.

Yours sincerely,

Houman Alipooramirabad
PhD student
School of Mechanical Engineering

The University of Adelaide

Investigating the effects of welding process on residual stresses, microstructure and mechanical properties in HSLA steel welds

Houman Alipooramirabad[1]*, Anna Paradowska[2, 3], Reza Ghomashchi[1], Mark Reid[2]

[1]School of Mechanical Engineering, the University of Adelaide, SA 5005

[2] Bragg Institute, Australian Nuclear Science and Technology Organisation (ANSTO), Lucas Heights, NSW 2234, Australia

[3]School of Mechanical and Manufacturing Engineering, UNSW, Sydney, NSW 2052, Australia

Tel 61 8 83135439

Fax 61 8 83134367

Abstract: One of the important steps in the design and fabrication of welded structures is the selection of the welding process and the filler consumables. This is because these two factors control the mechanics of thermal distribution and the chemistry of the welded join, which in turn affect weld integrity through the resulting microstructure and residual stresses. The present study employed neutron diffraction to investigate the effects of welding process on the residual stresses in high-strength low-alloy steel weld joints made by SMAW (Shielded Metal Arc Welding) and combined MSAW (Modified Short Arc Welding) and FCAW (Flux Cored Arc welding) processes. A significantly higher level of residual stress was found in the MASW+FCAW combination which was shown to be in line with the microstructural and mechanical properties. Higher levels of residual stresses may be related to the formation of bainite and Widmanstätten ferrite in the weld metal and HAZ of the combined MSAW and FCAW processes.

Key words: Welding process, Mechanical properties, Microstructural characterization, HSLA steels, Residual stress, Neutron diffraction technique

[1]*Corresponding author, E-mail: houman.alipooramirabad@adelaide.edu.au;

1. Introduction

Welding consumables and welding processes have significant effects on the integrity of welded structures and their performance in service [1-5]. This is because the chemistry of the filler material and the employed deposition mechanics control the phase transformation and thermal distribution in the weld metal respectively. The other important parametric welding setups are the mechanical design of the joint (geometry) and the applied heat input. These are the key factors for the evolution of microstructure and residual stress distribution of the weldments as well as the extent of heat affected zone [6]. The key parameter is the heat input because it determines the peak temperature at each location within the heat affected region as well as the cooling rate. Residual stress is caused by misfits due to different degrees of contraction in different region of the weld and is correlated with the thermal history [7]. The filler chemistry however determines the onset of phase transformation and the associated thermal strain offset by volume increases as detailed in a review study by Withers and Bhadeshia [8].

Amongst a range of welding processes shielded metal arc welding (SMAW) and a combination of modified short arc welding (MSAW) and flux cored arc welding (FCAW) processes are more acceptable routes in fabrication of high-strength low-alloy steel welded structures such as energy pipeline networks, ship building or pressure vessels. Welding with SMAW process offers several advantages including lower equipment cost, portability of equipment, and welding in various positions and confined spaces. If using cellulosic consumables, a faster welding speed and more penetrable welds could be achieved, although hydrogen dissolution may be an issue [9, 10]. At the same time using a combination of MSAW and FCAW processes is reported to provide excellent results including ensuring high deposition rate, i.e. improved productivity rates, low distortion and adaptability and ease of use of equipment [11]. For SMAW process, the heat input is usually higher than that of the MSAW resulting in formation of coarser bead structure due to having a slower cooling rate.

The wider arc column is another issue for SMAW to induce a wider fusion zone and HAZ [12]. For MSAW, the smaller bead size provides a higher energy density with having less spread of the fusion zone and HAZ along with a comparatively faster cooling rate [12]. This is not the case for FCAW used for fill passes where a higher deposition rate results in lower cooling rate when compared to that of the SMAW process [13]. The lower cooling rate results in FCAW having greater tempering effect on coarse grained heat affected zone (CGHAZ) in contrast to joints fabricated by the SMAW [14, 15].

In terms of the welded structure service integrity and performance, SMAW and coupled MSAW and FCAW respond differently. Balasubramanian and Guha [16] investigated the effects of welding process on toe cracking behaviour of load carrying cruciform joints. The joints were fabricated from pressure vessel grade steel (ASTM 515 grade F with 0.08-0.22% C and 0.55-1.10 Mn) using SMAW and FCAW processes. It was found that fatigue life is typically longer for SMAW joints than for FCAW fabricated joints. This difference in behaviour was attributed to the fatigue cracks that can easily propagate across a bainitic packet in FCAW with little resistance encountered at low angle boundaries within a pocket. The experimental study also revealed the importance of microstructural characteristics of the HAZ in the fatigue life and toe cracking behaviour of the joints. The findings showed that the HAZ of SMAW contained a low carbon martensitic structure and exhibited better fatigue resistance in comparison with the bainitic HAZ microstructure of FCAW joints. The variation in the microstructure of the HAZ can be explained by the higher heat input employed in FCAW (formation of bainite due to lower cooling rate) which lead to inferior fatigue performance of FCAW joints compared to SMAW joints.

The effects of welding process on the resulting residual stresses and distortion have also been previously studied [14, 15]. A range of welding processes including Gas tungsten arc welding (GTAW), also known as TIG, and Activated-TIG (A-TIG), submerged arc welding (SAW),

direct current gas metal arc welding (DCGMAW), also known as (MIG), Fronius cold metal transfer (CMT), autogenous laser and hybrid laser welding were used to highlight that both the magnitude and the distribution profile of residual stresses change with welding process [14, 15].

As briefly mentioned here, there is no report to examine the benefits and drawbacks of SMAW and combined MSAW+FCAW to eventually arrive at a cheaper and better quality welding process. The current study is therefore carried out to characterize both methods with respect to microstructure, and residual stresses and highlight the ways these factors affect the mechanical properties (hardness and tensile properties) of the welded joint in multi-pass welds. In this paper we present comparative results of microstructural/mechanical property investigations and residual stress measurements for the welded joints fabricated with SMAW and a combination of MSAW for the root pass and FCAW for the remaining passes of multi-pass high-strength low-alloy steel welds widely used in oil and gas pipelines.

2. Experimental procedure

2.1 Details of weld deposition procedure

The test specimens comprised of two 20 mm thick steel plates (API 5L grade X70) with the dimensions of 250x200 mm^2. The preparatory joint geometry is shown in Figs 1 and 3. A total of four (4) samples were fabricated. Two welded samples were used to measure the lattice spacing ($d_{0,hkl}$) in stress free mode and the other two samples were used to evaluate the residual stresses for both specimens. In order to prepare a stress-free sample, both SMAW and MSAW+FCAW specimens was cut in the manner shown in Figure 2. This is an especial cutting procedure employed, using electro-discharge machining (EDM), to relieve macro-stresses from the weld and HAZ region without introducing new stresses due to cutting [17]. In order to justify the comparison between the two different processes employed in this study, it was tried to have closely possible welding parameters such as heat input and number of

weld runs as well as welding consumables with similar mechanical properties. It should be noted that the average heat input for the SMAW and MSAW+FCAW was 0.767 and 0.667 kJ/mm, respectively. However, due to differences in deposition rates (e.g. higher deposition rate with flux cored arc welding) and the arc characteristics it was not possible to have similar number of weld runs. Therefore welding with the FCAW resulted in 25 weld runs along with the MSAW root pass while in SMAW 30 weld runs were deposited for exactly the same joint geometry and size. The welded specimen with the clamp position is shown in Fig.1.
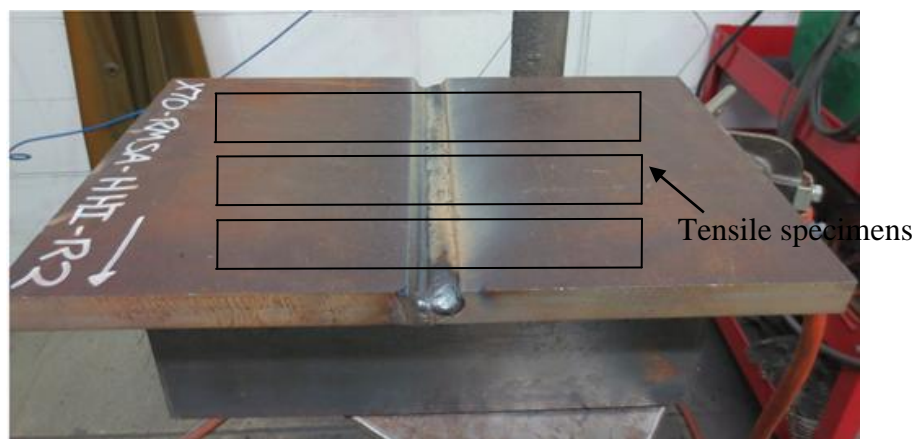
(a) Welded specimen
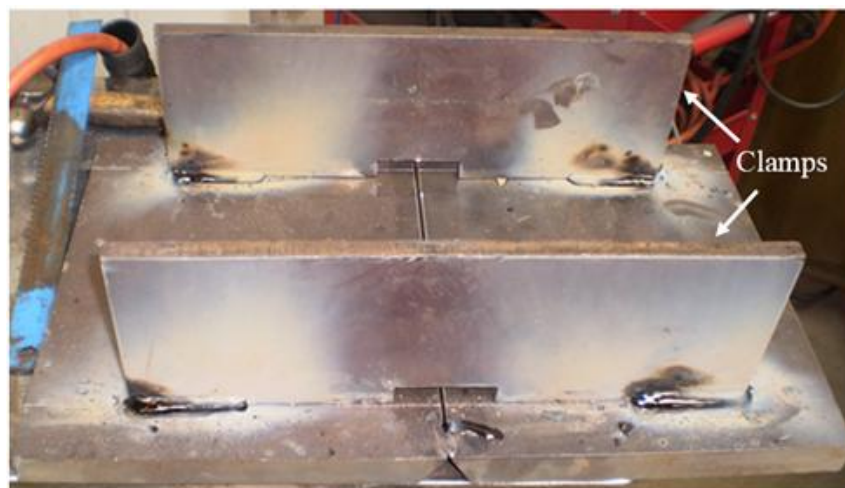
(b) Clamp position

Fig.1: welded specimen with the applied constraint
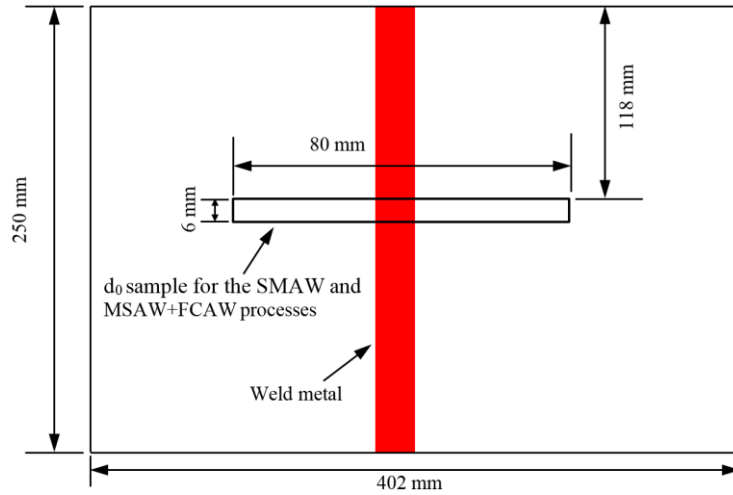
Fig. 2: Schematic drawing of prepared d_0 sample (stress-free sample)

Specimen series I: The welding process for these samples was SMAW. The weld consumable was specified to be E6010 electrode with a diameter of 3.2 mm for the root pass and E8010 electrode of 4 mm diameter for deposition of remaining passes. Fig. 3 specifies the detailed dimensions of the weld cross section for both samples and the deposition sketch for the SMAW processes. The chemical composition of the weld consumables is given at Table.1.

Table1: Chemical composition of welding consumables and parent metal

Chemical composition	ER 70S-6	E81T1-Ni 1M	E6010	E8010	Parent metal
%C	0.09	0.04-0.05	0.16	0.20	0.052
%Mn	<1.60	1.26-1.36	0.62	1.20	1.55
%S	0.007	0.006-0.009	0.009	0.03	0.0011
%Si	0.90	0.25-0.29	0.19	0.60	0.21
%P	0.007	0.005-0.008	0.009	0.03	0.0097
%Cu	0.20	-			0.15
%Cr	0.05	0.04-0.05	0.02	0.30	0.026
%Ni	0.05	0.86-0.96	0.2	1.00	0.19
%Mo	0.05	0.01	0.01	0.50	0.18
%V	0.05	0.02-0.03	≤0.01	≤0.10	0.029
%Ti	-	-			0.012
%NB	-	-			0.041

Fig. 3: Weld deposition sequence in specimen with SMAW process

Also, the details of the welding parameters is given in Table.2.

Specimen series II: The V-prep weld joints were manufactured using fluxed core arc welding (FCAW) processes with an ER70s-6 electrode for the root pass and modified short arc welding (MSAW) using E81TNi Flux cored wire for the remaining passes. The weld deposition sketch is shown in Fig. 4.
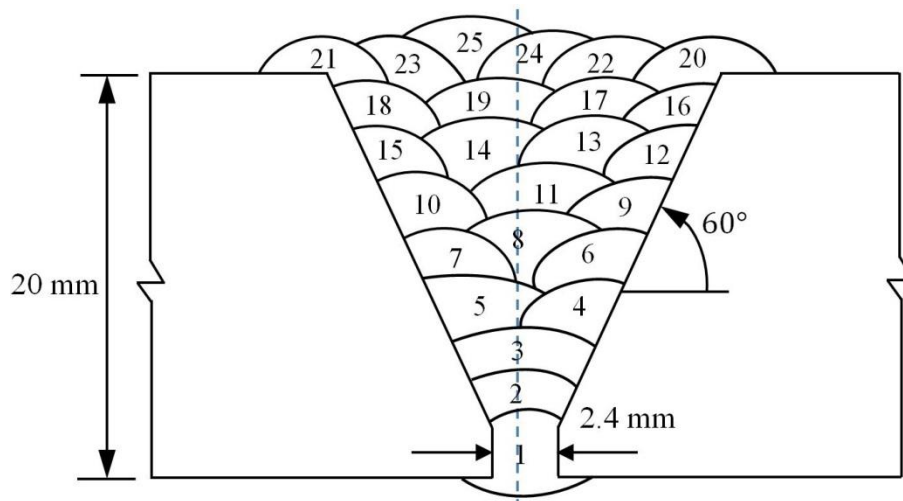
Fig. 4: Weld deposition sequence in specimen II (MSAW and FCAW process)

Table 2: Welding parameters used for SMAW process

Pass Number	Filler/Electrode		AMP	Volts	Speed	HI
	Size	Class	DCEP	DCEP	mm/min	kJ/mm
1	3.2	E6010	80.7	28.6	239	0.58
2	3.2	E8010	89	28.2	296	0.51
3	4	E8010	128.5	26.2	333	0.61
4	4	E8010	132.9	27	341	0.63
5	4	E8010	134.2	27.8	294	0.76
6	4	E8010	141.1	27.2	283.	0.81
7	4	E8010	139.5	26.8	277.8	0.81
8	4	E8010	144.9	26.4	324.6	0.71
9	4	E8010	143	27.2	282	0.83
10	4	E8010	144.5	27.4	288	0.82
11	4	E8010	144.7	27.8	321.2	0.75
12	4	E8010	143.8	28.1	294	0.82
13	4	E8010	144.1	26.1	289.6	0.78
14	4	E8010	143	26.4	294	0.77
15	4	E8010	141.4	27	283.5	0.81
16	4	E8010	141.5	27.8	289.6	0.82
17	4	E8010	142.8	26.2	279	0.80
18	4	E8010	143.2	27.5	287	0.82
19	4	E8010	139.8	26.4	279.8	0.79
20	4	E8010	142.3	27.4	286.8	0.82
21	4	E8010	138.8	27.4	280.4	0.81
22	4	E8010	143.6	27.5	306	0.77
23	4	E8010	142	27.3	287.3	0.81
24	4	E8010	141.9	26.5	289	0.78
25	4	E8010	134	27.2	283	0.77
26	4	E8010	140.7	26.6	288.5	0.78
27	4	E8010	143.5	26.7	295	0.78
28	4	E8010	141.9	26.8	290	0.79
29	4	E8010	142.7	27.1	277.8	0.84
30	4	E8010	141.5	26.8	267.8	0.85

The chemical composition of ER70s-6 and E81TNi can be seen in Table.1. The details of welding parameters are given in Table.3.

Table 3: Welding parameters used for MSAW and FCAW process

Pass number	Filler/Electrode		AMP	Gas		Volts	Speed	HI
	Size	Class		Type	Class	DCEP	mm/min	kJ/mm
1	0.9	ER70S-6	98	Argoshield	52	21	244	0.5
2	1.2	E81TNi	153	Argoshield	52	25	354	0.65
3	1.2	E81TNi	153	Argoshield	52	25	298	0.77
4	1.2	E81TNi	153	Argoshield	52	25	354	0.65
5	1.2	E81TNi	153	Argoshield	52	25	323	0.71
6	1.2	E81TNi	153	Argoshield	52	25	372	0.62
7	1.2	E81TNi	153	Argoshield	52	25	354	0.65
8	1.2	E81TNi	153	Argoshield	52	25	338	0.68
9	1.2	E81TNi	153	Argoshield	52	25	331	0.69
10	1.2	E81TNi	153	Argoshield	52	25	346	0.66
11	1.2	E81TNi	153	Argoshield	52	25	304	0.75
12	1.2	E81TNi	153	Argoshield	52	25	323	0.71
13	1.2	E81TNi	153	Argoshield	52	25	338	0.68
14	1.2	E81TNi	153	Argoshield	52	25	438	0.53
15	1.2	E81TNi	153	Argoshield	52	25	331	0.69
16	1.2	E81TNi	153	Argoshield	52	25	338	0.68
17	1.2	E81TNi	153	Argoshield	52	25	372	0.62
18	1.2	E81TNi	153	Argoshield	52	25	402	0.57
19	1.2	E81TNi	153	Argoshield	52	25	372	0.62
20	1.2	E81TNi	153	Argoshield	52	25	298	0.77
21	1.2	E81TNi	153	Argoshield	52	25	346	0.66
22	1.2	E81TNi	153	Argoshield	52	25	354	0.65
23	1.2	E81TNi	153	Argoshield	52	25	310	0.74
24	1.2	E81TNi	153	Argoshield	52	25	323	0.71
25	1.2	E81TNi	153	Argoshield	52	25	317	0.73

2.2 Hardness and microstructural analyses

The welded specimens were sectioned transversely half way through weld joint length (the weld centre), then ground and polished down to 1 μm diamond paste for hardness and metallographic analysis of the weld metal, HAZ and parent metal. Hardness testing was conducted according to the Australian standard AS.2205.6.1 (method 6.1). Measurements were taken on cross sections of the weld in 2 mm line intervals and hardness measurements 0.5 mm apart using a Vickers (HV) microhardness tester with the load of 0.5 Kg and with a loading time of 15 seconds. For microstructural analysis, the samples were etched in 5% Nital (5 % nitric acid in ethanol) or prepared by a double etching procedure using 2% Picral (2% picric acid in ethanol) and 2% Nital (2 % nitric acid in ethanol) solutions. Axio Zeiss optical

microscope and XL 30 FEG-SEM were used to examine the microstructure of the weld metal (WM), the heat affected zone (HAZ), and parent metal (PM).

2.3 Tensile tests

The tensile samples were machined out transversally to the weld joint (3 sample for each welding specimen), as shown in Fig.1. A special care was taken to have the weld zone at the middle of the tensile test samples. Also two strain gauges were mounted on both sides of the welded zone for each tensile specimen to measure the yield strength of the weld metal with high accuracy. Tensile testing was conducted according to the Australian standard AS.2205.2.1 using INSTRON 1282 with the loading capacity of 1000kN.

2.4 Neutron diffraction

Neutron diffraction utilises a beam of neutrons with a momentum p, and associated wavelength λ enabling the measurement of inter-crystalline plane space (d), a way to identify crystal structure or crystal strain, using the well-known Bragg diffraction law:

$$2d_{hkl} \cdot \sin\theta_{hkl} = n\lambda \ , \tag{1}$$

where d_{hkl} are the lattice spacing, n is an integer number representing the order of the reflection plane and θ is the angle between the incident ray and the scattering planes. A small change in the lattice spacing (Δd_{hkl}) will result in a change in the angular position of the diffraction peak ($\Delta\theta_{hkl}$) given by the following equation:

$$\Delta\theta_{hkl} = -\tan\theta_{hkl} \cdot \frac{\Delta d_{hkl}}{d_{hkl}} \tag{2}$$

The lattice normal strain ε is given by:

$$\varepsilon = \frac{d_{hkl} - d_{0,hkl}}{d_{0,hkl}} = -\Delta\theta_{hkl} \cdot \cot\theta_{0,hkl} \ , \tag{3}$$

Where $d_{0,hkl}$ is the strain-free lattice spacing for the hkl planes, and $\theta_{0,hkl}$ is the diffraction angle of the unrestrained lattice. The strains ($\varepsilon_{xx}, \varepsilon_{yy}, \varepsilon_{zz}$) convert to the three-dimensional stress ($\sigma_{xx}, \sigma_{yy}, \sigma_{zz}$) state by using the generalised Hooke's law, as follows:

$$\sigma_{xx} = \frac{E}{(1+v)(1-2v)}\left[(1-v)\varepsilon_{xx} + v(\varepsilon_{yy} + \varepsilon_{zz})\right] \tag{4}$$

Stresses in three directions can be calculated, using Eq.6. It should be noted that the Young's modulus of 224 GPa and Poisson's ratio (v) of 0.27 was used for stress calculations. Further details of instrumentation and general principles of neutron diffraction method (residual stress measurement) can be found in [18, 19].
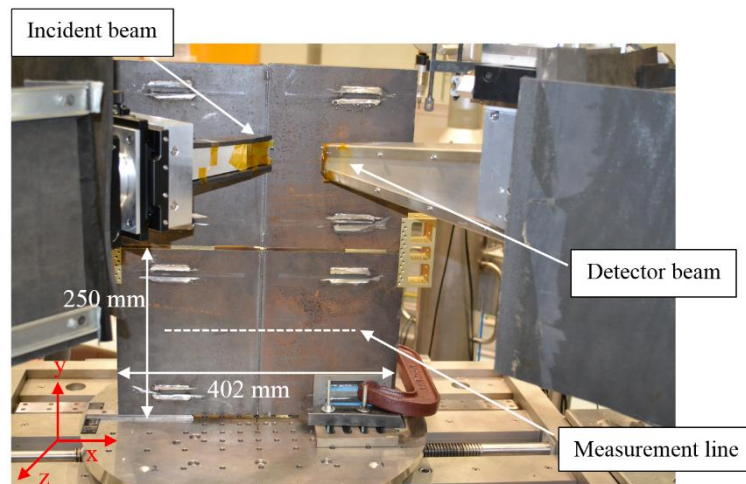
a) Kowari strain scanner at ANSTO facility. Sample I and II in position to measure normal strains. Strain scanning was performed in the middle of the specimen, as indicated by dotted line
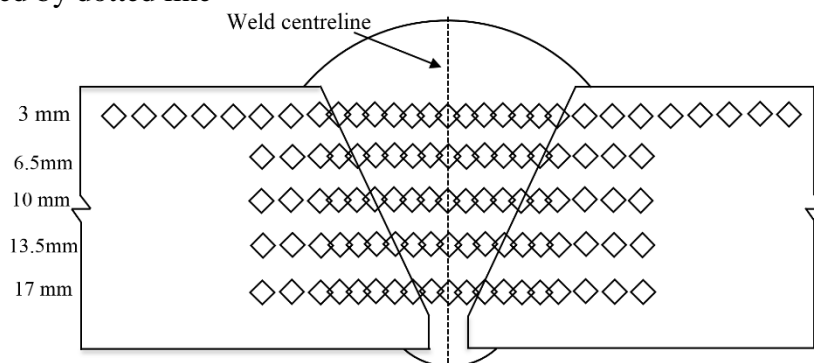
b) Schematic of measurement points

Fig. 5: Experimental set up and location of strain measurements

Residual stress measurements were conducted at ANSTO using KOWARI strain scanning instrument and a $3 \times 3 \times 3 \text{ mm}^3$ gauge volume, as shown in Fig.5. A monochromatic beam produced via diffraction from Si (400) planes of a bent single crystal monochromator, generating a neutron beam with the wavelength of 1.67Å was used in the present study. A detector angle, 2θ, was set at 90° corresponding to the αFe (211) diffraction peak. Residual strains were measured at 172 points (86 points for each sample) in three principal directions. The schematic of measurement points is shown in Fig. 5b. The reference stress-free samples were prepared using EDM (with a wire diameter of 0.2 mm) to obtain a 6mm thick slice from across the weld at the centre of the plate, as shown in Fig.2. The measurements of stress-free lattice spacing (d_0) for both SMAW and MSAW+FCAW specimens were conducted using a $3 \times 3 \times 3 \text{ mm}^3$ gauge volume. Reference lattice spacings were measured in all three principal directions to account for directional variation in peak position due to chemical composition heterogeneity around the weld and HAZ.

3   Results and discussion

The welding process, including the energy input and the resulted thermal distribution along with the thickness of parent metal control the cooling rate of the weld joint fusion zone and the extend of the HAZ. The cooling rate experienced by the weldment controls the microstructure and residual stresses. Both microstructure and residual stress are indicators for expected hardness of weld metal. The macrographs of both welded specimens are shown in Fig. 6. The size of each weld pass as well as the HAZ and root pass are clearly visible on the macrographs. The MSAW+FCAW welded joint appears to be more uniform with a HAZ that is having approximately the same width everywhere, in contrast to the SMAW with distinct but less uniform passes. The larger HAZ layer for SMAW is indicative of the wider arc column of this process. Both welds show some degree of texture, although the columnar structure is more dominant for the MSAW+FCAW combination. The formation of a

columnar structure is more pronounced for the later passes confirming that heat transfer is more effective through the top surface, as expected. The formation of columnar structure may result in anisoptropy in mechanical properties of welded joint affecting alloy distribution, segregation and especially micro-segregation and thus crack propagation in service.
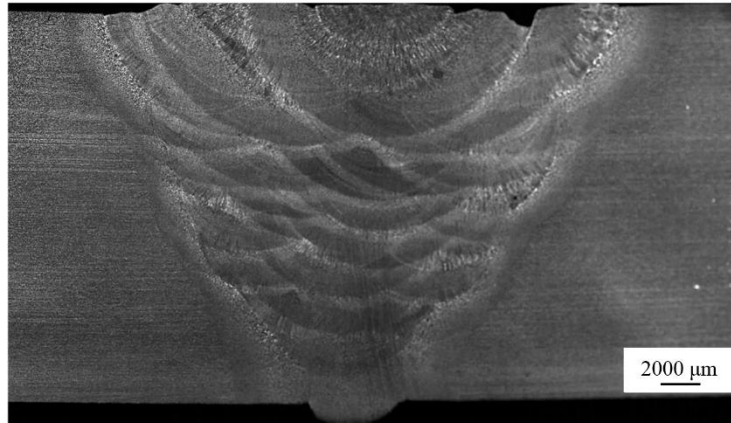
a) Macrograph of specimen I (SMAW process)
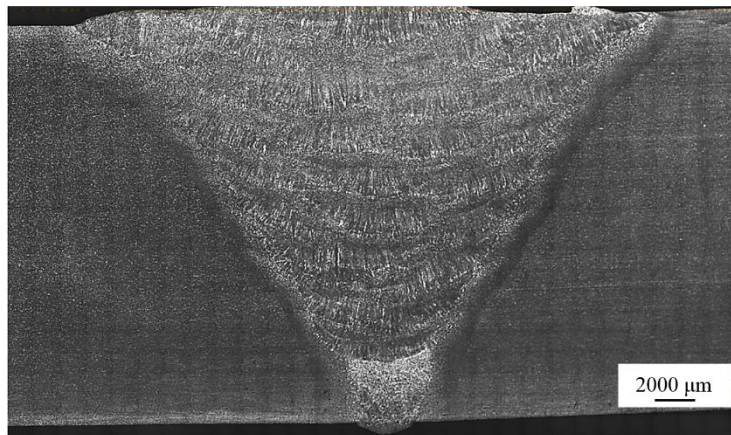
b) Macrograph of specimen II (MSAW and FCAW processes)

Fig. 6: Optical macrographs of V-perp weld joints for X70 HSLA steel

3.1 Microstructural analysis

The X70 parent plate steel contains bainite and acicular ferrite microconstituents with some polygonal ferrite as illustrated in Fig.7. There is also small percentage of pearlite as expected for a low carbon steel (0.05%C). Different regions within the HAZ and weld metal were also examined in great details to highlight the morphology of the weld metal microstructure, and the interface between weld passes to identify if passes are well fused together.
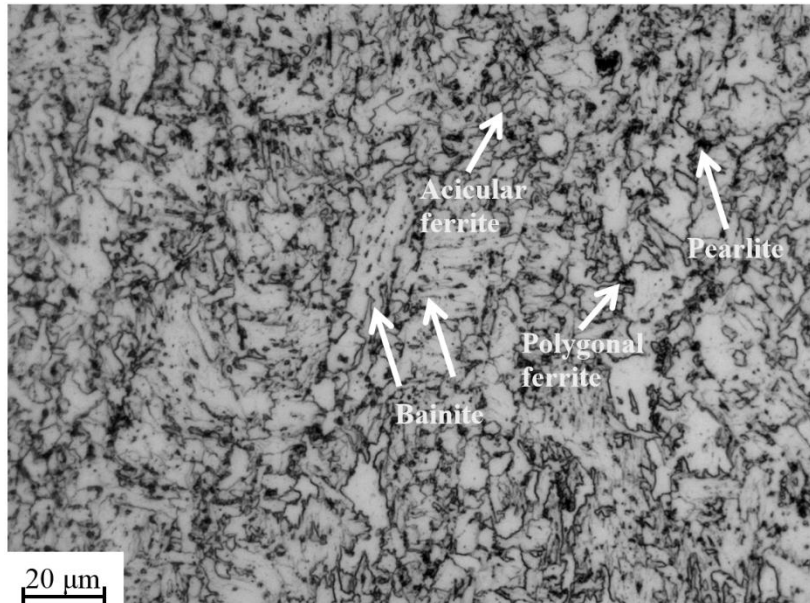
Fig. 7: Optical micrograph of the X70 steels showing bainite and acicular ferritic microstructure with some polygonal ferrite [7]

The microstructure of root pass of the MSAW is shown in Fig. 8a, where different morphologies of ferrite including Widmanstätten ferrite, acicular and polygonal ferrites are detectable. There was also a clear interface between the root pass and that of first pass of FCAW, as shown in Fig. 8b.
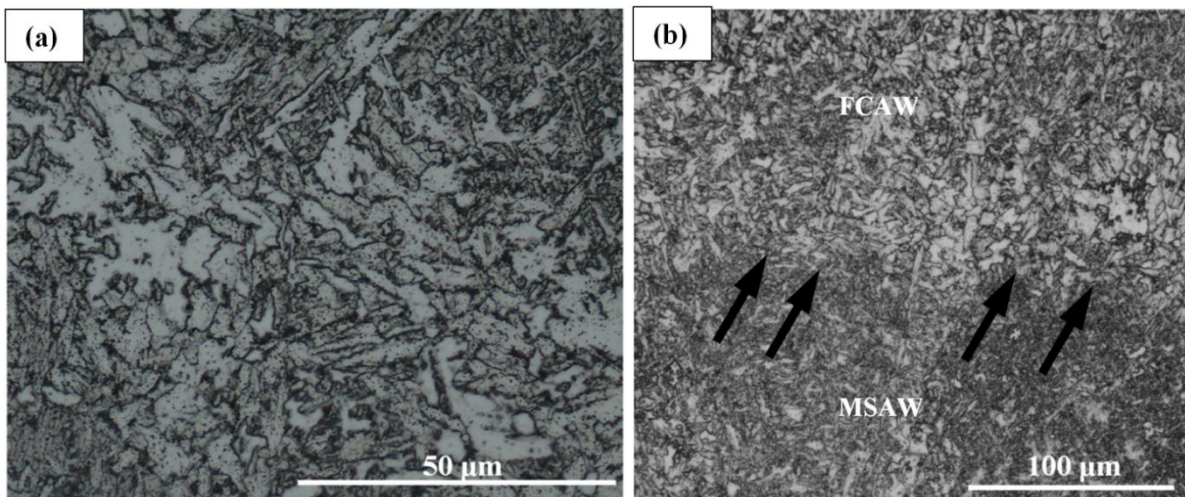
Fig. 8: Optical micrographs showing (a) the morphology of weld of the MSAW in the root pass (b) the boundary (Arrows) between the MSAW root pass and FCAW 1st pass
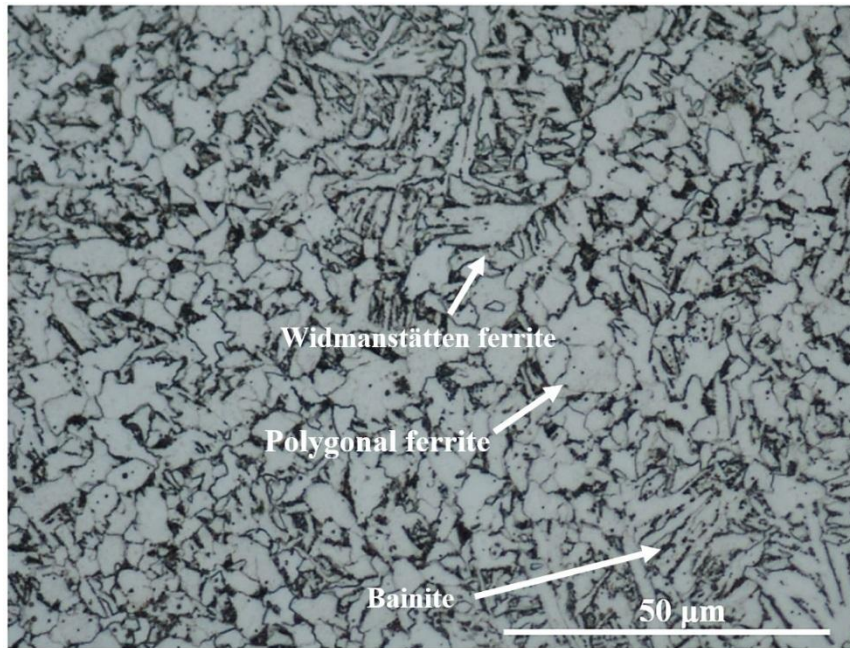
Fig. 9: Optical micrograph showing the root pass of the SMAW weld

The microstructure of the root pass of the SMAW, shown in Fig. 9, is mainly acicular ferrite, coarsened due to heating from subsequent passes, although Widmanstätten and polygonal ferrite morphologies along with some bainite are also detectable.
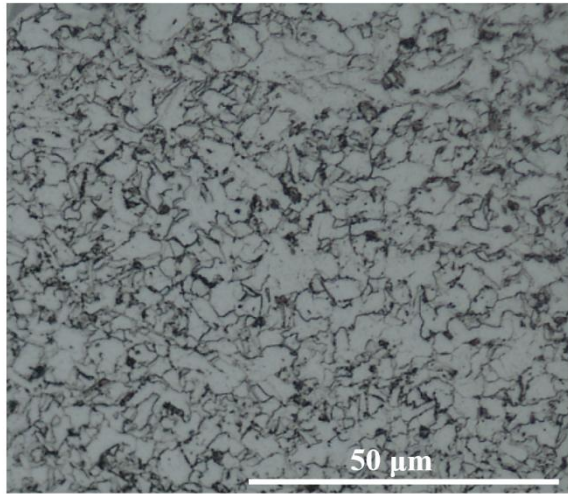
(a) HAZ, close to parent metal, SMAW
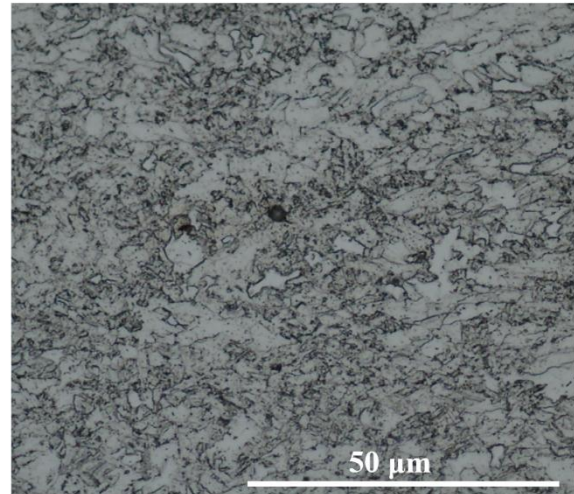
(b) HAZ, close to parent metal, FCAW
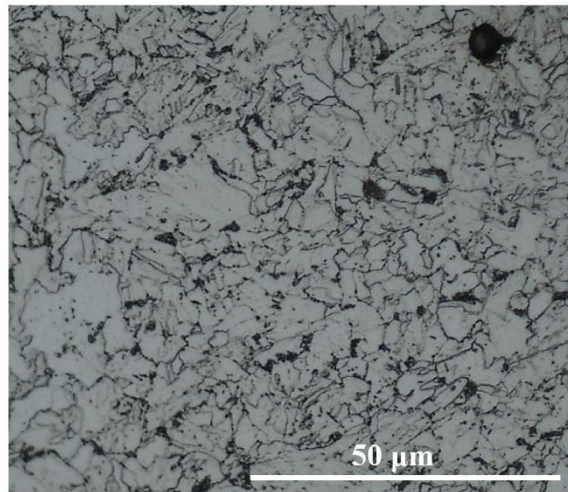
(c) HAZ, centre of HAZ, SMAW
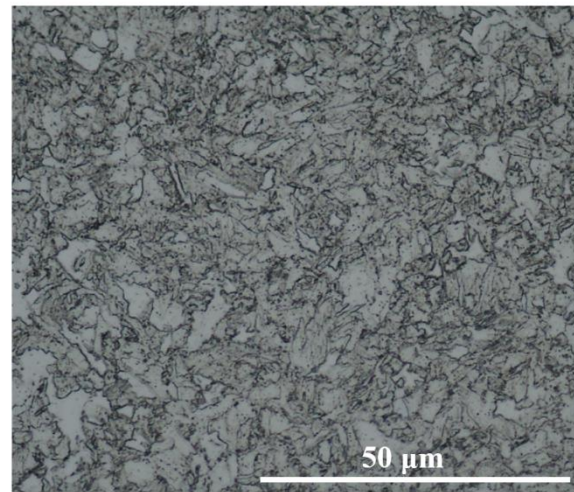
(d) HAZ, centre of HAZ, FCAW
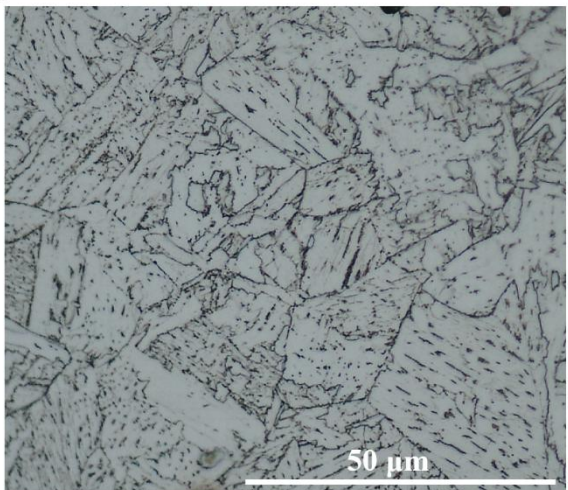
(e) HAZ, close to fusion zone, SMAW
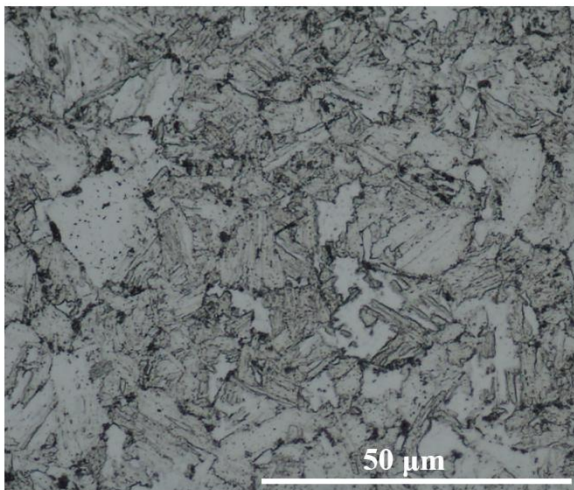
(f) HAZ, close to the fusion zone, FCAW

Fig. 10: Optical micrographs showing the HAZ in both SMAW (a, c, e) and combination of MSAW and FCAW (b, d, f).

Fig.10 provides representative microstructures of the specific HAZ regions examined in this work. The HAZ, as expected, comprises two distinct regions of coarse grained (CG) and fine grained (FG) microstructures, however, there is continuous grain growth toward the fusion zone with microstructure predominately acicular ferrite near the parent metal changing to polygonal ferrite and bainitic ferrite on approaching the fusion zone. One of distinctive contrasting feature of the two procedure is the finer grain structure of the MSAW+FCAW combination. This means the SMAW thermal distribution is as such that it brings about some reheating of the already deposited passes due to wider arc column in each pass. The tempering effect reveal itself with larger grain size for SMAW as seen in Fig. 10 in contrast to FCAW.

The optical micrographs in Fig. 11 are taken from the weld centreline half way through the weld length and weld throat (weld centre point) on the weld transverse direction. The weld metal structure with the MSAW and FCAW combination is predominantly composed of Widmanstätten ferrite, acicular ferritic and bainite. This may also confirm the fact that the higher cooling rate experienced during MSAW+FCAW has affected the scale of prior austenite grain size rendering a smaller prior austenite grain with more nucleation sites for phases with nucleation preference at the prior austenite grain boundaries, i.e. bainite and Widmanstätten ferrite [20]. When compared with FCAW, it is clear that the SMAW contains coarsened ferrites along with pearlite which are the indication of slower cooling rate enabling the formation of pearlite, something that is lacking in MSAW+FCAW combination.
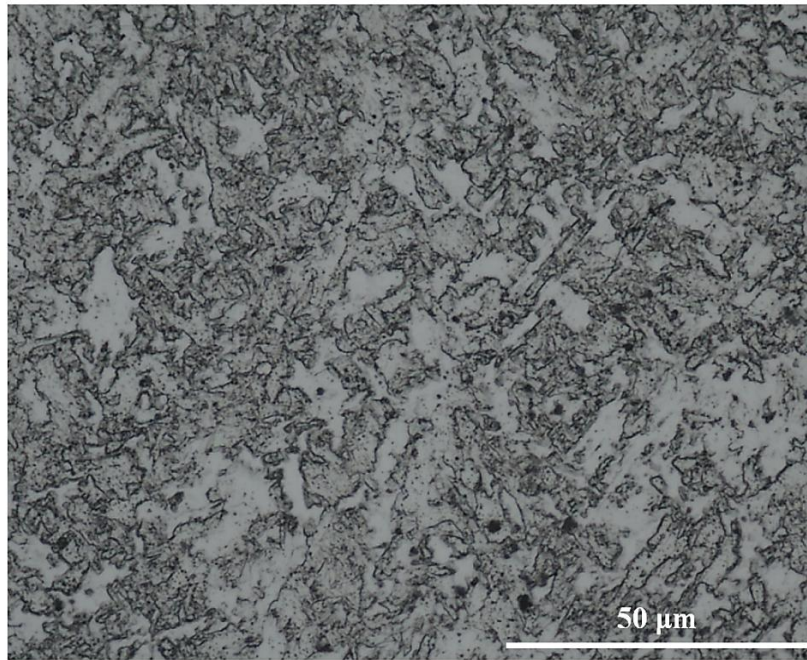
FCAW-Middle of the weld
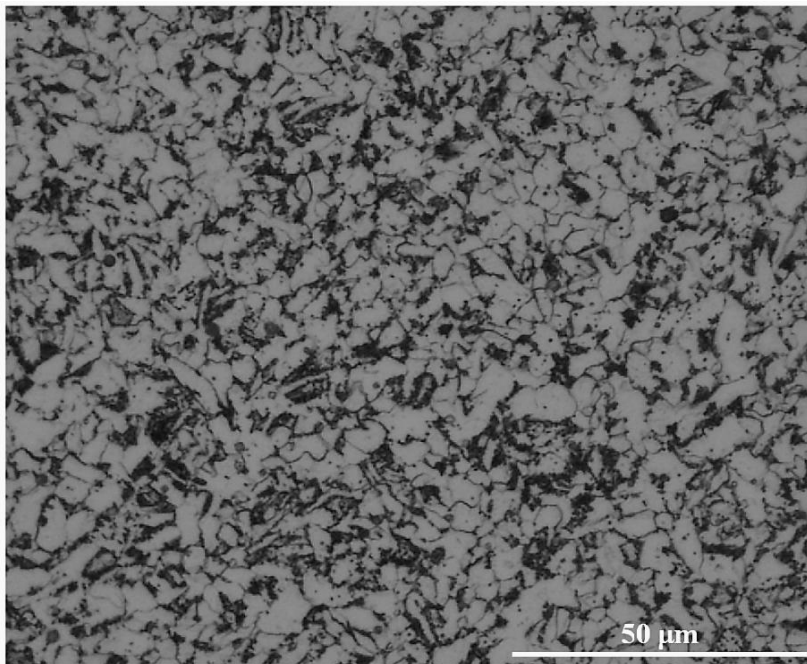
SMAW-Middle of weld

Fig. 11: Optical micrographs showing typical microstructure for middle of the weld of FCAW and SMAW welds

3.2 Tensile test

The tensile tests are carried out on the samples using INSTRON 1282 Servo-hydraulic tensile testing machine (with the loading capacity of 1000 kN). Fig. 12 shows the raptured tensile

specimen with the strain gauges mounted on both sides of the weld to measure yield strength of the weld metal. The stress-strain graph for both welded specimens is shown in Fig.13. One of the significant outcomes of these tests is that in all the tests the rupture occurred at the base material at a distance of 45-55 mm from the weld centreline. As a result, the strength of both HAZ and weld metal is higher than that of the parent material. The yield strength of weld metal for SMAW and MSAW+FCAW processes were 545 MPa and 558 MPa, respectively. Also the total percentage of elongation for SMAW and MSAW+FCAW processes were 21.3% and 22.1%, respectively.
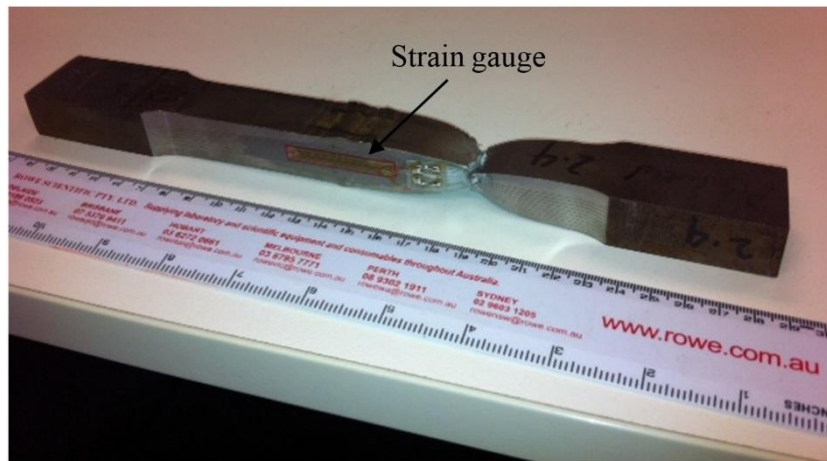
Fig. 12: Tensile test specimens of as weld specimen showing the fracture at the parent metal
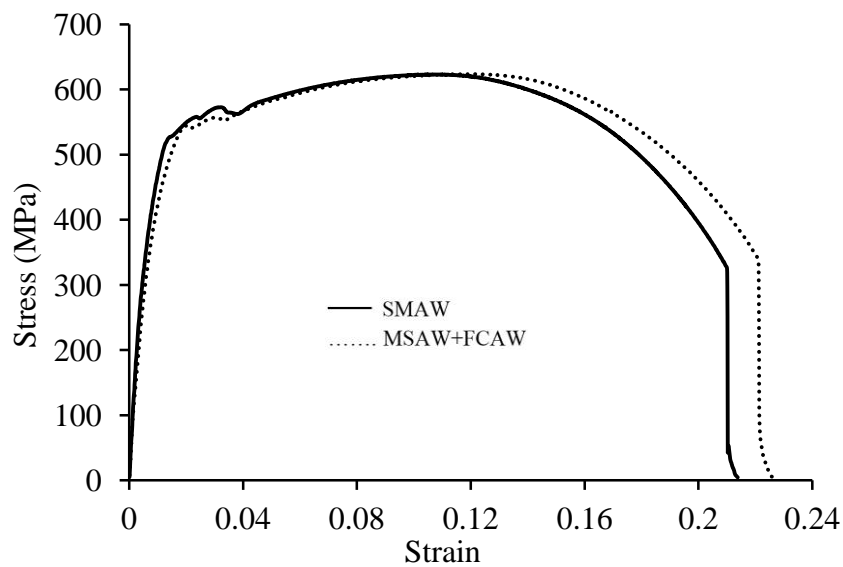
Fig. 13: Stress-strain curves for the middle of the plate tensile specimen for both FCAW and SMAW welds

3.3 Residual stress measurement

The effects of welding process on the residual stresses are presented for across the weld (transverse direction) and through the thickness (normal direction).

3.3.1 Across the weld

Fig.14 (a-e) shows the longitudinal and transverse residual stresses for the two different welding processes. The residual stress is tensile within the weld metal and heat affected zone but decreases within the parent metal to such an extent that becomes zero or even compressive further away within the parent metal. The peak value of longitudinal residual stress for the MSAW+ FCAW was 633 MPa, which is about 90-105 MPa above the yield strength of both the parent and weld metals. While the highest magnitude of longitudinal residual stress for the SMAW was 506 MPa which is lower than the yield strength of the deposited filler metal (E8010 electrode). The heat generated during deposition of the subsequent passes imparts tempering effect on the previous passes.

It is also evident that the residual stress is greatest within the weld centre line and HAZ for depths 3 and 6.5 mm below the weld top surface. Such findings is well in line with the fact that the weld metal and HAZ at these depths have the fastest cooling rates due to effective convection for the top passes (rapid solidification of weld pool) and the fact that later passes are less affected by the tempering effect of the heat generated by the subsequent passes; highest residual stresses. However as the depth of measurement increases (10-17 mm below the top surface) the residual stresses at the weld centre line decreases while the HAZ is now taking over as the highly stressed area. Such observation is in line with pronounced tempering effect of the weld metal for the lower weld passes due to V- geometry of the joint

(the heat concentration is more intense within weld metal with depth increasing). The HAZ is less influenced by this tempering effect.

Also it can be seen from Fig.14 (a-e), by using SMAW significant reduction in longitudinal residual stresses have been achieved. This was due to the lower weld deposition volume of each weld pass, relatively lower welding speed (higher heat input) and arc characteristics of SMAW (wider arc column) which reduces the rate of heat extraction from the weld pool due to reheating the surrounding region, facilitate the tempering effects. The intense heat generated during welding with SMAW process leads to the lower cooling rate and facilitated the tempering effect of this process. In addition to faster cooling rate in the combination of MSAW and FCAW processes, it may also be explained through microstructural constituents, i.e. formation of bainite and Widmanstätten ferrite in the combination of MSAW and FCAW processes as discussed in the previous sections. Similar finding was also reported in the literature where bainitic microstructure could lead to generation of higher level of residual stresses in welded structures [7, 21]. The maximum difference in longitudinal residual stress (185 MPa) for two welding processes was observed at 3 mm below the plate free surface. In general the uncertainties in the measured stresses were no greater than $\pm$ 18 MPa, to the point that the error bars do not extend beyond the data point markers.

This observation supports the finding of Balasubramanian and Guha [16] where welded joints with SMAW process exhibited superior fatigue performance (weld toe crack behaviour) compared to FCAW joints, simply due to lesser residual stresses in SMAW. Moreover, the distribution of transverse residual stresses in the sample with SMAW process shows a more uniform distribution with the significantly lower magnitude in comparison with the MSAW and FCAW processes.

It is also important to point out the effect of subsequent passes on the relieving of the residual stresses within the earlier passes, as for instance the peak longitudinal stress of 630 MPa (combination of MSAW and FCAW processes) measured within the final passes has reduced to less than 400 MPa at a depth of 17 mm below the surface. This reduction could be associated with the reduction of yield strength as a result of increasing cooling time and tempering effects [22].

The width of HAZ is increased for the SMAW welded specimen due to wider arc column of this process distinctly shown in the optical macrograph in Fig. 6a. As a result, wider residual stress distributions can be seen for SMAW process with respect to weld centreline.
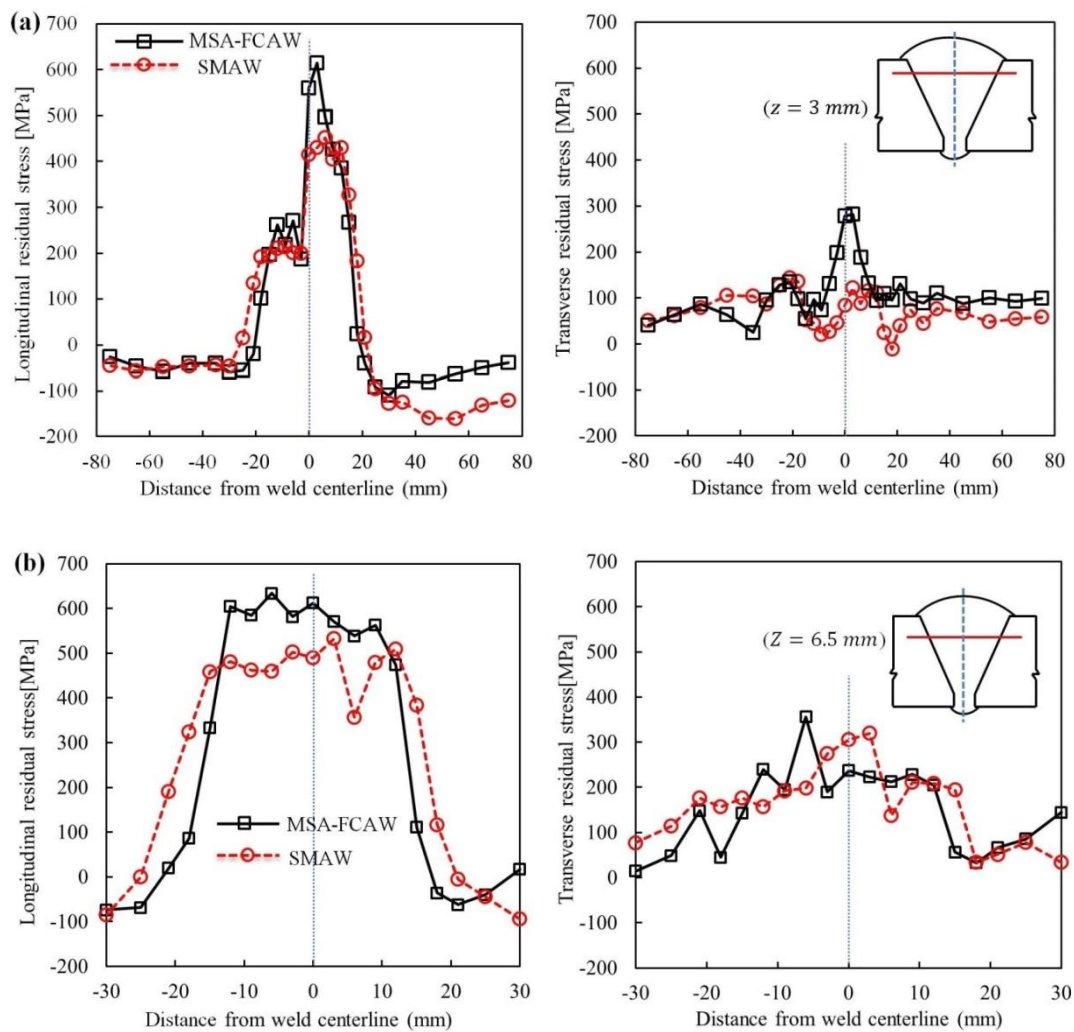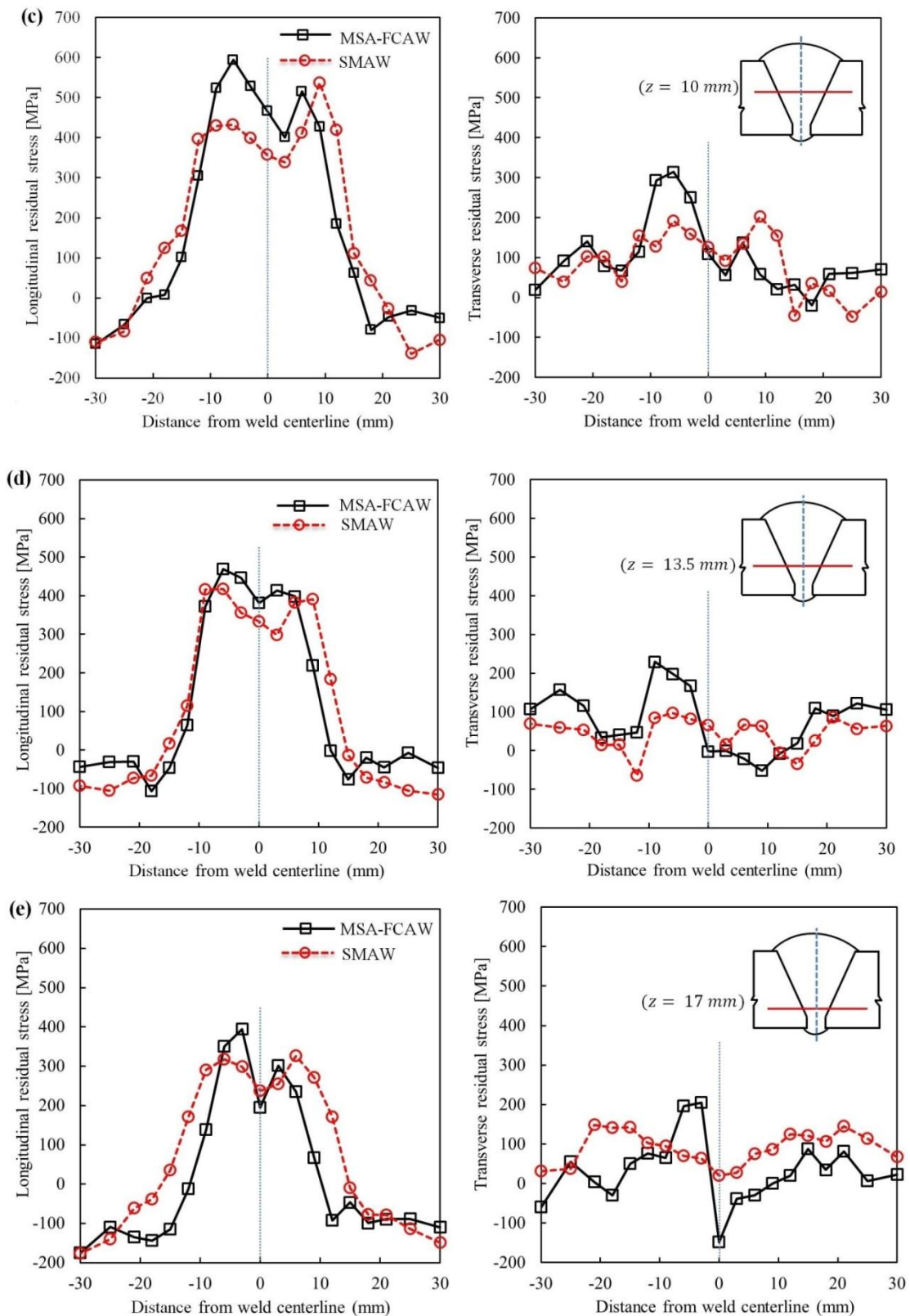
Fig. 14: Effects of welding process on longitudinal and transverse residual stresses - (a) 3 mm from the top surface; (b) 6.5 mm; (c) 10 mm; (d) 13.5 mm and (e) 17 mm from the top surface. SMAW: shielded metal arc welding; MSAW: Modified short arc welding; FCAW: flux cored arc welding.

3.3.2 Through thickness

Through thickness residual stress profiles in the parent metal (30 mm away from the weld centreline) for both specimens is shown in Fig.15 (a). Low magnitude of residual stresses can be seen for both specimens with a slight difference for transverse and longitudinal residual stress components. Fig.15 (b-d) shows the significance of the welding process on the residual stress profiles in the normal direction (z-direction) for different locations from the weld centreline, 3 mm and -6 mm away from the weld centreline. The welding process with the combination of MSAW and FCAW exhibits higher level of residual stresses in comparison with the shielded metal arc welding. The highest value of the generated residual stress in the combination of MSAW and FCAW process is about 90-105 MPa above the weld yield strength of the weld metal.
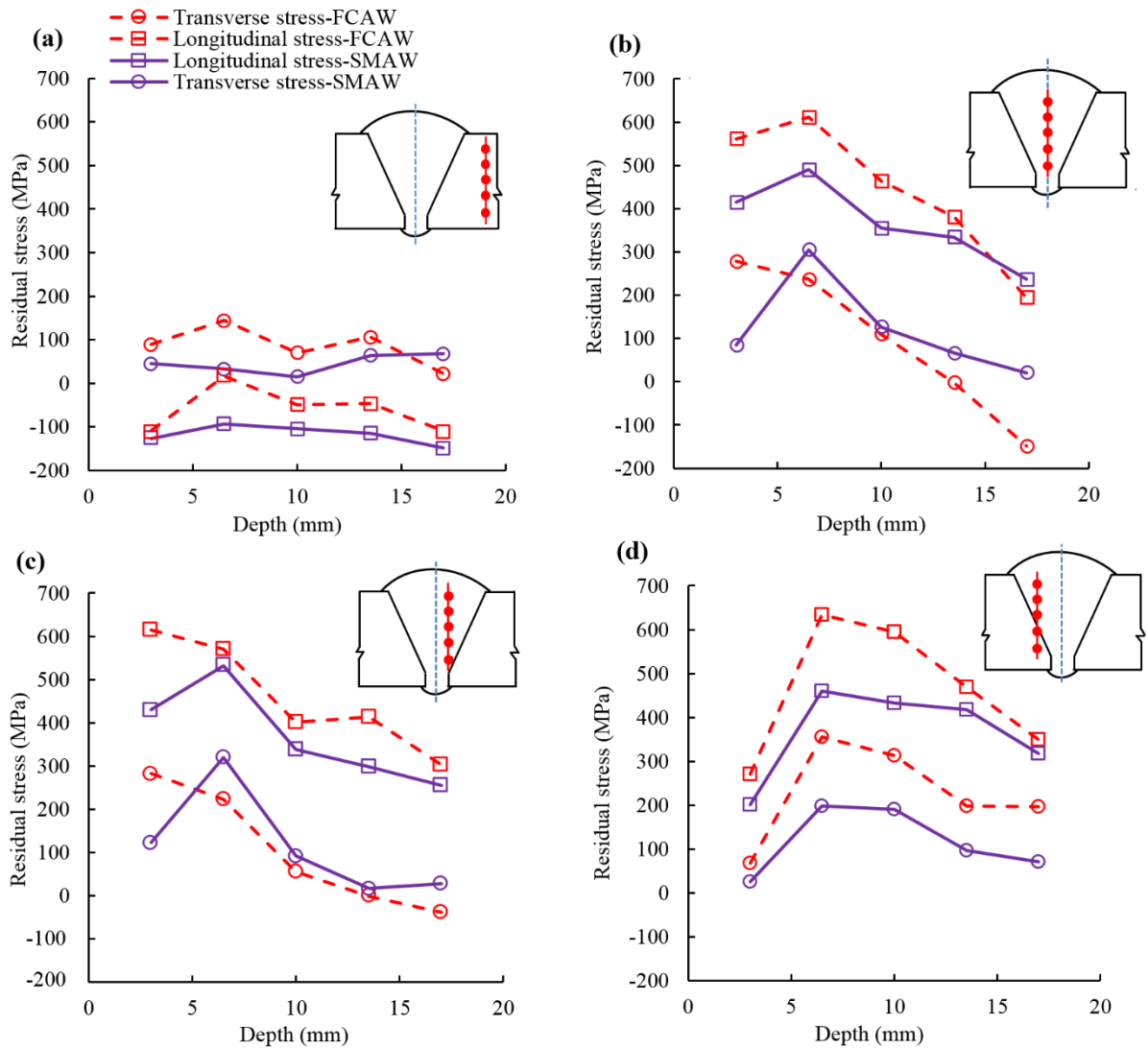
Fig. 15: Through thickness residual stress distributions measured for SMAW (specimen I) and MSAW with FCAW process (specimen III) welds: (a) 30 mm away from the weld centreline; (b) weld centreline; (c) 3 mm away from the weld centreline and (d) −6 mm away from the weld centreline; (solid line) SMAW (dashed line) MSAW with FCAW process

3.4 Hardness analysis

Fig.16 (a - b) shows the hardness map across the weld for SMAW and MSAW+FCAW combination. Generally hardness values for the sample with MSAW+FCAW process were higher than those with SMAW. This is due to the higher cooling rate for the specimen with MASW+FCAW weld with its direct effect on the microstructure as discussed before. As mentioned before, the formation of more bainitic and Widmanstätten ferrite and the smaller prior austenite grains (Figs. 10-11) are responsible for changes in hardness. Also existing of

columnar microstructure in different regions of weld metal for the MSAW+FCAW could lead to variations in the hardness for different weld beads. Furthermore, the higher hardness implies the material having higher yield stress thus could sustain higher residual stresses.
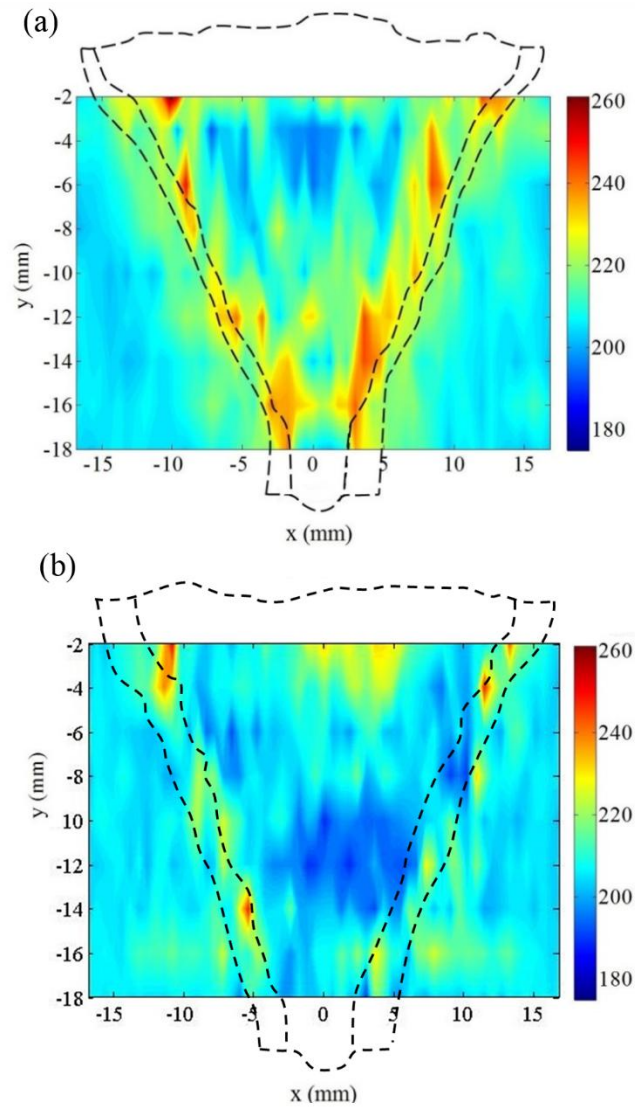

Fig. 16: Microhardness map for (a) MSAW and FCAW; (b) SMAW processes

4 Conclusions

The effects of welding process on the microstructure, residual stresses and hardness of high-strength low-alloy steel were investigated. The key findings of this experimental study were:

- With the SMAW process, the scale of fusion zone and HAZ area increased. As a result high levels of tensile residual stresses were found further away from weld centreline for the samples with SMAW process.

- The microstructure of weld changes with welding process where combination of MSAW and FCAW renders more bainitic and Widmanstätten ferrite resulted from smaller prior austenite grain size.

- Significantly higher level of longitudinal residual stresses was found in the specimen with MSAW and FCAW processes. This is in line with previous reports, where fatigue life and crack initiation life is longer in the specimen welded with SMAW in comparison with FCAW process

- Residual stresses in excess of yield strength were developed in the weld metal and HAZ particularly for the upper-layers of welds with MSAW+FCAW specimens. The magnitudes of residual stresses were also notably higher. Higher residual stress and hardness level in the joints fabricated with MSAW and FCAW process can be related to the microstructure constituent of bainite and Widmanstätten ferrite.

References:

[1] Shrikrishna KA, Sathiya P, Goel S. The impact of heat input on the strength, toughness, microhardness, microstructure and corrosion aspects of friction welded duplex stainless steel joints. Journal of Manufacturing Processes. 2015;18:92-106.

[2] Buchely M, Colorado H, Jaramillo H. Effect of SMAW manufacturing process in high-cycle fatigue of AISI 304 base metal using AISI 308L filler metal. Journal of Manufacturing Processes. 2015;20:181-9.

[3] Sakthivel T, Vasudevan M, Laha K, Parameswaran P, Chandravathi K, Mathew M, et al. Effect of welding processes on the creep rupture behaviour of type 316 LN stainless steel weld joints. Material Science and Engineering A. 2011;528:6971-80.

[4] Moraitis G, Labeas G. Prediction of residual stresses and distortions due to laser beam welding of butt joints in pressure vessels. International Journal of Pressure Vessels and Piping. 2009;86:133-42.

[5] Javadi Y, Akhlaghi M, Najafabadi MA. Using finite element and ultrasonic method to evaluate welding longitudinal residual stress through the thickness in austenitic stainless steel plates. Materials & Design. 2013;45:628-42.

[6] Kumar S, Shahi AS. Effect of heat input on the microstructure and mechanical properties of gas tungsten arc welded AISI 304 stainless steel joints. Materials & Design. 2011;32:3617-23.

[7] Alipooramirabad H, Ghomashchi R, Paradowska A, Reid M. Residual stress-microstructure- mechanical property interrelationships in multipass HSLA steel welds. Journal of Materials Processing Technology. 2016;231:456-67.

[8] Withers P, Bhadeshia H. Residual stress. Part 2–Nature and origins. Materials Science and Technology. 2001;17:366-75.

[9] Alipooramirabad H, Kotousov A, Ghomashchi R. Numerical analysis of welding stresses in WIC weldability test. 8th Australasian Congress on Applied Mechanics: ACAM 8. Melbourne2014. p. 731-8.

[10] Kotousov A, Borkowski K, Fletcher L, Ghomashchi R. A model of hydrogen assisted cold cracking in weld metal. 2012 9th International Pipeline Conference: American Society of Mechanical Engineers; 2012. p. 329-34.

[11] Alipooramirabad H, Paradowska A, Ghomashchi R, Kotousov A, Reid M. Quantification of residual stresses in multi-pass welds using neutron diffraction. Journal of Materials Processing Technology. 2015;226:40-9.

[12] Ragu Nathan S, Balasubramanian V, Malarvizhi S, Rao AG. Effect of welding processes on mechanical and microstructural characteristics of high strength low alloy naval grade steel joints. Defence Technology.

[13] Magudeeswaran G, Balasubramanian V, Madhusudhan Reddy G. Effect of welding processes and consumables on high cycle fatigue life of high strength, quenched and tempered steel joints. Materials & Design. 2008;29:1821-7.

[14] Magudeeswaran G, Balasubramanian V, Madhusudhan Reddy G. Effect of welding processes and consumables on fatigue crack growth behaviour of armour grade quenched and tempered steel joints. Defence Technology. 2014;10:47-59.

[15] Magudeeswaran G, Balasubramanian V, Madhusudhan Reddy G, S Balasubramanian T. Effect of Welding Processes and Consumables on Tensile and Impact Properties of High Strength Quenched and Tempered Steel Joints. Journal of Iron and Steel Research, International. 2008;15:87-94.

[16] Balasubramanian V, Guha B. Effect of welding processes on toe cracking behaviour of pressure vessel grade steel. Engineering Failure Analysis. 2004;11:575-87.

[17] Paradowska A, Finlayson TR, Price JWH, Ibrahim R, Steuwer A, Ripley M. Investigation of reference samples for residual strain measurements in a welded specimen by

neutron and synchrotron X-ray diffraction. Physica B: Condensed Matter. 2006;385–386, Part 2:904-7.

[18] Withers PJ. Mapping residual and internal stress in materials by neutron diffraction. Comptes Rendus Physique. 2007;8:806-20.

[19] Alipooramirabad H, Paradowska A, Ghomashchi R, kotooussov A, Hoye N. Prediction of welding stresses in WIC test and its application in pipelines. Materials Science and Technology. 2016; 32 (14):1462-1470.

[20] Ghomashchi R, Costin W, Kurji R. Evolution of weld metal microstructure in shielded metal arc welding of X70 HSLA steel with cellulosic electrodes: A case study. Materials Characterization. 2015;107:317-26.

[21] Smith C, Pistorius PGH, Wannenburg J. The effect of a long post weld heat treatment on the integrity of a welded joint in a pressure vessel steel. International Journal of Pressure Vessels and Piping. 1997;70:183-95.

[22] Venkata KA, Kumar S, Dey HC, Smith DJ, Bouchard PJ, Truman CE. Study on the Effect of Post Weld Heat Treatment Parameters on the Relaxation of Welding Residual Stresses in Electron Beam Welded P91 Steel Plates. Procedia Engineering. 2014;86:223-33.

CHAPTER 8

IN SITU NEUTRON DIFFRACTION MEASUREMENT OF STRAIN RELAXATION IN WELDS DURING HEAT TREATMENT

Houman Alipooramirabad[1]*, Anna Paradowska[2], Olivier Lavigne[1], Reza Ghomashchi[1], Mark Reid[2]

[1]School of Mechanical Engineering, the University of Adelaide, SA 5005

[2] Bragg Institute, Australian Nuclear Science and Technology Organisation (ANSTO), Lucas Heights, NSW 2234, Australia

Statement of Authorship

Title of Paper	In situ neutron diffraction measurement of strain relaxation in welds during heat treatment
Publication Status	☑ Published ☐ Accepted for Publication ☐ Submitted for Publication ☐ Unpublished and Unsubmitted work written in manuscript style
Publication Details	Alipooramirabad H, Paradowska A, Lavigne O, Ghomashchi R, Reid M. In situ neutron diffraction measurement of strain relaxation in welds during heat treatment. Science and Technology of Welding and Joining. 2016:1-12.

Principal Author

Name of Principal Author (Candidate)	Houman Alipooramirabad
Contribution to the Paper	I was responsible for the literature review required for this work, and designed the framework for the experimental conditions. I carried out mechanical property and microstructural behaviour analysis, wrote the first draft of the manuscript and incorporated and addresses all comments and suggestions by other authors in subsequent revesions of the manuscript. Interpertation of the data was primary my responsibility.
Overall percentage (%)	90%
Certification:	This paper reports on original research I conducted during the period of my Higher Degree by Research candidature and is not subject to any obligations or contractual agreements with a third party that would constrain its inclusion in this thesis. I am the primary author of this paper.
Signature		Date	30/01/2017

Co-Author Contributions

By signing the Statement of Authorship, each author certifies that:

  i.   the candidate's stated contribution to the publication is accurate (as detailed above);
  ii. permission is granted for the candidate in include the publication in the thesis; and
  iii. the sum of all co-author contributions is equal to 100% less the candidate's stated contribution.

Name of Co-Author	Anna Paradowska
Contribution to the Paper	I was joint supervisor of this work, assisted for conducting some part of the experiments at ANSTO, and jointly contributed to refining the manuscript.
Signature		Date	02/02/2017

Name of Co-Author	Olivier Lavigne		
Contribution to the Paper	I jointly contributed to conducting some part of the experiments and jointly contributed to refining the manuscript..		
Signature		Date	30/01/2017

Name of Co-Author	Reza Ghomashchi		
Contribution to the Paper	I was joint supervisor of this work and jointly contributed to refining the manuscript.		
Signature		Date	31/01/2017

Name of Co-Author	Mark Reid		
Contribution to the Paper	I jointly contributed to conducting some part of the experiments and jointly contributed to refining the manuscript..		
Signature		Date	31/01/2017

In situ neutron diffraction measurement of strain relaxation in welds during heat treatment

Houman Alipooramirabad, Anna Paradowska, Olivier Lavigne, Reza Ghomashchi & Mark Reid

Published online: 11 Dec 2016.

Submit your article to this journal

Article views: 17

View related articles

View Crossmark data

The Institute of Materials,
Minerals and Mining

Taylor & Francis
Taylor & Francis Group

In situ neutron diffraction measurement of strain relaxation in welds during heat treatment

Houman Alipooramirabad[a], Anna Paradowska[b], Olivier Lavigne[a], Reza Ghomashchi[a] and Mark Reid[b]

[a]School of Mechanical Engineering, The University of Adelaide, Adelaide, SA, Australia; [b]Bragg Institute, Australian Nuclear Science and Technology Organisation (ANSTO), Lucas Heights, NSW, Australia

ABSTRACT

Neutron diffraction (ND) is commonly used to investigate the stress redistribution before and after post-weld heat treatment (PWHT) in welded structures. However, there is a lack of information on the evaluations of strains during PWHT. The present work employed in situ ND to measure the relaxation of residual strains during conventional PWHT in multi-pass high-strength low-alloy steel welds. It was found that strain relaxation occurs principally during the heating stage of the heat treatment. The findings have important economic bearings and can be used to characterise comparable material combinations and optimise the PWHT process for high-strength low-alloy weld joints. This unique information also provides a valuable benchmark for the finite element modelling of this complex process.

Introduction

Post-weld heat treatment (PWHT) for steel structures is a stress-relieving process where a uniform heating is applied at subcritical temperatures for a specified period of time until the desired stress relief is attained. The selection of the subcritical temperature is dependent on the alloy chemistry, while the heat treatment time is thickness related [1]. The fact that temperature should be kept at subcritical level ($< E_{utectoid}$) is due to the phase transformation that occurs once the temperature is above the eutectoid temperature. Such high-temperature treatment is, therefore, detrimental to the steel's mechanical properties as it induces phase transformation (ferrite to austenite) and subsequent slow cooling to room temperature usually adopted during PWHT may result in the formation of a coarse microstructure. In such an unlikely event, the steel structure has to be re-heat-treated which results in an extra cost burden [2]. PWHT is often necessary for pressure vessels and piping components to relax or remove residual stresses for the purpose of increasing resistance to brittle fracture. So far, several experimental and numerical investigations have been carried out, comparing residual stress levels before and after PWHT. Paddea et al. [3] used a neutron diffraction (ND) technique to measure the distribution of the residual stresses in a P91 steel-pipe girth weld before and after PWHT. Before PWHT, the peak of the tensile residual stresses was shown to be 600 MPa, which

was located close to inner surface of the pipe on the boundary between the heat-affected zone (HAZ) and the adjacent parent material. The maximum tensile residual stress after PWHT in the vicinity of the HAZ was 120 MPa. Smith and Garwood [4] investigated the effects of PWHT on the residual stresses in a 50 mm thick ferritic steel weld using a hole drilling technique. A significant reduction in the surface residual stress levels was observed as a result of PWHT (the peak of the residual stresses was 740 MPa for as-welded condition which was reduced to 140 MPa after PWHT). Cho et al. [5] developed a 2D finite element model to evaluate the residual stresses in K- and V-type weld joints of thick plates for the as-welded condition and after PWHT. It was found that maximum residual stresses were 316 and 256 MPa, respectively, in the as-welded condition, which were reduced to 39.3 and 3.7 MPa, respectively, after PWHT.

A number of codes and standards exist, such as ASME Division 2 [6] and API 579RP [7], which generally specify a similar set of parameters. These include the application of uniform heating to a sufficiently high temperature below the lower transformation temperature (depending on steel grade/chemistry), heating rate and isothermal hold or soak time for a specified wall thickness [8]. According to recent investigations, the PWHT-related codes can be excessively conservative, particularly for the holding (soaking) time in thick sections. Zhang et al. [8] and Dong and Hong [9] used a

series of finite element models to predict weld residual stress relaxation in a furnace-based PWHT using the omega creep model. They found that the required hold time can be significantly reduced, in comparison with the codes and standards, with sufficient residual stress reduction as long as a reasonable PWHT temperature is applied. Chen *et al.* [10] used in situ ND to measure the residual stress relaxation during PWHT on butt-welded steel pipes. It was found the residual stress was relaxed completely during ramping up to 650°C. The authors [10] suggest that this may be due to the rearrangement of defects, including dislocations and resultant reduction in the yield stress of the material with temperature. Dodge *et al.* [11] used neutron diffraction to quantify strain evolution in dissimilar welds of 8630M low-alloy steel and Alloy 625 (ERNiCrMo-3) during PWHT. In addition, residual stress measurements before and after PWHT were also conducted. The findings showed reduction in localised strains during PWHT in all three principal directions. Residual stresses were substantially decreased in the PWHT samples, with a reduction of 400 MPa on the Alloy 625 side and a reduction of 200 MPa on the 8630M side. Lombardi *et al.* [12] used in situ neutron diffraction to measure the relaxation of residual strains in the cylinder bores of Al engine blocks during solution heat treatment. It was found that the residual strain was mainly relieved in two steps: an initial high rate of strain relief followed by a slower and relatively constant rate of strain relief. They concluded that primary creep was responsible for the initial step, while steady-state creep was responsible for strain relief in the second step. Despite the aforementioned experimental studies (in situ neutron diffraction during PWHT), there remains a number of questions on the mechanics of residual stress relief during PWHT. These include the rate of stress relaxation during holding (soaking), the onset temperature of relaxation of residual strain/stresses and the relationship between the ramp rate in the initial stages of PWHT and the relaxation of residual strains/stresses. Moreover, there are no reports on the in situ strain/stress relaxation during PWHT for high-strength low-alloy steel welds.

In order to address these fundamental questions, the present study employed in situ neutron diffraction during PWHT to measure the relaxation of residual strain during PWHT in HSLA welds. The experiments were conducted at Australian Nuclear Science and Technology Organisation using the KOWARI residual strain scanner. In addition, residual stress maps were obtained in and around the welds in the pre- and PWHT conditions. To complement the neutron diffraction data, microstructural and mechanical property studies were also performed on the samples. The findings of these experimental studies should lead to significant improvement in structural integrity and fitness for service assessments.

Materials and methods

Materials and sample preparation

The test specimens comprised two 20 mm thick steel plates (API 5L grade X70) with the dimensions of 250×200 mm^2, V-prep welded along the 250 mm side. The plates were cut from a single slab hot rolled to 20 mm thickness and were provided by Bao Steel, China. Two samples were fabricated utilising identical welding procedures. One was used for neutron diffraction analysis during in situ heat treatment and to evaluate the residual stresses before and after PWHT. The other was used to prepare a stress-free sample via electro-discharge machining (EDM) to relieve macro-stresses from the weld and HAZ region without introducing new stresses due to cutting [13]. The V-prep weld joints were manufactured using modified short arc welding with an ER70s-6 electrode for the root pass and fluxed core arc welding process, using E81TNi Flux cored wire for the remaining passes. The weld deposition sequence is shown in Figure 1. The yield strength of the parent and weld meal were 515 MPa and 538 MPa, respectively. The chemical composition for the parent metal (PM) and filler wires (ER 70s-6 and E81TNi) are given in Table 1.

Neutron diffraction measurements

ND measurements were performed using the KOWARI-ANSTO strain scanning instrument. The measurement
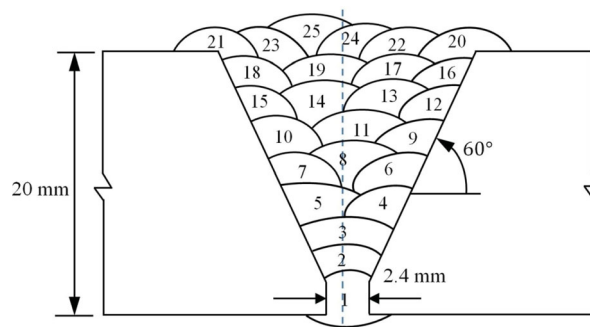

Figure 1. Weld deposition sequence in the welded specimens.

Table 1. Chemical composition of consumables (ER70S-6, E81T1-Ni 1M) and PM.

Chemical composition	ER 70S-6	E81T1-Ni 1M	PM
%C	0.09	0.04–0.05	0.052
%Mn	< 1.60	1.26–1.36	1.55
%S	0.007	0.006–0.009	0.0011
%Si	0.90	0.25–0.29	0.21
%P	0.007	0.005–0.008	0.0097
%Cu	0.20	–	0.15
%Cr	0.05	0.04–0.05	0.026
%Ni	0.05	0.86–0.96	0.19
%Mo	0.05	0.01	0.18
%V	0.05	0.02–0.03	0.029
%Ti	–	–	0.012
%NB	–	–	0.041

of strains and stresses by ND is based on the Bragg's law:

$$2d_{hkl} \cdot \sin\theta_{hkl} = n\lambda \qquad (1)$$

where d_{hkl} is the distance between adjacent lattice planes (lattice spacing), n is an integer number representing the order of the reflection plane and θ is the angle of incidence or reflection of neutron beam.

The lattice strain ε associated with hkl plane is given by

$$\varepsilon = \frac{d_{hkl} - d_{0,hkl}}{d_{0,hkl}} = -\Delta\theta_{hkl} \cdot \cot\theta_{0,hkl} \qquad (2)$$

where $d_{0,hkl}$ is the strain-free lattice spacing for the hkl planes, $\Delta\theta_{hkl}$ is the angular position of the diffraction peak and $\theta_{0,hkl}$ is the diffraction angle of the unrestrained lattice [14]. A monochromatic beam produced via diffraction from Si (400) planes of a bent single crystal monochromator, producing a wavelength of $\lambda = 1.1666$Å, was used in this investigation. The detector angle, 2θ, was set at $90°$ corresponding to the αFe (211) diffraction peak. To measure the relaxation of the residual strains during the PWHT, neutron diffraction was used in conjunction with heating blankets wrapped around the weld sample. The experimental set-up is shown in Figure 2. The heating blankets were made up from block-shaped elements of sintered alumina, containing resistance heating Ni-Cr wire. The heating elements were designed to wrap around the surface geometry with a gap of about 35 mm between them in order to allow the neutron beam to pass through the specimen without obstruction during the PWHT. The heating blankets were controlled using an Advantage3 controller to regulate the input current according to a centrally mounted control thermocouple. In order to monitor the temperature uniformity during the experiment, six thermocouples (K type) were spot welded to the specimen at different locations. The temperature distribution across the entire sample did not vary more than 10°C from the set PWHT temperature during the entire experiment. The strain measurements during heat treatment were made using a gauge
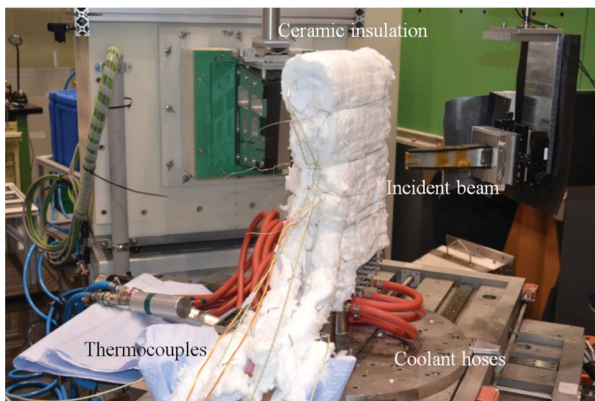
volume of $3 \times 3 \times 3 \text{ mm}^3$ and two different measurement times: 30 and 60s. The measurements were conducted only in the longitudinal direction (parallel to the welding direction) and at a single point where the highest value of tensile residual stress was found during neutron diffraction residual stress measurements for the as-welded condition (around 650 MPa). This location was at the weld centreline, below the weld cap and at a distance of 3 mm from the outer surface of the plate. It should be noted that stress in the transverse was found to be considerably lower than the maximum residual stress of 278 MPa in the as-welded specimen. The strain relaxation measured by neutron diffraction relies on the strain-free lattice spacing d_0 (equation 2). The measurement on the stressed weld was, therefore, followed by measurement on a mechanically stress relieved weld sample subjected to the same temperature regime. For the measurement of d_0 value during PWHT, a $6 \times 6 \times 20 \text{ mm}^3$ cube was extracted from the welded specimen with identical welding parameters using EDM to reduce the stress levels to zero. The stress-free reference cube (d_0 cube) was extracted from exactly the same region where the measurements were made during the heat treatment. The cube was attached to the sidewall of the weld sample using ceramic glue with the specific measures (i.e. placing extra insulation around the cube mounting area to prevent heat losses) to ensure temperature uniformity and consistency during the PWHT process.

A graph of strain measurement times (open circles) and the temperatures during PWHT is given in Figure 3. The as-welded sample was reheated at 5°C/min to a holding temperature of 600°C and was held isothermally at this temperature for 60 mins. At the end of holding time, the heating jacket (power source for PWHT) was turned off, but the heating blankets were left in place during the cooling to room temperature.

Figure 2. Experimental set-up for the measurement of strain relaxation by ND during PWHT.
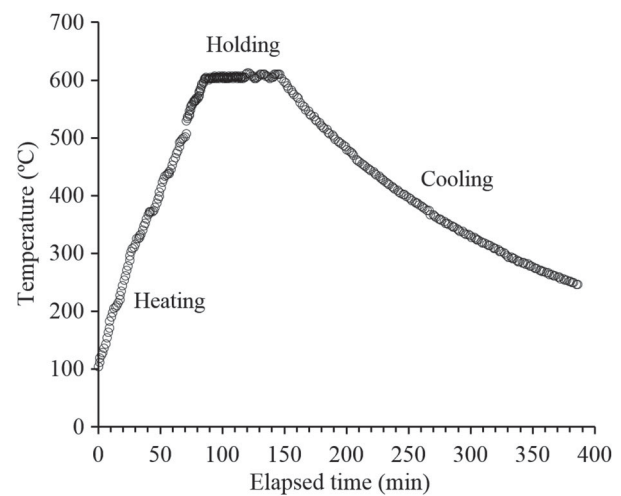
Figure 3. ND measurement points (open circles) and temperature variation during PWHT treatment using K-type thermocouple attached to the WM cap.
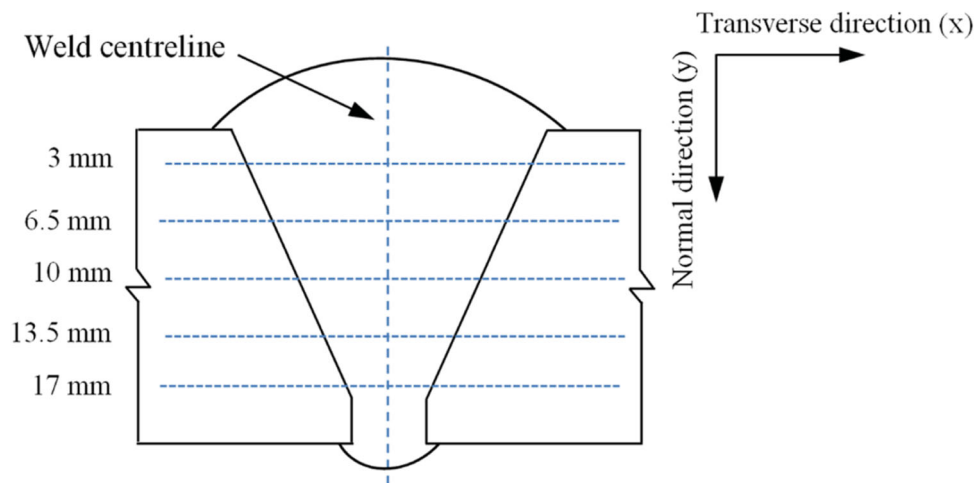
Figure 4. Schematic of the location of ND measurement points for the as-welded and PWHT samples.

Residual stress measurements were conducted on the as-welded and PWHT specimens again using a $3 \times 3 \times 3 \, mm^3$ gauge volume. Strain measurements were conducted at 86 points (schematically shown in Figure 4) in the three principal directions. The full scale (i.e. as opposed to the cube used during the PWHT measurements) reference stress-free sample was prepared using EDM to obtain a 6-mm thick slice from across the weld at the centre of the plate. The reference sample was also attached to the sidewall of the sample, using ceramic glue, during PWHT. This enabled measurement of d_0 values from the full-scale reference sample before and after PWHT. The residual stresses for the as-welded and PWHT samples were calculated, using the generalised Hooke's law. Further details of instrumentation and general principles of residual stress measurement via neutron diffraction can be found in [15–17].

Hardness and microstructural analyses

The welded specimens were sectioned transversely and polished down to 1 μm using semi-automatic polishing machine (Tegramin 25-Struers) for hardness and metallographic analysis. Measurements were taken on cross sections of the weld in 2-mm line intervals and hardness measurements of 0.5 mm apart, using a Vickers indenter (Leco-Lm700at) with the load of 0.5 Kg and with a loading time of 15 seconds. Selected samples were etched by a double etching procedure using 2% Picral (2% picric acid in ethanol) and 2% Nital (2% nitric acid in ethanol) solutions to reveal the microstructure. A Zeiss Axio imager optical microscope was used to examine the microstructure of the weld metal (WM), HAZ and PM.

### EBSD data collection and processing

A semi-automatic TegraPol polishing machine (Struers) was used for polishing the sample surfaces. Final polishing was achieved, using a porous neoprene disc with a colloidal silica suspension (0.04 μm). The EBSD scans were collected using a FEI Helios Nanolab 600-SEM equipped with an EBSD detector (EDAX Hikari™). The acceleration voltage and the electron beam current of the SEM were 30 kV and 2.7 nA, respectively. The step size was 30 nm with a hexagonal scan grid (scans were $100 \times 100 \, \mu m^2$). The TSL-OIM software was used for the data collection and analyses. The EBSD scans were conducted in the WM and HAZ of the as-welded and PWHT specimens.

Results

In situ neutron diffraction strain relaxation measurements

To distinguish between the changes due to thermal expansion in the reference sample and those due to stress relief, it was required to measure the interplanar spacing (d_0 for the longitudinal direction) of the stress-free sample prepared under the same heating and cooling conditions. A plot of stress-free measurement (d_0) that changes during PWHT is shown in Figure 5. Owing
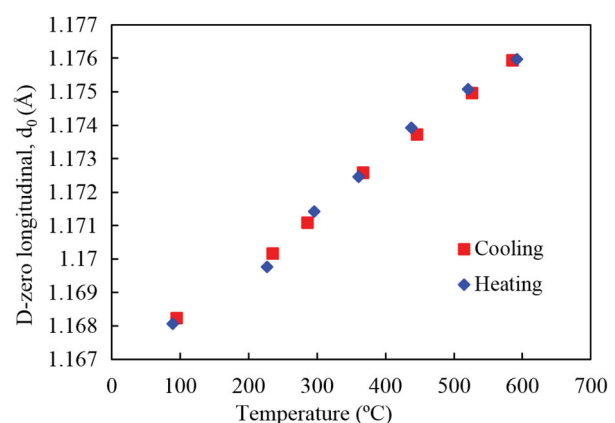
Figure 5. Longitudinal stress-free lattice parameter measurements during PWHT.

to the linearity of data (d_0) during cooling and heating, a linear regression fit was applied to calculate corresponding temperature-dependent d_0 values. Therefore, the following equation was employed to describe the trend for the calculation of d_0 at any temperature:

$$d_0 = mT + c \qquad (3)$$

where T is the temperature (°C), m is 0.00002 and c is 1.1665. R^2 is equal to 0.9931.

By calculating d_0 values (equation 3) corresponding with measured d-spacing values at any given temperature, the resultant strains for in situ heat treatment can be calculated according to the following equation:

$$\varepsilon_{xx}(T) = \frac{d_{xx}(T) - d_0(T)}{d_0(T)} \qquad (4)$$

Figure 6 shows the plot of the calculated longitudinal strain during heat treatment, after calculating d_0 values using equations (3) and (4). Given in Figure 6, are the results of the in situ strain relief experiment. During the heating phase of the PWHT, the measured stain falls from an initial value of $2588 \pm 82\ \mu\varepsilon$ at room temperature to a value of $601 \pm 112\ \mu\varepsilon$ on reaching the holding temperature (600 °C). During the holding phase, the stain further relaxes to a value of $318 \pm 124\ \mu\varepsilon$ over 60 minutes. This clearly indicates that the bulk of strain relaxation occurs during heating phase ($\sim 80\%$ as a fraction of total relaxation) with only a minor contribution during holding phase ($\sim 11\%$).

Neutron diffraction residual stress measurements before and after PWHT

The measured stresses at the 86 locations for the sample before and after PWHT were used to create contour maps in order to generate an overall impression of the residual stress distribution across the weld. The measured residual stresses before PWHT are given in Figure 7(a–c). The black cross markers on the contour plots indicate the measurement positions, while the broken lines represent the boundaries between the WM, HAZ and PM. The longitudinal residual stresses are in tensile mode in the WM, HAZ regions but become compressive and even zero in the PM, further away from the HAZ region. As noted in the experimental section, the residual stresses in the transverse and normal direction are far lower than the longitudinal stresses. The highest residual stress value was found in longitudinal direction at a depth of 3 mm below the surface (Figure 7(a)) reaching a peak value of 650 ± 16 MPa, which is about 95–110 MPa above the yield strength of both the parent and WM. This region is associated with the last weld pass and thus with the smaller tempering effects. It is also important to note that this tempering effect results in relief of the weld residual stresses, particularly for the initial passes up to the mid-plate thickness. The heat applied during deposition of the subsequent and final weld passes imparts this tempering effect on the previous passes.
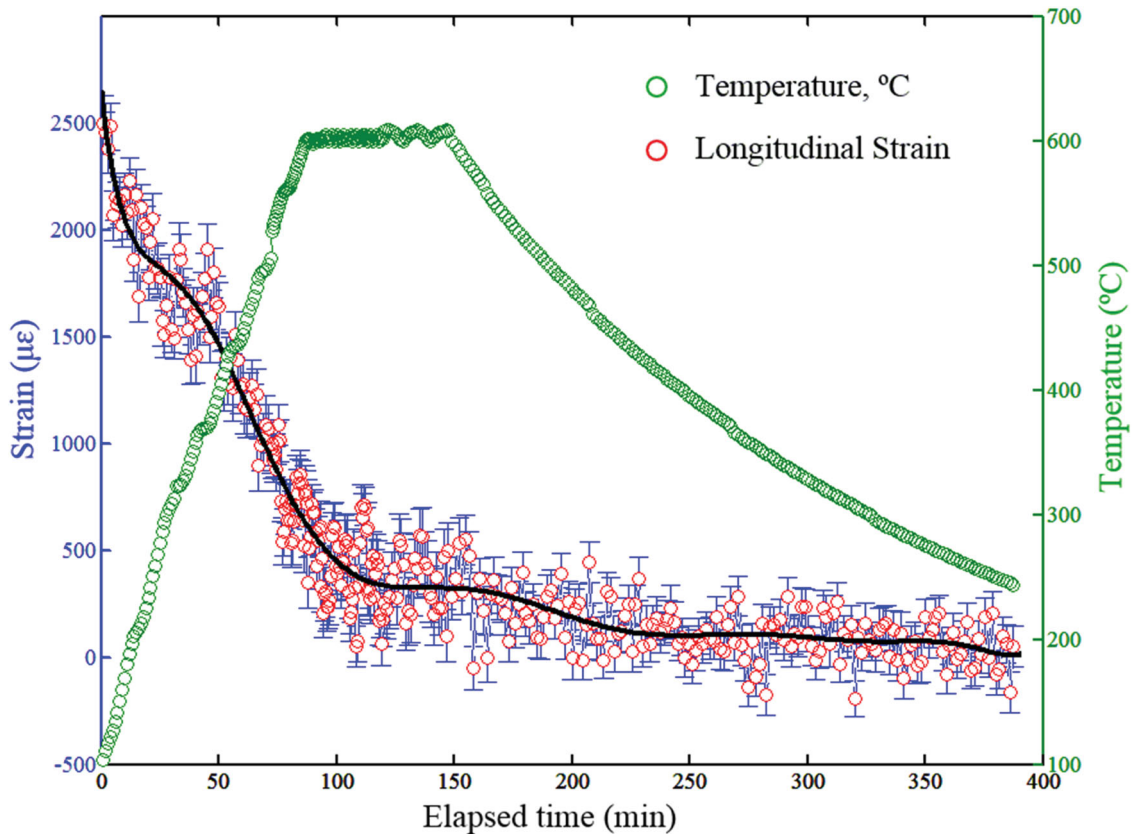
Figure 6. Measurements of longitudinal residual strains and the respected temperatures during PWHT cycle.
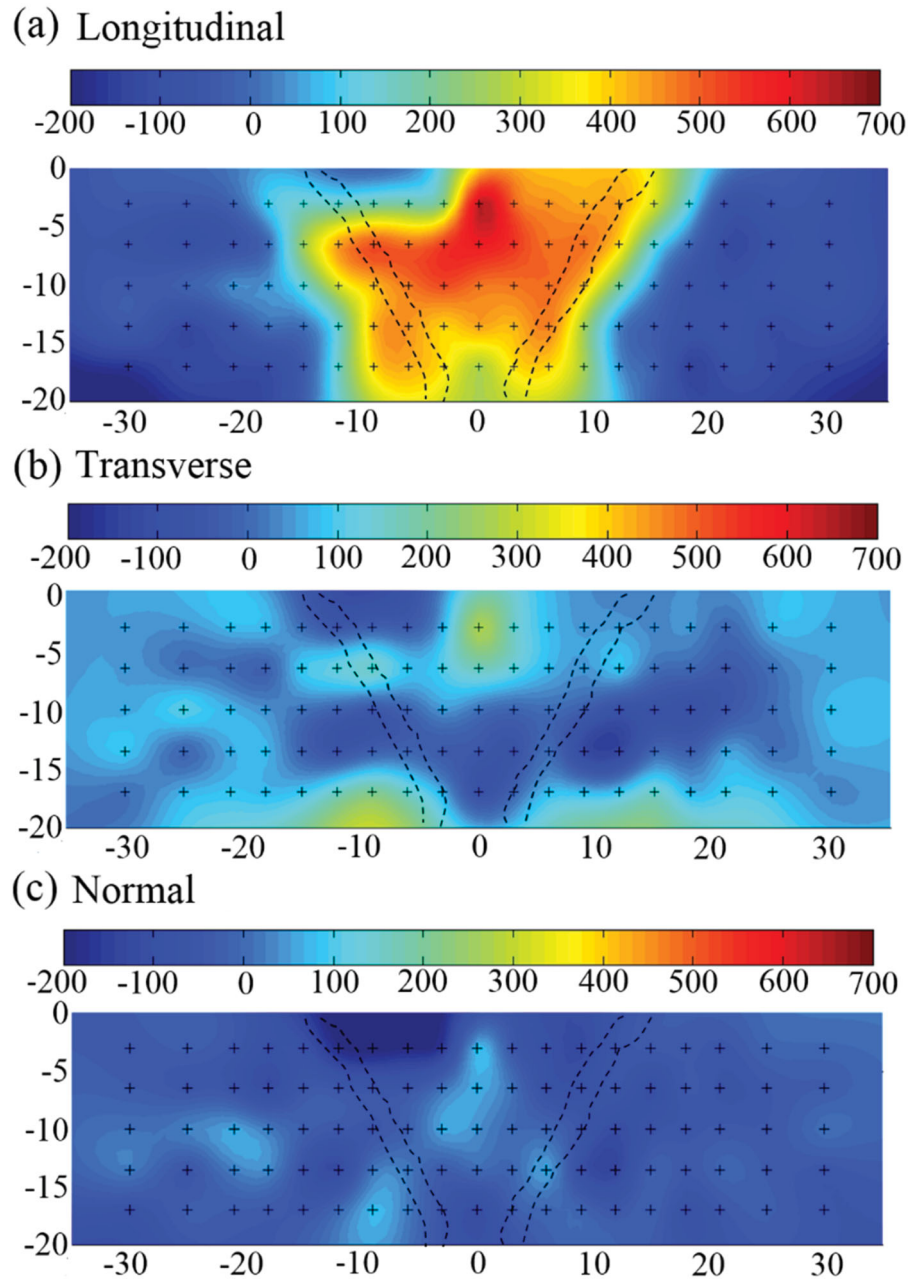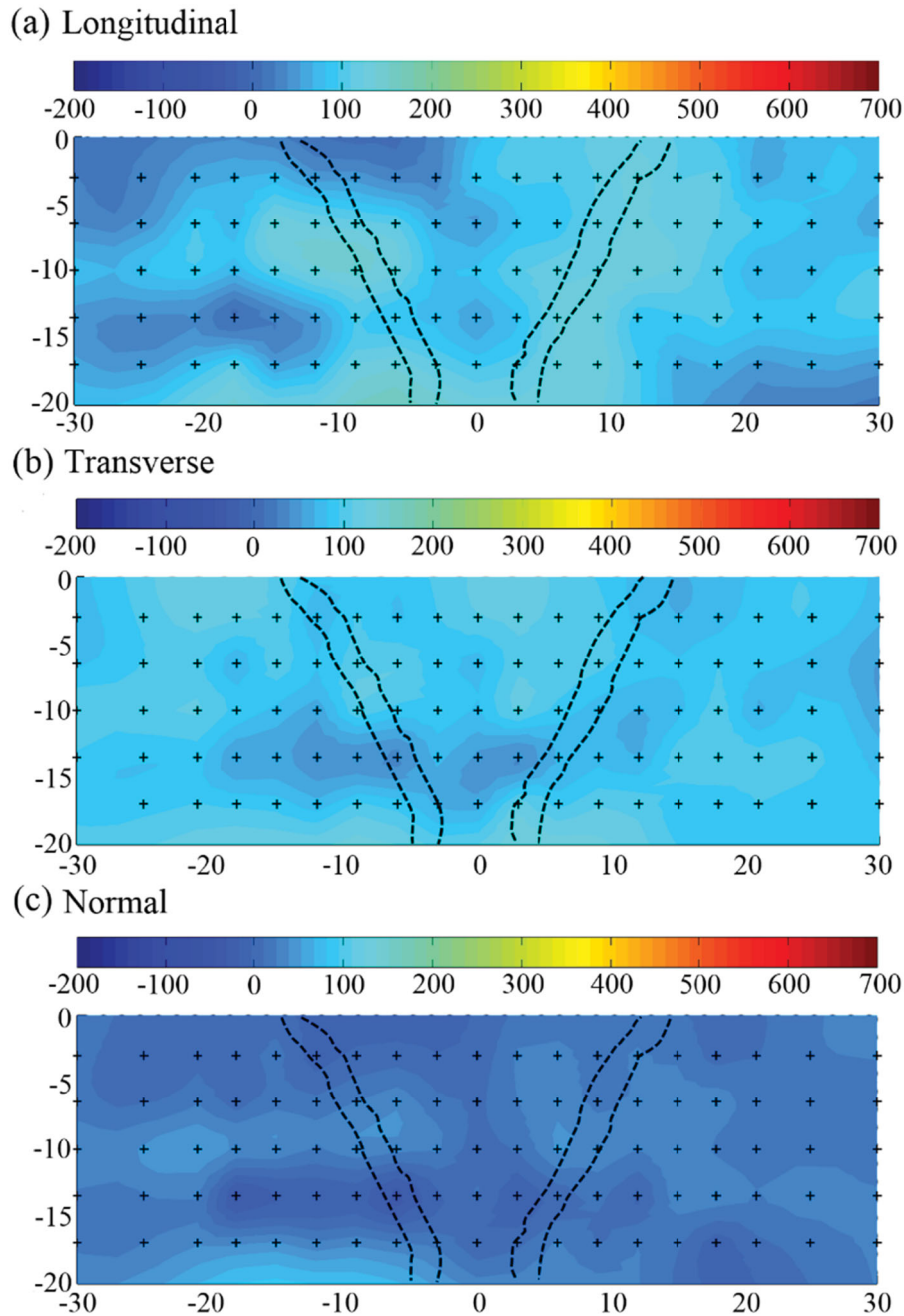
Figure 7. Residual stress (MPa) contour maps for the as-welded specimen (a) longitudinal, (b) transverse and (c) normal, components (x- and y-axes in mm).

Figure 8(a–c) shows the residual stress distributions in the three directions after the PWHT. It clearly reveals a substantial reduction in the magnitude of residual stresses after applying PWHT. The maximum longitudinal residual stress of $142 \pm 14\,MPa$ is found in the mid-thickness of the plate close to the fusion zone of the weld (Figure 8(a)).

EBSD residual strain measurement before and after PWHT

The residual strain distribution associated with inhomogeneous dislocation distribution was estimated using the kernel average misorientation (KAM) parameter measured by EBSD [18]. The KAM cartography represents the mean angle between the crystallographic orientation of each pixel and those of its nearest neighbouring pixels. It is important to note that misorientations above 5° are excluded from the calculation of KAM in order to avoid a high-angle grain boundary contribution. The second nearest neighbouring pixels were selected to define the kernel in this study. Figure 9 shows the superimposed image quality (IQ) and KAM maps for the weld centre regions of the as-welded and PWHT samples. It can be seen that the degree of misorientation between adjacent pixels has reduced (blue regions represent areas with less misorientation). The population of blue regions, representing less strained regions, has increased after the PWHT treatment. This is an indication of reduction in residual stress. The mean KAM values for these weld centre regions as well as for the coarse-grained heat-affected zone (CGHAZ)

Figure 8. Residual stress (MPa) contour maps for PWHT specimen (a) longitudinal, (b) transverse and (c) normal, components (x- and y-axes in mm).

and fine-grained heat-affected zone (FGHAZ) regions for the as-welded and PWHT samples are given in Figure 10. This figure confirms that the residual strains present in the microstructure in the WM, CGHAZ and FGHAZ decreased with the PWHT.

Hardness analysis

Figure 11 shows hardness maps for the as-welded and PWHT specimens. Hardness values varied between 197 and 264 HV for the WM and HAZ of the as-welded specimen (Figure 11(a)). There is a marked decrease in hardness in some regions of WM as a result of tempering of subsequent weld passes. PWHT specimens lead to a considerable decrease in hardness values in

the WM and HAZ regions (Figure 11(b)). The average hardness in the PM for the as-welded and PWHT specimens were very similar (around 211 HV).

Optical and EBSD microstructural analysis

The X70 parent plate steel contains bainite and acicular ferrite microconstituents with some polygonal ferrite as illustrated in Figure 12. There is also small percentage of pearlite as expected for a low carbon steel (0.05%C).

Figure 13 provides representative microstructures of the HAZ regions of the as-welded and PWHT samples. Two distinct regions of coarse- and fine-grained microstructures are evident within the HAZ region. However, there is a grain size gradient within the
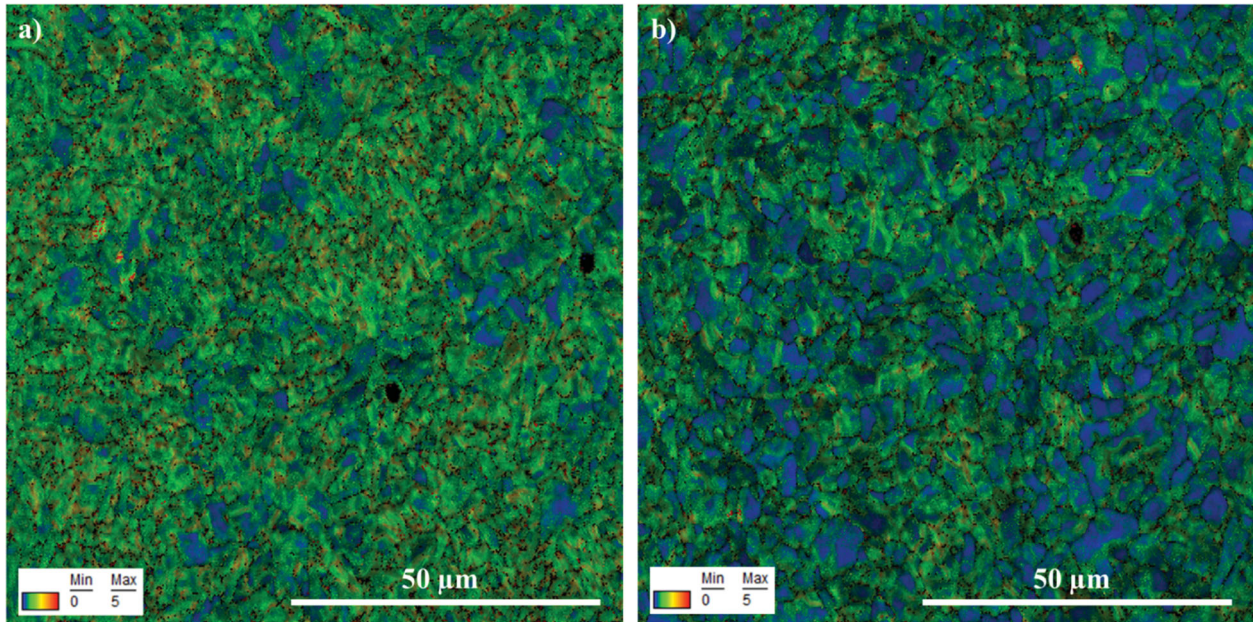
Figure 9. Superimposed IQ and KAM maps for the weld centre regions of the (a) as-welded (b) PWHT samples.
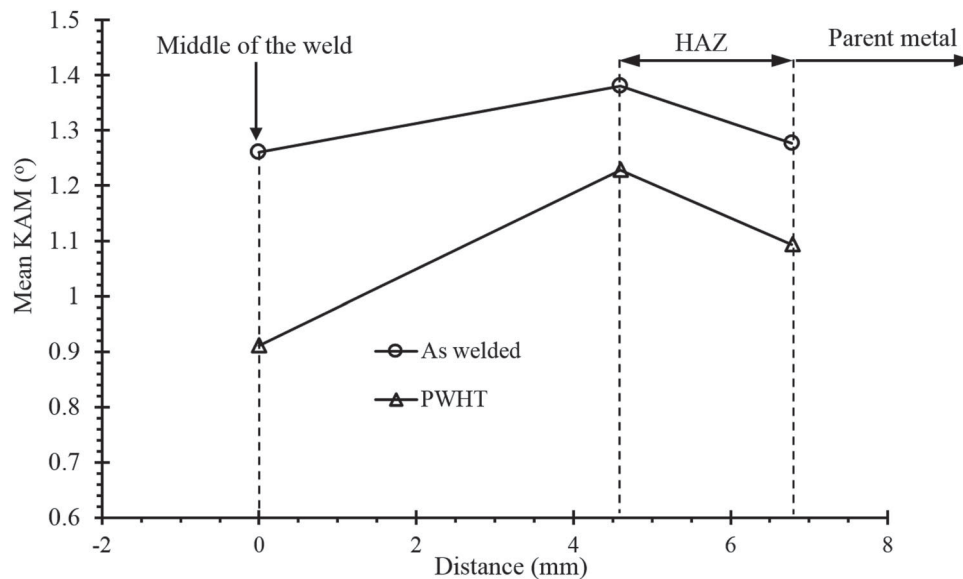
Figure 10. Mean KAM values of the WM, CGHAZ and FGHAZ for the as-welded and PWHT samples.

HAZ, particularly for the as-welded specimen, towards the fusion zone with the microstructure mainly acicular ferrite near the PM changing to polygonal ferrite and bainitic ferrite on approaching the fusion zone. The microstructure for the PWHT specimen is mainly slightly coarsened polygonal ferrite, grain boundary ferrite and acicular ferrite. It can also be seen that the microstructure across the weld/CGHAZ/FGHAZ zones is more homogeneous in terms of grain size for the PWHT sample. Furthermore, the Widmanstätten and bainitic ferrite that existed for the as-welded specimen was transformed into mainly polygonal ferrite.

The representative microstructures of the middle of the weld (mid-plate thickness at the weld centreline), for the as-welded and PWHT samples, are shown in Figure 14. The as-welded specimen contains

Widmanstätten ferrite, bainite and polygonal ferrite, but still is a mainly acicular ferritic weld. Owing to the tempering effects in PWHT, which resulted in the grain growth of the microstructure, a mainly equiaxed polygonal ferrite microstructure is observed.

The average spacing of grain boundaries (above $2°$ misorientation) determined by the linear intercept method in the EBSD scans (average of 10 lines) was found to increase after the heat treatment in the WM, the CGHAZ and the FGHAZ (Table 2). This indicates that the grains are larger in the PWHT sample compared to the as-welded sample in these regions.

The misorientation angle fractions of grain boundaries for the WM, CGHAZ and FGHAZ for the as-welded and PWHT samples were also determined from the EBSD scans. The results are presented in Table 3,

Figure 11. Micro-hardness ($HV_{0.5}$) map for (a) as-welded; and (b) after PWHT (x- and y-axes in mm).

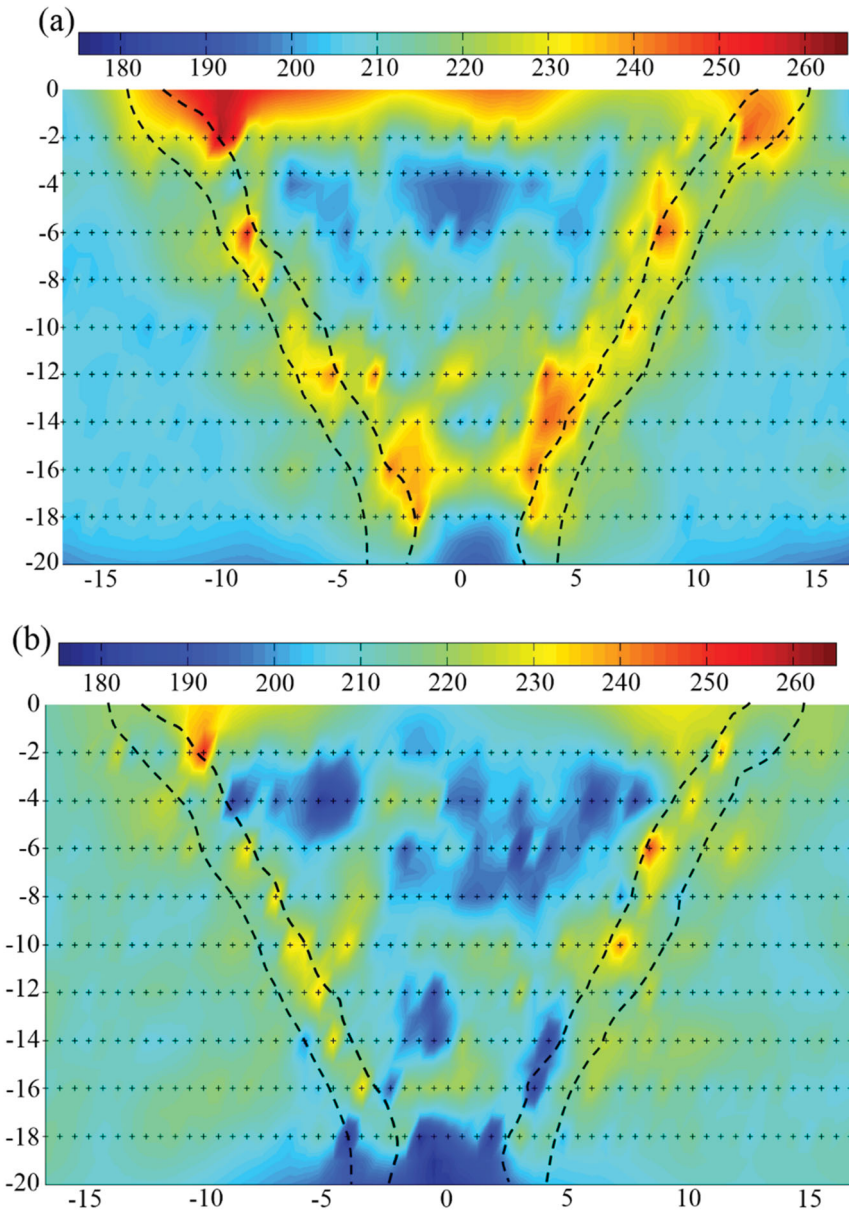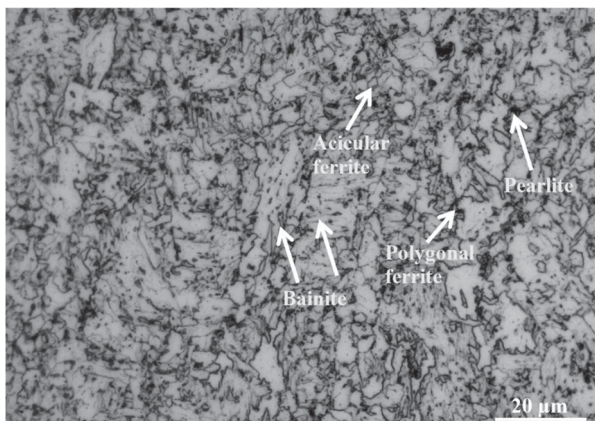**Figure 12.** Optical micrograph of the X70 steels showing bainite and acicular ferritic microstructure with some polygonal ferrite [19].
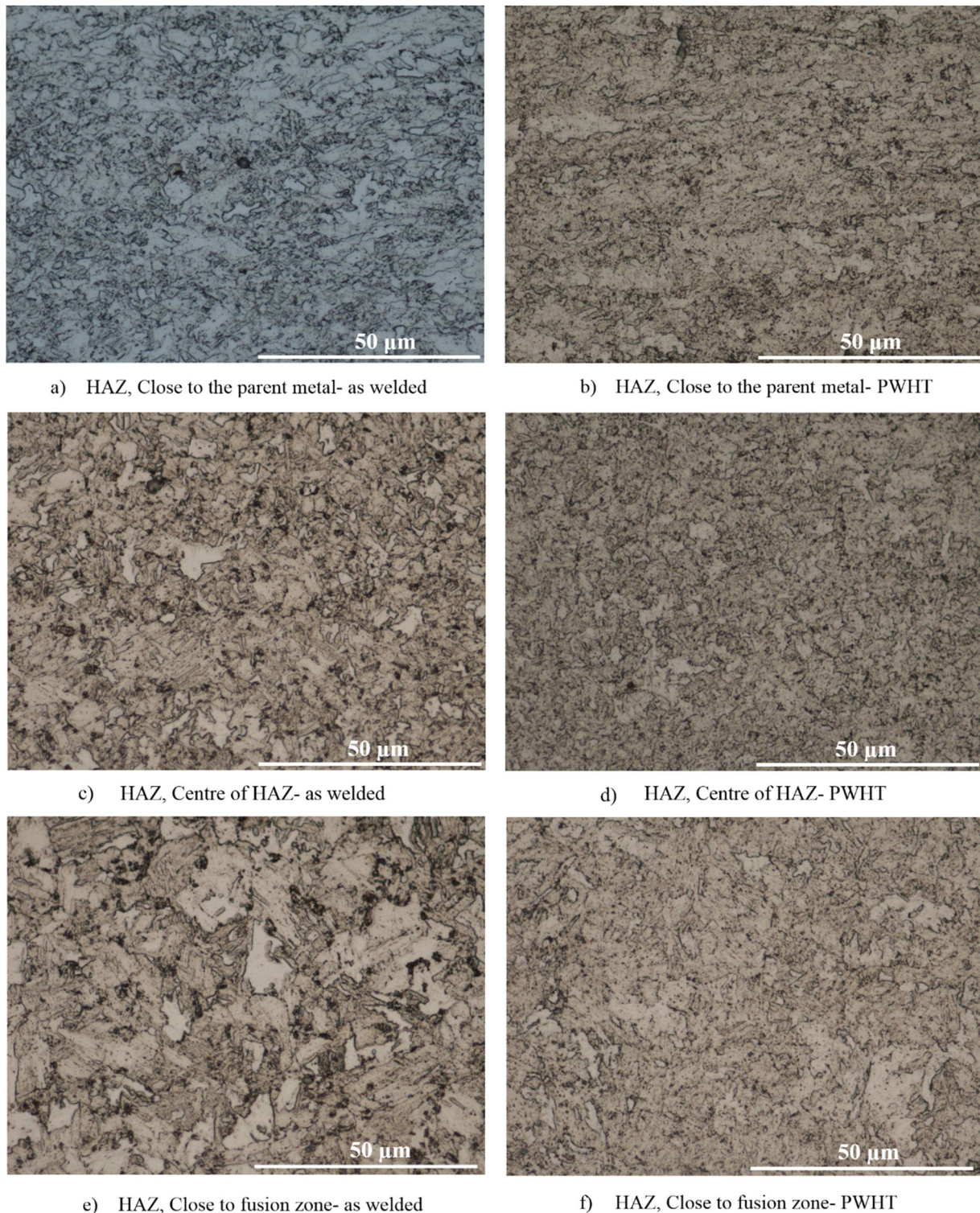
which shows that the fraction of high-angle boundaries (HAB $> 15°$) increases for these regions in the PWHT sample.

Discussion

The non-uniform temperature distribution and varied cooling rates during welding are responsible for the formation of residual stresses and distortion on cooling. The cooling rate and thermal gradients experienced by the material in and around the weld largely control the microstructure via grain size and phase transformation kinetics. These effects, in addition to thermal contraction effects, have a major contribution to the development of residual stresses. The presence of finer grains and microconstituents of bainite and Widmanstätten ferrite (Figure 13 (a, c, e) and Figure 14(a)) in the HAZ of the as-welded sample is the indication of higher cooling rate in this region during the welding process. These microstructures also account for the higher hardness values measured in the WM and HAZ for the as-welded sample as opposed to the PWHT sample (Figure 11(a)).

It has been clearly demonstrated by the in situ strain measurements during PWHT (Figure 6) that the

a)   HAZ, Close to the parent metal- as welded

b)   HAZ, Close to the parent metal- PWHT

c)   HAZ, Centre of HAZ- as welded

d)   HAZ, Centre of HAZ- PWHT

e)   HAZ, Close to fusion zone- as welded

f)   HAZ, Close to fusion zone- PWHT

Figure 13. Optical micrographs showing the microstructures across the HAZ in both as-welded (a, c, e) and after PWHT (b, d, f) samples.

residual strains (and by the association of the residual stresses) present in the as-welded specimen are largely relieved with the implemented heat treatment below the transformation temperature. Most importantly, the results indicated that the bulk of the strain relief occurred during the heating phase of the PWHT (80%), and that the holding time does not have significant effect on the relaxation of residual strains (only 11% of the strains were relieved during the holding time).

Previous numerical simulations, based on a creep model and analysis conducted by Zhang et al. [8] and Takazawa and Yanagida [20], showed that the relaxation of residual stresses mainly occurred during the heating stage to the PWHT isothermal holding temperature. Moreover, while Chen et al. [8] attributed the relaxation

a) As-welded, middle of the weld

b) PWHT, middle of the weld
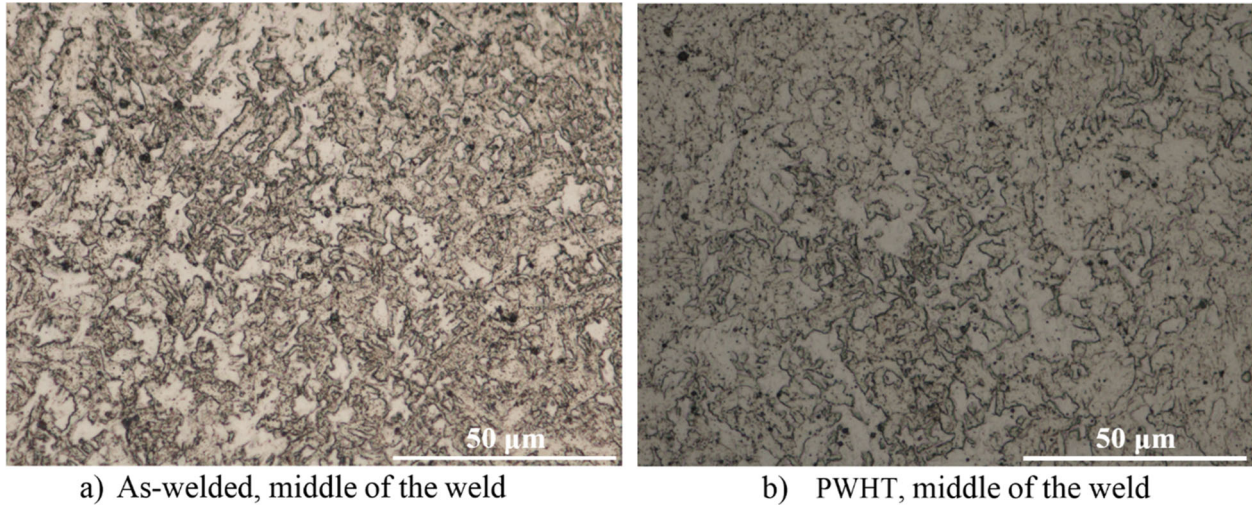
Figure 14. Optical micrographs showing typical microstructure for middle of the weld of (a) as-welded; and (b) after PWHT.

Table 2. Average spacing of grain boundaries with misorientations above 2° determined by the linear intercept method with random test lines on the EBSD scans.

	As-welded (µm)	PWHT (µm)
Weld middle	1.87	2.49
CGHAZ	1.95	2.27
FGHAZ	2.175	2.32

of the residual stresses, during the reheating stage, to the reduction in the steel yield stress with temperature. Further simulations by Dong *et al.* [21] showed that the most dominant stress relief mechanism during the temperature increase was creep strain-induced stress relaxation. In this [21], most of the strain is predicted to be released during the heating stage and it was suggested that PWHT holding time could be significantly reduced as far as residual stress relief was concerned. The in situ experimental results presented in Figure 6 of the current study confirm this suggestion. During the holding part of the PWHT at 600°C, the reduction in residual strains becomes less significant, which is attributed (analytically) to minor creep strain change during holding [8,20,21].

While the in situ measurements show only strain relaxation at one point of the sample during heat treatment, the strain/stress relaxation is confirmed in the whole cross section of PWHT sample (WM and HAZ) as shown by the residual stress (Figure 8), strain (Figure 9 and 10) and hardness measurements (Figure 11). It would be desirable to measure the strain relaxation during heat treatment in other location, particularly for the critical points (i.e. HAZ region) during the heating and holding stages of the PWHT. However, the strain measurements on the Kowari system are

somewhat time-intensive (i.e. as noted a minimum measurement time of 30 seconds for a given point was determined) and, as such in the interests of ensuring suitable time resolution during the strain relaxation process, the study was limited to a single point in the WM and associated regions.

Furthermore, residual stress measurements, which were conducted before and after PWHT, clearly show the substantial reduction in the magnitude of residual stresses (the stress relaxation after PWHT is evident in the residual stress contour maps, Figure 8). The peak of longitudinal residual stress for the as-welded and after PWHT was found to be 650 ± 16 MPa and 142 ± 14 MPa, respectively. It is also worth mentioning that the uncertainties for the measured stresses for the as-welded and PWHT samples were found to be no greater than ± 16 and ± 19 MPa, respectively.

During the heat treatment of the sample, the high temperature leads to microstructural changes, as shown by the optical micrographs (Figures 13 and 14) and evolution and enhancement of HAB fractions (Table 3), plus also some degree of grain growth (Table 2 and Figures 13 and 14). These experimental observations show that stress relaxation mainly occurs during the heating stage and explains the decrease in residual stress, strain and hardness in the PWHT specimen.

Conclusions

The key findings of this experimental study were

- The relaxation of residual stresses within the weld occurs mainly during heating stage of the PWHT,

Table 3. Grain boundary misorientation angle fraction for the WM, FGHAZ and CGHAZ for the as-welded and PWHT samples.

	WM		CGHAZ		FGHAZ	
Misorientation angle	As-welded	PWHT	As-welded	PWHT	As-welded	PWHT
(Low-angle g.b.) $< 15°$	0.484	0.340	0.717	0.565	0.613	0.535
(High-angle g.b.) $> 15°$	0.519	0.660	0.283	0.435	0.387	0.465

before reaching the isothermal holding temperature with ∼ 80% of the relaxation occurring in this stage. It was found that the relaxation of residual strain during the holding stage is a small percentage (about 11%) of the total strain relaxed.

- The magnitude of residual stresses decreased substantially after PWHT. In the as-welded sample, the maximum longitudinal stress was approximately 121% of the yield stress, while in the post-weld heat-treated sample the maximum longitudinal stress had fallen to approximately 26% of the yield strength of the WM.
- The Widmanstätten and bainitic ferrite which form within the as-welded specimen transformed into mainly polygonal ferrite. The grain size was found to be more homogeneous across the HAZ and WM for post-weld heat-treated sample compared to the as-welded sample.
- The unique information reported in this study should provide valuable data for the finite element modelling of this complex process. Clearly, this experimental approach supported by finite element simulations can optimise the PWHT and as a result significant cost savings may be achieved via reduction in PWHT times.

Disclosure Statement

No potential conflict of interest was reported by the author(s).

Funding

References

[1] Aloraier AS, Ibrahim RN, Ghojel J. Eliminating post-weld heat treatment in repair welding by temper bead technique: role bead sequence in metallurgical changes. J Mater Process Tech. 2004;153–154:392–400.

[2] Ebert H, Ballis W, Sperko W. Recommended practices for local heating of welds in piping and tubing. Miami: American Welding Society; 1990. 1990:260.

[3] Paddea S, Francis JA, Paradowska AM, et al. Residual stress distributions in a P91 steel-pipe girth weld before and after post weld heat treatment. Mater Sci Eng: A. 2012;534:663–672.

[4] Smith DJ, Garwood SJ. Influence of postweld heat treatment on the variation of residual stresses in 50 mm thick welded ferritic steel plates. Int J Press Ves Pip. 1992;51:241–256.

[5] Cho JR, Lee BY, Moon YH, et al. Investigation of residual stress and post weld heat treatment of multi-pass welds by finite element method and experiments. J Mater Process Tech. 2004;155–156:1690–1695.

[6] ASME boiler & pressure vessel code. Sec VIII Div 2 (2007 Edition)– an international code. The American society of Mechanical Engineers. New York: ASME Publication; August 2007.

[7] Standard API. 579-1/ASME FFS-1 Fitness for Service. Houston, TX: American Petroleum Institute; August 2007.

[8] Zhang J, Dong P, Song S. Stress relaxation behavior in PWHT of welded components. ASME 2011 Pressure Vessels and Piping Conference: American Society of Mechanical Engineers; 2011. p. 673–679.

[9] Dong P, Hong JK. Residual stress relief in post-weld heat treatment. ASME 2008 Pressure Vessels and Piping Conference: American Society of Mechanical Engineers; 2008. p. 321–329.

[10] Chen B, Skouras A, Wang YQ, et al. In situ neutron diffraction measurement of residual stress relaxation in a welded steel pipe during heat treatment. Mater Sci Eng: A. 2014;590:374–383.

[11] Dodge M, Gittos M, Dong H, et al. In-situ neutron diffraction measurement of stress redistribution in a dissimilar joint during heat treatment. Mater Sci Eng: A. 2015;627:161–170.

[12] Lombardi A, Sediako D, Machin A, et al. Transient analysis of residual strain during heat treatment of multi-material engine blocks using in-situ neutron diffraction. Mater Lett. 2015;157:50–52.

[13] Paradowska A, Finlayson TR, Price JWH, et al. Investigation of reference samples for residual strain measurements in a welded specimen by neutron and synchrotron X-ray diffraction. Phys B: Cond Matt. 2006;385–386, Part 2:904–907.

[14] Alipooramirabad H, Paradowska A, Ghomashchi R, et al. Prediction of welding stresses in WIC test and its application in pipelines. Mater Sci Tech. 2016;32:1462–1470.

[15] Alipooramirabad H, Paradowska A, Ghomashchi R, et al. Quantification of residual stresses in multi-pass welds using neutron diffraction. J Mate Process Tech. 2015;226:40–49.

[16] Kirstein O, Luzin V, Garbe U. The strain-scanning diffractometer Kowari. Neutron News. 2009;20:34–36.

[17] Withers P, Bhadeshia H. Residual stress. Part 1 – measurement techniques. Mater Sci Tech. 2001;17:355–365.

[18] Lavigne O, Gamboa E, Luzin V, et al. The effect of the crystallographic texture on intergranular stress corrosion crack paths. Mater Sci Eng: A. 2014;618:305–309.

[19] Alipooramirabad H, Ghomashchi R, Paradowska A, et al. Residual stress- microstructure-mechanical property interrelationships in multipass HSLA steel welds. J Mater Process Tech. 2016;231:456–467.

[20] Takazawa H, Yanagida N. Effect of creep constitutive equation on simulated stress mitigation behavior of alloy steel pipe during post-weld heat treatment. Int J Press Ves Pip. 2014;117–118:42–48.

[21] Dong P, Song S, Zhang J. Analysis of residual stress relief mechanisms in post-weld heat treatment. Int J Press Ves Pip. 2014;122:6–14.

CHAPTER 9

PUBLICATIONS TO BE SUBMITTED

Further work and future publication:

1) Title: Post weld heat treatment and its effects on the microstructure and mechanical properties of high strength low alloy steel welds.

2) Title: Effect of holding time on strain relaxation in high strength low alloy steel welds: an in-situ neutron diffraction approach.

The above mentioned work has been completed and the first draft of the papers have been submitted to supervisor. The abstracts are included.

Post weld heat treatment and its effects on the microstructure and mechanical properties of high strength low alloy steel welds

Houman Alipooramirabad[1]*, Reza Ghomashchi[1], Olivier Lavigne[1], Anna Paradowska[2]

[1]School of Mechanical Engineering, the University of Adelaide, SA 5005

[2] Bragg Institute, Australian Nuclear Science and Technology Organisation (ANSTO), Lucas Heights, NSW 2234, Australia

Abstract

Post weld heat treatment (PWHT) is often required for pressure vessel and piping components for relaxing residual stresses generated during welding and subsequent cooling to room temperature. This paper presents the effect of PWHT on the microstructure, mechanical properties and residual stresses in multi-pass, high strength low alloy steel, weld joints made by combined modified short arc welding (MSAW) and flux cored arc welding (FCAW) processes. Microstructural studies confirmed the formation of sub-grains in the PWHT specimen which is due to dislocation climb. This supports the creep-strain-induced, stress-relaxation mechanism during PWHT and explains the decrease of residual stress in the PWHT specimen. Furthermore, microstructural features evoulution due to PWHT explains the mechanical behaviour with the increase in the elongations (higher ductility) and a slight reduction in yield strenth for the PWHT specimen.

Effect of holding time on strain relaxation in high strength low alloy steel welds: an in-situ neutron diffraction approach

Houman Alipooramirabad[1]*, Anna Paradowska[2], Reza Ghomashchi[1], Olivier Lavigne[1], Mark Reid[2]

[1]School of Mechanical Engineering, the University of Adelaide, SA 5005

[2]Bragg Institute, Australian Nuclear Science and Technology Organisation (ANSTO), Lucas Heights, NSW 2234, Australia

Abstract

One of the consequence of welding is the generation of residual stresses which may play a deterimental role during service of welded structures. Post weld heat treatment (PWHT) is generally carried out to mitigate the residual stresses in weled structures. The two main parameters during PWHT are the time and temperature since the process of strain relieving is a diffusion controlled process. The present study therefore employed in-situ neutron diffraction to investigate the effects of holding time on relaxatin of residual strain for multi-pass high strength low alloy steel welds. Different holding times (0.5, 1 and 3 hours holding times) were utilized to monitor the residual strain evaluations during post-weld heat treatment. It was found that holding time has negligible effects on the strain relaxations as the bulk of strain relaxations occurs predominantly during the reheating stage of the heat treatment. Furthermore, the tensile, hardness and Charpy impact tests confirmed that lower holding time is beneficial for the mechanical and microstructural properties of the welded joints. The findings of this study can be used to optimize the current PWHT codes and standards. It can also be used for the validation studies of the finite element modelling of this process.

CHAPTER 10

CONCLUSIONS AND FURTHER SUGGESTIONS

10.1. Conclusions

The current research program was initiated to study the effect of stresses generated during welding and examine the effects such stresses impart on the susceptibility of weld metal to cracking and failure. The starting tests and modelling concentrated on effects of welding stresses on HACC susceptibility of line pipe girth welding using Welding Institute of Canada (WIC) weldability test.

3D finite element models (FEM) were developed to highlight the effects of welding parameters (heat input, thickness and restraint length) on the stresses, including residual stresses, generated during welding of the WIC weldability test. The numerical simulations were later validated against both the previously published results (the validation study was carried out for both thermal and residual stresses) and experimentally measured on WIC test coupons using neutron diffraction technique. The full detail of the work is presented in chapter 4. The key finding of this study were:

- The numerical results indicated that the heat input (constant welding speed) is an important factor affecting the welding stresses, specifically at low restraint intensity or for relatively small diameter pipelines and small wall thicknesses. This is an interesting justification for the use of low heat inputs at least for the first weld pass, which is the most critical stage with respect to the risk of HACC. However, low heat inputs also lead to higher cooling rates of the WM and trapping hydrogen within the weld. It is not clear how these two competitive mechanisms (lower cooling time and lower welding stresses) affect the overall risk of HACC. This should be subject of further investigation.

- The numerical results also confirmed the existence of a critical restraint length, below which the further decrease of the restraint length has no effect on the welding stress field. As a practical outcome, this finding allows the consideration of just one value of the restraint length in this region as it will be representative for all restraint intensities above a critical level. The computational results indicate that this critical length is between 25 and 50 mm.

However after initial modelling for single pass (root) girth welding, the project was focused on residual stresses measurements for multi-pass welding of HSLA to further highlight the issue of pipeline welding with further passes of hot, fill and cap, usually deposited for pressure vessels/pipeline construction. The work is presented in chapters 5-7 for this section.

To carry out the investigations, neutron diffraction was employed to study the effects of heat input, pass sequence and welding process on the magnitude and distribution of residual stresses for multi-pass high strength low alloy steel plates. Neutron diffraction measurements were performed at the Australian Nuclear Science and Technology Organization (ANSTO). The detailed measurements were performed in cross sections of weld and through different depths of the plate. Moreover, the combined effects of heat input (in the context of travel speed and resulting cooling rate), pass sequence and welding process on the microstructural and mechanical properties of high strength low alloy steel welds were investigated and how such properties could be affecting residual stresses in multi-pass welded joints was also detailed.

Some of the core findings of this study are listed below:

- Residual stresses in excess of yield strength were developed in the weld metal and HAZ of the MSAW+FCAW specimen. The residual stresses were notably higher than the SMAW process. Higher hardness levels in the joints fabricated with MSAW and FCAW process was attributed to the higher residual stresses and the microstructural constituents of bainite and Widmanstätten ferrite.

- The conducted measurements confirmed that the heat input (changing the weld speed) is one of the major factors affecting the field of residual stresses. With an increase of weld travel speed, and subsequent decrease of the heat input, the magnitude of residual stresses significantly increased. It was also found with the increase of heat input, the size of fusion zone and HAZ area also increased. As a result the maximum tensile residual stresses (longitudinal stresses) were located further away from weld centreline for the samples with higher heat input.

- The current results indicated no significant difference in the distribution of residual stresses as a result of changing the weld deposition direction. This could be attributed to the length of the specimen, which was rather long and negated the thermal effects associated with the change of the weld deposition direction. Another reason is that the measurements were conducted in the central part of the Specimens, which is lesser affected by this change. It is expected that the effect could be more pronounced at the weld start and end locations.

- The residual stresses were notably higher in the specimen with MSAW and FCAW processes, in comparison with SMAW process. This has been

previously reported, as well as the possibility that crack growth is faster in the MSAW and FCAW processes due to the presence of bainitic packets. Both these two factors may be used to explain the findings reported in the literature where crack initiation time and fatigue life of SMAW welds are longer than FCAW welds.

As mentioned earlier, there is a lack of study of the stress evaluation during heat treatment particularly for HSLA welds. Therefore, the in-situ neutron diffraction studies were employed during PWHT to investigate the rate of stain relaxation during heat treatment, holding time effects and the underlying mechanism behind stress relaxation for HSLA welds. In addition to the in-situ neutron diffraction studies, microstructural characterization (optical microscopy, scanning electron microscopy, EBSD and TEM) and mechanical property tests were also conducted to fully characterize the PWHT effects in multi-pass HSLA welds. The results of such investigations are presented in chapter 8 and future publications as detailed in chapter 9. The key findings of these experimental investigations were:

- It was found that the relaxation of residual stresses are mainly developed during reheating stage (about 89% of the total strain relaxed), before PWHT isothermal holding temperature. It was found that the relaxation of residual strain during the holding stage is a small percentage (about 11%) of the total strain relaxed.

- The magnitude of residual stresses decreased substantially after PWHT (about 26% of yield strength of the weld metal in the longitudinal direction and 20% in the transverse direction).

- The findings of three different holding times (0.5, 1 and 3 hours) proved that holding time has negligible effects on relaxation of residual stresses. This was also confirmed with the residual stress measurements after PWHT as well as the plastic strain measurements using kernel average misorientation data. The results of mechanical property analysis also confirmed the effectiveness of lower holding time for the mechanical property studies. The article to report this extra results is under preparation and will be submitted for publication soon.

- The Widmanstätten and bainitic ferrite which existed for the as-welded specimen was transformed into mainly polygonal ferrite after heat treatment. Also more homogeneous microstructure in terms of grain size was found after the PWHT process (HAZ and weld metal)

- High temperature leads to microstructural changes by assisting diffusion and increasing dislocation mobility, i.e. Dislocation climb – This could be due to the creep strain induced stress relaxation mechanism which may be active during PWHT and justifies the decrease of residual stress and hardness in the PWHT specimen. Further studies may be needed to fully clarify the hypothesis.

10.2. Recommendation for further works

Future studies will be investigating the effects of plate thickness and the type of material effects on strain relaxation behaviour for various weld joints. Clearly such investigation will help to establish a complete "time-temperature-rate of relaxation-thickness-holding time-material type" envelope which offers the prospect of more rational and economic heat treatment standards that combine cost savings with

optimised mechanical properties and residual stress states. Furthermore, development of effective finite element modelling for prediction of relaxation of residual strains/stresses during PWHT, in conjunction with above mentioned experimental studies, could lead to optimization of PWHT process with significant cost savings.